Slip systems, dislocation boundaries and lattice rotations in deformed metals

Winther, Grethe

Publication date:
2009

Document Version
Publisher's PDF, also known as Version of record

Risø DTU
National Laboratory for Sustainable Energy

DTU

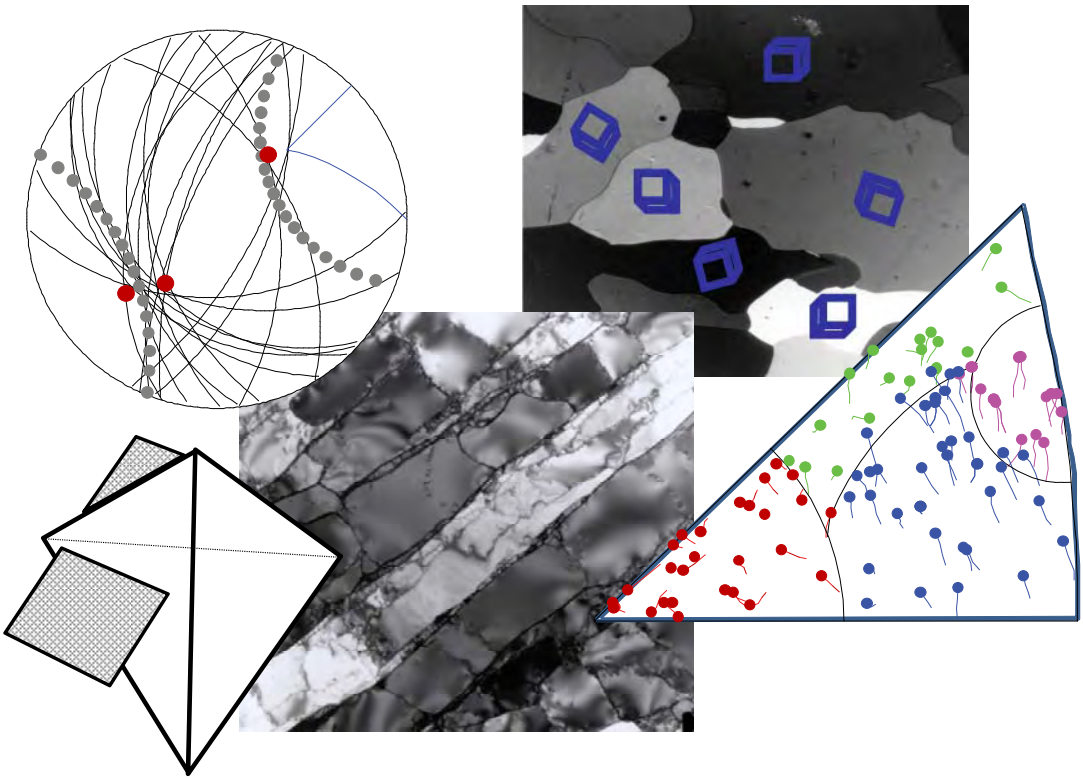

Slip systems, dislocation boundaries and lattice rotations in deformed metals

Grethe Winther

Dr. techn. thesis

Center for Fundamental Research:
Metal Structures in Four Dimensions
Materials Research Division

Risø-R-1686(EN)

ISSN 0106-2840

ISBN 978-87-550-3741-0

Risø-R-1686(EN)

Slip systems, dislocation boundaries and lattice rotations in deformed metals

Grethe Winther

Dr. techn. thesis

Center for Fundamental Research:
Metal Structures in Four Dimensions
Materials Research Division
Risø National Laboratory for Sustainable Energy
Technical University of Denmark

Denne afhandling er af Danmarks Tekniske Universitet antaget til forsvar for den tekniske doktorgrad. Antagelsen er sket efter bedømmelse af den foreliggende afhandling.

Kgs. Lyngby, den 23. marts 2009

Lars Pallesen
Rektor

/Martin P. Bendsøe
Dekan

This thesis has been accepted by the Technical University of Denmark for public defence in fulfilment of the requirements for the degree of Doctor Technices. The acceptance is based on this dissertation.

Kgs. Lyngby, 23 March 2009

Lars Pallesen
Rector

/Martin P. Bendsøe
Dean

Contents

A6: Dislocation structures. Part II. Slip system dependence by G. Winther and X. Huang, Phil. Mag., 2007

A7: Modelling flow stress anisotropy caused by deformation induced dislocation boundaries by G. Winther, D. Juul Jensen and N. Hansen, Acta Materialia, 1997

A8: Effect of grain orientation dependent microstructures on flow stress anisotropy modelling by G. Winther, Scripta Materialia, 2005

A9: Lattice rotations of individual bulk grains Part II: correlation with initial orientation and model comparison by G. Winther, L. Margulies, S. Schmidt and HF. Poulsen, Acta Materialia, 2004

A10: Slip systems extracted from lattice rotations and dislocation structures by G. Winther, Acta Materialia, in print

Preface

The subject of this thesis is the internal structures that develop in a metal upon deformation, i.e. texture and dislocation structures, and how these are controlled by the microscopic deformation mechanisms operating in each grain, namely slip systems. Fcc metals of medium to high stacking fault energy, such as aluminium and copper, deformed by tension and rolling at room temperature have been investigated.

The thesis presents methods and results of analyses of TEM data on the alignment of dislocation boundaries and 3DXRD data on the lattice rotations of grains. The experimental data underlying the analyses are obtained by co-workers. The focus of the analyses is to demonstrate that both dislocation boundaries and lattice rotations originate from the ensemble of active slip systems, and to identify predictive relations between especially dislocation boundary alignment and slip systems. The grain is seen as the basic entity assumed to have a set of representative active slip systems, even though some variations in these systems across a grain occur. The analysis consequently concentrates on the grain orientation dependence of dislocation boundary alignment, lattice rotations and slip systems rather than interactions between neighbouring grains and dislocations.

The studies behind this thesis have been conducted over a period of about 10 years, and ten selected papers describing the main results are included as appendices. Throughout the thesis these are referred to as A1-A10. Other papers by the author are referred to as A11-A21. Papers of other authors are cited by the numbers 22-119. Chapters 1 to 10 of the thesis present a coherent summary of the included papers in a common context, emphasizing the overall purpose and flow of the analysis both historically and thematically.

1 Introduction

Metals are a natural part of our everyday life, to which we normally do not pay much attention. To our ancestors the introduction of metals, however, marked new eras, i.e. the Bronze and Iron Ages, with new technological possibilities compared to the Stone Age. Since then processes have been developed to produce other metals and well-controlled alloys, e.g. a wide range of steels, which is still the dominating metal type. The discovery and technological exploitation of aluminium is relatively new. The first isolation of aluminium by the Dane Hans Christian Ørsted took place in 1825 and production in large quantities was not possible until much later in the century. Metals continue to be important as demonstrated by the large quantities produced each year. In 2006, about 1200 million tons of steel and 27 million tons of aluminium were produced and the production is steadily increasing.

The technologically important mechanical properties of metals are, for example, strength and formability through thermomechanical processing, involving plastic deformation at various temperatures, e.g. rolling of sheets. Such sheets may then be further processed to their final form by, for example, drawing operations. The discipline of metal science aims at elucidating the fundamental mechanisms controlling the properties to eventually provide predictive models to the metal industry which can guide the mechanical manufacturing process and product development. This involves studies of the internal structures of the metal.

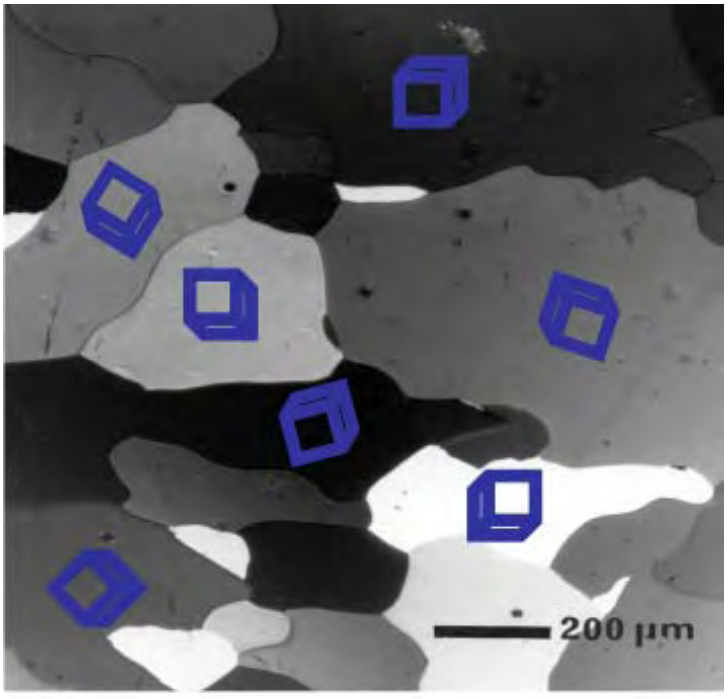

Fig. 1. Optical micrograph of polycrystalline metal surface, illustrating individual grains represented by different shades of grey. The orientation of the crystallographic lattice differs from grain to grain as illustrated by the blue cubes.

1.1 Metal Structures

Metals are crystalline and most often metals are used in the form of polycrystals, i.e. they are built up of individual grains (see Fig. 1). The crystallographic lattice in the individual grains is not oriented in the same way as illustrated by the blue cubes in the figure. The orientation of the crystallographic lattice with respect to the deformation mode, typically represented by the stress and strain axes of the sample, is referred to as the crystallographic *grain orientation*. The overall distribution of such grain orientations in the sample is the *texture*.

In the crystallographic lattice deformation takes place by slip, which is the sliding of certain crystallographic planes past each other in certain directions like a deck of sliding cards, which causes a shape change of the sample. The combination of such a plane and direction is called a *slip system*. As a result of the boundary conditions imposed slip is typically accompanied by *lattice rotation*, i.e. rotation of the crystallographic lattice to change the grain orientation. These rotations ensure that all grains remain connected to each other.

Seen at a smaller scale line defects in the crystallographic lattice, termed *dislocations*, glide on the slip plane. The gliding dislocation has characteristics which depend on the slip system. The dislocations in many metals accumulate in *dislocation boundaries*. An example of such boundaries observed by transmission electron microscopy (TEM) is shown in Fig. 2. Many such boundaries are formed within a grain. The spacing between them is typically of the order of a few micrometres but may also be smaller.

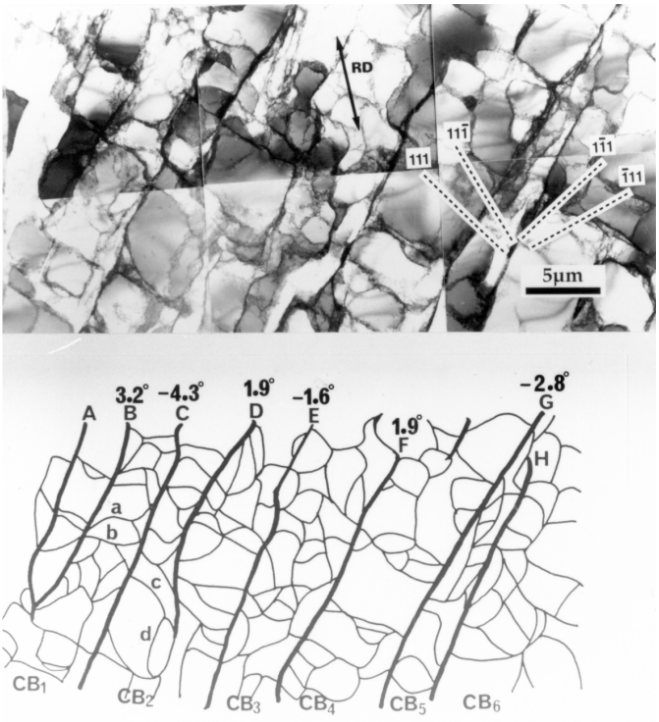

Fig. 2. Transmission electron micrograph of the typical deformation-induced dislocation structure in aluminium deformed to low strains. The dislocations assemble in dislocation boundaries, which are marked in the tracing below together with the crystallographic misorientation across some of the boundaries. From [22].

1.2 Modelling slip systems, texture evolution and dislocation boundaries

Traditionally studies of deformation-induced texture and dislocation boundaries have been two separate scientific fields addressed by different communities. This thesis demonstrates that texture and dislocation boundaries are coupled in the sense that they both depend on the slip systems.

1.2.1 Slip systems and texture evolution

Direct observation of slip is only possible at surfaces, where slip lines develop during deformation. Indirectly slip systems may be studied through the lattice rotations with which they are inherently associated. At the bulk level lattice rotations lead to deformation texture evolution so that the intensity of certain stable orientations (deformation texture components) increases at the expense of the intensity of unstable orientations. Deformation texture evolution is typically measured at the bulk level on small samples cut out of a larger material volume before and after deformation. The limitation of only having bulk data complicates analysis of the active slip systems in individual grains immensely and essentially prevents solid conclusions in many cases. Measurements of the orientation of individual grains at a metal surface are also possible. The rotation of surface grains can therefore be measured but may not necessarily be representative of the vast majority of grains, which are deeply embedded in the bulk of the metal. To overcome this, experiments designed to mimic bulk conditions have been designed, e.g. by pressing two metal surfaces tightly together during deformation [23-25] or using columnar grains where surface data in the initial state can be assumed to be valid also for the part of the grains far from the surface [26-29]. However, data for real bulk grains are obviously to be preferred.

In parallel with the experimental observations, a huge effort has been put into the development of models of deformation texture evolution over the past ~80 years. The wide range of models proposed involves a common step of slip system prediction and subsequent derivation of the lattice rotations. The iterative procedure typical for simulation of deformation textures is sketched in Fig. 3. The deformation is simulated as a number of small deformation steps. In each step and for each grain the slip systems are calculated from the initial grain orientation (arrow 1). Subsequently the lattice rotation is calculated (arrow 2), leading to an updated grain orientation, which is then the basis for the next deformation step (arrow 3). The flow stress may be derived from the slip system activity (arrow 4), often involving a hardening law, which may also be updated.

The proposed models differ in the degree of enforcement of stress equilibrium and strain compatibility between neighbouring grains. The simplest models see a grain as an independent entity characterised solely by its orientation. These models then apply various stress/strain boundary conditions to this orientation to calculate the slip systems. The most widely known models of this type are the model by Sachs [30], which enforces neither stress equilibrium nor strain compatibility but base the prediction on stress considerations, and the models arrived at by Taylor [31] and Bishop-Hill [32], which ignore stress equilibrium and strictly enforce strain compatibility in the sense that all grains are assumed to deform with the same strain as the sample. A wide range of variants of the Taylor model has been proposed, including i) introduction of a strain rate sensitivity (e.g. [33]), which is more important for deformation at elevated temperatures, and ii) grain shape effects (e.g. [34]), which are especially important at high strains where the shape often becomes asymmetric. These models typically predict textures that are too sharp, i.e. with more intensity around the stable components than observed experimentally. In addition, the

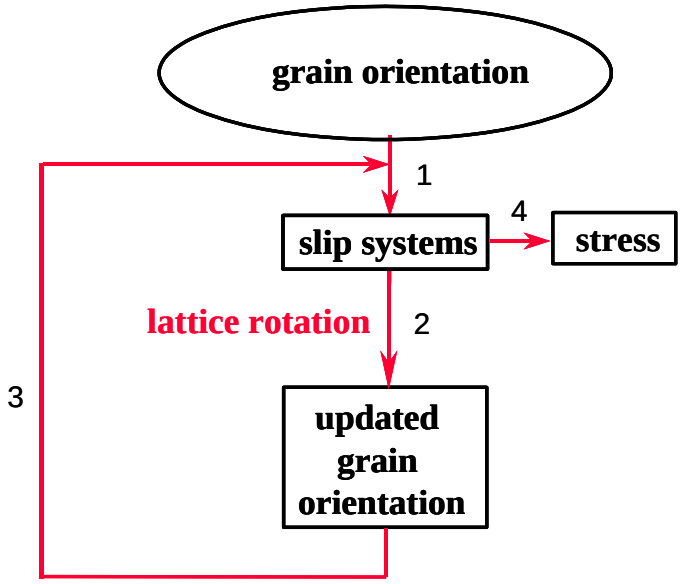

Fig. 3. Sketch of the typical polycrystal plasticity model.

relative intensities of the stable texture components are also difficult to predict, which suggests more fundamental problems in the slip system prediction.

Some of these inadequacies may be overcome by introducing more elaborate modelling of the grain interaction effects, ranging from self-consistent models (see e.g. [35]) that take the interaction between a grain and a matrix representing the other grains into account, over specific interactions between two or more grains (e.g. the LAMEL model [36]) to models considering the detailed interactions of all grains, often based on finite element methods (e.g. [37]), or more recently based on Fourier transformations [38].

While the field is sufficiently advanced to provide reasonably satisfactory models for prediction of bulk textures, the models are difficult to validate at the grain level due to the general lack of experimental data. Data for individual grains, which are indisputably deeply embedded in the bulk of the metal, have recently become available with the development of the three-dimensional X-ray diffraction technique (3DXRD) [A11, A12, A13]. These data constitute the experimental basis for this thesis, together with dislocation structure data.

1.2.2 Dislocation boundaries

While slip systems have always been an essential part of modelling of lattice rotations and deformation textures, they are not traditionally a primary parameter in the modelling of dislocation structures. Often the dislocation structure is modelled in terms of the dislocation density, as the stress in general is proportional to the square root of this density [39, 40]. The spatial arrangement of the dislocations is, however, complex as dislocations in many metals assemble in dislocation boundaries, which form three-dimensional networks within each grain.

Fig. 2 shows a two-dimensional TEM image of the typical morphology of dislocation structures after monotonic deformation in fcc and bcc metals of medium to high stacking fault energy. The dislocation boundaries are typically classified in two groups [41], namely

extended planar boundaries and short, randomly oriented cell boundaries. The randomly oriented cell boundaries are believed to originate from statistical trapping of dislocations and they are termed incidental dislocation boundaries (IDBs). The trace of an extended planar boundary is seen as a long line in the TEM image. Such lines are emphasized in the tracing included in Fig. 2. The extended planar boundaries are termed geometrically necessary boundaries (GNBs) as they are believed to accommodate systematic slip differences in the grain. This is also in agreement with the typically alternating sign of the misorientation across adjacent GNBs. As seen from the parallel traces in Fig. 2 the GNBs exhibit a common alignment within a grain.

The absolute magnitude of misorientation angles and boundary spacings vary substantially with the metal type, for example being smaller in copper than in aluminium [42, 43]. Variations with the grain size are also seen [44]. Nevertheless, the evolution of angles and spacings with the strain follows some common principles: as the strain increases, the boundary spacings decrease while the misorientation angles increase. The mean misorientation angle for GNBs is found to increase exponentially with the strain and is proportional to $\varepsilon^{2/3}$ while the angle for the IDBs is proportional to $\varepsilon^{1/2}$ [45]. The difference in exponents is related to the different origin of the two types of boundaries: a random capture has been theoretically shown to lead to an exponent of ½ [46, 47] while the higher exponent of 2/3 has been theoretically traced to a transition from 0 to 1 with increasing strain [48]. Furthermore, a scaling law applies to the distributions of boundary spacings [49] and misorientation angles [45]: the distributions are similar when normalized with the average value. The boundary spacings scale independently of metal type, deformation mode and strain level [49], which has been demonstrated for average boundary spacings in the range between 10 nm and 10 μm [50]. For high strains ($\varepsilon>2$) scaling of the misorientation angles for the GNBs breaks down as the distribution becomes bimodal [51, 52].

Another invariant feature of the GNBs is their characteristic alignment within a grain which is independent of grain size and strain level up to low and moderate strains ($\varepsilon<1$) [A14]. Instead the GNB alignment, characterised in terms of the crystallographic GNB plane, varies systematically with the grain orientation and the crystal structure of the metal. This crystallographic alignment of the GNBs and its grain orientation dependence is the experimental basis of the dislocation structure studies in this thesis.

Dislocation boundaries are often believed to be low energy dislocation structures (LEDS) [53], meaning that the dislocations in the boundaries screen each others' stress fields so that the boundaries are free of long range stresses. Detailed studies of individual GNBs have revealed that a large fraction of the dislocations in the boundary corresponds to those generated by the expected active slip systems [54, 55]. These observations are in agreement with calculations assuming that the GNBs are low energy dislocation structures [54-56]. However, the LEDS principle has not been capable of predicting the spatial arrangement of the dislocation structure, including the GNB alignment, although modelling of the evolution of GNBs based on this principle has been proposed [A15, 57].

The grain orientation dependence of the crystallographic GNB alignment is believed to originate from an underlying dependence of the active slip systems, implying that the GNB alignment is a new indirect way to investigate slip systems. This thesis analyses the GNB alignment to the point of formulating a general predictive model relating slip systems and crystallographic GNB planes.

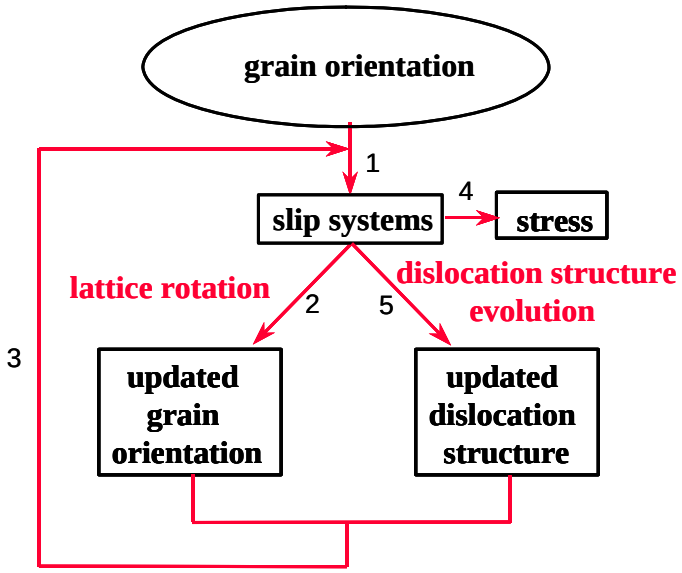

Fig. 4. Modification of the standard modelling scheme for prediction of lattice rotations (see Fig. 3) to model the coupling of lattice rotations and dislocation structures thrgout the slip systems. From [A1].

1.3 Introducing coupling of lattice rotations and dislocation structures

With the realisation that both lattice rotations and dislocation structure alignment depends on the slip systems, modelling the evolution of deformation induced textures and of dislocation structures should be coupled as proposed in Fig. 4. The author first presented this coupled modelling scheme in 1998 [A16] in a preliminary form and subsequently in its present form in 1999 in the following paper, which is included in the appendix:

A1: Coupling textural and microstructural evolution by G. Winther, Proc. ICOTOM12, 1999.

As seen in Fig. 4 the coupling introduces a new branch into the classical modelling scheme outlined in Fig. 3. This new branch consists of prediction of the dislocation structure changes from the slip systems, in parallel to the prediction of the changes in the grain orientation. The coupling also means that the effect of the dislocation structure on the slip systems and the flow stress must be considered.

The experimental lattice rotation and dislocation structure alignment data on which this thesis is based clearly depend on the grain orientation, which implies that the grain orientation is the dominant parameter controlling the slip systems. In Fig. 4 and throughout the thesis the grain is therefore the basic entity and the intragranular orientation spread, which evolves with increasing strain, is considered a secondary phenomenon. As a first approximation it is consequently assumed that the same ensemble of active slip systems operates in the entire grain. By conducting the investigations at the grain scale it was possible to demonstrate the coupling between lattice rotations and dislocation structure alignment through their common relation to the slip systems. Using the methods and results of this thesis future refinement of the scale to consider orientation gradients and grain subdivision as well as the systematic misorientations across GNBs may be possible.

The results and conclusions of this thesis are generally applicable to cold deformation of fcc metals of medium to high stacking fault energy in relatively pure form and a broad range of grain sizes (demonstrated for the range 4-300 μm). Grain orientation dependent dislocation structure alignment has also been observed in bcc metals, such as IF steel [58]. It is therefore expected that analogous results can be derived for bcc metals upon future characterisation of their lattice rotations and dislocation structure alignment to the same level of detail as for the fcc case.

1.4 Purpose of this thesis

At the time of the first formulation of the schematic modelling framework in Fig. 4, the author also evaluated to what extent the modelling components represented by the arrows were available. As the coupled modelling scheme is an extension of the standard polycrystal plasticity modelling in Fig. 3 models for prediction of slip systems (arrows 1 and 3), lattice rotations (arrow 2) and flow stress (arrow 4) were obviously available, but of course improvements might be possible and even necessary. Models for inclusion of dislocation structure alignment in the prediction of mechanical properties (arrow 4) had also been devised, first at the bulk level [59] and subsequently extended to the grain level with the author in a leading role [A7, 60]. By contrast, prediction of dislocation structure alignment from the slip systems (arrow 5) was at a rudimentary state: the author had proposed a model applying only to a specific case [A4] and generalisation of this was not immediately foreseeable. As mentioned above other models based on the LEDS principle were also in their infancy [A15, 57]. In fact, the gap in this part of the proposed modelling scheme was so serious that an alternative was suggested in the form of a data base with experimental dislocation structure information, in which the updated dislocation structure alignment could be looked up once the updated grain orientation was found [A1]. At the time, the experimental data required to build the data base were, however, also limited.

Note that a similar modelling scheme has subsequently been implemented for bcc metals in [61, 62]. The focus of those studies was, however, on application of the model to predict the stress/strain curve during complex strain paths while the present thesis focuses more on fundamental studies of lattice rotations, dislocation structure alignment and slip systems at the grain scale to build up the experimental and theoretical basis for subsequent modelling of phenomena at the scale of the sample.

This thesis presents a coherent compilation of the research conducted to advance the modelling scheme to a state where its practical application has become realistic. Significant progress has been made for most of the modelling components (arrows), tightly following the availability of new experimental data. The majority of the author’s efforts has been aimed at filling the largest gap, i.e. prediction of the dislocation structure alignment based on slip systems, which is now generally possible. The technological relevance of such prediction is exemplified by the modelling of mechanical anisotropy of rolled sheets.

Another key issue has been the prediction of slip systems from the grain orientation. The Taylor model was initially selected to calculate the slip systems. Throughout the thesis, predictions of dislocation structure alignment and lattice rotations from these systems show that the Taylor model is often successful but its limitations have also been revealed. Although not explicitly formulating a new predictive model, the thesis devises methods for determination of the active systems based on dislocation structure alignment studies, which may also be supplemented by data on lattice rotations.

In addition to this introduction, the thesis contains nine chapters. Two of these (chapters 2 and 3) contain introductory background material and the remaining seven present the results of nine of the author's key papers in the context of Fig. 4. These papers are included in the appendix, together with the original paper proposing the scheme. More specifically, the thesis contains the following chapters:

Chapter 2: ***Materials, deformation modes and experimental characterisation***. This chapter gives an overview of the experimental data underlying this thesis. These data have been acquired by the author's co-workers, although the author has sometimes been involved.

Chapter 3: ***Introduction to dislocation structure alignment***. This chapter provides a historic overview of significant advances in the characterisation and understanding of dislocation structure alignment, in particular the planes of GNBs.

Chapter 4: ***Dislocation structure alignment - Grain orientation dependence***. The author has contributed to the investigation of the grain orientation dependence of dislocation boundary planes by development and application of a method to determine the 3D orientation of the boundary plane from analysis of dislocation boundary traces in 2D observed by TEM. This established the grain orientation as a governing parameter in all cases. The findings inspired even more detailed characterisation by TEM, the results of which are also included to describe the full experimental basis for the analysis in the subsequent chapters.

A2: Critical comparison of dislocation boundary alignment studied by TEM and EBSD: Technical issues and theoretical consequences by G. Winther, X. Huang, A. Godfrey and N. Hansen, Acta Materialia, 2004.

A3: Crystallographic and macroscopic orientation of planar dislocation boundaries – correlation with grain orientation by G. Winther, X. Huang and N. Hansen, Acta Materialia, 2000

Chapter 5: ***Dislocation structure alignment - Slip system dependence***. The slip systems rather than the grain orientation are established as the parameter controlling the dislocation structure alignment. The development of models relating slip systems and dislocation structure alignment is described, in particular focusing on GNBs aligned with {111} planes and specific deformation modes.

A4: Dense dislocation walls and microbands aligned with slip planes – theoretical considerations by G. Winther, D. Juul Jensen and N. Hansen, Acta Materialia, 1997

A5: Slip patterns and preferred dislocation boundary planes by G. Winther, Acta Materialia, 2003

Chapter 6: ***Dislocation structure alignment - Slip class dependence***. The concept of slip classes is introduced to detach the analysis from a particular grain orientation and

deformation mode and obtain a universal model. The analysis is also extended to consider the crystallographic alignment of all GNBs.

A6: Dislocation structures. Part II. Slip system dependence by G. Winther and X. Huang, Phil. Mag., 2007

Chapter 7: ***Prediction of dislocation structure alignment in rolling and its effect on mechanical anisotropy***. This chapter illustrates the technological relevance of studies of dislocation structure alignment, using the flow stress anisotropy of rolled sheets as an example. At first the capability to predict the dislocation structure alignment in rolling is evaluated. Subsequently, modelling of the coupled effects of texture and dislocation structure alignment on the flow stress anisotropy is presented and it is demonstrated that the current understanding of grain orientation dependent dislocation structure alignment is sufficient to allow good predictions of the anisotropy.

A7: Modelling flow stress anisotropy caused by deformation induced dislocation boundaries by G. Winther, D. Juul Jensen and N. Hansen, Acta Materialia, 1997

A8: Effect of grain orientation dependent microstructures on flow stress anisotropy modelling by G. Winther, Scripta Materialia, 2005

Chapter 8: ***Lattice rotations during tension - Grain orientation and slip system dependence***. Lattice rotation data during tension obtained with the 3DXRD technique are analysed to determine their grain orientation dependence. The experimental data and their grain orientation dependence are also compared with the predictions of standard crystal plasticity models (including the Taylor model), showing that while these capture some of the features, some phenomena remain unaccounted for.

A9: Lattice rotations of individual bulk grains Part II: correlation with initial orientation and model comparison by G. Winther, L. Margulies, S. Schmidt and HF. Poulsen, Acta Materialia, 2004

Chapter 9: ***Slip systems in tension determined from coupling of dislocation structure alignment and lattice rotations***. By combining the grain orientation dependence of dislocation structures and lattice rotations in tension, the grain orientation dependence of the slip systems is deduced. By means of the slip class concept slip systems leading to both the observed lattice rotations and dislocation structure alignment are identified, leading to a discussion of the stress/strain conditions experienced by each grain. This truly establishes the slip systems as the underlying factor coupling lattice rotations and dislocation structure alignment.

A10: Slip systems extracted from lattice rotations and dislocation structures by G. Winther, Acta Materialia, in print

Chapter 10: ***Conclusions and outlook***, which summarises the results and outlines the main implications for future studies.

2 Materials, deformation and experimental characterisation

The experimental data sets on which the thesis have been acquired by co-workers but with strong interaction between experiment and analysis/modelling (with the author's contribution lying on the analysis/modelling front). In total the thesis analyses 12 data sets, which are summarised in Table 1. Throughout the thesis these data have been supplemented by other relevant data found in the literature, especially data for single crystals, which exhibit the same alignment of the dislocation structure as grains in polycrystals of similar orientation.

2.1 Materials

The investigation concerns metals of medium to high stacking fault energy, here represented by aluminium and copper. The selected materials had purities in the range 99.999% to 99.5% and grain sizes between 4 and 300 μm (see Table 1 for a complete list). In two cases dislocation structure characterisation and lattice rotation measurements were conducted on the same materials (but not on the same samples).

2.2 Deformation

The materials have been deformed by uniaxial tension and rolling (data sets 1-6+10-12 and 7-9 in Table 1, respectively). All deformation took place at room temperature at low strain rates and the strain level spans from 5 to 50 % deformation.

The advantage of tensile deformation is that it may be assumed to exhibit axial symmetry, meaning that only the crystallographic direction of the tensile axis needs to be considered. This limits the relevant orientation space to one of the 24 stereographic triangles, which can realistically be covered by experimental data. Rolling was selected due to its industrial relevance. It is assumed that deformation by rolling is equivalent to plane strain compression. In addition inclusion of two deformation modes was necessary to demonstrate that the slip systems – rather than the grain orientation – control the dislocation structure alignment.

Table 1. Overview of the experimental data sets forming the primary basis for this thesis.

Data set	Material	Grain size μm	Deformation mode	Strain ε_{vM}	Strain rate s^{-1}	Data from ref.
Dislocation structure characterisation by TEM						
1	Al (99.996 %)	300	tension	0.05, 0.14, 0.22, 0.34	$8 \cdot 10^{-4}$	[63]
2	Al (99.5 %)	75	tension	0.10, 0.22	$8 \cdot 10^{-4}$	[A14]
3	Cu (99.999 %)	190	tension	0.05, 0.14, 0.22	$1.7 \cdot 10^{-4}$	[64]
4	Cu (99.999 %)	50	tension	0.10, 0.14, 0.20	$1.7 \cdot 10^{-4}$	[65]
5	Cu (99.999 %)	4	tension	0.05, 0.14, 0.22, 0.28	$1.7 \cdot 10^{-4}$	[44]
6	Cu (99.99 %)	90	tension	0.15, 0.20	$4 \cdot 10^{-4}$	
7	Al (99.99 %)	300	rolling	0.06, 0.12, 0.41,0.8	6	[22, 66]
8	Al (99.5 %)	75	rolling	0.15, 0.33	6	[A14]
9	Cu (99.99 %)	90	rolling	0.13, 0.22, 0.78	6	[A14, 43]
Lattice rotation characterisation by 3DXRD						
10	Al (99.996 %)	300	tension	0-0.1	$1.6 \cdot 10^{-4}$	[A11]
11	Al (99.95 %)	75	tension	0-0.05	$1.6 \cdot 10^{-4}$	[A13]
12	Cu (99 %)	35	tension	0-0.05	$1.6 \cdot 10^{-4}$	[A12]

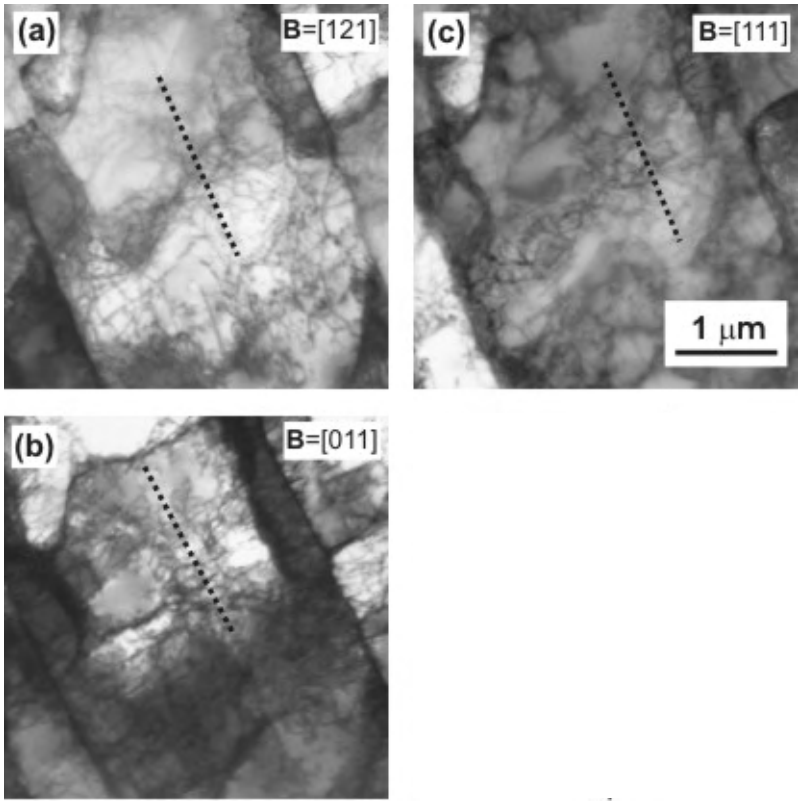

Fig. 5. TEM images of the same ($\bar{1}1\ \bar{1}$) aligned boundaries in a grain in 25 % cold rolled AA1050. The images a-c are taken at different tilts, i.e. with the beam B parallel to different crystallographic directions. a) The boundary traces are sharp, i.e. the boundaries are seen edge-on, b) tilting around an axis perpendicular to the boundary plane still gives a very sharp trace, i.e. edge-on conditions are maintained, and c) after tilting around an axis parallel to the boundary plane, edge-on conditions no longer apply resulting in a very wide trace. From [A2].

2.3 Dislocation structure characterisation

The data on the GNB alignment analysed in this thesis have been provided by TEM as TEM is the only technique capable of determining the crystallographic plane of an individual boundary in one process. The procedure is described in detail in [A2, 67] and outlined in Fig. 5. The basic principle is to tilt the foil until the boundary trace is sharp and narrow, at which point the electron beam is parallel to the boundary plane and the boundary is viewed edge-on (Fig. 5a).

The edge-on condition may be verified by tilting the foil around an axis perpendicular to the boundary plane, which should not change the edge-on conditions (Fig. 5b), while tilting around an axis parallel to the boundary plane causes the boundary to appear wider as it is no longer seen edge-on (Fig. 5c).

A further advantage of the TEM is its high resolution which reveals the details of the boundary structure, e.g. that boundaries often consist of planar segments, which are parallel but slightly shifted with respect to each other as demonstrated in Fig. 6 [A14]. While individual segments are planar as evidenced by the straightness of their traces, the steps in between segments may give the GNB a curved character over longer distances.

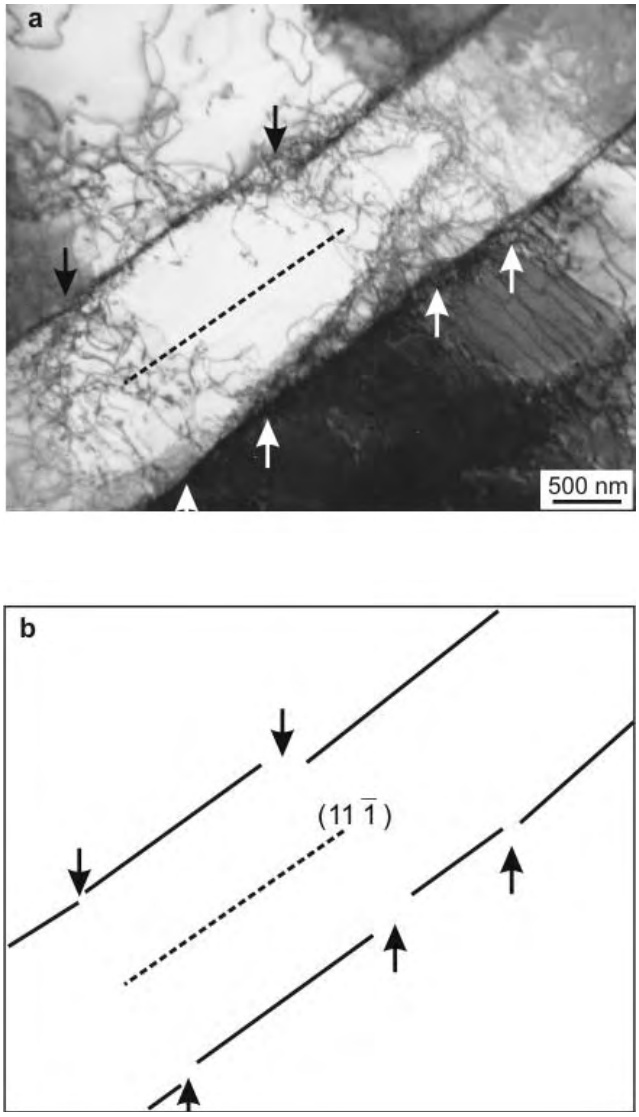

Fig. 6. An example showing the GNB plane determination for grain with GNBs aligned with the (11-1) slip plane. (a) An edge-on image of two GNBs taken in the beam direction of $[1\bar{2}\bar{1}]$. Small steps are indicated by arrows. (b) A sketch showing an approximately parallel relationship between the straight segments forming the GNB. From [A14].

Detailed TEM [68] and EBSD [69] studies of the parts of the grain that lie in the vicinity of grain boundaries and triple junctions compared to the grain interior have revealed that the dislocation structure in general exhibits localized changes near triple junctions. Analogous changes near grain boundaries are less frequent and in many (but clearly not all) cases the GNBs exhibit an unaltered directionality when approaching the grain boundary as illustrated in Fig. 7. In the case of orientation differences across a grain – presumably as a result of deformation – the local dislocation structure follows the local crystallographic orientation as demonstrated in Fig. 8 for a grain splitting up into regions of alternating orientation.

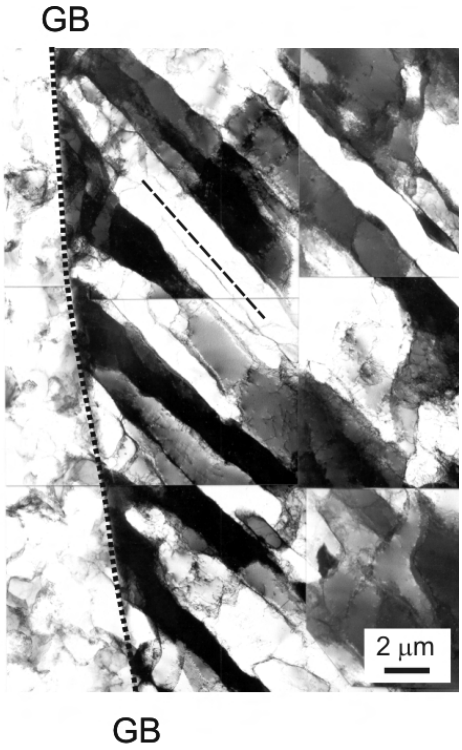

Fig. 7. TEM image showing a uniform structure extending from the grain boundary (GB and dotted line) toward the grain interior. The primary slip plane trace is indicated by a dashed line and the GNBs remain parallel to this as is also the case in the grain interior (not shown). From [A14].

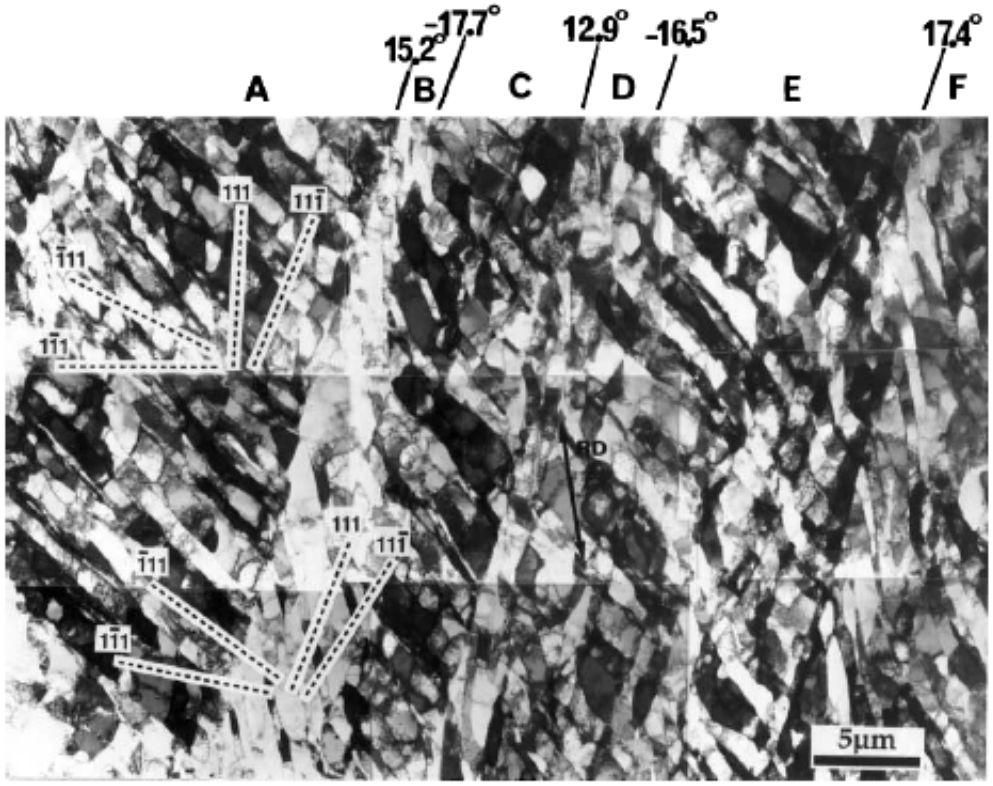

Fig. 8. TEM image of a grain subdivided into different regions (A, B, C, D, E, and F). Regions A, C and E have similar dislocation structure alignment and similar orientation, which differ from those in regions B, D and F. From [22].

The data forming the basis for this thesis come from nine TEM studies (data sets 1-9) including a total of about 500 grains, with all foils taken from the central parts of the samples to ensure bulk conditions. The majority of these studies were conducted by Dr. Huang. Within each grain the crystallographic alignment of the GNB planes has been determined with respect to the local grain orientation, often involving several positions in the same grain which typically yielded the same local crystallographic GNB plane even if the local crystallographic orientations exhibited differences (as exemplified in Fig. 8b). For such grains a representative grain orientation is normally reported together with the common crystallographic GNB plane, i.e. the grain is considered an entity with a crystallographically uniform GNB alignment.

2.4 Lattice rotation characterisation

The lattice rotation data analysed in this thesis originate from the 3DXRD microscope [70]. This technique has the penetrating power to monitor the rotation of grains deeply embedded in the sample and sufficient resolution to follow individual grains.

Using the 3DXRD microscope, two different methods were employed to ensure that the data cover only grains deeply embedded in the bulk of the sample. In the first experiment [A11] the radial position of the reflections was used to determine the location of the grains along the beam direction. In the subsequent experiments [A12, A13] a conical slit was introduced in the 3DXRD microscope as illustrated in Fig. 9. The slit only allows diffraction spots originating from a volume of 5 x 5 x ~300 μm^3 located in the centre of a sample to reach the detector.

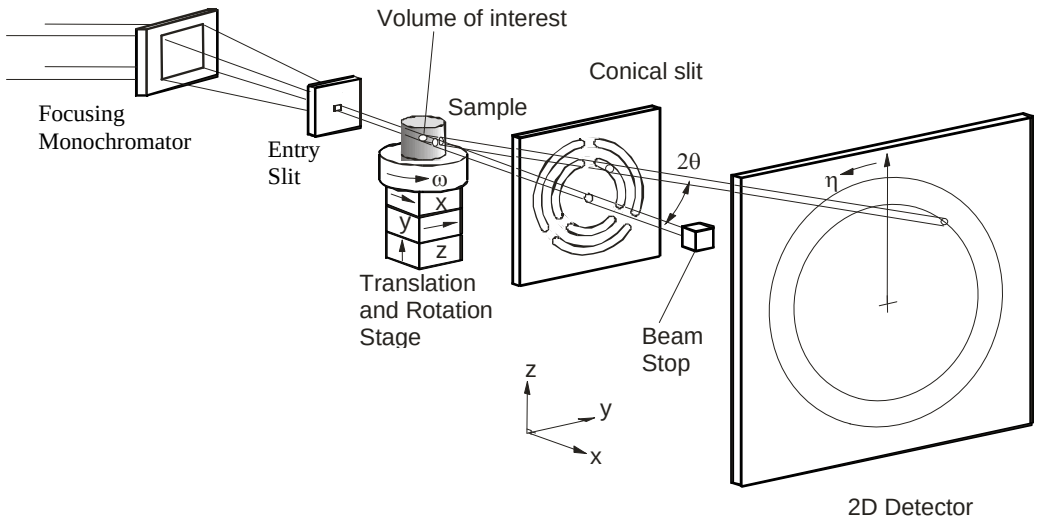

Fig. 9. Sketch of the experimental set-up in the 3DXRD microscope. The co-ordinate system (x,y,z) and angles 2θ (Bragg angle), ω (sample rotation) and η (azimuthal angle) are defined. The axis of the mounted tensile rig (not shown) is parallel to y for ω = 0. The first experiment was conducted without the conical slit.

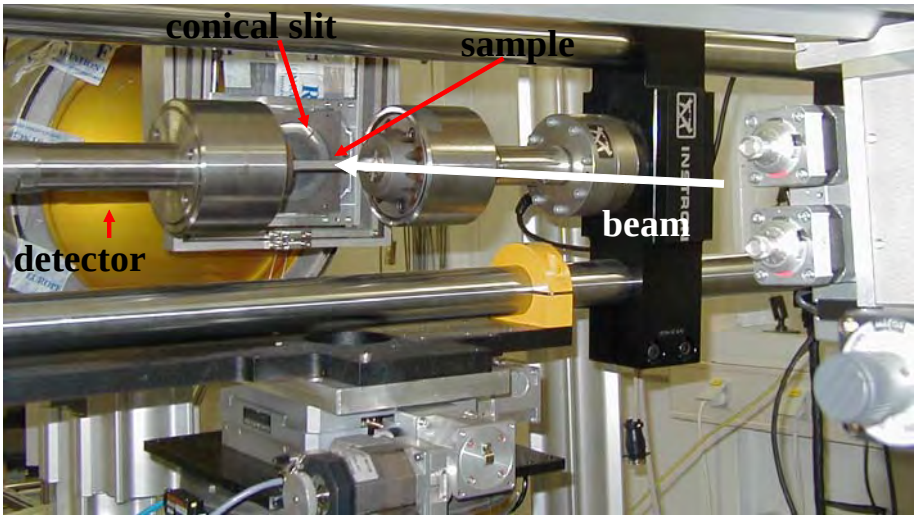

Fig. 10. Photo showing the sample mounted in the tensile rig (Note the x-direction points from left to right, i.e. the view is opposite that of Fig. 9).

Measurements were made in several positions along the tensile axis of the sample (all located well away from the grips) to monitor a large number of grains. The diffracting volume at each position contained several grains in parts which typically spanned over both grain boundary and grain interior. Straining typically took place in steps of 2 % elongation. After each step the sample (and tensile rig) was rotated in ω to record sponts from a sufficient number of crystallographic planes from each grain. The volumes investigated at the different strains were not exactly identical and also at each strain the volume changed due to rotation in ω of the sample to obtain diffraction from other planes.

Fig. 11 shows an example of the recorded diffraction spots and also illustrates how these move and broaden with strain as the grain rotates and develops an internal orientation spread. The spots were analysed by Dr. Margulies with the GRAINDEX program [71] which identifies the centre-of-mass of each spot and determines the grain orientation best matching the centre-of-mass positions of the spots. The rotation path of the grain is identified by comparing the orientations measured at the same position of the sample at the individual strain steps and identifying orientations which constitute a continuous and fairly smooth rotation path over several strain steps.

Multiple positions investigated within one very large grain yielded the same rotation behaviour [A12]. In the present data sets 10-12 the spread of the individual diffraction peaks is also often in the form of tails trailing behind the main spot along the rotation direction, indicating operation of the same slip systems but with different activities. These observations are furthermore in agreement with recent EBSD studies of rolled metals where orientation gradients in the direction of the expected lattice rotations were often seen [72] and X-ray studies of several positions within one grain, which rotated in the same direction but with different angles [73].

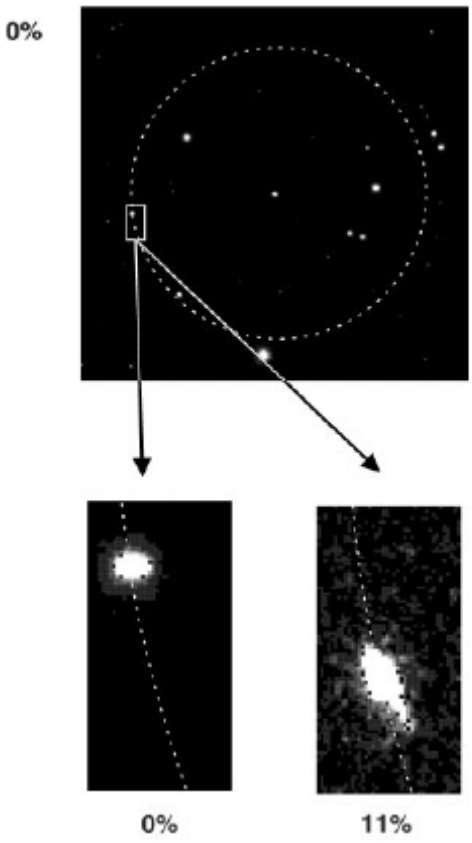

Fig. 11. Example of raw data for ω=1° and 0% strain (top). The circle marks the (220) Debye-Scherrer ring, and the box identifies a single spot related to grain 1. The enlarged areas (bottom) show the movement and broadening of this spot on the ring, by comparison with a corresponding image at ω=-5° and 11% strain. From [A11].

In summary, these studies indicate a fairly uniform deformation of a grain, resulting from activation of the same slip systems although possibly with different relative activities. It should, however, be noted that a few examples of grains that split in two distinct orientations were also observed in grains near symmetry lines in the stereographic triangle where two slip systems are equally stressed [A13].

For the present purpose the lattice rotation of a grain is taken as the change in the mean orientations (centre-of-mass) measured, i.e. the grain is considered a homogenous entity. Averaged over many grains the magnitude of this rotation is more than twice the magnitude of the developing internal orientation spread measured as the full-width-half-maximum value of the diffraction spots at 6% strain [A13], confirming that the grains may, to a first approximation, be considered a homogenous entity.

3 Introduction to dislocation structure alignment

This chapter presents a historic overview of significant advances in the characterisation and understanding of dislocation structure alignment, in particular the planes of GNBs.

3.1 Single crystal observations

The earliest studies of the plane of dislocation boundaries date back to the 1960's and were primarily conducted on copper single crystals oriented for single glide in tension [74-77]. In these crystals the dislocation boundaries align with the primary {111} slip plane. However, the boundaries do not exactly coincide with the slip plane but deviate a few degrees from it [74, 75, 78]. Also tensile deformed crystals oriented for conjugate or coplanar double slip have been observed to form boundaries aligned with the active slip planes [79]. In addition slip-plane-aligned boundaries have been observed in rolled crystals of copper [80-83], aluminium [84-88] and nickel [89].

However, it is now clear that not all boundaries in deformed single crystals align with slip planes [82, 87, 90, 91]. Furthermore, some crystals do not form extended planar boundaries but only randomly oriented cells, as after tension along the [100] direction [90].

3.2 Polycrystal observations

Inspired by the initial findings of boundaries aligned with slip planes in many single crystals, the trace of dislocation boundaries in polycrystal grains was in the 1980's compared with the trace of slip planes and also other crystallographic low index planes [42, 92]. However, no unique crystallographic boundary plane was found. Also more recent studies both from observation of a single sample section in torsion [93] and by combining traces observed for different grains in different sample sections in rolling [94] concluded that in general boundaries do not lie on {111} slip planes.

3.2.1 Macroscopic alignment

Around 1990 it was observed that the GNBs had a preferred orientation with respect to the sample co-ordinate system defined by the deformation axes: Boundaries tend to cluster around the macroscopically most stressed planes [92, 95]. This was first observed for rolling and most studies of rolled polycrystals throughout the 1990's analysed the boundary planes with respect to the macroscopic sample axes, see for example [96-98]. As shown in Fig. 12, the distribution of boundary trace angles to the sample axes is rather wide and the mean inclination of boundaries to the rolling direction in the plane spanned by the rolling direction and the rolling plane normal is often closer to 30° than the 45° of the macroscopically most stressed planes. This has been found for both fcc and bcc metals in cold and warm deformation [58, 94, 97, 99].

Studies of rolled samples were followed up by investigations of other deformation modes. In torsion results comparable to rolling were found [98], i.e. GNBs aligned with two approximately perpendicular planes, which are the most stressed sample planes. For tension and compression the number of macroscopically most stressed planes is infinite. All planes inclined 45° to the deformation axis are highly stressed. Analysis of the distribution of the three dimensional boundary plane around the deformation axis revealed good agreement between the experimental and calculated boundary trace distributions,

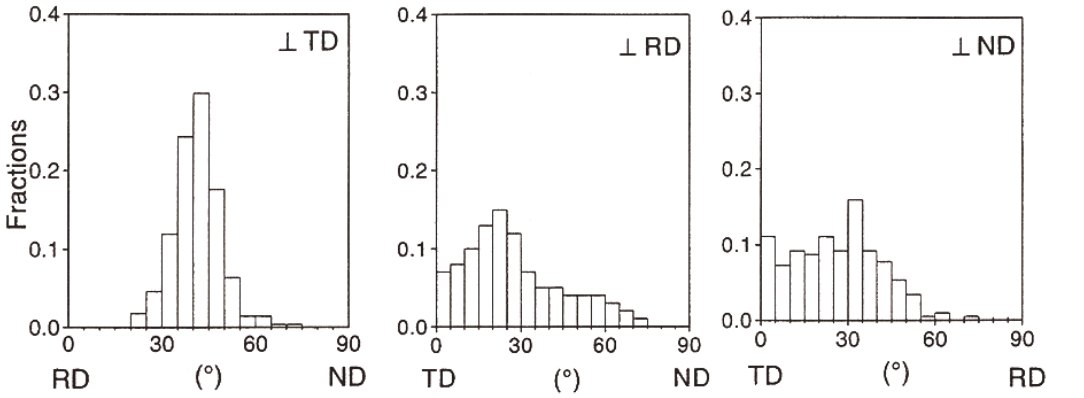

Fig. 12. Distribution of boundary traces in polycrystalline copper cold rolled to 11 % observed in the three sample planes perpendicular to the deformation axes (from ref. [100]).

assuming a mean inclination of boundaries to the tensile axis of approximately 45° and random distribution around the tensile axis [101]. The exact mean inclination angle is, however, sensitive to reversal of the deformation mode as demonstrated for tension vs. compression [101] and forward and reverse torsion [93].

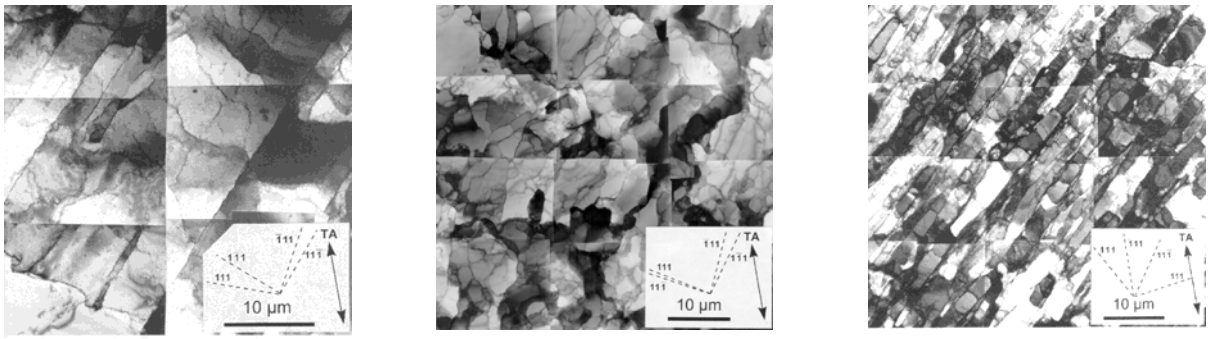

a b c

Fig. 13. a-c) TEM images of different dislocation structures in tensile deformed pure aluminium. Traces of the {111} slip planes are marked on the images. a) slip-plane-aligned GNBs, b) no planar GNBs but only cells, c) not-slip-plane-aligned GNBs and d) stereographic triangle presenting the grain orientation dependence of the three structure types. (a-c from [63], d from [A14] (data set 1)).

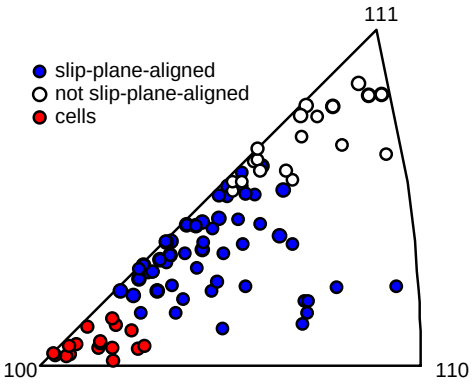

d

3.2.2 Grain orientation dependent crystallographic alignment

In the late 1990's, it was realized that the crystallographic plane of extended planar dislocation boundaries in individual grains in a polycrystal depends on the crystallographic orientation of the grain: Some grain orientations have boundaries lying close to {111} slip planes while boundaries in grains of other orientations lie far from slip planes. This was demonstrated for both rolling [22, 66] and tension [63, 65]. An example for tension is shown in Fig. 13, where it is seen that the grains with the tensile axis in the middle of the stereographic triangle have slip-plane-aligned GNBs, grains near [111] in the triangle have not-slip-plane-aligned GNBs, and grains near [100] do not have planar GNBs but only an equiaxed cell structure.

3.3 Macroscopic vs. grain orientation dependent alignment

At the time of writing this thesis, the existence of grain orientation dependent dislocation structure alignment in polycrystals is still disputed by some researchers. They consider the occurrence of slip-plane-aligned GNBs to be merely coincidental [94]. According to that view, the GNBs align with most stressed planes and deviations from alignment with the exact macroscopically most stressed planes of the sample are believed to be caused by deviations in the local strain due to grain interactions [94, 102]. This interpretation is in strong contradiction to the results and conclusions of this thesis, which ultimately traces the alignment of the GNBs with different but grain orientation dependent crystallographic planes to the activation of certain slip systems and furthermore correlates these with the observed lattice rotations during deformation. However, the grain orientation dependent crystallographic GNB planes undoubtedly tend to cluster around macroscopically most stressed planes. One reason for this is that many (but not all) GNBs align with either an active slip plane or an active slip direction.

In the author's opinion part of the origin of the continued discussion about the macroscopic vs. grain orientation dependent alignment of the GNBs is to be found in limitations of some of the microscopy techniques employed as well as problems with derivation of GNB planes from trace observations (to be addressed in general terms in the next chapter). Probably the apparently common misunderstanding that grain orientation dependent GNB planes mean that all GNBs align with a slip plane is also a factor. The latter misunderstanding may partly be traced to the historic sequence of the findings in this field outlined above as well as issues related to the terminology, which has also undergone development over the years.

3.3.1 Terminology

The papers included in the appendices of this thesis employ the following terminologies:

GNBs aligned with a slip plane have been referred to as crystallographic and the other GNBs as non-crystallographic [A4], implicitly suggesting that the non-crystallographic (=not-slip-plane-aligned) might not have a specific crystallographic relation. It was indeed for a while suspected that these GNBs aligned with macroscopically most stressed sample planes. This suggestion has, however, since been disproven [A3, A14]. Less misleading but still with a strong focus on the GNBs aligned with {111} slip planes, the terms slip-plane-aligned and not-slip-plane-aligned GNBs have been used [A5].

With the increasing characteristaion of the crystallographic planes of the not-slip-plane-aligned GNBs, the Miller indices of the crystallographic GNB plane were introduced to distinguish between different types of alignment [A6, A10]. The geometric deviation of these planes from the nearest {111} slip plane is, however, often reported in the form of an

axis around which the GNB plane is rotated away from the {111} slip plane and the corresponding rotation angle.

In the parts of the thesis where the focus is on the slip-plane-aligned GNBs (in particular Chapter 5) the terms slip-plane-aligned and not slip-plane-aligned GNBs are heavily used. Otherwise Miller indices are preferred, sometimes together with the deviation axis and angle from the nearest slip plane to relate the GNB plane to the slip systems.

4 Dislocation structure alignment – Grain orientation dependence

As described in the previous chapter, the discovery of the grain orientation dependence of the crystallographic GNB planes was first based on the observation that some grain orientations had GNBs which aligned closely with a {111} slip plane while the GNBs in grains of other orientations did not. In these initial studies, no further attempt was made to determine the precise GNB plane.

This chapter describes the boundary trace analysis conducted by the author to determine the crystallograpic plane of the GNBs not aligned with slip planes [A2, A3]. This analysis also discovered more details about the small deviations of the slip-plane-aligned GNBs from the exact {111} plane. These results have since been refined in studies employing tilting of the sample in the TEM conducted by Dr. Huang [A14].

4.1 Methods for determination of GNB planes from boundary traces

Geometrically, the trace of a planar boundary is the intersection line between the boundary plane and the plane of inspection. When only observing the trace in one inspection plane no information can be retrieved on the inclination between boundary plane and inspection plane as an infinite number of boundary planes with different inclinations share the same trace. Full determination of the boundary plane therefore requires trace observations from different inspection planes.

Such methods are well-known for rather large planar features, e.g. planar grain boundaries [103]. Typically, the inspection sections are perpendicular but this is not a requirement. Even two parallel planes may be employed so that the inclination of the boundary to the inspection planes is calculated from the small displacement of the traces between the two inspection planes and the distance between these.

For GNBs it is more common to exploit the fact that they are not isolated features but occur as a set of parallel planes. This means that one does not necessarily have to observe the same boundary in different inspection planes. This obviously simplifies the experimental procedure. It is, however, important that in case of multiple sets of intersecting parallel boundaries care is taken to combine the right boundary traces in the determination of the boundary planes. In such cases inspection of a third sample section may be used to verify the determination. The method has been widely used for single crystals which are typically large and homogenous enough to produce several good inspection planes [78, 80, 81, 84, 87, 88, 90].

Analogous inspection of GNBs in the same grain in a polycrystal in more than one section has been carried out by EBSD [94]. However, typically information from different grains observed in different inspection planes has been combined. For example, the realisation described in the previous chapter that GNBs in polycrystalline samples preferentially align with the most stressed sample planes came from observations in perpendicular sample sections. For rolling, this has been refined by combining the distributions of GNB traces observed in three perpendicular sample sections to derive the distribution of GNB planes in the rolling co-ordinate system [100]. Distributions of GNB planes have also been calculated from trace distributions from different sample planes focusing on grains within 20° [94] or 15° [102] of selected reference orientations. However, when analysing such distributions a number of general issues must be taken into account.

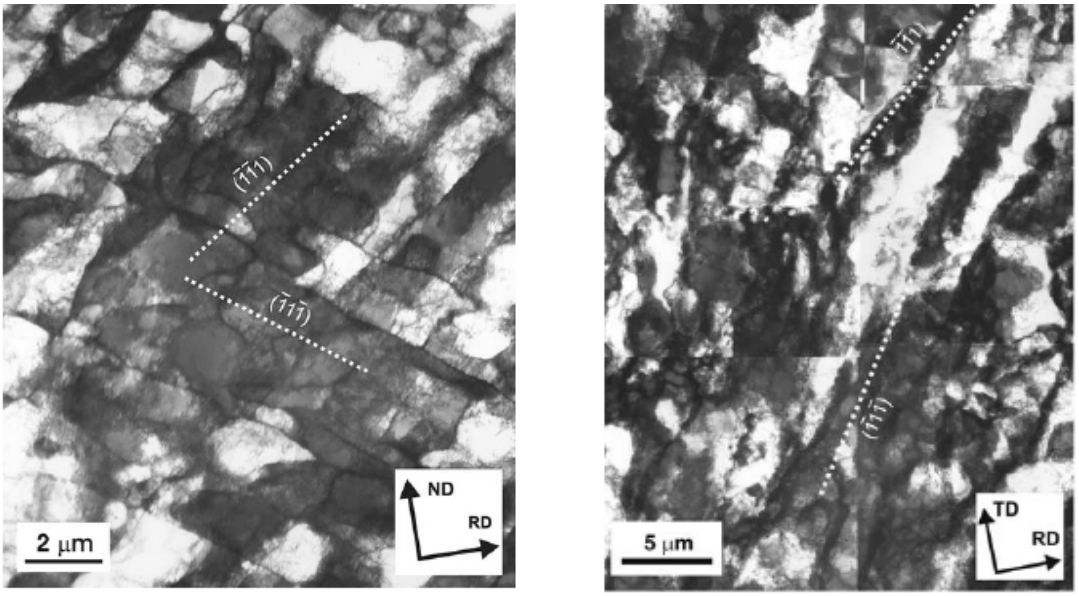

Fig. 14. TEM images of two grains of near Brass orientation in rolled aluminium with two sets of GNBs aligned with {111} planes. The GNBs are observed in two different sample sections, and it is seen that the image to the left from the rolling plane is much less clear than the image to the right, which is partly due to the fact that the two GNBs share the same trace and partly because they are only inclined 30° to the rolling plane. The traces in the plane spanned by the rolling plane normal and the rolling direction in the left image are different, the GNBs are inclined about 45° to the inspected sample plane and the foil has furthermore been tilted to give the best image. From [A2].

4.2 Issues to be considered in analysis of GNB traces and GNB planes

4.2.1 Selection of the inspection plane

Not all sample planes are well-suited for observation of GNB traces. In particular two issues affect the visibility of the GNB trace (apart from problems relating to the sampling of discrete points on a grid by EBSD, which may distort the trace direction in the EBSD map):

The GNB inclination to the inspection plane. GNBs which are not sufficiently inclined to the inspection plane can be practically invisible by TEM because the projected boundary becomes very wide and small irregularities may be emphasised. It is not as serious a problem for EBSD where the electrons penetrate much less into the metal. Still, GNBs close to being parallel to the inspection plane will have widely spaced traces and their detection consequently more difficult.

Interference between different sets of GNBs approximately sharing the same trace. This is a serious problem for both TEM and EBSD, which renders some sample sections useless because it results in a messy image/map in which one cannot distinguish any coherent traces over longer distances.

Assuming that the GNBs lie close to the macroscopically most stressed planes, it has been shown for rolling that only the sample plane spanned by the rolling and normal directions is suitable due to interference problems in combination with difficulties to detect GNBs

almost parallel to the inspection plane [A2]. This is illustrated in Fig. 14. For tension, the macroscopically most stressed planes are all planes inclined 45° to the tensile axis. Due to the rotational geometry around the tensile axis, the GNB inclination with respect to inspection planes parallel to the tensile axis will in general be steeper than 45° and some GNBs will be almost perpendicular to the inspection plane. Consequently, inspection planes parallel to the tensile axis should in general be preferred.

4.2.2 Co-ordinate system

Alignment of GNBs may be studied in any co-ordinate system but the systems defined by the deformation axes of the sample or the crystallographic axes of the unit cell are the two obvious choices. As outlined in Chapter 3, the GNBs align with a fairly narrow range of planes in the sample co-ordinate system while the alignment in the crystallographic co-ordinate system involves a much wider range of crystallographic planes. Analysis in the crystallographic lattice therefore gives the highest resolution, and therefore often the better chance to detect variations in the GNB plane depending on the grain orientation. The grain orientation dependence may, however, also be observed in the sample co-ordinate system. For example, it has been shown that grains in warm-rolled IF-steel with orientations on the α- and γ-fibres of the rolling texture have mean trace angles with respect to the rolling direction which are about 10° smaller than the trace angles found in grains of other orientations [58].

It is of course clear that as long as the crystallographic grain orientation is still associated with the determined GNB plane, one may easily convert between the two co-ordinate systems. Preserving the relation between the individual GNB and the crystallographic grain orientation is furthermore essential when analysing the grain orientation dependence of GNB planes, irrespective of the selected co-ordinate system.

4.2.3 Sample and crystal geometry

Symmetries of the crystal lattice and the deformation mode may be exploited to reduce the grain orientation space, which must be considered. The reduced orientation space may then serve as a reference subspace into which all the available data are folded.

Transformation of crystallographic grain orientations to the same variant of, for example, the 24 equivalent orientations in the case of cubic crystal symmetry is trivial. If the crystallographic GNB plane is determined before this transformation, the transformation must of course also be applied to this plane so that all the GNB planes refer to the same variant of the grain orientation.

When working with observations of individual grains, the symmetry of the deformation mode must be considered a little more carefully than when working at the bulk level. The orientation of each grain with respect to the sample axes has to be considered as if the grain were a single crystal. At the bulk level the orthorhombic symmetry of rolling, for example, eliminates the need to keep track of the sign of the rolling, transverse and normal directions. This sign cannot be ignored when determining the angle between a GNB trace and the sample direction. However, once the trace angle is determined with the correct sign both the grain orientation and the trace angle can be transformed to the same reference frame by inverting the sign of the sample directions and trace angle appropriately.

As described below, uniaxial deformation of the cubic crystal geometry is especially advantageous as the reference orientation space is small and the rotational symmetry around the deformation axis offers additional advantages.

4.2.4 Subdivision of grain orientation space

When analysing for grain orientation effects the orientation space is typically divided into subspaces, within which the grains exhibit GNBs aligned with the same planes. Particularly interesting grain orientations may be selected as references, e.g. the typical deformation texture components. It is, however, not certain that such reference orientations constitute the centre of a region of the orientation space with the same GNB alignment. Nor can anything be known in advance about the extension of such a region. The determination of regions of the orientation space within which the GNB alignment is the same therefore has to be data-driven so that definition of a region is a result of the analysis rather than a predefined input.

4.3 Grain orientation dependent GNB planes in tensile deformed polycrystals

To study tension, the author developed a geometric analysis taking advantage of uniaxial symmetry allowing use of data from only one sample section.

4.3.1 Terminology

The assumed uniaxial symmetry of tensile deformation substantially reduces the relevant grain orientation space to one of the 24 stereographic triangles in the full inverse pole figure. Throughout this thesis the triangle spanned by [100]-[111]-[110] is selected as the reference orientation space for uniaxial tension. This triangle is illustrated in Fig. 15 where also the terms critical, conjugate and cross slip systems are defined. Easy and difficult cross slip, respectively, refer to situations where the cross slip is assisted or inhibited by the externally applied tensile stress.

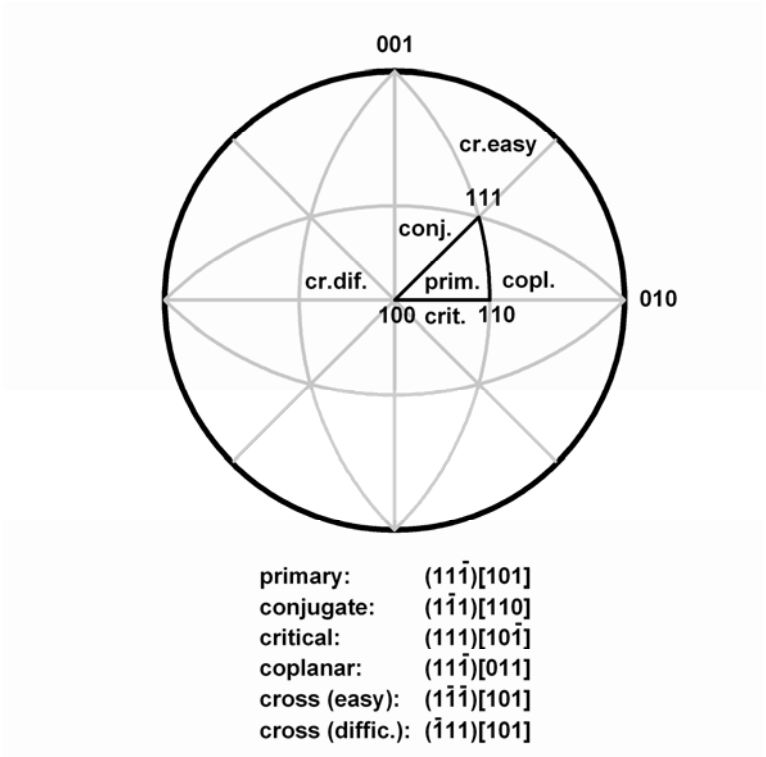

Fig. 15. Stereogram showing the triangle used to present the orientation of the tensile axis. The primary slip system in this triangle is listed as well as the terminology used to describe the dominant systems in some of the neighbouring triangles. From [A6].

4.3.2 Determination method

Due to the rotational symmetry grains with the tensile axis in the same crystallographic direction may be oriented differently with respect to an inspection plane parallel to the tensile axis. If the crystallographic GNB plane depends only on the crystallographic tensile axis, observations of such grains in the same sample section is therefore equivalent to inspecting grains in different sample sections.

The trace analysis leading to determination of the GNB plane involves calculation of all the crystallographic planes, which share the same trace on the observed sample section. A specific crystallographic plane is represented as a point in a pole figure, in which the intersection of the plane normal with a sphere spanned by the three <100> crystallographic axes is projected onto the plane spanned by two of the three <100> crystallographic axes (the third one being perpendicular to these). In this representation, the range of planes with the same trace constitutes an arc starting and ending on the circumference (see Fig. 16a). When having several grains with the same crystallographic tensile axis but oriented differently with respect to the observed sample section, these arcs intersect in the point representing the crystallographic GNB plane (Fig. 16b). This is of course only valid if the GNB plane in the considered grains is actually the same, i.e. the assumption that the tensile axis uniquely determines the GNB plane holds. In order to check this underlying assumption, more than two trace observations should be combined in this analysis. This is particularly important in the case of two intersecting sets of GNBs in the observed grains, in analogy with the need for a third section in single crystal studies described in section 4.1.

As described above in section 4.2.4 a result of the analysis must also be the region of grain orientations with GNBs aligned with the same crystallographic plane. A substantial number of experimental observations are obviously required to establish a range of grain orientations for which the arcs intersect in a common point.

For traces determined by TEM the additional information that the crystallographic GNB plane is sufficiently inclined to the inspected sample section to give a good image may be added. In practice this means that the extension of the arcs is limited so that they do not traverse the full pole figure. No definite inclination angle can be given (and also tilting of the foil in the TEM has an influence) meaning that this has to be done with caution. In practice, however, the determined intersection points to be described in the next section involved arc segments with inclination angles between about +45° and -45°.

Misalignment of the foils in the TEM causes systematic errors in the crystallographic grain orientation but the crystallographic analysis of the trace is not affected. Additional errors may arise – and did as demonstrated at the end of the chapter – from problems with the underlying assumption of only one type of GNB planes in a given grain orientation region.

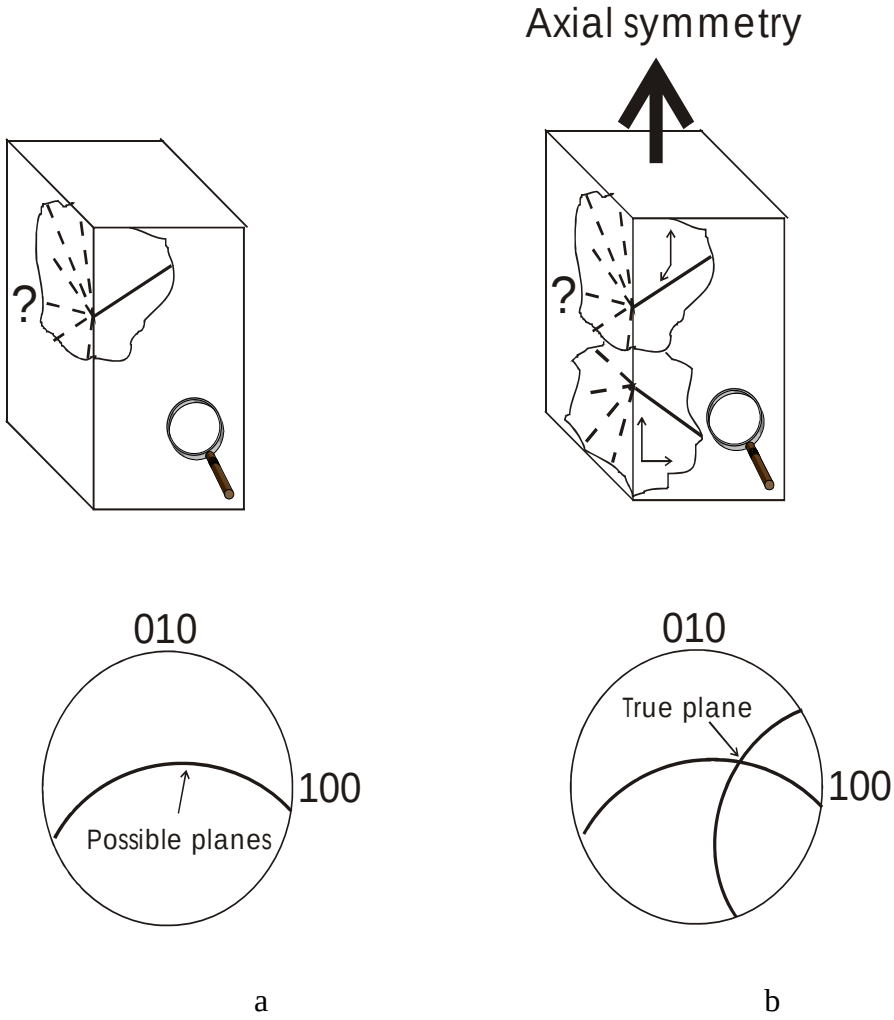

Fig. 16. Determination of crystallographic GNB planes in grains in a polycrystal with a) showing the arc representing all possible planes with the trace observed in one grain in one inspection plane and b) showing the boundary plane as the intersection between arcs from two grains with a similar orientation of the tensile axis but differently oriented with respect to the inspection plane. From [A3].

4.3.3 Determined grain orientation dependent crystallographic GNB planes

The experimental data analysed with the developed method came from data set 1. Dr. Huang kindly provided the trace angles of all the investigated GNBs in this data set. The arcs representing the range of possible crystallographic GNB planes for each trace were drawn as described in the previous section. Based on these the stereographic triangle was subdivided into four regions with different GNB planes as shown in Fig. 17. In addition, there is a region in the immediate vicinity of [100] with no GNBs but only cells. Note that the distinction between regions A and B, in particular, is ill-defined with a large overlap between the two regions. In some regions two sets of GNBs were observed, in which case not all of the arcs intersect in one point but each arc goes through at least one such intersection point. The arcs for each region and their intersection points are shown in Fig. 6 of [A3]. The identified crystallographic GNB planes for the regions labelled A-E in Fig. 17 were:

Region A: The GNBs align with the primary slip plane $(11\bar{1})$ but lie between this and a plane, which is rotated 10° away from the slip plane around the $[1\bar{2}\,\bar{1}]$ axis, which is perpendicular to the primary slip direction. Near the [100]-[111] line of the stereographic triangle some GNBs align with the conjugate slip plane $(1\bar{1}\,1)$ with a similar small deviation. A few GNBs aligned with the critical slip plane (111) are also found.

Region B: The GNBs align with the primary and conjugate slip planes and deviate from the ideal slip plane by rotation around the same axes as in region A. However, the rotation is in the opposite direction.

Region C: No clear intersection point was identified. It was concluded – also considering the inclination of the GNB planes to the inspected sample sections – that the most likely GNB planes deviate from the primary and cross slip planes by 10-35° rotation around axes which lie between the <112> axis perpendicular to the primary and cross slip directions, respectively, and another <112> axis, which is inclined 30° to this slip direction. The Miller indices of the planes rotated 35° away from the slip planes around these <112> axes are of the {315} type.

Region D: By analogy with region C it was concluded that the most likely GNB planes are rotated 10-35° away from the conjugate and cross slip planes around an axis which lies between two <112> variants.

Region E: No planar GNBs are found. The structure only consists of equiaxed cells.

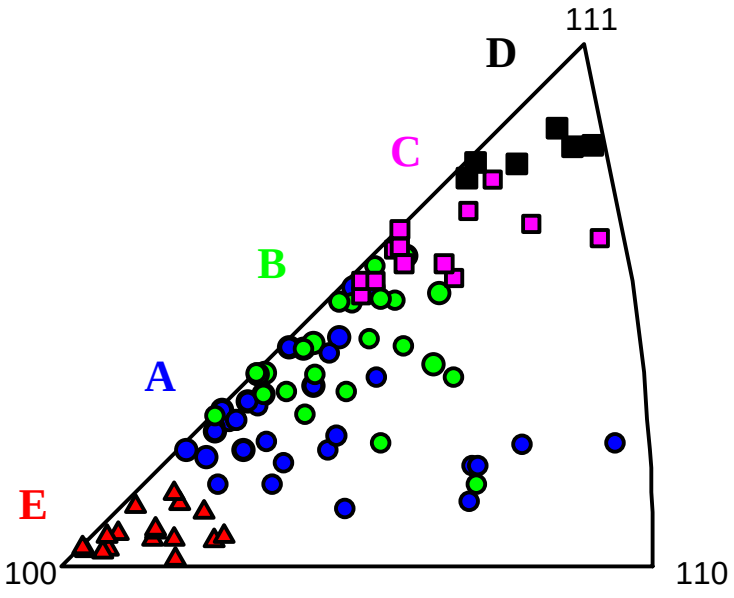

Fig. 17. The symbols mark the tensile axis of the investigated grains. The colours define regions A-E, which have different dislocation structure alignment as described in the text. From [A3].

While the analysis in [A3] determined some GNBs to align with the critical slip plane these were concluded not to be frequent. Such GNBs have been more clearly detected after hot-tensile-testing of aluminium [17]. However, reanalysis of the data in [A3] shows that a substantial number of the arcs may originate from GNBs aligned with the critical slip plane, which happen to be studied in grain orientations where the traces of the primary and critical slip planes approximately coincide and both are rather steeply inclined to the inspection plane, meaning that the analysis could not in reality differentiate between GNBs aligned with these two {111} planes.

4.4 Crystallographic vs. macroscopic alignment

The analysis in [A3] clearly demonstrated that all GNBs, i.e. also the GNBs which lie far from a slip plane, have specific crystallographic preferences and do not merely align with macroscopically most stressed planes. Even the small deviations from the slip plane for the slip-plane-aligned GNBs are systematic, involving rotation away from the slip plane around a specific axis, and the sign of the deviation angle depends on the grain oirentation. It has further been shown that these deviations do not always bring the GNB plane closer to the macroscopically most stressed plane [A19].

Nevertheless, the detemined GNB planes are also close to macroscopically most stressed planes, which for uniaxial tension are all planes inclined 45° to the tensile direction. Fig. 18 shows a histogram of the inclinination of the identified GNB planes to the tensile axis for regions A-D in Fig. 17. In all cases a broad peak around the 45° of the macroscopically most stressed planes is seen. Regions A and B exhibit the narrowest peaks with a width of about 30°. This width is to be compared with the spread in the crystallographic lattice where the GNBs lie within 10° of the {111} planes. A substantially larger spread of the GNB planes in the macroscopic co-ordinate system than in the crystallographic lattice has also been observed in a study of grains of near Brass orientation after rolling [A2, A14]. For the asymmetric S orientation in rolling it has furhter been shown that also the alignment of GNBs which lie far from any slip plane depend on the crystallography. The traces of the GNBs in the four symmetric variants of this orientation exhibit the same alignment with respect to the highly stressed slip planes while the macroscopic alignment changes signs depending on the variant [104]. These result demonstrate that the crystallographic alignment is stronger than the macroscopic.

The stronger crystallographic alignment is also revealed when the arcs are drawn in the pole figures. In these figures the macroscopically most stressed planes form a circle around the tensile axis as exemplified in Fig. 19, which also includes arcs drawn based on traces observed in grains lying in the middle of the triangle in hot-tensile-deformed aluminium (350° C , 15 % elongation, $\dot{\varepsilon} = 0.1$) (not included in the table in Chapter 2, see [17] for details). The arcs drawn in Fig. 6 of [A3] and Fig. 19 in this chapter do not intersect such a circle in a random manner. Instead the the arcs intersect each other in certain points near the circle, showing that the GNB planes are close to macroscopically most stressed sample planes but any such sample plane cannot be a GNB plane.

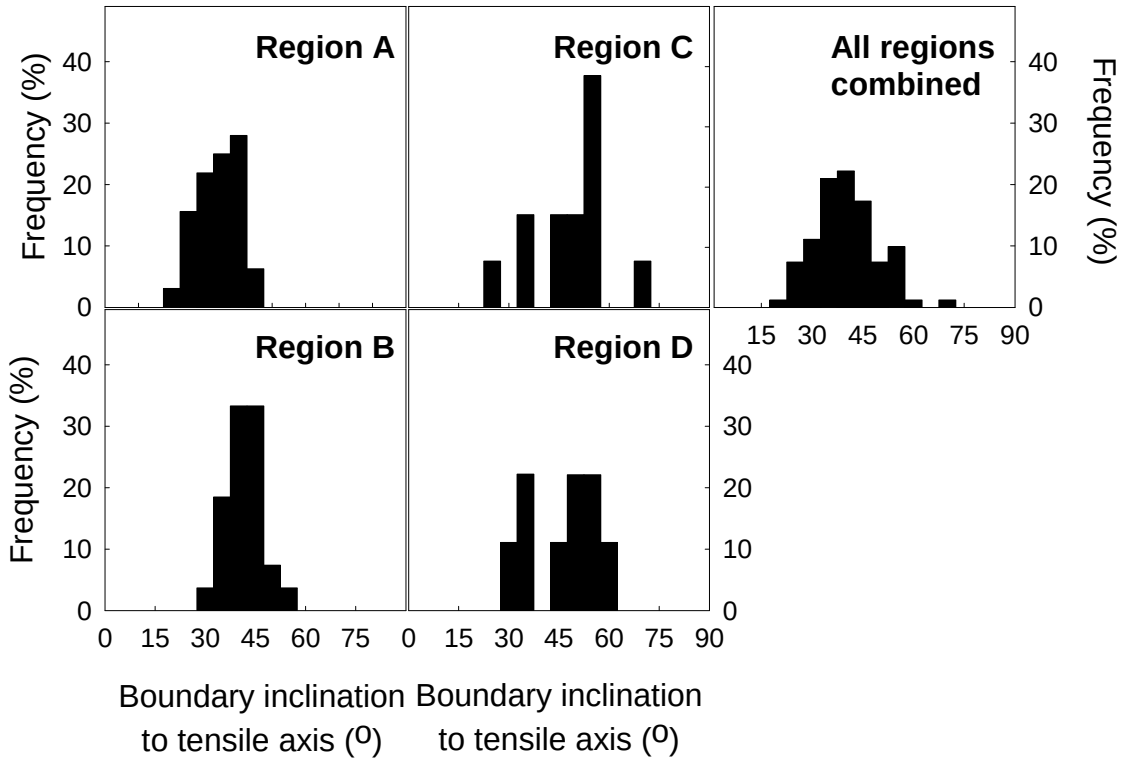

Fig. 18. Distributions of the inclination of the GNB plane to the tensile axis for grains in regions A-D in Fig. 17. From [A3].

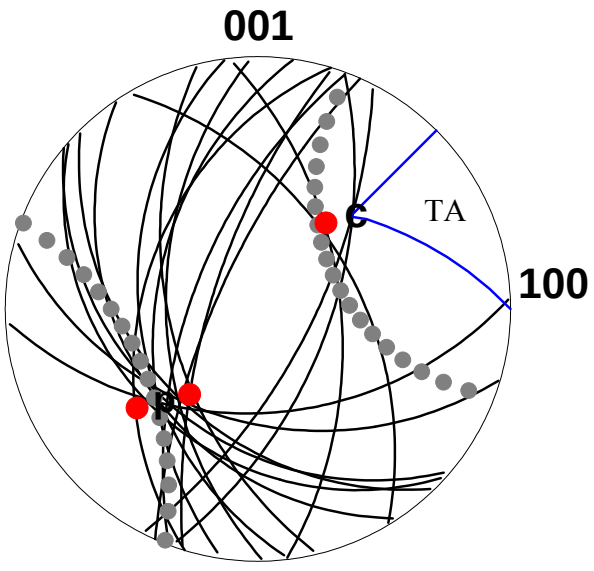

Fig. 19. GNB plane determination for aluminium tensile deformed at 350° C. The arcs represent all possible GNB planes with the observed traces for grains with the tensile axis (TA) approximately in the middle of the indicated triangle (blue line). The letters p and c mark the primary and critical slip planes and the red dots designate planes rotated 10° from these around <112> axes. The grey dots mark the approximate location of the macroscopically most stressed planes inclined 45° to the tensile axis. From [A17].

4.5 Subsequent TEM studies of tensile deformation

Subsequent studies using tilting in the TEM performed by Dr. Huang determined the GNB planes after tensile deformation with more precision [A14, 67]. The tilting confirmed the findings above for regions A and B. The existence of regions C and D near [111] with different GNB alignment was also confirmed, however, the identity of the GNB planes was not accurately determined in [A3]. In region C the precise determination showed that the GNBs align with the $(35\bar{1})$ plane, which is within the range determined in [A3]. However, GNBs related to the cross slip plane were not found. Instead some GNBs were found to align with $(35\bar{1})$, which is related to the conjugate slip plane by a similar rotation around a <112> axis and within the range originally determined for region D.

The GNB planes in region D were found by tilting to align with {115} planes of different variants, in conflict with the assumption of unique GNB planes within a grain orientation region. The existence of GNBs aligned with {115} variants was not suspected in the analysis in [A3]. However, the occurrence of {115} planes is in retrospect in good agreement with preliminary results of arcs drawn from trace observations in tensile deformed copper (data set 4) in region D, which were, however, abandoned because no clear intersection points were determined and the preliminary results seemed to be in conflict with the aluminium data.

Combination of all the presently available data on the grain orientation dependence of GNB planes after tension (data sets 1-6) yields the subdivision of the triangle shown in Fig. 20 [10]. This figure shows the occurrence of slip-plane-aligned and not-slip-plane-aligned GNBs as well as the occurrence of only cells. The regions with slip-plane-aligned and not-slip-plane-aligned GNBs are the same for all the data sets, with a slight overlap between the two regions. However, the extension of the region with cells depends slightly on the metal type, being larger for copper than aluminium [A14, 67]. The region shown in Fig. 20 is determined for AA1050 [A14, 67]. On top of this subdivision of the triangle the occurrence of specific crystallographic GNB planes is illustrated. The question mark indicates an area of the triangle which has not been investigated in detail but it is clear that the GNBs lie far from a {111} slip plane.

4.6 Grain orientation dependent GNB planes in rolled polycrystals

Using the tilting method to establish whether a GNB is aligned with a slip plane or not, the grain orientation dependence was determined for rolled polycrystals in studies conducted by Prof. Q. Liu [22, 66] and Dr. X. Huang [A14, 43] giving rise to data sets 7-9. Note that the classification of the GNB alignment used in data set 7 differs from data sets 8 and 9 by only considering GNBs aligned with slip planes and GNBs not-aligned with slip planes while the coexistence of these two was not addressed. The results are presented in Fig. 21a-c in the form of three-dimensional ODFs. All three ODFs exhibit the same features, which become even clearer in the combined ODF in Fig. 21d: grains on the α-fibre of the typical rolling texture, extending from Goss to Brass have slip-plane-aligned GNBs while grains on the β-fibre extending from Brass via S to Cu typically have one set of slip-plane-aligned GNB together with one set of not-slip-plane-aligned GNBs. The occurrence of slip-plane-aligned GNBs also spans from the α-fibre to the 45° ND rotated Cube orientation marked as RC in the figure. Grains near the Cube orientation have not-slip-plane-aligned GNBs. Within 15° of the ideal Cube orientation equiaxed structures are found in copper polycrystals. Single crystals of aluminium with the ideal Cube orientation

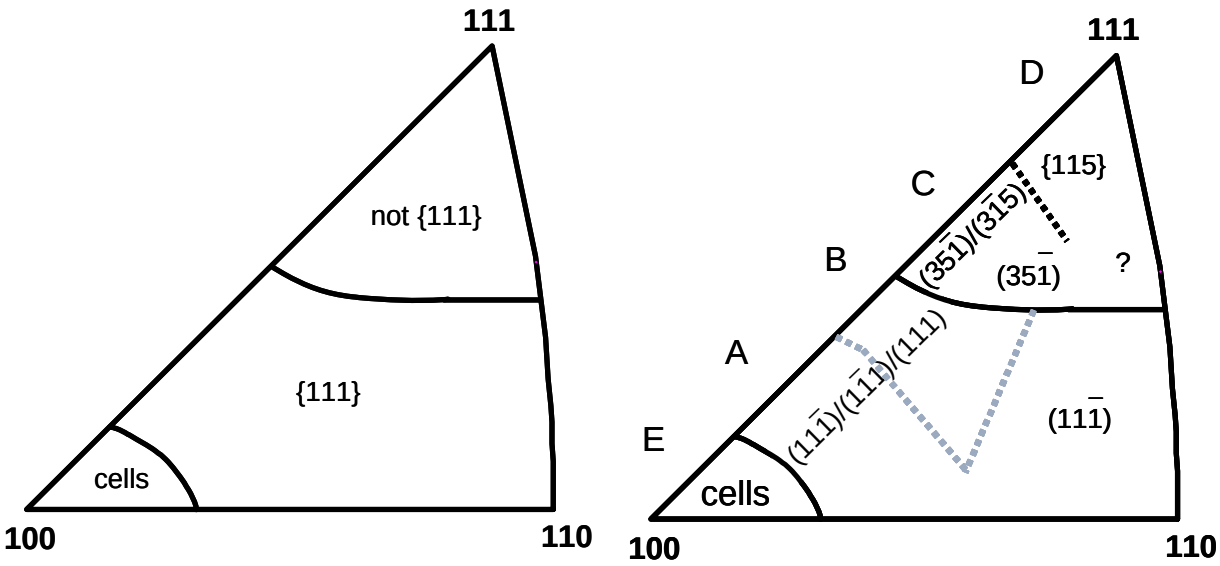

a b

Fig. 20. The grain orientation dependence of dislocation structure alignment in tensile deformation. a) classification into only cells and GNBs aligned or not-aligned with {111} planes and b) addition of the more detailed crystallographic GNB planes obtained by careful tilting in the TEM (from [10]). The letters A-E labeling the regions are repeated from Fig. 17. The grey line marks the approximate location of the changing sign of the small deviation from the {111} plane between regions A and B in Fig. 17.

have also been seen to have only cells but this structure has not been observed in grains of near Cube orientation.

More specific investigations of individual orientations have also been conducted as listed in Table 2 [A14]. According to this table two sets of intersecting GNBs are found in all orientations. It should, however, be emphasized that these are not always equally developped, and in fact sometimes only one of the sets are observed.

Table 2. Crystallographic GNB planes determined for specific orientations in rolled polycrystals (from [A14]).

Grain orientation	GNB planes
Goss $(011)[100]$	(111); $(\bar{1}11)$
Brass $(011)[2\bar{1}1]$	(111); $(\bar{1}11)$
S $(123)[63\bar{4}]$	(111); (113)
Copper $(112)[11\bar{1}]$	(111); (001)
Cube $(001)[100]$	*only cells near ideal*; *otherwise* (101) / $(10\bar{1})$

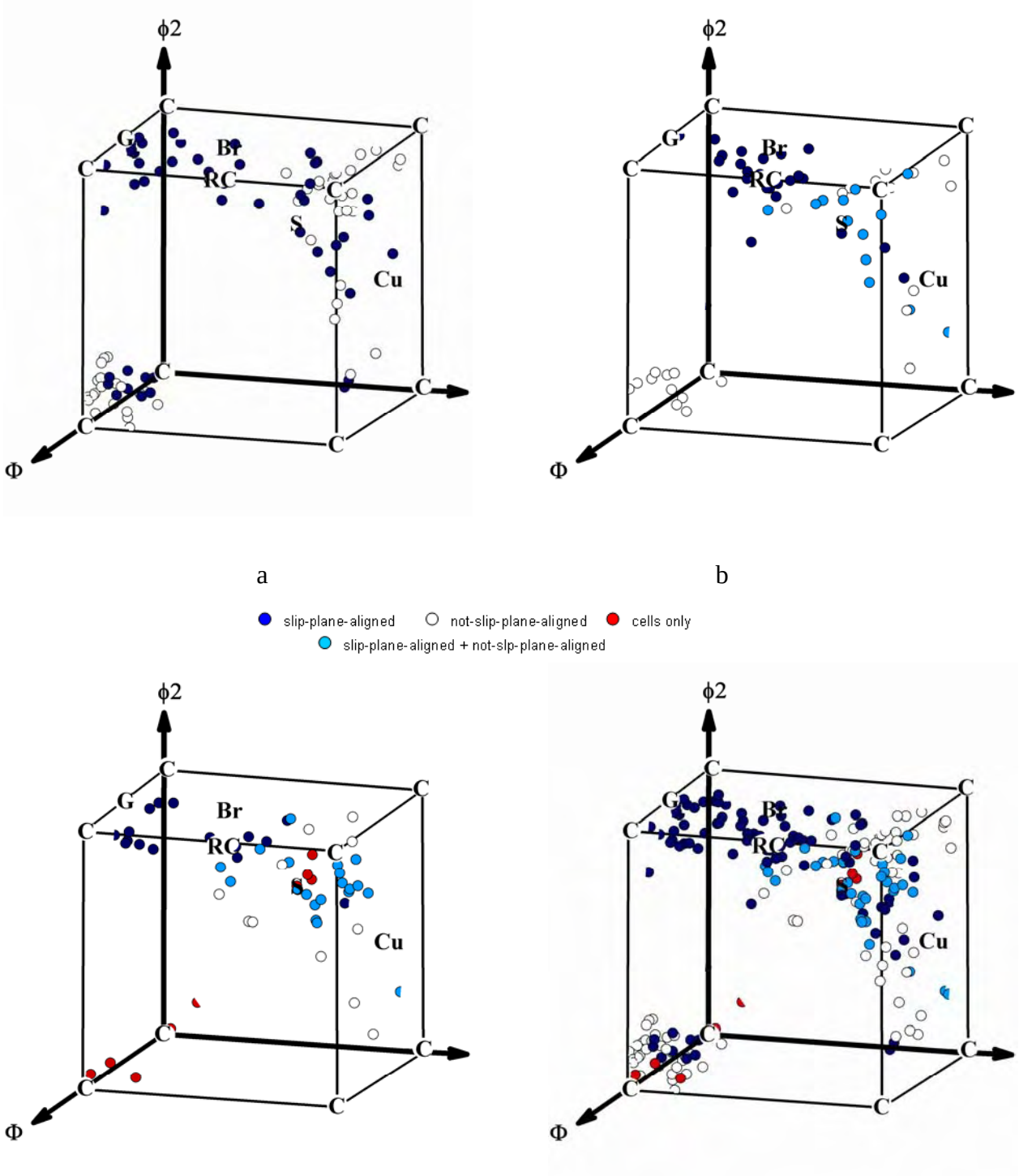

Fig. 21. Three-dimensional ODFs showing the grain orientation dependence of the occurrence of slip-plane-aligned and not-slip-plane-aligned GNBs and cells in all the rolled polycrystals included in the table of Chapter 2. The figures are: a) data set 7: aluminium (99.99 %), 300 μm, b) data set 8: aluminium (99.5 %), 75 μm, c) data set 9: copper (99.99 %), 90 μm, and d) all the data from a-c.

4.7 Conclusions

Combining all the studies, a coherent and reproducible picture of grain orientation dependent dislocation structure alignment in polycrystals is well established for fcc metals of medium to high stacking fault energy subjected to low and moderate strains in different deformation modes. The grain orientation dependence is assumed to originate from an underlying dependence on the active slip systems. The following two chapters investigate and prove this hypothesis. As also described here the studies establishing the grain orientation dependence of the dislocation structure alignment have been conducted in several steps over a number of years. The parallel analysis and modelling of the slip system dependence have consequently also evolved from focusing on specific features and deformation modes as described in Chapter 5 to a more general state described in Chapter 6.

5 Dislocation structure alignment – Slip system dependence

Analysis of the grain orientation dependence of crystallographic GNB planes in terms of slip systems aims at formulation of models for prediction of these planes - assuming that the slip systems can be predicted by the Taylor model. A model capable of such GNB predictions is the missing component of the proposed modelling scheme for the coupled evolution of texture and dislocation structures with further prediction of the resulting mechanical properties outlined in Chapter 1.

This chapter presents the studies relating slip systems and GNB planes conducted in the period 1997 to 2003. These relate to specific types of GNBs or deformation modes. Based on the initialassumption that the GNBs are LEDS, i.e. on the dislocation content of the GNBs, the author formulated a model capable of predicting the grain orientations in which slip-plane-aligned GNBs evolve during rolling [A4]. While the GNBs may be LEDS it soon became clear that the problem was too complex to continue this approach and identification of relations between slip systems and GNB planes without considering the specific dislocation content or the LEDS principle became the focus of the studies. This allowed extension of the model developed for rolling to slip-plane-aligned GNBs in tension [A5]. Finally the increasingly better characterisation of also the GNB planes not aligned with any slip plane revealed that the slip systems calculated with the Taylor model could not adequately explain the grain orientation dependence of the GNB plane [A3].

5.1 Slip-plane-aligned GNBs in rolling

According to the LEDS principle dislocations assemble in boundaries in order to screen each other's stress fields, thereby creating boundaries free of long-range stresses. Frank [105] established an equation, which must be fulfilled for such boundaries, relating dislocation content, boundary plane and boundary misorientation:

$$V \times a = \sum_i b_i \left(\frac{1}{2D_i \sin(\theta/2)} (n \times \xi_i) \cdot V \right). \qquad \text{Eq. 1}$$

In this equation V is any vector in the boundary plane with normal n. b_i, D_i and ξ_i are the Burgers vector, spacing of and dislocation line unit vector of dislocation set i, and a and θ are the normalised misorientation axis and the misorientation angle.

According to this equation a boundary aligned with a {111} slip plane cannot be constructed from one set of dislocations. However, twist boundaries consisting of two sets of dislocations with Burgers vectors and dislocation lines in the slip plane, in this case equal to the GNB plane, fulfil this equation. In rolled aluminium polycrystals it has furthermore been established experimentally that the slip-plane-aligned GNBs have a much stronger twist character than those not aligned with slip planes [22].

Based on these considerations, it was expected that grains with slip-plane-aligned GNBs occur when two slip systems producing such dislocations are highly active. In order to define a threshold for the coplanar slip activity which separates grain orientations with slip-plane-aligned and not-slip-plane-aligned GNBs, the fraction of the total slip in the grain which comes from such systems was calculated based on the slip systems predicted by the Taylor model. In this calculation the problem of ambiguous solutions giving the same Taylor factor and strain but having different slip systems was handled by taking the

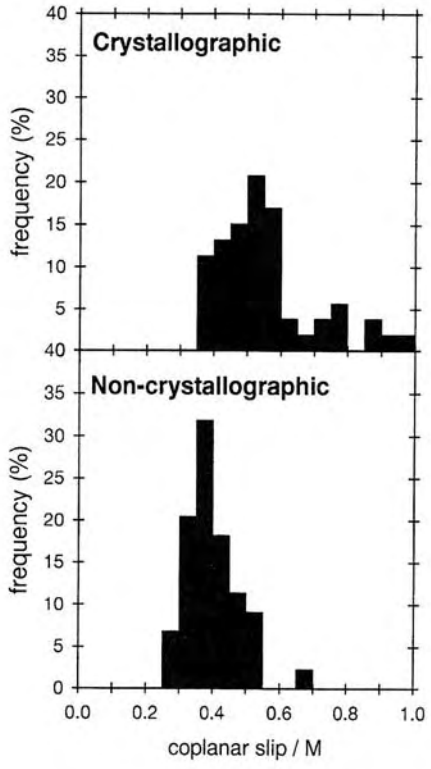

Fig. 22. Histogram showing the distribution of the coplanar slip fraction in grains experimentally observed to have slip-plane-aligned and not-slip-plane-aligned GNBs in rolled aluminium (here termed crystallographic and non-crystallographic, respectively). The coplanar slip fractions are calculated from the slip systems predicted by the FC Taylor model and by ignoring contributions from cross slip systems. From [A4].

average solution with six or eight active systems. This was done for grain orientations in which the GNBs had been experimentally observed to align or not-align with slip planes, respectively. The distributions of coplanar slip fractions in the grains observed to have either slip-plane-aligned or not-slip-plane-aligned GNBs were compared as shown in Fig. 22.

There is some overlap between the two coplanar slip fraction distributions in Fig. 22. Nevertheless, about 75 % of the grains with slip-plane-aligned GNBs have coplanar slip fractions above 45 % while a similar percentage of the grains with not-slip-plane-aligned GNBs had coplanar slip fractions below 45 %. The threshold value was therefore defined to be 45 %.

The general validity of the coplanar slip criterion and the determined threshold value is illustrated in Fig. 23. The predicted occurrence of slip-plane-aligned GNBs calculated from the slip systems predicted by the Taylor model and using the criterion of 45 % coplanar slip is illustrated by the grey shading in the ODFs. The experimental observations from data sets 7-9 are superimposed on the prediction. At the time this model was proposed only data set 7 was available but the prediction is seen to match data sets 7 and 8 equally well.

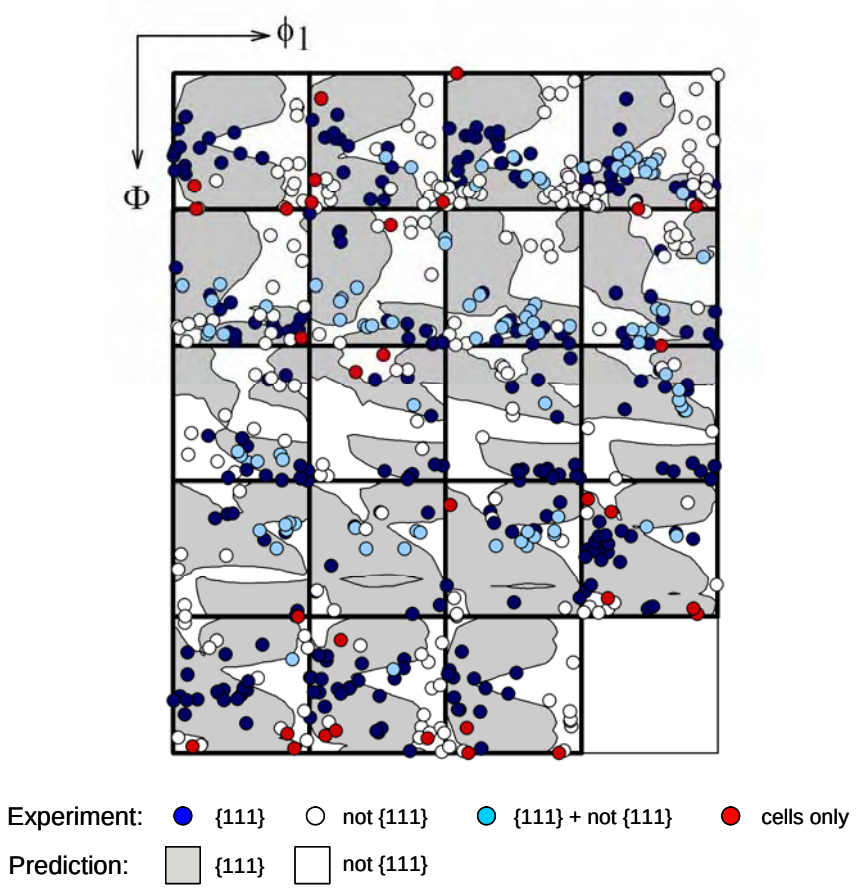

Fig. 23. ODF showing the predicted dislocation structure alignment based on the fraction of coplanar slip. The experimental GNB planes in grain orientations from data sets 7-9 are included as coloured symbols. Cells are only observed in copper (data set 9).

Please remember that data sets 8 and 9 introduced classification also of grain orientations, in which both slip-plane-aligned and not-slip-plane-aligned GNBs were observed. Interestingly these were primarily found in the vicinity of predicted transitions between slip-plane-aligned and not-slip-plane-aligned GNBs, i.e. the border between white and grey areas. The model was not designed for prediction of cells vs. not-slip-plane-aligned GNBs but the cells occurring near the Cube orientation in copper (data set 9) also lie at the border between white and grey areas.

5.2 Slip-plane-aligned GNBs in tension

The applicability of the model for prediction of slip-plane-aligned GNBs was subsequently investigated for tension. Apart from being a survey of the general validity of the model for other deformation modes, this is a critical test of the underlying assumption that the slip systems control the GNB planes: the slip system characteristics identified as inducing slip-plane-aligned GNBs in rolling must also induce similar GNBs in other deformation modes.

The prediction for tension in Fig. 24a is made with the same criteria as for rolling above. This is to be compared with the experimental subdivision of the triangle in Fig. 24d. It is immediately seen that this prediction is rather poor.

Comparison with single crystal studies reveals the origin of the failure of the prediction: single crystals oriented for single glide exhibit slip-plane-aligned GNBs, i.e. two coplanar slip systems are not required. As described above a slip-plane-aligned GNB which is free of long-range stresses cannot be constructed from one set of dislocations. To fulfil the LEDS criterion, additional dislocations from other slip systems are needed. As the slip activity of the additional systems may be so low that it is not predicted by crystal plasticity models (as would obviously be the case for the single crystals oriented for single slip) further analysis of the dislocation content and potential LEDS character of the GNBs is not pursued further in this thesis.

Modification of the model to include both single and coplanar slip leads to the concept of slip concentration. A grain orientation is defined to have concentrated slip when the fraction of slip (on one or two systems) on a slip plane exceeds 45 %. The prediction based on this criterion of concentrated slip is illustrated in Fig. 24b. The prediction has improved significantly so that slip-plane-aligned GNBs are now predicted in almost the entire region where they are experimentally observed. Further improvement is obtained from selecting a particular solution to the Taylor ambiguity problem, namely the one with most slip concentrated on one system instead of the average of all the solutions. The result of this is shown in Fig. 24c.

It should be noted that the change in modelling criterion from coplanar slip to the slip concentration does not noticeably alter the predictions for rolling. Selecting the solution with most slip on a single system instead of the average solution does not alter the qualitative features of the prediction but the quantitative agreement with experiment becomes somewhat poorer.

In conclusion, the occurrence of slip-plane-aligned GNBs is in general well predicted by the model developed based on the slip concentration. A limitation of the model is obviously its focus on only slip-plane-aligned GNBs. With the realisation that all GNBs align with specific crystallographic planes depending on the grain orientation, the analysis and modelling efforts were naturally extended to cover the dislocation structure alignment in the entire grain orientation space of tension.

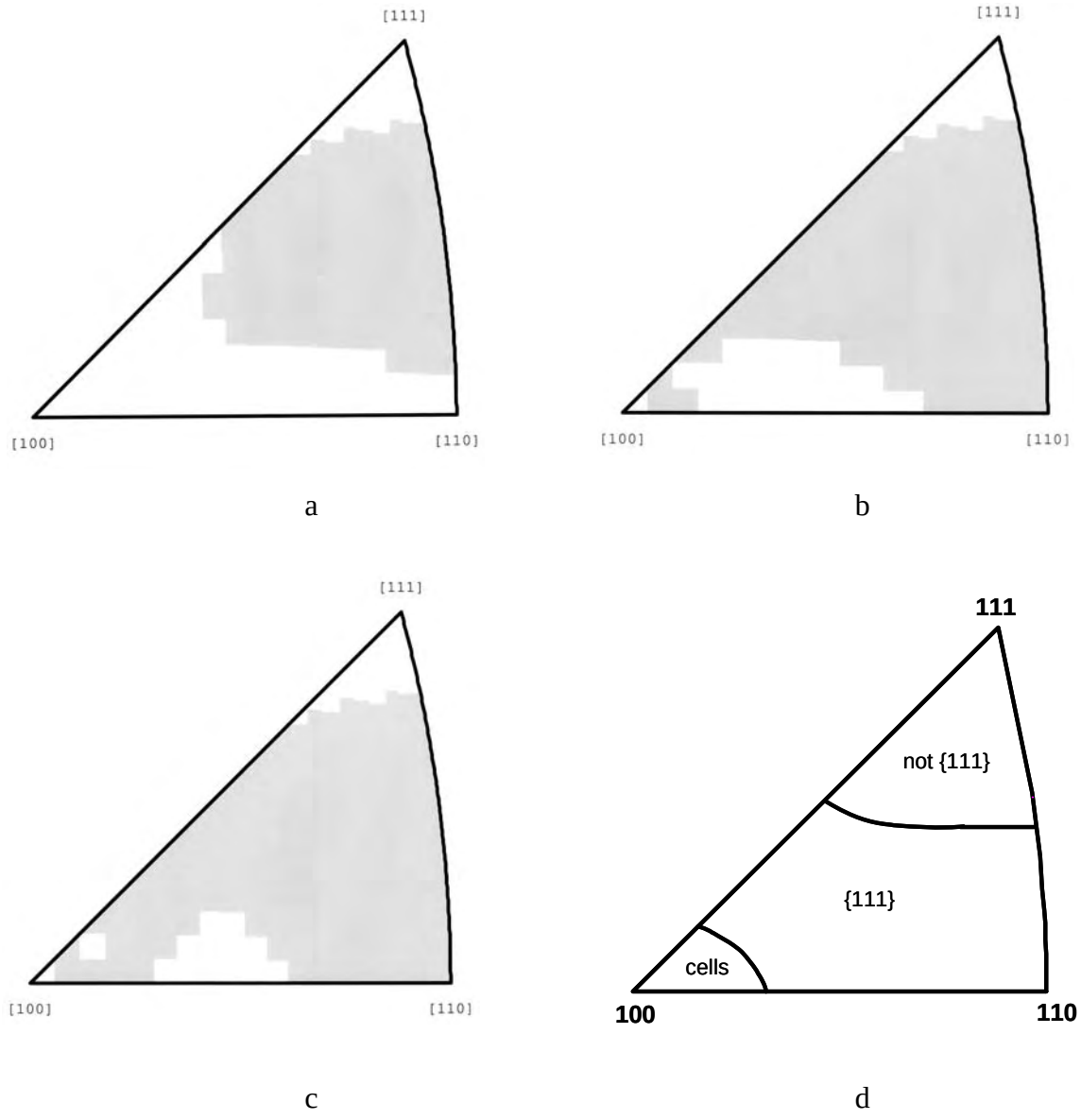

Fig. 24. Stereographic triangles showing predictions of the occurrence of slip-plane-aligned GNBs (in grey areas) using modelling criteria involving the a) coplanar slip fraction based on the average solution to the Taylor ambiguity, b) coplanar slip fraction based on the ambiguity solution with maximum slip on one system [A5]), c) concentrated slip fraction based on the ambiguity solution with maximum slip on one system, and d) experimental data (from Chapter 4). Please note that the a, b and c differ slightly from those in [A5] due to use of another grid in orientation space and less smoothing.

5.3 All GNBs and cells in tension

While the concept of slip concentration worked well for prediction of slip-plane-aligned GNBs, more details of the slip systems had to be considered to account for the occurrence of several types of crystallographic GNB planes and their grain orientation dependence.

The basic assumption that the grain orientation dependence of GNB planes reflects the grain orientation dependence of the slip systems suggests a comparison of the regions with different GNB planes or cells with the prediction of regions with different slip systems. Such a comparison is conducted in Fig. 25 for the systems predicted by the Taylor model. It is seen that the number of dislocation structure regions is larger than the number of slip system regions. While the slip system variation predicted by the Taylor model may explain the transition between regions B and C and also the occurrence of cells only near [100], it does not explain the transitions A/B and C/D. Furthermore, dislocation structure regions A and E both extend over two regions with different slip systems. The Taylor model therefore does not seem to predict the slip systems adequately for tension.

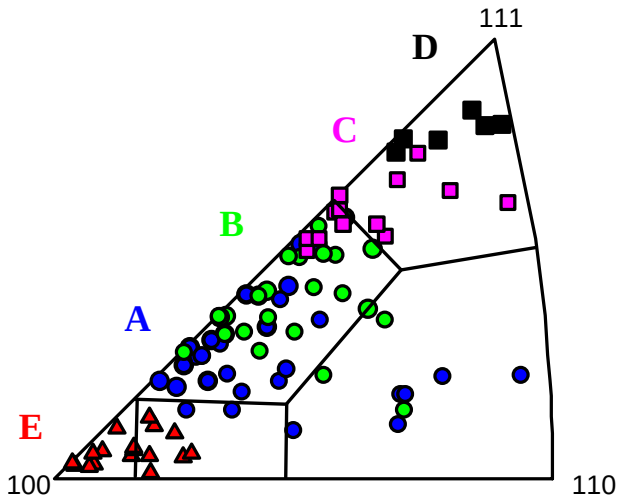

Fig. 25. Comparison of regions of the stereographic triangle with different GNB planes with regions with different slip systems as predicted by the Taylor model. From [A3].

Substituting the subdivision according to the Taylor model with the subdivision according to Schmid factors gives better agreement. Fig. 26 shows the triangle subdivided into regions within which the same four, five and six slip systems, respectively, have the highest Schmid factors. The subdivision best matching the regions with different GNB planes is the one with five slip systems as seen in Fig. 27, although the sixth system must be invoked to separate out the region containing only cells near <100>[1]. By analogy with the comparison for the Taylor prediction, dislocation structure region A extends over two regions with significantly different slip systems but otherwise all the regions are separated.

[1] Note that [A3] does not mention the need for the sixth slip system. This error was subsequently corrected in [A17].

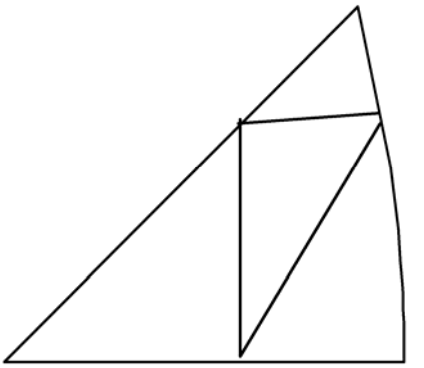

a

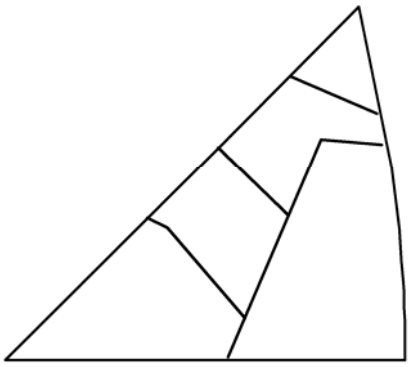

b

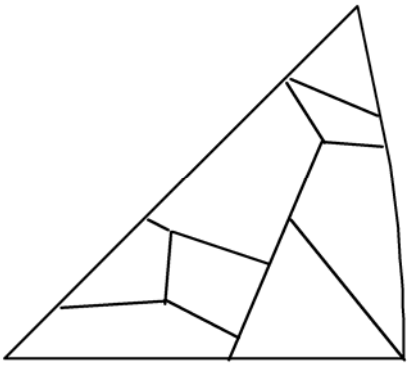

c

Fig. 26. Subdivision of the stereographic triangle into regions within which the same slip systems have the highest Schmid factors. The number of slip systems considered is a) four, b) five and c) six. From [A18].

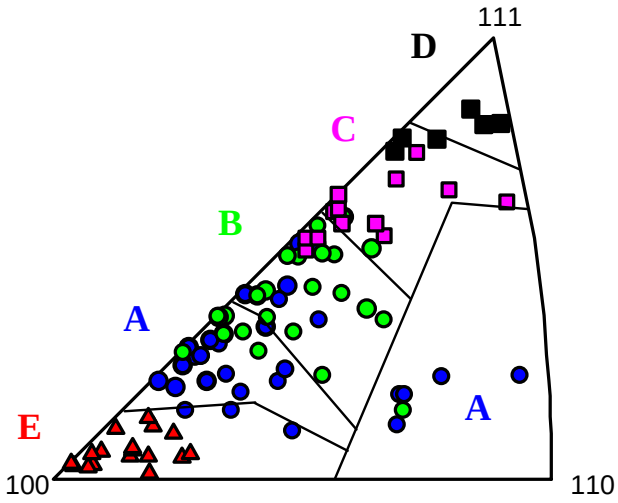

Fig. 27. Comparison of regions of the stereographic triangle with different GNB planes with regions within which the same five slip systems have the highest Schmid factors. The sixth highest Schmid factor is also considered to separate the two regions closest to [100]. From [A3].

5.4 Conclusions

This chapter demonstrated that the slip systems control the crystallographic dislocation structure alignment and that the grain orientation dependence of the alignment is due to the grain orientation dependence of the slip systems. Predictive modelling was obtained for the slip-plane-aligned GNBs by means of slip fractions. Good agreement was obtained when assuming that the active slip systems are those calculated with the Taylor model. For the prediction of more details of the dislocation structure alignment, including also the grain orientation dependence of the GNBs not aligned with a slip plane, the Taylor model, however, proved inferior to a Schmid factor analysis.

Clearly, a model capable of predicting the crystallographic GNB plane, whether slip-plane-aligned or not, is desired, and this model further should be applicable to all deformation modes. The next chapter derives such a model by considering ideal cases where the slip systems are unambiguously identifiable to focus on the relations between slip systems and dislocation structure alignment rather than the problem of slip system prediction. The analysis is furthermore generalised to consider slip classes rather than individual slip systems.

6 Dislocation structure alignment – Slip class dependence

This chapter describes the studies carried out since 2003 to derive a model relating slip systems and dislocation structure alignment, which is not limited to GNBs aligned with a specific plane (e.g. a {111} slip plane). In addition the concept of *slip classes* [A6] is introduced to detach the model from a particular grain orientation and deformation mode. A slip class describes the geometric relationship between a set of slip systems which leads to a particular crystallographic dislocation structure alignment. If the same slip class is activated in both tension and rolling (which is not always possible), similar dislocation structure alignment should be found. The establishment of such similarities will prove that the slip systems are more important for the alignment than the macroscopic deformation mode.

The analysis leading to identification of the fundamental slip classes and their resulting dislocation structure alignment is described in detail in [A6]. In the following the experimental basis for the analysis and the main results are summarised, focusing on demonstration of the slip class concept and outlining how it will be employed in the subsequent chapters.

6.1 Experimental basis for the analysis to identify slip classes

In order to avoid uncertainties associated with the identity of the active slip systems care is taken to base the analysis on experimental data for which the Taylor model and the Schmid factors both predict the same systems and furthermore roughly equal activity on these. In the analysis the observations from data sets 1-9 of the dislocation structure alignment in individual grains of a polycrystal are supplemented by single crystal data from the literature. The orientations investigated for rolling and tension are listed in Table 3 and Table 4, respectively. Also in the tables the active slip systems and the observed dislocation structure alignment are listed. In [A6] this experimental basis is analysed in the order of increasing complexity, going from single slip over double slip to multislip cases. In this process the slip system configurations investigated are decomposed into more fundamental slip classes, each of which is associated with a specific crystallographic GNB plane (except for one class, which only gives rise to cells). The slip classes are listed in Table 2 of [A6] and summarised below.

Table 3. Specific crystal/grain orientations for rolling.

Orientation	**Slip systems**	**Slip class**	**GNB planes**	**Sgl/poly**
Goss $(011)[100]$	$(111)[10\bar{1}], (111)[1\bar{1}0]$ $(\bar{1}11)[\bar{1}0\bar{1}], (\bar{1}11)[\bar{1}\bar{1}0]$	*coplanar*; *coplanar*	(111); $(\bar{1}11)$	s&p
45^0 *ND rot. Cube* $(001)[110]$	$(111)[10\bar{1}], (111)[1\bar{1}0]$ $(\bar{1}11)[\bar{1}0\bar{1}], (\bar{1}11)[\bar{1}\bar{1}0]$	*coplanar*; *coplanar*	(111); $(\bar{1}11)$	s
*S** $(123)[63\bar{4}]$	$(111)[10\bar{1}], (111)[01\bar{1}]$ $(\bar{1}11)[\bar{1}\bar{1}0], (1\bar{1}1)[\bar{1}\bar{1}0]$	*coplanar*; *codirectional***	(111); (113)	p
Copper $(112)[11\bar{1}]$	$(111)[10\bar{1}], (111)[01\bar{1}]$ $(\bar{1}11)[\bar{1}\bar{1}0], (1\bar{1}1)[\bar{1}\bar{1}0]$	*coplanar*; *codirectional*	(111); (001)	s&p
Cube $(001)[100]$	$(111)[10\bar{1}], (\bar{1}1\bar{1})[10\bar{1}]$ $(\bar{1}11)[\bar{1}0\bar{1}], (11\bar{1})[\bar{1}0\bar{1}]$	*codirectional*; *codirectional*	*only cells near ideal*; *otherwise* $(101)/(10\bar{1})$	s&p
$(\bar{1}13)[741]$	$(111)[10\bar{1}]$	*single*	(111)	s

* two sets of coplanar systems are expected from the Schmid factors (which was unfortunately not mentioned in [A6]). The mentioning of three coplanar slip planes predicted by the Taylor model in [A4] is due to negligible slip on two other systems.

** one codirectional system being twice as active as the other

Table 4. Specific crystal/grain orientations for tension.

Orientation	**Slip systems**	**Slip class**	**GNB planes**	**Sgl/poly**
$[100]$	$(11\bar{1})[101], (1\bar{1}\bar{1})[101]$ $(111)[10\bar{1}], (111)[10\bar{1}]$ $(1\bar{1}1)[110], (111)[110]$ $(11\bar{1})[xxx], (111)[xxx]$	*codirectional**; *codirectional**; *codirectional**; *codirectional**	*No GNBs*; *only cells*	s&p
[100]-[211]	$(11\bar{1})[101]; (1\bar{1}1)[110]$	*2 x single*	$(11\bar{1}); (1\bar{1}1)$	s&p
[211]-[111]	$(11\bar{1})[101], (11\bar{1})[011]$, $(1\bar{1}1)[110], (1\bar{1}1)[011]$	*2 x dep. copl&codir*	$(35\bar{1}); (3\bar{1}5)$	s&p
Near [111]	$(11\bar{1})[101], (11\bar{1})[011]$, $(1\bar{1}1)[110], (1\bar{1}1)[011]$, $(\bar{1}11)[101], (\bar{1}11)[110]$	*more dep. copl&codir*	$\{001\} - \{115\}$	p
[111]	$(11\bar{1})[101], (11\bar{1})[011]$, $(1\bar{1}1)[110], (1\bar{1}1)[011]$, $(\bar{1}11)[101], (\bar{1}11)[110]$	*more dep. copl&codir*	$(35\bar{1}); (3\bar{1}5)$; $(44\bar{1})$	s
[111]-[221]	$(11\bar{1})[101], (11\bar{1})[011]$, $(\bar{1}11)[101], (1\bar{1}1)[011]$	*2 x dep. copl&codir*	$(44\bar{1})$	s
[221]-[110]**	$(11\bar{1})[101], (11\bar{1})[011]$	*coplanar*	$(11\bar{1})$	s
[110]-[100]	$(11\bar{1})[101]; (111)[10\bar{1}]$	*2 x single*	$(11\bar{1}); (111)$	p
Midtriangle	$(11\bar{1})[101]$	*single*	$(11\bar{1})$	s&p***

* easy cross slip
** two additional systems are expected from the Schmid factors (see discussion in [A6])
*** single slip is not confirmed in polycrystal case

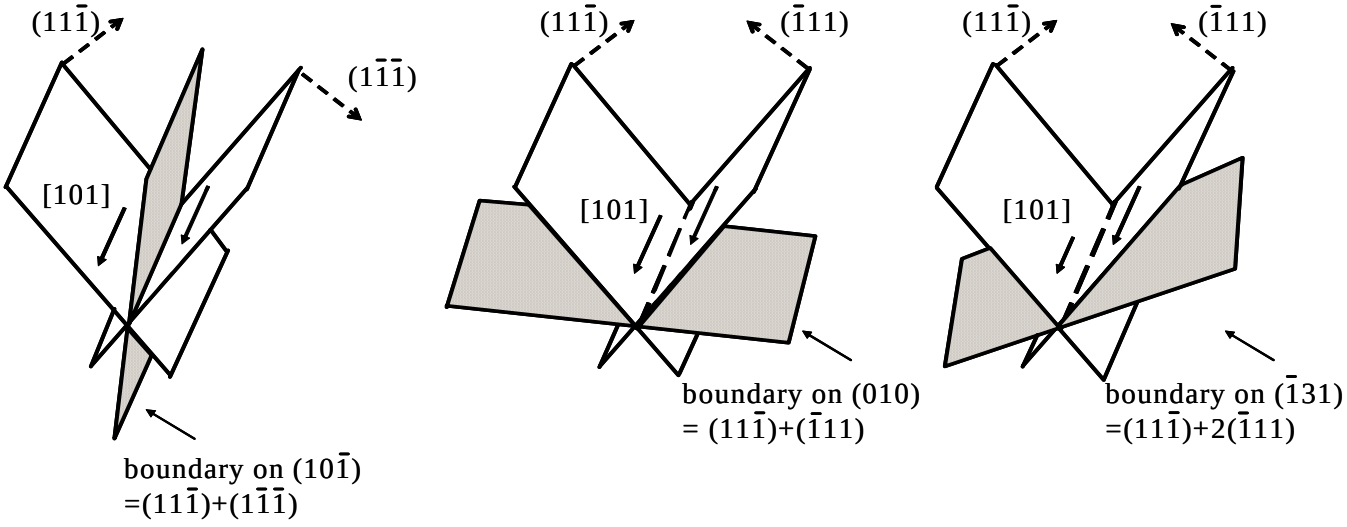

Fig. 28. GNB planes resulting from codirectional slip in different configurations: a) symmetric easy cross slip, b) symmetric difficult cross slip, and c) asymmetric difficult cross slip with one of the systems being twice as active as the other. From [A6].

6.2 Identified slip classes

In total five fundamental slip classes have been identified:

- Both the *single slip* class and the *coplanar slip* class lead to slip-plane-aligned GNBs, but the GNB planes are slightly (<10°) rotated away from the ideal slip plane around two different crystallographic axes[2].
    - Conjugate and critical double slip are in fact two-fold activation of the single slip class, leading to one set of GNBs aligned with the primary slip plane and a second set aligned with the conjugate or critical slip plane, respectively.

- *Codirectional slip* results in GNBs in between the two active slip planes, however, closer to the more active plane in the case of asymmetric activation.
    - Codirectional slip systems may be oriented for easy or difficult cross slip, defined here as cross slip, which is either assisted or inhibited by the applied force. The difference between GNBs arising from the two types of cross slip is that they bisect the acute or obtuse angle between the two slip planes (see Fig. 28a-b).
    - In case of asymmetric activation of the two codirectional systems the GNB plane is the linear combination of the two slip planes, weighted by their respective activities (see Fig. 28c). These planes are of the type {xyy}.

[2] In principle, coplanar slip may be seen as a two-fold activation of the single slip class, with a deviation axis which is the sum of the two <211> axes perpendicular to the two coplanar slip directions.

- *Two-or-more-fold activation of codirectional slip oriented for easy cross slip* gives rise to only cells.

- *Dependent coplanar slip and codirectional slip*, involving only three systems of which one is coplanar and codirectional, respectively, to the other two is a special class, giving rise to GNBs aligned with {351} planes. The geometry of the fundamental slip class is illustrated in Fig. 29a. The faces of the tetrahedron represent the slip planes and the edges the slip directions. The active slip systems are indicated by arrows. The dislocation boundary plane is rotated away from the slip plane around a <211> axis.
    - Two-fold activation of this slip class may occur in three different configurations as illustrated in Fig. 29b-d. One configuration involves four systems on two slip planes giving rise to two sets of GNBs aligned with two {351} planes. The other configurations, involve four systems on three slip planes and six systems on three slip planes, respectively. In these two cases the GNBs align with planes, which are linear combinations of {351} planes. Especially in the last case there is a significant variation in the GNB plane ranging from {001} to {115}. However, it is characteristic that all of the GNBs contain a common <110> direction.

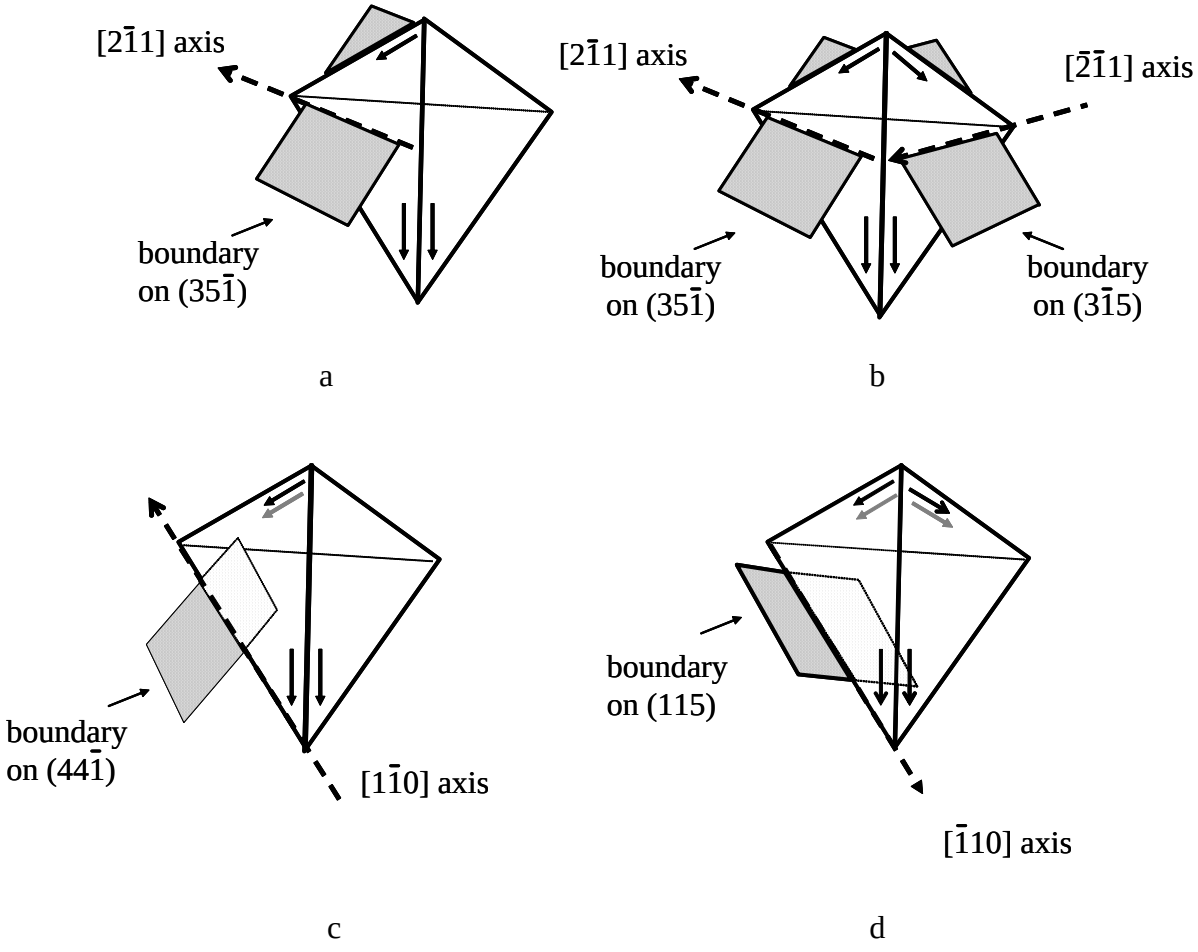

Fig. 29. Illustration of the dependent coplanar and codirectional slip class in different configurations: a) fundamental slip class, b) two-fold activation with four systems on two slip planes, b) two-fold activation with four systems on three slip planes, and c) two-fold activation with six systems on three slip planes. From [A6].

6.3 Demonstration of the slip class concept

This section focuses on identification of cases where activation of slip systems representing the same slip class lead to lead to a similar dislocation structure alignment in different deformation modes. The following three examples clearly demonstrate that the slip class controls the dislocation structure alignment:

6.3.1 Single slip class

Single crystals lying in the middle of the stereographic triangle and deformed in tension results in boundaries closely aligned with the {111} slip plane. While not frequent in rolling, the single slip class has been activated in a rolled single crystal of $\{\bar{1}13\}<741>$ orientation deforming with a significant shear component [82]. The GNBs in this crystal aligned with the active slip plane.

6.3.2 Coplanar slip class

The coplanar slip class results in boundaries aligned with the active {111} slip plane but rotated slightly away from this around a <101> axis as found along the [110]-[211] line in tension [79] and in the 45° ND rotated Cube [106, 107] orientations in rolling. That the coplanar slip class leads to GNBs aligned with {111} is also demonstrated in the rolled Goss orientation.

Furthermore activation of the coplanar slip class in the rolled S and Copper orientations results in GNBs align with {111}, showing that the additional activation of the codirectional slip class in these orientations does not interfere with the slip class.

6.3.3 Multiple activation of codirectional slip class oriented for easy cross-slip

Two or more sets of codirectional slip systems oriented for easy cross slip lead to cell structures with no planar GNBs, when activated in either tension along [100] [A14, 90] or rolling of the exact Cube orientation [A14, 82, 108].

6.4 Prediction of dislocation structure alignment in shear deformation

Shear was not among the deformation modes serving as the experimental basis for the identification of the slip classes. Evaluation of the slip class concept for prediction of the dislocation structure alignment after shear deformation is therefore a relevant and critical test.

The active slip systems in typical shear texture components obtained with the Taylor model and a Schmid factor analysis are identical and listed in Table 5, which also identifies the corresponding slip class and the predicted GNB plane. As the dislocation structure alignment after shear (or torsion) has not been investigated at the same level of detail as in tension and rolling these predictions cannot be completely verified. Nevertheless, the predicted GNB planes coincide with the shear plane in the sample coordinate system, in agreement with the general observations after torsion to high strains. The fact that GNBs aligned with a plane perpendicular to the shear plane are also frequent at low strains while the majority of the grains typically have other orientations, further supports the prediction.

Table 5. Typical shear texture orientations.

Grain orientation	**Slip systems**	**Slip class**	**GNB planes**
(001)[110]	$(\bar{1}11)[110], (1\bar{1}1)[110]$	*codirectional*	(001)
(111)[11$\bar{2}$]	$(111)[01\bar{1}], (111)[10\bar{1}]$	*coplanar*	(111)
(111)[110]	$(111)[1\bar{1}0]$	*single*	(111)

6.5 Parameterisation of the slip class concept for general prediction

General application of the slip class concept to slip system combinations involving many systems with different relative activities requires that the slip classes are transformed into a number of quantitative parameters, which can be evaluated. Following the success of the criterion of concentrated slip used in Chapter 5 for prediction of slip-plane-aligned GNBs, the fraction of the total slip in a grain which belongs to a slip class is the basis of these parameters:

- F_{single}, which is the fraction of the total slip in the grain occurring on the most active slip system.
- F_{sgl}^2, which is the fraction of the total slip in the grain occurring on the most active slip system and its conjugate or critical system (two-fold activation of the single slip class).
- F_{copl}, which is the fraction of the total slip in the grain occurring on the most active set of coplanar slip systems.
- F_{codir} , which is the fraction of the total slip in the grain, which occurs on the most active set of codirectional slip systems.
- $F_{\{351\}}$, which is the maximum fraction of the total slip which occurs on three systems, of which one is coplanar and codirectional, respectively, with the two others. This combination leads to a boundary plane near {351}.
- $F_{\{351\}}^2$, $F_{\{441\}}$, $F_{\{115\}}$ which are the fractions of the total slip accounting for multiple activation of the dependent coplanar and codirectional slip class. This may occur in three different geometries, involving four systems on two or three slip planes or six systems on three slip planes. These geometries lead to two sets of boundaries near {351}, one boundary near {441}, or one boundary near {115}, respectively.
- F_{cell}, which is the fraction of the total slip which occurs on two or more sets of codirectional slip systems, which are oriented for easy cross slip.

A high value of one of these nine parameters is evidence that the corresponding slip class dominates over the others and therefore the dislocation structure alignment must be the one typical for this slip class. Two slip classes and their corresponding alignment of the dislocation structure may coexist, as for example observed in the rolled copper orientation where two sets of GNBs from the coplanar and codirectional slip classes are found, in which case two parameters may have comparable values. When considering the possibility of simultaneous activation of two slip classes, care must, however, be taken to ensure that these are activated independently, i.e. that they do not involve the same slip system.

6.6 Conclusions

The concept of slip classes is a new tool for analysis and prediction of dislocation structure alignment, which is not related to a specific deformation mode, grain orientation or GNB plane. The relations between slip classes and dislocation structure alignment can be used in two ways: i) to predict dislocation structures from slip systems and ii) to deduce slip systems from dislocation structures. Prediction of dislocation structure alignment has already been demonstrated for shear deformation. Prediction by means of the proposed parameterisation of the slip class concept will be pursued further for rolling in the next chapter, where also the technological relevance of such predictions is illustrated. In this

process deduction of slip systems from experimentally observed dislocation structure alignment is also briefly demonstrated, and such slip system deduction is explored in much more detail for tension in Chapter 9 where also information from lattice rotations during deformation are included in the analysis.

7 Prediction of dislocation structure alignment and its effect on mechanical anisotropy in rolling

This chapter illustrates the technological relevance of studies of dislocation structure alignment, using the flow stress anisotropy of rolled sheets as an example. In Chapter 5 the occurrence of grain orientations having GNBs aligned with {111} was successfully predicted based on the concept of concentrated slip. A prediction based on the slip class concept derived in Chapter 6 is presented here and evaluated. For the purpose of modelling the flow stress anisotropy of rolled sheets the presently best available prediction of GNB planes is constructed.

Modelling of the coupled effects of texture and dislocation structure alignment on the flow stress anisotropy is presented and the importance of considering the grain orientation dependent dislocation structure alignment is demonstrated.

7.1 Prediction of dislocation structure alignment

The parametrisation of the slip class concept giving the fraction of slip belonging to each slip class is applied to the slip systems calculated from the Taylor model. Due to the fact that fcc metals have four slip planes and six slip directions and the Taylor model in general predicts more than five active systems when using the average solution to the ambiguity problem, the class of dependent coplanar and codirectional slip must be activated in many grain orientations. Direct consideration of the highest parameter consequently leads to GNB plane predictions (not shown here) in which practically all grain orientations were predicted to have GNBs aligned with {351}, {441} or {115}. The predictions were improved by introduction of a threshold value so that each slip system must account for at least 10 % of the slip accounted for by the dependent coplanar and codirectional class. The threshold of 10 % was selected by trial and error to give the best agreement with the experimental observations. The prediction is shown in Fig. 30a where also the experimental points from data sets 7-9 are included. To facilitate comparison and to avoid unnecessary complication of the figures no distinction is made between the GNBs originating from the single and coplanar slip classes. In both cases these are closely aligned with {111}, only differing in their small deviations from the exact {111} plane, which have furthermore not been characterised for data sets 7-9. With respect to the GNBs not aligning with {111} in data sets 7-9 the exact plane is not known. It is, nevertheless, known from other studies [A14] that grain orientations close to the β-fibre of the rolling texture have one set of GNBs aligned with {111} and another with {xyy}. To compare this information with the prediction, Fig. 30a distinguishes between GNBs predicted on {xyy} planes from the codirectional slip class and GNBs on one of the planes resulting from the dependent coplanar and codirectional slip class (i.e. {351}, {441} or {115}).

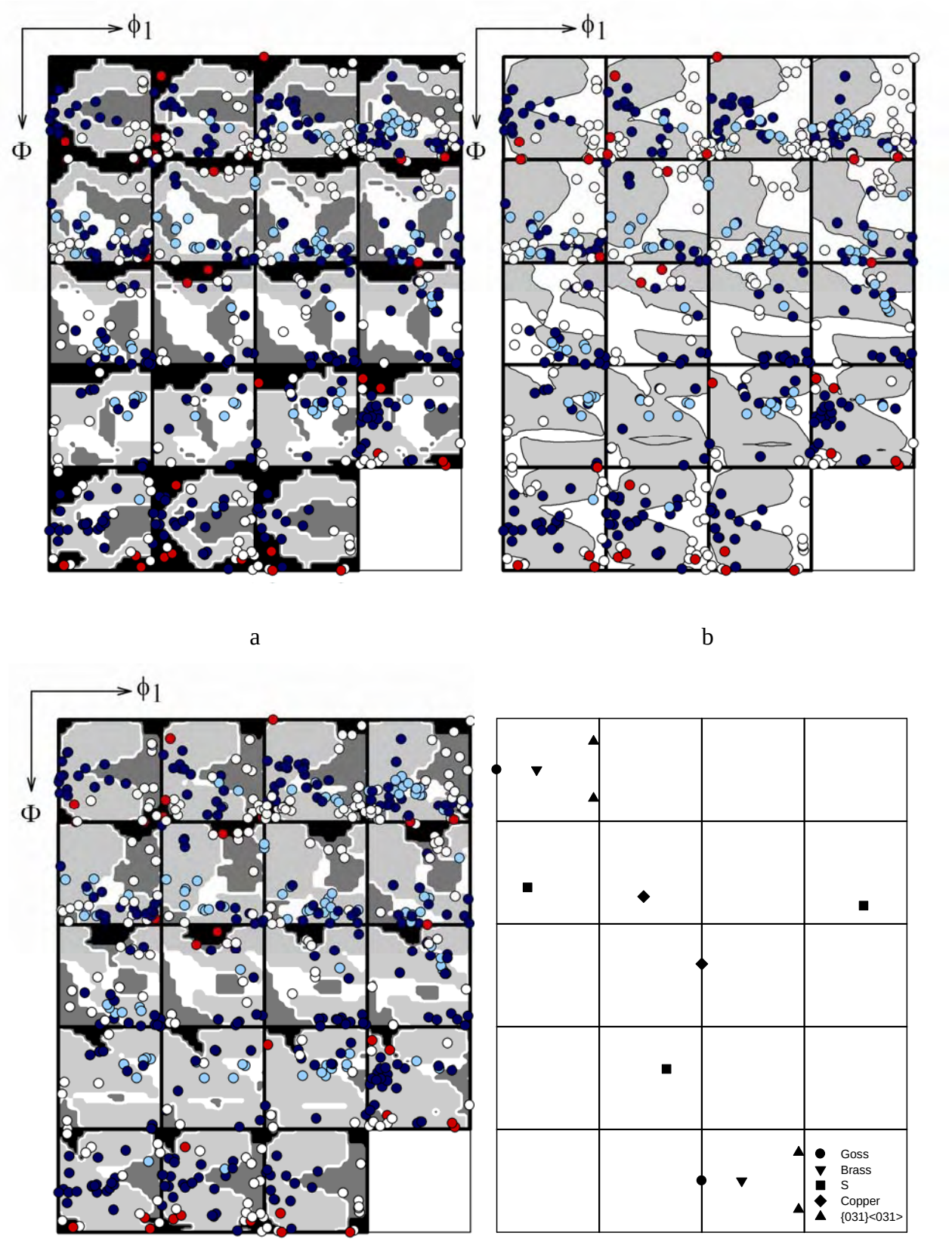

(Caption on next page)

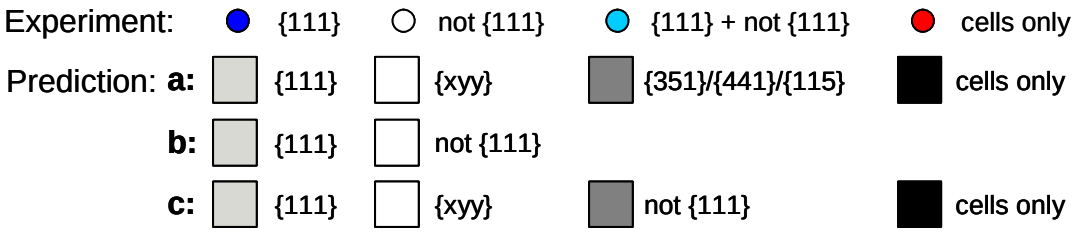

Fig. 30. ODF showing the predicted dislocation structure alignment based on a) the dominant slip class as judged from its slip fraction, b) the fraction of concentrated slip (repeated from Chapter 5), c) the hybrid model (see text) and d) reference orientations used in the discussion. The experimental GNB planes in grain orientations from data sets 7-9 are included as coloured symbols. Cells are only observed in copper (data set 9).

Analysis of the prediction in Fig. 30a and comparison with the previous prediction from Chapter 5 based on the fraction of concentrated slip repeated here as Fig. 30b reveals that each of these models has its strengths and weaknesses:

- The concept of concentrated slip is better at separating grain orientations aligned with {111} from orientations with GNBs aligned with other planes or only cells.
- The advantage of the model based on slip classes is its ability to correctly predict the occurrence of {xyy} planes and cells, even if the range of orientations predicted to have cells seems overestimated.

Three orientations or orientation ranges are particularly interesting (see Fig. 30d for the position of these in the ODF):

- Near the α-fibre of the rolling texture (spanning from the Goss to the Brass orientation) the experimental data clearly show that the GNBs align with {111}. Both models reproduce this, although the one based on concentrated slip better predicts the extension of this orientation range. Close to the ideal Brass orientation, however, both models predict GNBs not aligned with {111}, which is in strong contrast to experimental observations of two sets of GNBs aligned with {111} in both grains [A2, A14] and single crystals [80-82, 86, 88] of this orientation.
- Along the β-fibre of the rolling texture (spanning from the Brass over the S to the Copper orientation) the slip-class-based model predicts GNBs aligned with {xyy} planes, which is also seen experimentally together with a second set aligned with {111}. More detailed analysis of the slip systems in these grains (not included here) confirmed that while the codirectional slip class is responsible for the largest fraction of the slip in these grains, the coplanar slip class also accounts for a substantial slip fraction. The predicted dominance of the {xyy} aligned GNBs is also generally observed experimentally, at least for orientations closer to the β-fibre. This has been observed both in a Copper oriented single crystal [87] and in S-oriented grains [104] where these GNBs are much more frequent.
- Orientations near {031}<013> are in Fig. 30a predicted to have GNBs aligned with {111}, in strong contrast to the large number of GNBs aligned with other planes experimentally observed. This deficiency is not seen in Fig. 30b using the concentrated slip criterion.

7.2 Origin of the problems of the prediction based on slip classes

The comparison of the prediction based on slip classes with the experimental data shows that the model fails for two specific orientations. These cases are analysed in more detail here by considering the experimentally observed GNB alignment and the possible active slip systems to see whether the discrepancies are due to limitations of the Taylor model or of the slip class concept.

7.2.1 Brass orientation

For the Brass orientation the slip class predicted by the Taylor model is two-fold activation of the dependent coplanar and codirectional slip class in the configuration giving rise to two GNBs aligned with {351} planes. The two sets of GNBs experimentally observed to align with {111} deviate from the slip planes by rotation around a <101> axis [A14], i.e. the GNBs have the characteristics originating from the coplanar slip class. The class must be two-fold activated as two sets of GNBs are found. The specific variants of the {111} planes of the GNBs and the <110> axis allows deduction of the two sets of coplanar

systems, which must be active. They are also the systems with the four highest Schmid factors.

It should furthermore be noted that activation of these systems are in agreement with the observed stability of the Brass orientation but the strain they produce is an ideal plane strain compression with no shear strains. The Taylor model has often been seen to underestimate the intensity of the Brass texture component, which further warrants a correction of the model prediction for this orientation.

7.2.2 {031}<013>

The system calculated by the Taylor model for this orientation represent two-or-more fold activation of the single slip class, i.e. only have one highly active system on each slip plane and none of these are codirectional. This slip class obviously should give rise to GNBs aligned with {111}. The fact that this is in clear disagreement with the experimental observations shows that the Taylor systems are not those actually operating.

Considering the Schmid factors, eight slip systems have comparable values. If they are all activated they will represent multiple activation of the coplanar and codirectional slip class, and therefore not give rise to GNBs aligned with {111} planes.

By analogy with the Brass case, the active systems should be deducible from the observed GNB alignment. The exact GNB planes needed to do this have not been determined for data sets 7-9. The only available data set consists of one grain of {013}<031> orientation [109] deformed in hot plane strain compression. This grain had GNBs aligned with several variants of {351} planes. These planes are in agreement with the multiple activation of the dependent coplanar and codirectional slip class as expected from the Schmid factors. To fully resolve the slip systems in this orientation range further experimental characterisation of the GNB plane is needed.

7.3 Best available prediction of dislocation structure alignment

It is concluded above that the poor prediction originates from problems with the Taylor model. The finding that the active slip systems often are in better agreement with a Schmid factor analysis than with the Taylor model inspired predictions based on the application of the slip class concept to the systems with high Schmid factors rather than those calculated by the Taylor model. As expected from the analysis above better agreement with experiment was obtained in parts of the ODF. However, the agreement in other parts, and in particular near the β-fibre of the rolling texture, deteriorated by replacing the Taylor systems with those having high Schmid factors, where two sets of GNBs aligned with {111} planes were then frequently predicted instead of the observed alignment with {xyy} and {111} planes.

From a technological point of view good prediction of the dislocation structure alignment in orientations which are frequent is obviously more important than in orientations which are less frequent and eventually expected to disappear with increasing rolling strain. For this reason a hybrid model was devised based on the slip systems from the Taylor model and using the concentrated slip criterion to predict the orientations which have GNBs aligned with {111} and the slip class concept for the remaining orientations to predict the occurrence of {xyy} aligned GNBs and cells. Orientations which do not fall into any of these categories probably have GNBs from the dependent coplanar and codirectional slip class, i.e. GNBs aligned with {351}, {441} or {115}. This is, however, not well documented and furthermore cannot be determined from the present models for slip system

prediction. The predicted grain orientation dependence of the plane of the dominant GNBs using the hybrid model is compared with the experimental observations for aluminium (data sets 7 and 8) in Fig. 1c where good agreement is seen over the entire orientation space.

7.4 Modelling flow stress anisotropy of rolled sheets

The mechanical anisotropy of rolled sheets is an industrially relevant problem because the anisotropy influences the formability of the sheet. Typically, the flow stress (here taken as the $\sigma_{0.2}$ values) in tensile tests along different directions in the sheet is measured.

The crystallographic texture is an important source of mechanical anisotropy, which is, however, not always enough to account for the experimentally observed anisotropy in rolled sheets. The flow stress perpendicular to the rolling direction systematically exceeds that along the rolling direction [95, 110, 111], even after correction for texture effects. The suggestion that this is due to the alignment of the dislocation structure has been confirmed by experiments showing that this additional anisotropy can be suppressed by annealing of the sheet [110, 111], addition of solutes [95, 110, 111] and processing of the sheet by cross-rolling instead of conventional monotonic rolling [112], which destroys or alters the dislocation structure.

7.4.1 Anisotropic critical resolved shear stresses

Slip systems which interact with many GNBs, i.e. systems which frequently intersect the GNBs, are assumed to have a higher critical resolved shear stress than systems which glide almost parallel to the GNBs and practically never intersect one. The spacing between the GNBs as experienced by the individual slip systems therefore becomes the important parameter changing the critical resolved shear stress from system to system. This spacing is obviously proportional to the perpendicular GNB spacing in the material but must be multiplied by a geometric factor, which takes into account the orientation of the GNB plane relative to each slip system. With the GNB spacing as the governing parameter for the stress, modeling by means of a Hall-Petch type relation is natural, as also proposed in a model calculating the contributions from texture and GNBs independently and assuming that they are additive [59]. When modelling at the grain scale the two contributions are included in the critical resolved shear stress of slip system *i*, which is given by:

$$\tau_{crss,i} = \tau_0 + x \cdot K^{-1/2} \cdot d_i^{-1/2}, \qquad \text{Eq. 2}$$

where τ_0 is the isotropic part common to all slip systems, x the Hall-Petch slope, K the perpendicular GNB spacing, and d_i the geometric factor giving the distance between the GNBs experienced by the slip system. This geometric factor may take various forms, for example giving the distance measured along the slip direction (two other approaches have also been tested, in general with qualitatively similar results [A7, A20].

The value of the perpendicular GNB spacing, K, can be determined directly by electron microscopy studies of the rolled metal. Considering various mechanistic models, the parameter x has been seen to be proportional to the misorientation angle across the GNBs [113], which can also be measured.

The isotropic part of the critical resolved shear stress, τ_0, is the sum of contributions from the friction stress of the undeformed metal and from the randomly oriented part of the dislocation structure, namely the IDBs and loose dislocations in between the boundaries.

The latter contributions are given by the dislocation densities, which can also be determined by electron microscopy, normally relating the dislocation density for the IDBs to their misorientation angle and spacing [114].

The author's contribution to the flow stress anisotropy modelling has been to explore the impact of the increasingly better understanding of the dislocation structure alignment and its grain orientation dependence on the modelled flow stress anisotropy by incorporating the anisotropic critical resolved shear stress in Eq. 1 into the conventional Taylor model and otherwise following standard procedures.

7.4.2 Importance of grain orientation dependent GNB planes

Here the flow stress anisotropy is predicted for three aluminium samples (AA1050) with different grain sizes. The anisotropy of these materials is investigated experimentally in [95], where it is also established that all the materials have weak rolling textures. The parameters τ_0 and x of Eq. 1 used in the following predictions are those calculated in [A20] based on typical microstructural data for aluminium. The three materials are assumed to have identical parameters except for the GNB spacing, *K*, which for the coarse grained material is measured to be almost twice that of the two other materials [95].

Three different flow stress predictions are included in Fig. 31, differing by the model used to predict the dislocation structure alignment induced by the rolling deformation prior to the calculation of the flow stress anisotropy. In all cases only one set of GNBs is predicted in each grain, as experimental evidence for aluminium shows that one set is often much more closely spaced than the other and therefore should control the anisotropy.

7.4.2.1 Macroscopically aligned GNBs

The first flow stress anisotropy calculation is made assuming that the GNBs align with the macroscopically most stressed planes. More specifically half of the grains were assumed to have one set of GNBs inclined +45° to the rolling direction while the other half had GNBs inclinded -45°. In Fig. 31 this dislocation structure prediction (black curve) is seen to overestimate the absolute value of the flow stress and in particular for the medium grain size to underestimate the anisotropy. While fine tuning (with an element of fitting) of the parameters in Eq. 1 can bring the absolute flow stress level in agreement with experiment the degree of anisotropy for the medium grain size cannot be modelled quantitatively assuming only macroscopically aligned GNBs.

7.4.2.2 Introducing GNBs aligned with {111}

The first grain orientation dependent dislocation structure prediction introduced in the flow stress anisotropy calculation is the one from Fig. 30b, which has GNBs aligned with {111} planes in the grain orientations with a high slip concentration and macroscopically aligned GNBs (similar to those described above) in the remaining orientations. As it is known that the GNBs always deviate a little from the ideal {111} plane they are given a deviation of 3° in the calculations.

The introduction of the GNBs aligned with {111} has a major impact on the flow stress anisotropy as seen from the blue curve in Fig. 31 where the absolute flow stress level is now lowered to the experimentally observed values and also the anisotropy is increased to match the experimental observations fairly well. In particular for the medium grain size the prediction is now much better.

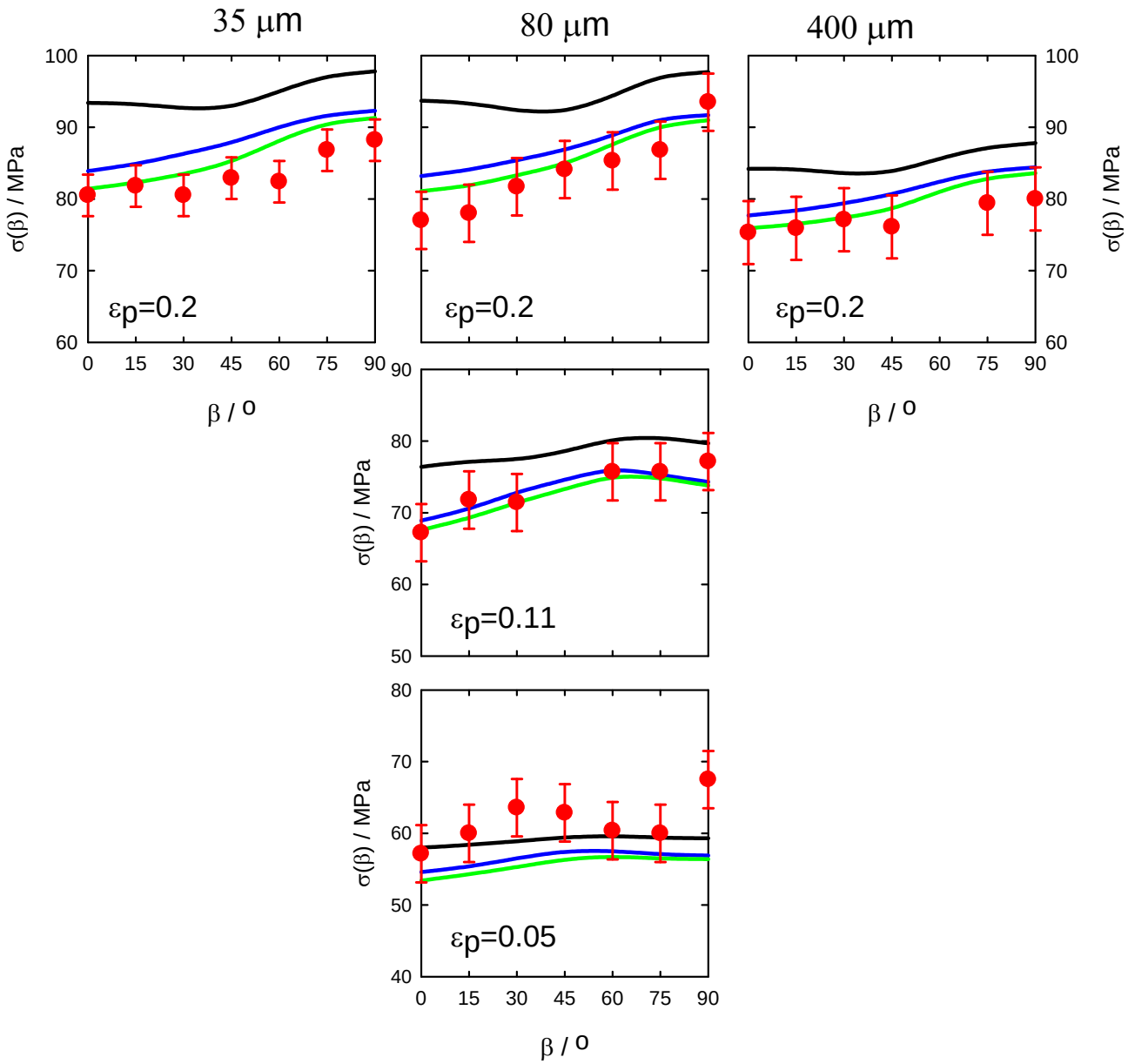

Fig. 31. Flow stress anisotropy for three aluminium samples with different grain sizes and rolled to different prestrains (ε_p) before tensile testing along different directions in the sheet given by the angle β, with β=0° along the rolling direction and β=90° along the transverse direction. Experimental data (red symbols) are taken from [95]. The anisotropy is calculated using different models to predict the dislocation structure alignment: i) macroscopically aligned GNBs (black curve), ii) slip-plane-aligned and macroscopically aligned GNBs (blue curve), and iii) dislocation structure alignment with the hybrid model (green curve).

The large impact of the GNBs aligned with {111} is due to the fact that the slip directions of all systems on that plane as well as their cross slip systems, are almost parallel to the GNBs and therefore experience much longer GNB spacings than the other systems, i.e more anisotropy. An increase in GNB spacing means a lower critical resolved shear stress and slip on such systems therefore significantly lowers the flow stress.

7.4.2.3 Prediction by the hybrid model

The dislocation structure alignment predicted using the hybrid model from Fig. 30c includes GNBs aligned with {111} as in the previous prediction and separates the remaining GNBs into three categories, namely no GNBs, GNBs aligned with {xyy} planes (parallel to the codirectional slip direction) and GNBs on macroscopically aligned planes. By analogy with the modelling of the GNBs aligned with {111} the GNBs aligned with {xyy} planes are tilted 3° out of the exact {xyy} plane to make all slip systems feel the effect of the GNBs. For the grain orientations with no GNBs but only cells x is set equal to 0 in Eq. 2.

It is seen from the green curve in Fig. 31 that the hybrid model for the dislocation structure alignment leads to changes in the flow stress anisotropy analogous to those following the introduction of the {111} aligned GNBs: the flow stress level is lowered and the anisotropy increased. The origin of this effect is also the same, namely that some of the slip directions in grains with GNBs aligned with {xyy} planes are almost parallel to the GNB plane, resulting in a relatively low critical resolved shear stress for these systems.

While the introduction of GNBs aligned with {111} was seen to have a huge impact on the flow stress anisotropy prediction, the effect of going to the hybrid model is minor. In fact the difference between the two flow stress anisotropy calculations based on grain orientation dependent dislocation structure alignment predictions is so small that considering the error bars on the experimental data one cannot be deemed better than the other. The relatively small effect is due to the lower fraction of grains predicted to have GNBs aligned with {xyy} compared to the fraction of {111} aligned GNBs. Furthermore, the grains of near Cube orientation no longer have anisotropic critical resolved shear stresses as they are not predicted to form GNBs. This fraction is, however, low.

The knowledge about the exact plane of the GNBs in the grains modelled as having macroscopically aligned GNBs with the hybrid model is limited. It is, however, known that these are not aligned with {111} and while some of them may align with {xyy} planes, it is expected that many of them align with planes originating from the dependent coplanar and codirectional slip class, i.e. {351}, {441} or {115}. These planes do not align with any of the slip systems and they will therefore not induce as large a difference in the critical resolved shear stresses of a grain as GNBs aligned with {111} or {xyy}. The effect of knowing the exact GNB plane in these orientations is therefore comparable to knowing whether a macroscopically aligned GNB is inclined positively or negatively to the rolling direction. The effect of the latter has been demonstrated to be small [A8], leading to the conclusion that further improvements of the dislocation structure alignment prediction will not in practice affect the flow stress anisotropy calculations.

7.5 Conclusions

Exploring the potential for prediction of the dislocation structure alignment after rolling based on the slip class concept revealed limitations of the models used for slip system calculation: The systems from the Taylor model were confirmed in some cases while those with high Schmid factors were better in others.

For technological purposes, the uncertainties in the slip system calculation have been circumvented by construction of a hybrid model for dislocation structure alignment prediction, yielding good agreement with experiment. The understanding of the dislocation structure alignment and its consequences was proven to be sufficiently advanced to successfully predict the resulting flow stress anisotropy, i.e. the modelling scheme proposed in Chapter 1 for the coupled effects of texture and dislocation structure alignment has been demonstrated to be applicable to technological problems.

Scientifically, the major result obtained in this chapter is that analysis of the experimentally observed dislocation structure alignment using the slip class concept is an important new tool, allowing evaluation and improvement of models for slip system prediction. This will be explored further for tension in Chapter 9.

8 Lattice rotations during tension – Grain orientation and slip system dependence

The crystal plasticity model employed in the previous chapters for the prediction of slip systems from the grain orientation and deformation mode has been the Taylor model, which is well-established as a model giving a good overall agreement with experimentally observed deformation textures, although the predicted textures are generally too sharp. The predictions of dislocation structure alignment obtained in Chapters 5 and 7 from the slip systems calculated by the Taylor model also showed general good agreement with the experimental observations. However, deficiencies in the predictions were also evident. These were ascribed to deficiencies in the slip system calculation rather than in the prediction of the dislocation structure alignment from the calculated systems.

The lattice rotations measured by 3DXRD of individual grains deeply embedded in the bulk of the metal provide an additional method to evaluate the quality of the slip system predictions of the Taylor model. This is the subject of the present chapter, which also compares the experimental rotations to examples taken from the literature of lattice rotations predicted by models, which include contributions from grain interactions, i.e. self-consistent and finite element based polycrystal plasticity models. The purpose of this comparison is to evaluate the hypothesis of this thesis that the slip systems - and therefore dislocation structure alignment and lattice rotations - primarily depend on the grain orientation with respect to the deformation axes, while grain interactions are secondary effects.

8.1 Grain orientation dependence of lattice rotations

As described in Chapter 2, three data sets of lattice rotations measured by 3DXRD during tensile deformation of aluminium and copper to 6-11 % elongation are available (data sets 10-12). The rotations of the tensile axes of the individual grains are shown in Fig. 32. Data set 11 on the 6 % elongated AA1050 sample (Fig. 32b) is by far the most extensive encompassing about 100 grains. This is the reason why the analysis is concentrated on this data set. It is, however, emphasized that data sets 10 and 12 are in agreement with the conclusions drawn from data set 11.

First of all it is observed that the lattice rotations in Fig. 32 correspond to the overall evolution of bulk textures after tension where the intensity concentrates around a major and minor fibre centred on [111] and [100], respectively. The observed rotations of the grains near [110] towards the [100]-[111] line are also in agreement with high texture intensities close to this line at intermediate strains while the intensity at the [110] corner of the triangle is rapidly vanishing.

Turning to the level of individual grains, visual inspection of Fig. 32b reveals four different types of rotation behaviour depending on the grain orientation. The four regions of the stereographic triangle with different rotation behaviours are shown in Fig. 33a. The rotation characteristics in each region are:

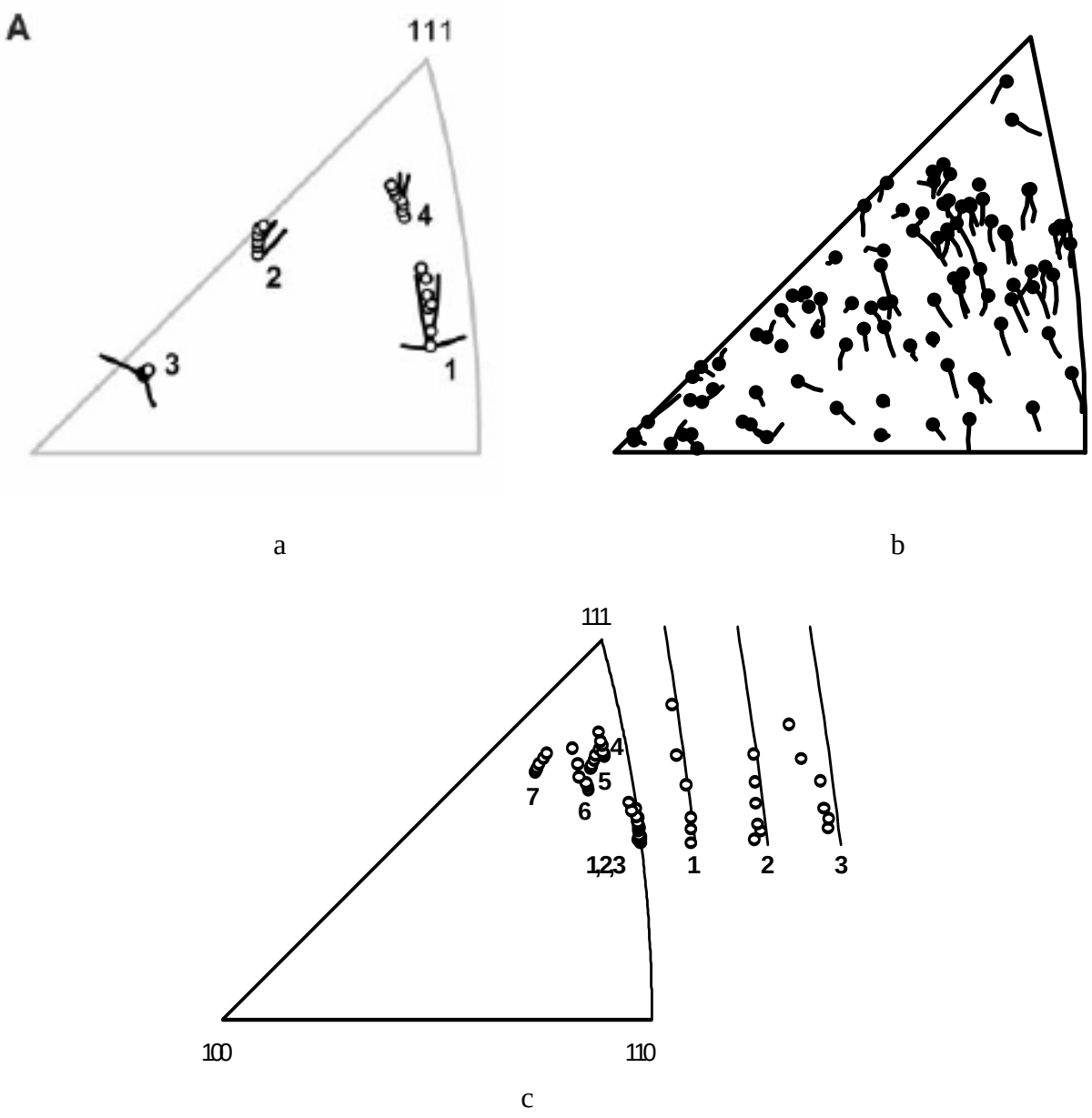

Fig. 32. Rotations of the tensile axes: a) 11 % tensile elongation of aluminium with a grain size of 300 μm (data set 10 from [A11]), b) 6 % elongation of aluminium (AA1050) with a grain size of 75 μm (data set 11 from [A13] and c) 6 % elongation of copper with a grain size of 35 μm (data set 12 from [A12]). The rotations for grains 1-3 are shown in enlargement. For a) and c) the initial orientation is marked with the numbers. For b) the circular symbols mark the final orientation after deformation.

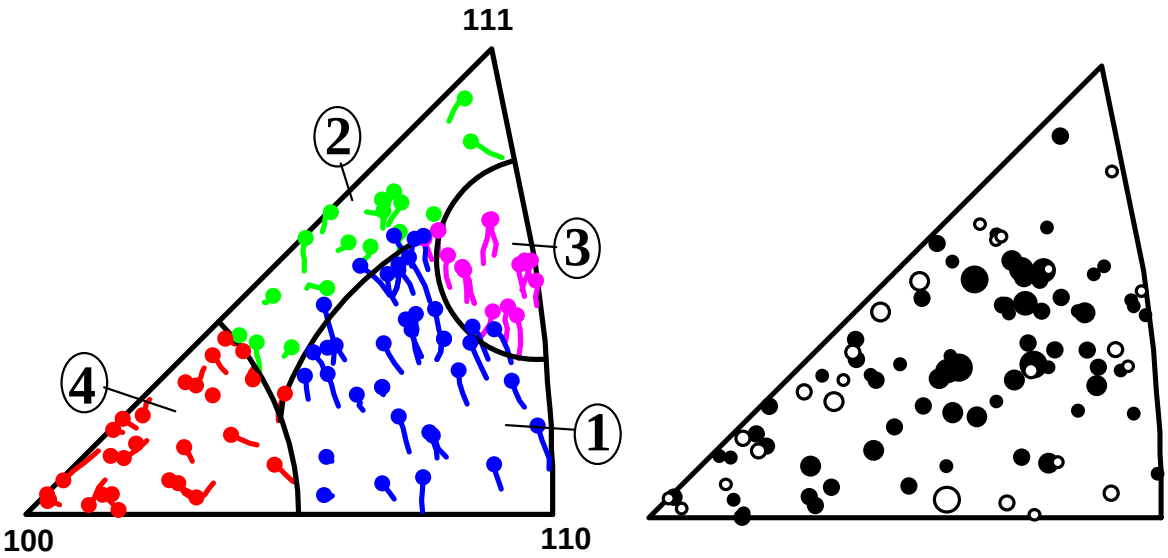

a b

Fig. 33. Stereographic triangle showing the grain orientation dependence of the lattice rotations from data set 11. a) Rotation of the tensile axis (direction and angle). The triangle from Fig. 32b is subdivided into four regions with different behaviours. From [A9]. b) Rotation angle around the tensile axis. Open circles designate clockwise rotation around the tensile axis while filled circles represent counter-clockwise rotations. The size of the symbol reflects the magnitude of the rotation with the largest rotation being 2.5°. From [A13].

Region 1: Grains in the [110] corner rotate towards the [100]-[111] line.

Region 2: Grains at the [100]-[111] line rotate along this line towards [111].

Region 3: Grains half way up the [110]-[111] line, i.e. close to [221], rotate directly towards [111].

Region 4: Grains near [100] do not exhibit a common rotation trend.

The rotations around the tensile axis for data set 12 are shown in Fig. 33b. The majority of the grains rotate counter-clockwise around the tensile axis. However, rotations in the opposite direction are found near the edges of the triangle.

8.2 Variation within regions

Within all of the regions there is some variation in the axes around which the tensile direction rotates and the corresponding rotation angles. However, the characteristics of these variations differ from region to region, i.e. exhibit grain orientation dependence:

Region 5: The rotation angles form a broad peak around the mean value of 2.7°. The mean rotation axis does not vary with the distance from [110] but more between the upper right and lower left parts of the region.

Region 6: The distribution of rotation angles is fairly flat ranging from practically no rotation to 3° (mean angle of 1.7°). The rotation axes exhibit some variation but distinct trends could not be discerned.

Region 7: The rotation angles form a narrow peak with a mean value of 2.5°. The rotation axes also exhibit very little variation.

Region 8: The distribution of rotation angles is bimodal and the rotation angles also exhibit large variations. Analysis revealed that three distinct rotation trends coexist: 4I) rotation towards the [100]-[111] line, 4II) rotation along the [100]-[111] line towards [100] and 4III) virtually no rotation of the tensile axis.

8.3 Comparison with the Taylor model

Many studies based on rotations measured for surface or surface-like grains (e.g. [23-29]) conclude that the Taylor model is not successful in predicting the rotations at the grain scale but reproduces the main trend for the bulk textures. The present comparison is conducted at an intermediate level by evaluating if the Taylor prediction captures the main trends of the four identified rotation regions.

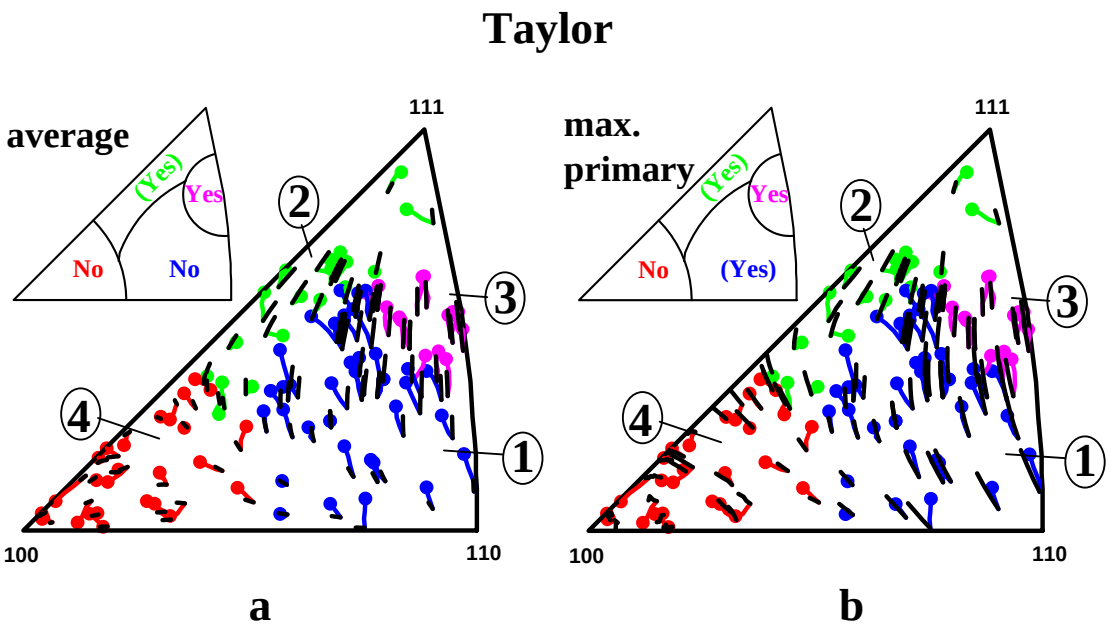

Fig. 34. Comparison with the rotations from the Taylor model (black lines) using a) the average solution to the Taylor ambiguity problem, and b) the solution with most slip on a single system. The small triangles indicate whether acceptable agreement is found for the individual regions. From [A9].

In Chapter 5 two different approaches to the ambiguity problem inherently associated with the Taylor model were used, namely the average solution and the solution with maximum slip on a single system. In general the dislocation structure alignment predicted based on the slip systems from the Taylor solution with maximum slip on a single system gave better agreement with experiment for tension. Following up on these investigations, the experimental lattice rotations are also compared to the rotations calculated from the Taylor model using both of these solutions to the ambiguity problem.

The comparisons are shown in Fig. 34 with the average solution in Fig. 34a and the solution with maximum slip on a single system in Fig. 34b. In general both predictions lead to smooth rotation fields where the only variation with the grain orientation lies in the fact that grains in the upper right part of the triangle rotate more towards [111] while those in the lower left part head more towards [100]. The predictions in Fig. 34a and b for region 3 are practically identical and in good agreement with the experimental data. In region 2 the main experimental trend of a strong rotation component towards [111] is also found in both Fig. 34a and b but the experimental scatter in the form of additional rotation components towards and away from the [100]-[111] line is not predicted. However, pronounced disagreements between the experimental and predicted rotations are found in regions 1 and 4:The solution with most slip on a single system (Fig. 34b) is significantly better than the average solution (Fig. 34a) in most of region 1, both with respect to rotation direction and rotation magnitude. However, in the upper left part of region 1 (marked with a circle in the figures), where the rotations in Fig. 34a and b are practically identical, the predictions do not match the experimental observations, in the sense that they head more vertically towards [111] than the experimental rotation paths.

In region 4 near [100] the predictions in Fig. 34a and b are different but neither prediction agrees with the variation in the experimental rotations. Yet, the solution with most slip on a single system (Fig. 34b) reproduces one of the three experimental trends (4I) in this region well. Further analysis of the Taylor ambiguity in this region was therefore conducted: with a tensile axis close to [100] the Taylor model predicts six solutions, of which only four are in agreement with the experimental observations for the rotation of the tensile axis (two agree with rotation trend 4III and the other two with 4I and 4II, respectively). The remaining two solutions lead to rotations of the tensile axis which are in the opposite directions to the trends 4I and 4II, respectively, and consequently in disagreement with the observations.

In summary, the Taylor model has problems in region 4 but reasonably well captures the main trends for the other three regions when selecting the solution to the ambiguity problem with most slip on a single system. The variations observed for grains lying within the same region are, however, not accounted for by the Taylor model, not even when allowing for ambiguous slip system solutions.

8.4 Comparison with models including grain interaction effects

The deficiencies of the Taylor model is generally expected to lie in its basic assumption that all grains experience the same strain. In the following the experimental rotations are therefore compared with predictions including grain interaction effects. A variety of models has obviously been proposed and the present comparison is restricted to typical examples taking fundamentally different approaches. The number of predictions for tensile deformation in the literature is limited, probably due to the higher industrial relevance of rolling, where also the mechanical effects of, for example, friction from the rolls may be considered.

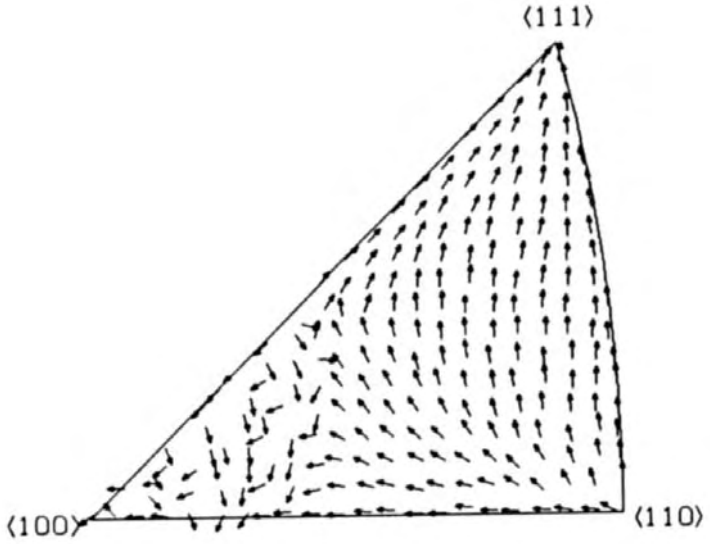

Fig. 35. Self-consistent prediction of the rotation of the tensile direction of aluminium from 3% to 5% elongation. The arrows represent the rotation direction and not the angle. From [115].

8.4.1 Self-consistent model

Self-consistent models consider the interaction between a grain and a matrix representing the rest of the material. An example of rotations predicted by a self-consistent model is shown in Fig. 35. It is seen that the rotation field in a large part of the triangle exhibits the same form of grain orientation dependence as the Taylor model with rotations heading towards [111] and [100], respectively, in a manner resembling the predictions with the average solution to the ambiguity problem. Near [100] rotations in different directions are predicted, in analogy with the experimental data. However, the self-consistent model does not correctly reproduce the three distinct rotation trends found in this region.

8.4.2 Specific interactions between neighbouring grains

Finite element based polycrystal plasticity calculations, in which the interaction between neighbouring grains, have been performed for a few tensile deformed quasi-columnar grains [116] and polycrystals built up of up to 100 grains with free or periodic boundary conditions [117]. The quasi-columnar predictions were too few to allow an actual comparison with the 3DXRD data. The rotations predicted for the larger grain ensemble did not exhibit any clear grain orientation dependence [117]. Closer comparison with the 3DXRD data reveals that the rotations towards the [100]-[111] line in region 1 are well predicted but that the existence of regions 2-4 cannot reliably be detected. Furthermore, the predicted variations within regions 2 and 4 are too small.

8.5 Comparison with Schmid factor based modelling

The analysis of the dislocation structure alignment in the previous chapters concluded that for some grain orientations the slip systems are controlled by the Schmid factors, i.e. the stress state, rather than strain compatibility as enforced by the Taylor model.

The ‘modified Sachs model’ [118, 119] is based on stress considerations and activates only the most stressed slip system (with the highest Schmid factor) in each iteration step. It differs from the original Sachs model by adding random stresses in each iteration step to induce multislip and account for grain interaction effects.

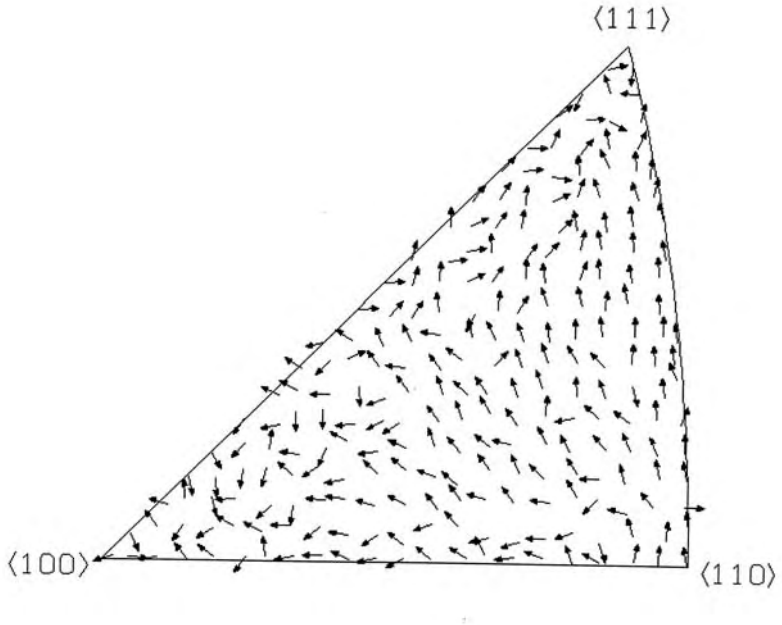

Fig. 36. Prediction of the rotation of the tensile axis by the modified Sachs model. The arrows represent the rotation direction and not the angle. From [A21] with model described in [118, 119].

The directions of the lattice rotations predicted with the modified Sachs model are shown in Fig. 36. Remarkably, an orientation dependence matching the experimentally observed is discerned: the predicted rotation directions of grains in regions 1-3 more or less follow the experimental rotations, except for a larger variation in region 1 in the [110] corner. Near [100] in region 4 the model predicts rotations in different directions as experimentally observed. By analogy with the self-consistent prediction some orientations are, however, predicted to rotate away from the [100]-[111] line in disagreement with the experimental trends.

8.6 Conclusions

The comparisons conducted here are obviously not a complete survey of all possible models and furthermore the predictions are not based on the ensemble of grains investigated experimentally. Nevertheless, the results suggest that inclusion of specific interactions with neighbouring grains does not *per se* lead to predictions generally better than those of the Taylor model or the modified Sachs model, which are based on the orientation of the grain without consideration of its neighbours.

In recent years the focus has mainly been on modelling of grain interactions. The fundamental crystal plasticity model, which is part of all polycrystal plasticity models, has not received as much attention. The results of the comparisons made here as well as the strong grain orientation dependence of both lattice rotations and dislocation structures indicate that progress can still be gained from research focusing on the individual grains to predict the slip systems. Such research is the subject of the next chapter.

9 Slip systems in tension determined from coupling of dislocation structure alignment and lattice rotations

The previous chapters demonstrate a strong grain orientation dependence of both dislocation structure alignment and lattice rotations which originates from the grain orientation dependence of the active slip systems.

Chapter 6 identified the relations between slip classes and the type of dislocation structure alignment. In chapter 7 these were applied to the slip systems calculated by the Taylor model revealing limitations. It was furthermore briefly demonstrated that the active slip systems may be deduced from the experimentally observed dislocation structure alignment by means of the slip class relations. It must, however, be expected that only the dominant systems can be identified in this way and that additional systems may be active without having a noticeable impact on the dislocation structure.

Chapter 8 compared experimentally measured lattice rotations with rotations from slip system predictions. The limitation of such comparisons is that lattice rotations do not give direct evidence of the individual systems but are the combined effect of all the active systems.

As dislocation structure alignment and lattice rotations are coupled through their mutual dependence on the slip systems (and therefore the grain orientation) but elucidate different aspects, combination of the two sets of data in the deduction of the slip systems is an obvious new method emerging from the results of this thesis. This is pursued in [A10] for tension and the main techniques and results are summarised here.

The first step taken is to merge the grain orientation dependence of the two types of data to obtain the grain orientation dependence of the slip systems. Subsequently, slip systems which agree with the dislocation structures and lattice rotations, respectively, are determined independently, and finally the two sets of slip systems are compared to demonstrate that systems which agree with both data sets exist. The deduced slip systems are then compared to the predictions of the Taylor model and the Schmid factors.

9.1 Grain orientation dependence of slip systems

It must be expected that some changes in the active slip systems when going from one part of the stereographic triangle to another have a larger impact on the dislocation structure alignment than on the lattice rotations and vice versa. To construct the subdivision of the triangle according to slip systems one should therefore start by combining the subdivisions of the triangle according to dislocation structure alignment and rotation behaviour established in Chapters 4 and 8, respectively. Fig. 37a and b repeat these subdivisions and Fig. 37c shows the result of their superposition. The two subdivisions in Fig. 37a and b are clearly not identical and do not even agree on the number of regions. As shown in Fig. 37d two simplifications are made to the superposition in Fig. 37c. Fig. 37d is henceforth taken as the subdivision according to slip systems forming the basis of the analysis. New labels (A-G) have also been introduced to identify the individual regions. These are inspired by the previous labeling of dislocation structure types in Chapter 4 but it was also necessary to add new labels.

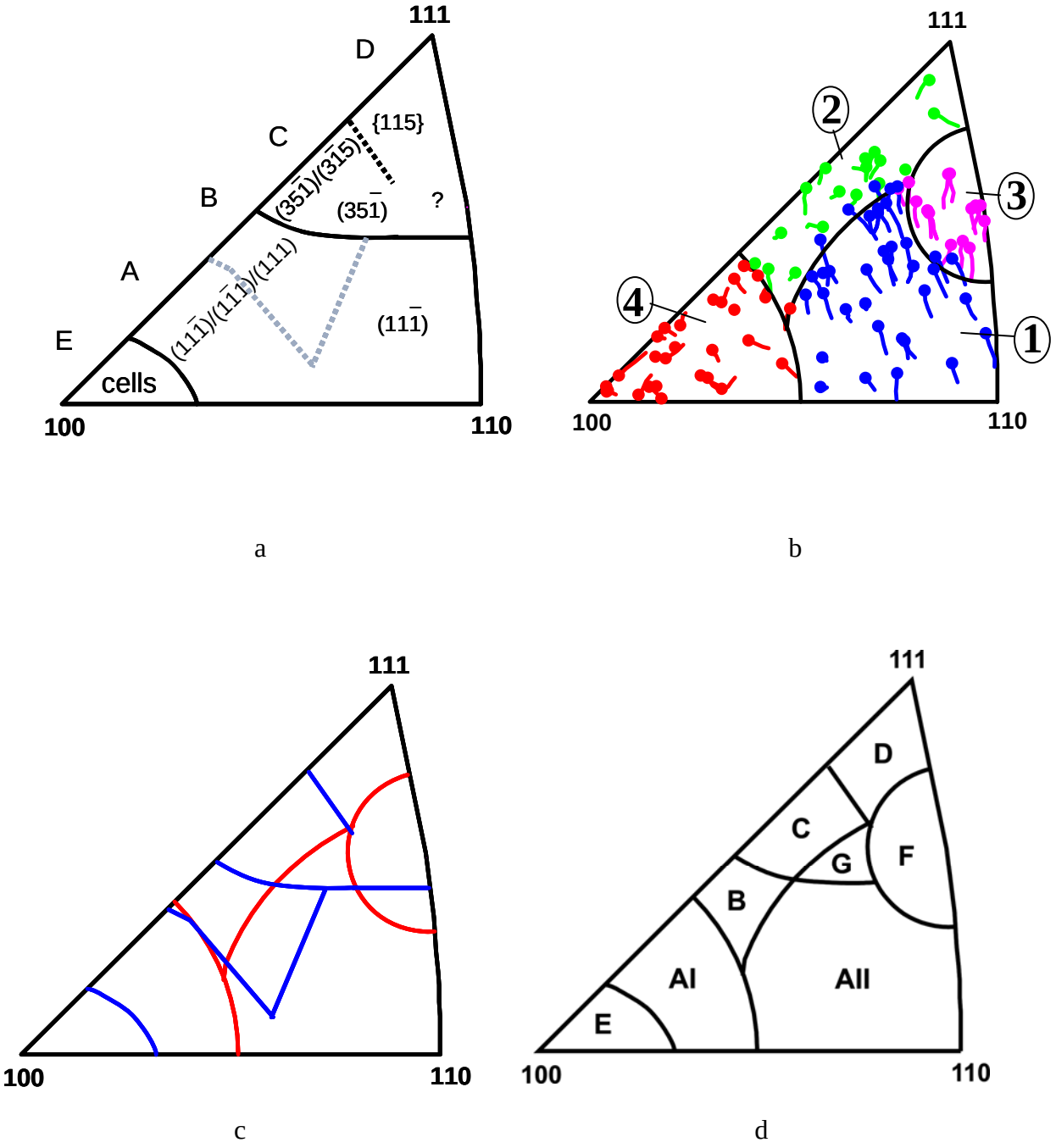

Fig. 37. Grain orientation dependence of a) dislocation structure alignment (from Chapter 4), b) lattice rotations (from Chapter 8), c) superposition of a and b (from [A10]), and d) deduced grain orientation dependence of the slip systems and the labelling of the different regions used in the remainder of this chapter (from [A10]).

The two simplifications made in Fig. 37d are:

- Slip system region F corresponds to rotation region 3, although the GNBs in the lower part of region F align with {111} while the GNBs in the upper part do not. This is because single crystals on the part of the [110]-[111] line delineating region F systematically increase their deviation from the {111} plane [79]. This indicates the operation of the same slip systems although with a gradual change of their relative intensities. A further pragmatic argument for keeping this as one region is that the lack of detailed GNB planes for grains in polycrystals with the tensile axis lying in the interior of this region prevents firm conclusions in the subsequent analysis.
- The transition between slip system regions AII and B is taken as the one given by the lattice rotations because this transition is very sharp while that of the dislocation structure alignment is more diffuse.

9.2 Slip systems from dislocation structure alignment

The dislocation structure alignment in the individual regions is listed in Table 6. By means of the relations derived in Chapter 6 between GNB planes and slip systems the corresponding slip class is easily identified. Consideration of the actual variant of the GNB plane, e.g. among the four {111} slip planes, allows further deduction of the actual slip systems. The results of this analysis is also presented in Table 6. Note that the slip systems are designated in the Bishop-Hill notation (see Table 7) and that the primary, conjugate, critical and cross slip systems are –b2, d3, -a2 and -c2, respectively. Due to the poorly characterised GNB planes in Region F all the possibilities are included with a question mark in the table.

It is typical for the regions close to the [100]-[111] line of the triangle that GNBs aligning with different planes of the same type are found, alone or coexisting within a grain. For example, the GNBs in Region AI align with three different slip planes but all of them are of the type resulting from the single slip class, as evidenced by the small deviation of the GNBs from the ideal slip plane by rotation around {112} axes. Analogously, GNBs may align with one or two slip planes in region B and with two different variants of {315} planes in region C. This means that the slip class may be one- or two-fold activated.

Identification of the dominant slip class in a region based on the dislocation structure alignment also shows which of the parameters defined in Chapter 6 characterising the fraction of the total slip belonging to a slip class that must be high. These parameters are included in the fourth column of Table 6. The last columns in the table show whether the expected parameters are in fact the highest for the ensembles of slip systems calculated based on the lattice rotations as described in the next section.

Table 6. Crystallograhpic GNB plane, deduced slip class and the active slip systems belonging to this slip class for the different slip system regions of the stereographic triangle in Fig. 37d. The slip systems are given in the notation of Table 7. The parameters quantifying the fraction of the slip that is accounted for by the slip class are also listed. Note that / separates slip classes or slip systems, which may or may not be active at the same time while , separates classes or systems which must be simultaneously activated. The ?'s for region F reflect the uncertainty about the GNB plane. The ✔'s in the last columns refer to comparisons with the slip systems calculated from lattice rotations (see the subsequent sections).

Region	GNB plane	Slip class	Slip systems	Exp. parameter	axi	int	unr
AI	$(11\bar{1})/(1\bar{1}1)/(111)$	sgl. or two-fold sgl.	-b2/d3/-a2	F_{sgl}/F_{sgl}^2	✔	✔	✔
B	$(11\bar{1})/(1\bar{1}1)$	sgl. or two-fold sgl.	-b2/d3	F_{sgl}/F_{sgl}^2		✔	✔
AII	$(11\bar{1})$	sgl.	-b2	F_{sgl}			
C	$(35\bar{1})/(3\bar{1}5)$	one or two-fold dep. copl. and codir.	-b2,b1,-d1/ d3,-d1.b1	$F_{\{135\}}/F_{\{135\}}^2$	✔	✔	
G	$(35\bar{1})/(3\bar{1}5)$	one or two-fold dep. copl. and codir.	-b2,b1,-d1/ d3,-d1.b1	$F_{\{135\}}/F_{\{135\}}^2$	✔	✔	
D	{115}	two-fold dep. copl. and codir.	-b2,b1,-d1, d3,c2,-c3	$F_{\{115\}}$	✔	✔	
E	cells only	two-fold easily cross slipping codir.		F_{cell}	✔		
F	$(44\bar{1})$?	two-fold dep. copl. and codir.	-b2,b1,-d1,c2	$F_{\{441\}}$	✔		
	$(35\bar{1})/(3\bar{1}5)$?	two-fold dep. copl. and codir.	-b2,b1,-d1/ d3,-d1.b1	$F_{\{135\}}/F_{\{135\}}^2$		✔	
	$(11\bar{1})$?	copl.	-b2,b1	F_{copl}			✔

Table 7. Slip systems in the Bishop-Hill notation.

Plane	(111)			$(\bar{1}\bar{1}1)$			$(\bar{1}11)$			$(1\bar{1}1)$		
Direction	$[01\bar{1}]$	$[\bar{1}01]$	$[1\bar{1}0]$	$[0\bar{1}\bar{1}]$	[101]	$[\bar{1}10]$	$[01\bar{1}]$	[101]	$[\bar{1}\bar{1}0]$	$[0\bar{1}\bar{1}]$	$[\bar{1}01]$	[110]
Notation	a1	a2	a3	b1	b2	b3	c1	c2	3	d1	d2	d3

9.3 Slip systems from lattice rotations

The five strain components (ε_{ij}) and the three rotation components (r_{ij}), which constitute the symmetric and antisymmetric parts, respectively, of the displacement gradient tensor are related to the shears on the individual slip systems (γ^k) according to the following equation:

$$\varepsilon_{ij} = \sum_{k=1}^{8} \gamma^k (b_i^k n_j^k + b_j^k n_i^k)/2$$
$$r_{ij} = \sum_{k=1}^{8} \gamma^k (b_i^k n_j^k - b_j^k n_i^k)/2 \qquad \text{Eq. 3}$$

with b=(b_1,b_2,b_3) and n=(n_1,n_2,n_3) being the unit vectors representing the slip direction and slip plane normal, respectively, in the sample coordinate system.

Three different calculation methods imposing different bounds on the strain components have been employed in the present study. The elongation along the tensile axis is fixed to the nominal elongation of the sample (in this case 6%) in all the methods but the contraction ratio of each grain as well as the shear strain components are allowed different degrees of freedom:

- The *axisymmetric method* enforces an axisymmetric strain with no shear strains.
- The *intermediate method* allows shear strain components and deviations from symmetric contraction of up to 15 % of the elongation.
- The *unrestricted method* requires that the largest component of the strain is elongation but otherwise allows the contraction as well as shear strains to vary freely.

of inequalities and equations (see [A10] for details). By analogy with the conventional Taylor model numerous slip system combinations satisfying the criteria are possible but the one giving the minimum plastic work, assuming identical critical shear stresses of all systems, is selected.

The fraction of slip belonging to each slip class is determined based on the calculated slip systems and using the parametrisation from Chapter 6. Within the two regions (AI and E) where three rotation trends coexist the calculations have been made separately for each

trend. Tables listing these parameters for each of the regions in Fig. 37d calculated with each of the three methods are found in the appendix of [A10].

9.4 Slip systems from both dislocation structure alignment and lattice rotations

Table 6 includes the result of comparing the highest parameter obtained from the lattice rotations with that expected from the dislocation structure alignment. At least one of the three calculation methods succeeded in all regions, except for region AII. In general, the axisymmetric and intermediate methods each produced slip systems in agreement with the dislocation structure for six of the eight regions.

For region AII, where single slip is expected based on the dislocation structure, the slip systems matching the lattice rotations do not give the highest value for F_{sgl} for any of the three methods. However, for the unrestrictred method F_{sgl} is the second highest parameter (after F_{sgl}^2) and inspection of the detailed slip systems reveals that a single system on average accounts for most (58 %) of the total slip calculated with the unrestricted method, which may also be achieved with a bound on the shear strains and contractions of 25 % of the elongation instead of the 15 % used in the intermediate method, i.e. still with fairly tight bounds on the strain tensor.

The identified slip systems are reported in Table 8 in the form of the dominant systems, which are those deduced to be active based on both dislocation structure alignment and lattice rotations. These dominant systems account for 54-90 % of the total slip, depending on region and calculation method. A more detailed analysis of the slip system activity as calculated from the rotations reveals that each of the dominant systems is active in practically all the grains in the region and accounts for at least 8 % of the total slip. Additional systems are also active in some regions as listed in Table 8, where a major additional system is interpreted as a system, which on average accounts for 5 % or more of the slip in the region and is also active in at least half of the grains. By contrast to the dominant systems the identity and number of additional major systems depend on the calculation method, i.e. on the enforced bounds on the strain. Together the dominant and major additional systems account for more than 70 % of the slip and in most cases this approaches 90 %.

Table 8. Dominant slip systems and major additional systems identified for each region. The major addional systems depend on the calculation method.

Region	Dominant systems	Method	Additional major systems
AI-down	-a2>>-b2,d3	axi	a3,b3,-c3,c2
		int	a3
		unr	a3,b3
AI-none	-b2,d3>>-a2	axi	a3,b1,-d1
		int	a3
		unr	a3,-d2
AI-up	-b2>>d3,-a2	axi	a3,-d1,b1
		int	a3,-d1
		unr	none
B	-b2,d3	int	-d1,b1,-a2,a3
		unr	-d1,-a2
AII	-b2	unr	b1 ,-a2
C	-b2,b1,-d1,d3	axi	none
		int	none
G	-b2,b1,-d1	axi	a3,-c3,c2,d2
		int	a3
D	-b2,b1,-d1, d3,c2,c3	axi	none
		int	none
E-down	a3,b3,-a2,-d2	axi	c2,-c3,-b2
E-none	-b2,-c2,c3, d3,a3,b3	axi	-a2
E-up	-b2,-c2,a3,b3	axi	-a2,-d1
F	-b2,b1,c2,-d1	axi	none
	-b2,b1,-d1	int	c2
	-b2,b1	unr	-d1

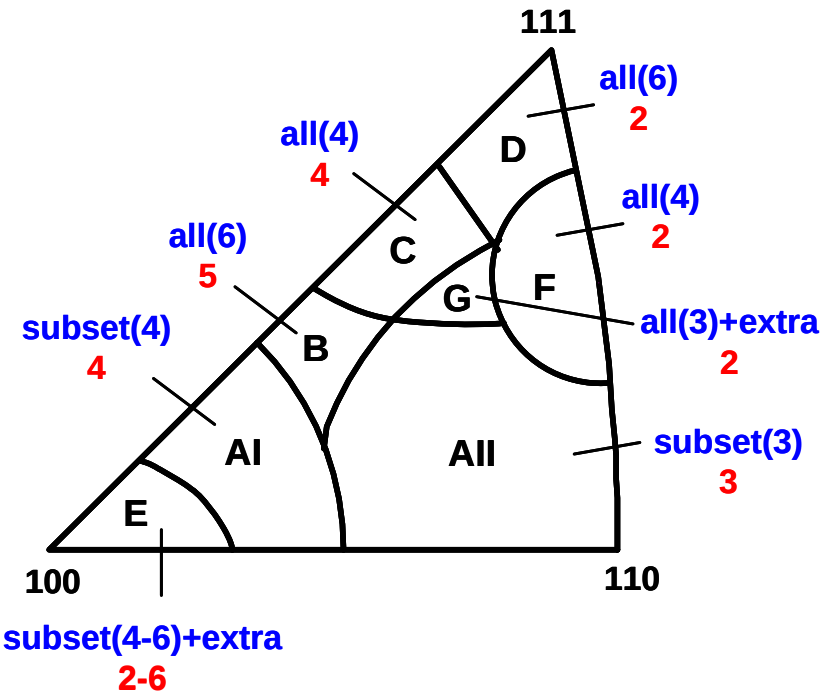

Fig. 38. Comparison with the Taylor model (average ambiguity solution) and Schmid factors. Blue labels indicate that the systems identified here are all or a subset of the Taylor systems (number of common active systems indicated in parenthesis; +extra indicates systems not predictged by Taylor). Red labels designate how many of the identified systems correspond to those with the highest Schmid factors.

9.5 Comparison with the Taylor model and Schmid factors

While the slip systems calculated by the Taylor model have in the previous chapters been seen to lead to predictions of dislocation structure alignment and lattice rotations which reproduce some of the main trends observed in the experimental data, it was concluded that limitations of the Taylor model resulted in inaccurate prediction of many details. In parallel to the comparisons with the Taylor model, comparisons with slip systems predicted based on Schmid factors have also been made throughout the thesis, sometimes showing better agreement with the experimental observations. Comparison of the systems identified here in Table 8 with the systems predicted by the Taylor model and those with the highest Schmid factors is therefore of interest. The slip systems calculated with the intermediate method are selected for this comparison, except for regions E and AII where only the axisymmetric and unrestricted method, respectively, was successful.

The comparison with the Taylor model is conducted using the average solution to the ambiguity problem. The criterion applied to the Taylor systems to identify the dominant and additional major systems is analogous to those used in Table 8 for the systems identified here, requiring that the systems must account for more than 5 % of the total slip fraction. Note that this criterion gives another subdivision of the triangle than that normally seen for the Taylor model (and used for the comparison in Chapter 5), where all systems are included. The number of common systems for the Taylor model and the method used

here is given for each region in Fig. 38. In all cases the systems deduced here include all or a subset of those predicted by the Taylor model.

The number of systems identified here, which are also the systems with the highest Schmid factors, is also stated in Fig. 38. It is seen that in all cases at least the two systems with the highest Schmid factors are activated. A closer analysis reveals that system –d1 is often activated even though its Schmid factor is not among the highest (it is typically about half of the highest value). The fact that this system is among the Taylor systems shows that it is activated to maintain strain compatibility. In the cases where a large number of systems with high Schmid factors are active (e.g. regions C and D) they may also have Schmid factors which differ by a factor of about two, showing that besides the uniaxially applied stress the effect of the constraints from the other grains must be considered. The consistent deduction of the same systems within a region, however, shows that the effect of having an environment of neighbouring grains is larger than the effects originating from the specific orientation, shape, etc. of these neighbours.

9.6 Variations within regions

With respect to the variations within each region, it is noted that the variations in both dislocation strucuture alignment and lattice rotations in regions B and C originate from different relative activation of the primary and conjugate systems (-b2 and d3), which have the same Schmid factors exactly on the [100]-[111] line. Dominance of the primary system results in GNBs aligned with the primary slip plane and rotations towards the [100]-[111] line while the conjugate system leads to GNBs aligned with the conjugate slip plane and rotation away from the line.

In region AI the dominant system varies between the primary, conjugate and critical systems, which have the three highest Schmid factors, giving rise to the three observed rotation trends in the regions and GNBs aligned with one or two slip planes. Although the rotations in region E are similar to those in region AI, region E exhibits no GNBs but only cells. This difference is remarkably well accounted for by differences in the identified slip systems, which in region E also include the cross slip systems to the primary, conjugate and critical systems. By analogy with region AI the three trends in region E can be attributed to preferred activation of one or two of the three most stressed systems. These systems appear to somehow exclude each other. As only the axisymmetric method succeeded in region E, grain-to-grain variations in the strain does not seem to explain this. The origin of the three trends is therefore likely to be a factor not considered here, for example specific dislocation interactions.

9.7 Conclusions

The existence of slip systems which are in agreement with both dislocation structure alignment data and measured lattice rotations validates the basic idea of the modelling scheme presented in Chapter 1 for coupled evolution of deformation textures and dislocation structures.

In agreement with this modelling scheme, the grain orientation is identified as the primary parameter controlling the slip systems as also evidenced by the fact that the identified systems are in overall agreement with those predicted by the Taylor model and the Schmid factors, i.e. with standard boundary conditions in terms of strain and stress on individual grains.

The variation between the regions of the stereographic triangle originates from activation of different ensembles of slip systems in grains of different orientation. The variation within each region is traced to selection of the most active system among those with the highest Schmid factors. The factor controlling the latter variations may to some extent be local stress/strain variations but not all variations were directly explainable by this.

While not directly extendable to a model for slip system prediction, the method introduced here may be applied to determine the active slip systems and their relative activities also for other cases, e.g. rolling. Such an expansion to other deformation modes may eventually provide sufficient insight to formulate a predictive model. In the mean time a critical test of existing models for slip system prediction is to evaluate their ability to reproduce the coupling between dislcoation structure alignment and lattice rotations.

10 Conclusions and outlook

The validity of the modelling scheme proposed in Chapter 1 for the coupled evolution of deformation textures and dislocation structures through their mutual dependence on the slip systems has been demonstrated for fcc metals of medium to high stacking fault energy deformed to low and intermediate strains. The studies concluded that:

- The crystallographic orientation of a grain with respect to the deformation axes is the basic parameter to be considered in the modelling:
  - The dislocation structure alignment is grain orientation dependent. In particular extended planar dislocation boundaries (GNBs) align with crystallographic planes specific to the grain orientation, of which some are slip planes while others are not, as demonstrated for low and intermediate strains.
  - Lattice rotations of individual grains deeply embedded in the bulk of the sample also exhibit grain orientation dependence, as demonstrated at low strain.
- The role of the grain orientation is to determine the dominant active slip systems. The active slip systems are the true factor on which the dislocation structure alignment and lattice rotations depend:
  - Unambiguous relations between slip systems and the dislocation structure alignment have been established in the form of slip classes, i.e. slip system combinations with a specific geometric relationship, which when activated in grains of different orientations and in different deformation modes lead to a specific crystallographic alignment of the dislocation structure.
  - Slip systems which are in agreement with data on both dislocation structure alignment and lattice rotations have been identified, proving the coupling of the two types of internal structural evolution in metals.
- Analysis of the dislocation structure alignment – supplemented by lattice rotations – demonstrates that the dominant active slip systems are those expected from a Schmid factor analysis or the Taylor model.
  - For tension such analysis has been conducted over the entire orientation space.
  - For rolling such analysis has been conducted for the stable rolling texture orientations and preliminary results have demonstrated the potential for other orientations. Further characterisation of the dislocation structure alignment is needed to cover the entire orientation space.
- The technological relevance of the inclusion of the dislocation structure alignment in crystal plasticity modelling is two-fold:
  - The slip class concept allows prediction of the dislocation structure alignment when the slip systems are known. At the time of proposing the modelling scheme this was the major missing component. That this gap is now sufficiently filled to allow practical implementation of the modelling scheme is exemplified by the modelling of the flow stress anisotropy of rolled sheets, showing that inclusion of the aligned dislocation structure provides significant improvements to predictions based on texture alone.

  - The slip class concept allows deduction of the slip systems when the dislocation structure alignment is known. This is a new tool for direct evaluation and improvement of models for slip system prediction and therefore also better deformation texture simulations.

- The results of this thesis, which apply to the scale of the entire grain, form a solid basis for future studies at a smaller length scale:
  - Establishment of the active slip systems at the grain scale opens up for studies of the slip system differences within the grain, which lead to formation and evolution of the GNBs. Most importantly the GNBs resulting from the different slip classes should be investigated separately. While they may adhere to a common underlying principle, for example LEDS, their differences imply that the dislocation interactions involved are somewhat different.

References

Author's own references:

[A1] Winther G. In: Szpunar, editors. Proceedings of ICOTOM 12. Montreal; 1999. p. 387.
[A2] Winther G, Huang X, Godfrey A, Hansen N. Acta Mater. 2004;52:4437.
[A3] Winther G, Huang X, Hansen N. Acta Mater. 2000;48:2187.
[A4] Winther G, Juul Jensen D, Hansen N. Acta Mater. 1997;45:5059.
[A5] Winther G. Acta Mater. 2003;51:417.
[A6] Winther G, Huang X. Phil. Mag. A 2007;87:5215.
[A7] Winther G, Juul Jensen D, Hansen N. Acta Mater. 1997;45:2455.
[A8] Winther G. Scripta Mater. 2005;52:995.
[A9] Winther G, Margulies L, Schmidt S, Poulsen HF. Acta Mater. 2004;52:2863.
[A10] Winther G. Acta Mater. in print.
[A11] Margulies L, Winther G, Poulsen HF. Science 2001;291:2392.
[A12] Winther G, Margulies L, Poulsen HF, Schmidt S, Larsen AW, Lauridsen EM, Nielsen SF, Terry A. Mat. Sci. Forum 2002;408-412:287.
[A13] Poulsen HF, Margulies L, Schmidt S, Winther G. Acta Mater. 2003;51:3821.
[A14] Huang X, Winther G. Phil. Mag. A 2007;87:5189.
[A15] Driver JH, Winther G. La Revue de Metallurgie-CIT/Science et Genie des Materiaux 1997:1021.
[A16] Winther G. In: Carstensen JV, Leffers T, Lorentzen T, Pedersen OB, Sørensen BF, Winther G, editors. Proceedings of 19th Risø Symposium. Risø, Denmark; 1998. p. 185.
[A17] He Y, Huang X, Hansen N, Winther G. Mat. Sci. Techn. 2005;21:1471.
[A18] Winther G. Mat. Sci. Eng. 2001;A309-310:486.
[A19] Winther G. In: Hansen N, Huang X, Juul Jensen D, Lauridsen EM, Leffers T, Pantleon W, Sabin TJ, Wert JA, editors. Proceedings of 21st Risø International Symposium on Materials Science: Recrystallization - Fundamental aspects and relations to deformation microstructure. Risø, Denmark; 2000. p. 653.
[A20] Li ZJ, Winther G, Hansen N. Acta Mater. 2006;54:401.
[A21] Winther G, Leffers T, Clausen B. In: Szpunar J, editors. Proceedings of ICOTOM 12. Montreal; 1999. p. 399.

Other references:

[22] Liu Q, Juul Jensen D, Hansen N. Acta Mater. 1998;46:5819.
[23] Barrett CS, Levenson LH. Transactions of the American Institute of Mining and Metallurgical Engineers 1940;137:112.
[24] Panchanadeeswaran S, Doherty RD. Scripta Metall. Mater. 1993;28.
[25] Panchanadeeswaran S, Doherty RD, Becker R. Acta Mater. 1996;44:1233.
[26] Bhattachayya A, El-Danaf E, Kalidindi SR, Doherty RD. Int. J. Plast. 2001;17:861.
[27] Wu GL, Godfrey A, Liu Q. Texture and deformation structure evolution during rolling of individual grains of columnar grain nickel. Textures of Materials, Pts 1 and 2, vol. 408-4. 2002. p.589.
[28] Kalidindi SR, Bhattacharyya A, Doherty RD. Proc. Phys. Soc. 2004;460:Surya R. Kalidindi.
[29] Kalidindi SR, Bhattachayva A, Doherty RD. Advanced Materials 2003;15:1345.
[30] Sachs G. Z. Ver. Deu. Ing. 1928;72:734.
[31] Taylor GJ. Journal of the Institute of Metals 1938;62:307.
[32] Bishop J, Hill R. Phil. Mag. 1951;42:414.
[33] Canova GR, Fressengeas C, Molinari A, Kocks UF. Acta Metall. 1988;36:1961.
[34] Kocks UF, Canova GR. In: Hansen N, Horsewell A, Leffers T, Lilholt H, editors. Proceedings of 2nd Risø international symposium on deformation of polycrystals: Mechanisms and microstructures. Risø, Denmark; 1981. p. 35.
[35] Molinari A, Canova GR, Ahzi S. Acta Metall. 1987;35:2983.
[36] Van Houtte P, Delannay L, Samajdar I. Textures Microstruct. 1999;31:109.
[37] Mika DP, Dawson PR. Mat. Sci. Eng. A 1998;257:62.
[38] Lebensohn R. Acta Mater. 2001;49:2723.
[39] Kocks U. J. Eng. Mater. Technol. 1976;98:76.
[40] Kocks U, Mecking H. Prog. Mater. Sci. 2003;48:171.
[41] Bay B, Hansen N, Hughes DA, Kuhlmann-Wilsdorf D. Acta Metall. Mater. 1992;40:205.
[42] Gil-Sevillano J, Torrealdea FJ. In: Hansen N, Jones AR, Leffers T, editors. Proceedings of 2nd Risø International Symposium on Metallurgy and Materials Science: Deformation of Polycrystals: Mechanisms and Microstructures. Risø, Denmark; 1981. p. 185.
[43] Huang X, Leffers T, Hansen N. In: Bilde-Sørensen JB, Carstensen JV, Hansen N, Jensen DJ, Leffers T, Pantleon W, Pedersen OB, Winther G, editors. Proceedings of 20th Risø International Symposium on Materials Science: Deformation-Induced Microstructures: Analysis and Relation to Properties. Risø, Danmark; 1999. p. 365.
[44] Huang X, Hansen N. Mat. Sci. Eng. A 2004;387-389:186.
[45] Hughes DA, Liu Q, Chrzan DC, Hansen N. Acta Mater. 1997;45:105.
[46] Nabarro FRN. Scripta Metall. Mater. 1994;30:1085.
[47] Pantleon W. Acta Mater. 1998;46:451.
[48] Pantleon W. Mat. Sci. Eng. A 2005;400-401:118.
[49] Godfrey A, Hughes DA. Acta Mater. 2000;48:1897.
[50] Hughes DA, Hansen N. Phys. Rev. Let. 2001;87:135503.
[51] Hughes DA, Hansen N. Acta Mater. 2000;48:2985.
[52] Liu Q, Huang X, Lloyd DJ, Hansen N. Acta Mater. 2002;50:3789.
[53] Kühlmann-Wilsdorf D. Mat. Sci. Eng. 1989;A113:1.
[54] Hughes DA, Khan S, Godfrey A, Zbib H. Mat. Sci. Eng. A 2001;309:220.
[55] McCabe RJ, Misra A, Mitchell TE. Acta Mater. 2004;52:705.

[56] Wert JA, Liu Q, Hansen N. Acta Metall. Mater. 1995;43:4153.
[57] Basson F, Driver JH. Mat. Sci. Eng. A 1998;A256:243.
[58] Haldar A, Huang X, Leffers T, Hansen N, Ray R. Acta Mater. 2004;52:5405.
[59] Hansen N, Juul Jensen D. Acta Metall. Mater. 1992;40:3265.
[60] Rollett AD, Juul Jensen D, Stout MG. In: Andersen SI, Bilde-Sørensen JB, Hansen N, Jensen DJ, Leffers T, Lilholt H, Lorentzen T, Pedersen OB, Ralph B, editors. Proceedings of 13th Risø Symposium. Denmark; 1992. p. 93.
[61] Peeters B, Kalidindi SR, Van Houtte P, Aernoudt E. Acta Mater. 2000;48:2123.
[62] Peeters B, Seefeldt M, Teodosiu C, Kalidindi SR, Van Houtte P, Aernoudt E. Acta Mater. 2001;49:1607.
[63] Huang X, Hansen N. Scripta Mater. 1997;37:1.
[64] Huang X, Borrego A, Pantleon W. Mat. Sci. Eng. A 2001;319-321:237.
[65] Huang X. Scripta Mater. 1998;38:1697.
[66] Liu Q, Hansen N. Phys. stat. sol. (a) 1995;149:187.
[67] Huang X. Mat. Sci. Techn. 2005;21:1379.
[68] Barlow C, Bay B, Hansen N. Phil. Mag. A 1985;51:253.
[69] Randle V, Hansen N, Juul Jensen D. Phil. Mag. A 1996;73:265.
[70] Poulsen HF. Three-dimensional X-ray diffraction microscopy. Mapping polycrystals and their dynamics: Springer, Berlin, 2004.
[71] Lauridsen EM, Schmidt S, Suter RM, Poulsen HF. J. Appl. Cryst. 2001;34:744.
[72] Kang J-Y, Bacroix B, Re´gle´ H, Oh KH, Lee H-C. Acta Mater. 2007;55:4935.
[73] Joo H, Kim J, Kim K, Tamura N, Koo Y. Scripta Mater. 2004;51:1183.
[74] Steeds JW. Proc. Roy. Soc. A 1966;292:343.
[75] Basinski ZS. Disc. Faraday Soc. 1964;93:38.
[76] Basinski ZS, Basinski SJ. Phil. Mag. 1964;9:51.
[77] Essmann U, Raap M, Wilkens M. Acta Metall. Mater. 1968;16:1275.
[78] Kawasaki Y. Journal of the physical society of Japan 1974;36:142.
[79] Kawasaki Y. Relationship between deviations from slip planes and slip systems of layered dislocation structures in deformed copper single crystals. In: Oikawa, editor. Strength of materials. The Japan Institute of Metals, 1994. p.187.
[80] Malin A, Huber J, Hatherly M. Z. Metallk. 1981;72:310.
[81] Nakayama Y, Morii K. Transactions of the Japan Institute of Metals 1982;23:422.
[82] Wróbel M, Dymek S, Blicharski M, Gorczyca S. Z. Metallkd. 1994;85:415.
[83] Wróbel M, Dymek S, Blicharski M, Gorczyca S. Textures and Microstuctures 1988;10:9.
[84] Morii K, Mecking H, Nakayama Y. Acta Metall. 1985;33:379.
[85] Morii K, Nakayama Y. Scripta Metall. 1985;19:185.
[86] Driver JH, Juul Jensen D, Hansen N. Acta Metall. Mater. 1994;42:3105.
[87] Godfrey A, Juul Jensen D, Hansen N. Acta Mater. 1998;46:835.
[88] Godfrey A, Juul Jensen D, Hansen N. Acta Mater. 1998;46:823.
[89] Feller-Kniepmeier M, Wanderka N. In: Kallend JS, Gottstein G, editors. Proceedings of ICOTOM 8. 1988. p. 517.
[90] Kawasaki Y, Takeuchi T. Scripta Metall. 1980;14:183.
[91] Wert JA, Liu Q, Hansen N. Acta Mater. 1997;45:2565.
[92] Bay B, Hansen N, Kuhlmann-Wilsdorf D. Mat. Sci. Eng. 1989;A113:385.
[93] Lopez-Pedrosa M, Wynne B, Rainforth W. J. Microscopy 2006;222:97.
[94] Hurley PJ, Bate P, Humphreys FJ. Acta Mater. 2003;51:4737.
[95] Juul Jensen D, Hansen N. Acta Metall. Mater. 1990;38:1369.
[96] Wilson DV, Bate PS. Acta Mater. 1996;44:3371.

[97] Akbari GH, Sellars CM, Whiteman JA. Acta Mater. 1997;45:5047.
[98] Hughes DA, Hansen N. Mat. Sci. Techn. 1991;7:544.
[99] Bay B, Hansen N, Kuhlmann-Wilsdorf D. Mat. Sci. Eng. 1992;A158:139.
[100] Leffers T, Christoffersen H. Mat. Sci. Forum 1998;273-275:77.
[101] Zhu Q, Sellars CM. Scripta Mater. 2001;45:41.
[102] Humphreys FJ, Bate PS. Acta Mater. 2006;54:817.
[103] Randle V. Journal of Microscopy-Oxford 1999;195:226.
[104] Fengxiang L, Godfrey A, Liu Q. Key Engineering Materials 2007;353-358.
[105] Frank F. In: editors. Proceedings of Plastic deformation of crystalline solids. Mellon Institute, Pittsburgh; 1950. p. 150.
[106] Becker R, Butler JF, Hu H, Lalli LA. Met. Trans. A 1991;22A:45.
[107] Li ZJ, Godfrey A, Liu Q. Scripta Mater. 2001;45:847.
[108] Liu Q, Hansen N. Proc. Roy. Soc. A 1998;454:2555.
[109] Knudsen T. An experimental study of plastic deformation in metals. PhD thesis. Roskilde University, 2008.
[110] Eardley ES, Coulet A, Court SA, Humphreys F, Bate P. Mat. Sci. Forum 2003;426-432:363.
[111] Eardley ES, Humphreys F, Court SA, Bate P. Mat. Sci. Forum 2002;396-402:1085.
[112] Juul Jensen D, Hansen N. In: Brandon DG, Chaim R, Rosen A, editors. Proceedings of ICSMA 9. Haifa; 1991. p. 179.
[113] Hansen N. Mat. Sci. Eng. A 2005;409:39.
[114] Hansen N, Huang X, Hughes DA. Mat. Sci. Eng. 2001;A317:3.
[115] Lorentzsen T, Clausen B, Leffers T. In: Carstensen JV, Leffers T, Lorentzen T, Pedersen OB, Sørensen BF, Winther G, editors. Proceedings of 19th Risø International Symposium on Materials Science: Modelling of Structure and Mechanics of Materials from Microscale to Product. Roskilde, Denmark; 1998. p. 345.
[116] Delaire F, Raphanel JL, Rey C. Acta Mater. 2000;48:1075.
[117] Haldrup K, McGinty R, McDowell D. Submitted for publication.
[118] Leffers T. Phys. stat. sol. (a) 1995;149:69.
[119] Leffers T. In: Haasen P, Gerold V, Kostorz G, editors. Proceedings of 5th International Conference on Strength of Metals and Alloys. Aachen; 1979. p. 769.

Acknowledgements

The author gratefully acknowledges the Danish National Research Foundation for supporting the Center for Fundamental Research: Metal Structures in Four Dimensions, within which the vast majority of the studies behind this thesis have been conducted. She also wishes to thank all present and former members of the Center as well as members of the Materials Research Department for their help and interest in these studies. Similarly, Department and Center heads are thanked for providing excellent working conditions, in particular Dorte Juul Jensen and Niels Hansen who have encouraged this project and followed it closely from start to finish in various functions.

Special thanks are due to the co-authors of the included papers: Larry Margulies, Søren Schmidt and Henning Friis Poulsen for their work with 3DXRD and Xiaoxu Huang, Andrew Godfrey, Dorte Juul Jensen and Niels Hansen for fruitful collaboration on dislocation boundaries. Finally, my family deserves to be acknowledged for their patience and support, the technicians and secretaries of the department for all sorts of practical assistance and Brian Ralph for commenting on my manuscripts.

Dansk resume (Summary in Danish)

Opdagelsen af metallers formbarhed og styrke har haft stor betydning for udviklingen af det moderne samfund, hvor metaller stadig er en vigtig materialegruppe, der produceres og forarbejdes i store mængder. Formbarheden skyldes den særlige binding mellem atomerne i det krystallinske metalgitter, men metallets egenskaber er også betinget af strukturelementer på større skala, som kan manipuleres ved termomekanisk processering. En fundamentel forståelse for de mekanismer, der kontrollerer strukturudviklingen og ikke mindst de tilhørende mekaniske egenskaber, er vigtig for at opstille gode modeller, der kan anvise retningslinjer for optimering af processer og produkter i den metalliske industri.

Som illustreret i fig. 1 er et metal sammensat af mange forskellige korn, og de enkelte korn adskiller sig fra hinanden ved at deres krystallografiske gitter har forskellig orientering. Fordelingen af de krystallografiske kornorienteringer kaldes metallets *tekstur*. Ved mekanisk deformation af metallet ændres teksturen, dvs. det krystallografiske gitter for hvert korn roterer. Under formgivning af metallet dannes der desuden dislokationer inden i hvert korn, som samler sig i dislokationsvægge, som underopdeler kornet som vist i fig. 2. Nogle af disse vægge er kendetegnet ved at være plane og at følge det samme krystallografiske plan. I fig. 2 ses disse vægge som parallelle linjer.

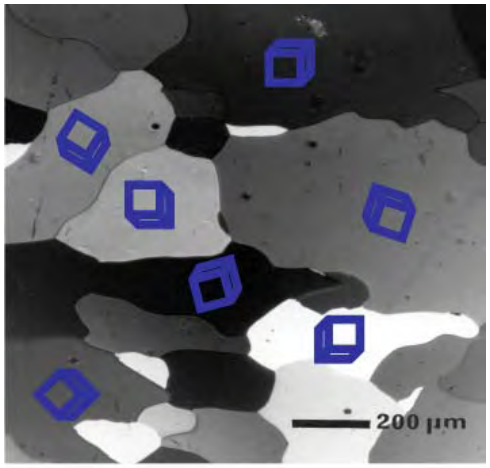

Figur 1. Optisk mikroskopibillede af en polykrystallinsk metaloverflade. De enkelte korn er representeret ved forskellige gråtoner. Orienteringen af det krystallografiske gitter i hvert korn er forskellig, som illustreret af de blå terninger.

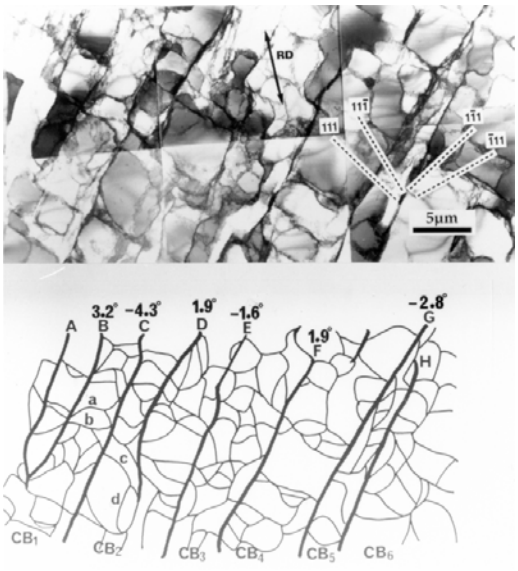

Figur 2. Transmissionselektron-mikroskopibillede af en typisk dislokationsstruktur i det indre af et korn efter en lav deformationsgrad ($\varepsilon<1$). Dislokationerne samles i dislokationsvægge, som er optegnet i den nederste del af figuren, hvor også den krystallografiske misorientering over nogle af de plane vægge er angivet.

Emnet for denne afhandling er analyse og modellering af orienteringen af de enkelte korns krystallografiske gitter, og specielt hvordan dette gitter roterer under plastisk deformation, samt de planer, som de parallelle dislokationsvægge ligger på i de enkelte korn. Udgangspunktet for arbejdet er de to fænomeners fælles relation til den mikroskopiske deformationsmekanisme i metallet, nemlig dislokationsglidning ved slip. Slip sker på bestemte krystallografiske planer i bestemte retninger – såkaldte slipsystemer. Det overordnede princip for modellering af den fælles afhængighed af slipsystemerne, som foreslået af forfatteren, er skitseret i figur 3. Det nye i dette princip i forhold til den traditionelle modellering er, at dislokationsstrukturen indgår som et centralt element. Ved dette arbejdes begyndelse var en sådan modellering overhovedet ikke mulig. Afhandlingen viser rigtigheden af princippet om den fælles afhængighed af slipsystemerne og udvikler en model til forudsigelse af dislokationsvæggenes planer. Princippets anvendelighed til modellering af mekaniske egenskaber demonstreres endvidere.

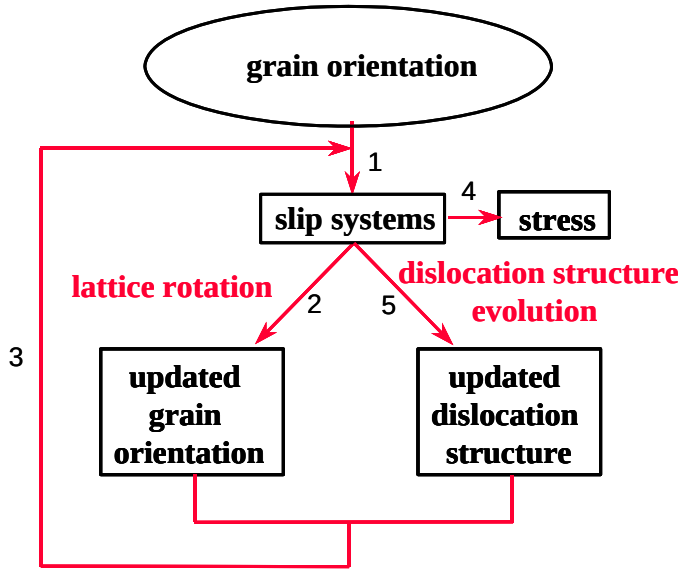

Figur 3. Illustration af princippet om at kornrotationer og dislokationsstrukturer er koblede gennem en fælles afhængighed af de aktiverede slipsystemer i det enkelte korn.

Den eksperimentelle basis for afhandlingen er data fra studier af dislokationsvægges planer med transmissionselektronmikroskopi og data fra studier at enkelte korns gitterrotationer med tredimensionel røntgendiffraction (3DXRD). Disse eksperimentelle undersøgelser er foretaget af forfatterens samarbejdspartnere, undertiden med medvirken fra forfatteren.

De undersøgte materialer er aluminium og kobber med forskellige renheder og kornstørrelser, og al deformation er foretaget ved stuetemperatur (see **afhandlingens kapitel 2** for en komplet oversigt). Undersøgelserne har ikke påvist væsentlige forskelle mellem disse materialer, og resultaterne i denne afhandling anses derfor for at være repræsentative for relativt rene metaller med fladecentreret kubisk krystalstruktur og middel til høj stabelfejlenergi.

Arbejdet er beskrevet i 10 videnskabelige artikler, der er vedlagt som bilag. Afhandlingen kan inddeles i et antal hovedafsnit, hvoraf de to første omhandler henholdsvis dislokationsvægge og gitterrotationer og det tredje kobler de to fænomener gennem deres fælles afhængighed af slip systemerne.

1 Dislokationsvægge

Denne del af arbejdet er den mest omfattende og falder i tre underafsnit:

Afhandlingens kapitel 4: ***Bestemmelse af det kornorienteringsafhængige krystallografiske plan for dislokationsvæggene***, hvor forfatterens bidrag primært har været at fastslå, at vægplanet ikke nødvendigvis er et krystallografisk slipplan, men altid afhænger af kornorienteringen. I det makroskopiske koordinatsystem givet af deformationsakserne ligger væggene tæt på de planer, der har den største resulterende spænding, men analysen viser, at ikke alle sådanne makroskopiske planer faktisk er dislokationsvægplaner, og at den krystallografiske præference er stærkere end den makroskopiske. Netop dette spørgsmål har i mange år været debatteret, og afhandlingens resultat viser, at den videre modellering af væggene skal baseres på de krystallografiske slipsystemer.

Afhandlingens kapitel 5 og 6: *Analyse og modellering af relationerne mellem dislokationsvæggenes krystallografiske planer og slipsystemer* - først med fokus på de vægge, der ligger på slipplaner, og siden udvidet til at omfatte alle de vægplaner, der optræder efter deformation med to forskellige metoder, nemlig valsning og træk. Netop anvendelsen af mere end én deformationsmetode har været væsentlig for at foretage en generel analyse og at demonstrere, at det er slipsystemerne, der er årsag til de foretrukne krystallografiske vægplaner. Mere konkret er der etableret entydige relationer mellem visse kombinationer af slipsystemer (her kaldet slipklasser) og dislokationsvægge på specifikke krystallografiske planer. Hver slipklasse består af slipsystemer, der geometrisk er relateret til hinanden på en bestemt måde. Relationerne mellem slipklasser og vægplaner gælder uanset kornorientering og deformationsmetode og kan således anvendes prædiktivt.

Afhandlingens kapitel 7: *Anvendelse af slipklassebegrebet til modellering af dislokationsvægplaner og deraf følgende mekaniske egenskaber.* Det valgte eksempel er den anisotrope flydespænding i en valset metalplade, der er betydningsfuld i forbindelse med mange formgivningsoperationer. Det er tidligere vist, at dislokationsvæggenes foretrukne planer i forhold til de makroskopiske deformationsakser giver et betydeligt bidrag til anisotropien. I afhandlingen modelleres væggenes krystallografiske planer i de enkelte korn og derefter deres bidrag til de mekaniske egenskaber vha. deres interaktion med de enkelte slipsystemer. Det vises, at en god forudsigelse af dislokationsvæggenes krystallografiske planer er vigtig for en succesrig modellering af flydespændings-anisotropien. Udover dette teknologisk vigtige resultat viser eksemplet, at den mest udbredte krystalplasticitetsmodel (Taylormodellen) til forudsigelse af hvilke slipsystemer, der aktiveres i enkelte korn, i nogle tilfælde er utilstrækkelig.

2 Gitterrotationer

Afhandlingens kapitel 8: ***Kortlægning af kornorienteringsafhængigheden af gitterrotationerne*** for et stort antal korn under deformation i træk konkluderer, at gitterrotationerne udviser en tydelig kornorienteringsafhængighed. Hele det rum af kornorienteringer, der er relevant for træk, underopdeles i regioner med karakteristiske rotationer. De eksperimentelle rotationer sammenlignes med eksempler på forudsigelser fra forskellige typer modeller. Sammenligningen, der dog ikke er fuldstændigt komplet, viser, at modeller, der inkluderer specifikke interaktioner mellem nabokorn, ikke nødvendigvis giver en bedre overordnet forudsigelse end modeller, der udelukkende baserer sig på det enkelte korns orientering. I lighed med konklusionerne omkring dislokationsvægge afsløres visse uoverensstemmelser mellem Taylormodellens forudsigelser og de eksperimentelle data.

3 Kobling af dislokationsvægge og gitterrotationer

Afhandlingens kapitel 9: Koblingen mellem dislokationsvægge og gitterrotationer gennem den fælles relation til slipsystemerne udnyttes til at bestemme de aktive slipsystemer under trækdeformation. Over hele orienteringsrummet for trækdeformation anvendes slipklassebegrebet til at deducere slipsystemerne ud fra de observerede krystallografiske planer af dislokationsvæggene, og uafhængigt heraf gennemføres en tilsvarende slipsystemanalyse for gitterrotationerne. Der er god overensstemmelse mellem de to sæt slipsystemer i alle regioner af orienteringsrummet. De identificerede systemer er i stor udstrækning dem, der forventes ud fra enten Taylormodellen eller en Schmidfaktoranalyse, hvilket giver retningslinjer for fremtidig forbedring af de krystalplasticitetsmodeller, der i teknologisk sammenhæng også bruges til modellering af udviklingen af deformationsteksturer. Især analyse af dislokationsvæggenes krystallografiske planer etableres hermed som et nyt og væsentligt værktøj til identifikation af de dominerende slipsystemer.

APPENDICES:

Published papers

A1: Coupling textural and microstructural evolution by G. Winther, Proc. ICOTOM12, 1999.

Proc. ICOTOM 12, Montreal, 1999, ed. Szpunar, p. 387-392

COUPLING TEXTURAL AND MICROSTRUCTURAL EVOLUTION

Coupling textural and microstructural evolution

G. Winther
Materials Research Department, Risø National Laboratory, Roskilde, Denmark

Abstract

A new modelling scheme which couples the evolution of texture and dislocation microstructure is presented. One component of this modelling is an extension of standard polycrystal plasticity models which predicts the slip pattern from the crystallographic orientation of a grain and its dislocation microstructure. The other components consist of updating steps of both texture and dislocation structure. The current status of the components in the model are discussed and a realistic implementation is proposed.

Keywords: Polycrystals, microstructure, dislocation boundaries, texture

1 Introduction

Plastic deformation occurs by slip on a number of slip systems in the individual grains in a polycrystal. Slip pattern prediction is therefore the essential element in modelling of polycrystal plasticity. Traditionally, polycrystal plasticity models are used to calculate the slip pattern in individual grains merely from their crystallographic orientation by enforcing various types of boundary conditions concerning strain and stress compatibility between the grains.

Contributions from microstructures within the grains have not been included in the polycrystal plasticity models although there is experimental evidence that both crystallographic precipitates in alloys (Vasudévan et al. 1996) and twins in fcc metals of low stacking fault energy (Leffers 1996) have an effect on texture, which cannot be modelled by the standard polycrystal plasticity models.

In fcc metals of medium to high stacking fault energy, the dominant microstructure consists of long, parallel dislocation boundaries. The fact that the grains are subdivided by these boundaries, which have a spacing of a few micrometers, must influence the slip pattern in the grain and the boundaries must therefore be considered in the models used to predict the slip pattern.

The dislocations in the dislocation boundaries are generated by slip on the active slip systems and the boundary characteristics, e.g. orientation and strength, therefore evolve during deformation. There is thus a coupling between the evolution of texture and microstructure that must be taken into account in the modelling. Neither textural nor microstructural evolution can be treated alone.

This paper presents a modelling scheme for the coupling. The scheme consists of a combination of a) slip pattern prediction taking the current texture and dislocation boundaries into account and b) prediction of the evolution of both texture and dislocation boundaries. Finally, the current state of the various components in the coupling model is discussed and an implementation which can be realised in the near future is proposed.

2 Effect of microstructure on slip pattern

The long parallel dislocation boundaries are geometrically necessary boundaries which separate small volumes of crystallographically misoriented material. The slip pattern in the misoriented material volumes must be different in order to create and increase the misorientation with strain. From geometric reasons alone, the presence of boundaries in the grain must therefore affect the slip pattern and it is basically incorrect to predict only one slip pattern in a grain with dislocation boundaries - although an average slip pattern may be obtainable.

Apart from being associated with slip pattern differences, the boundaries can also directly affect the slip pattern by offering resistance to slip like grain boundaries (Hansen and Juul Jensen 1992), which also separate material with different crystallographic orientations. The resistance may be enhanced by the fact that the boundary spacing is of the order of the slip length. Due to the resistance, slip parallel to the boundaries is easy while slip perpendicular to the boundaries become difficult. In addition to strengthening the material, this effect can be sufficient to activate slip systems that would not be active in the absence of the boundaries.

3 Microstructure, crystallographic grain orientation and slip pattern

There is a strong correlation between the type of dislocation structure developed in a grain and the crystallographic orientation of the grain for fcc metals deformed in both tension (Huang and Hansen 1997; Huang 1998) and rolling (Liu and Hansen 1995; Liu et al. 1998). A recent study of tensile deformed aluminium has shown that the dislocation boundaries form on certain crystallographic planes and that the crystallographic boundary orientation depends on the grain orientation. Based on the crystallographic orientation of the boundaries, the stereographic triangle representing all grain orientations in axisymmetric tension can be divided

into six regions. The details of this study will be presented elsewhere.

The correlation between grain orientation and microstructure is explained in terms of the slip pattern. Grains with similar orientations, i.e. grains lying in the same region in the triangle, have similar slip patterns. The active slip systems feed the dislocations to the boundaries and the boundary orientation in grains with similar slip patterns must therefore also be similar.

The subdivision of the triangle into regions with different microstructures is also a subdivision into regions with different slip patterns and microstructural studies can therefore provide new important information on the slip pattern.

The subdivision of the triangle is based on microstructural observations in aluminium deformed to tensile strains between 0.05 and 0.34. In this strain range the boundaries do not change their crystallographic orientation with strain. Still, the dislocations in the boundaries are accumulated over the whole deformation history and a strain effect must also be expected. In rolling, for example, the boundaries in samples deformed to low and high strains have neither the same crystallographic nor macroscopic orientations. At low strains the boundaries are inclined about 45° to the macroscopic rolling direction and at high strains they become roughly parallel to the rolling plane. This macroscopic orientation change cannot be explained by the macroscopic orientation change of boundaries on fixed crystallographic planes due to texture evolution and the crystallographic boundary plane in each grain must therefore change when going from low to high strains.

4 Modelling scheme for coupled textural and microstructural evolution

The coupling between textural and microstructural evolution is caused by the dependence of the slip pattern in an individual grain on both the crystallographic grain orientation and the microstructure combined with the fact that the slip pattern determines the evolution of both texture and microstructure.

Modelling of the coupled evolution of texture and microstructure must therefore follow the scheme outlined in Fig. 1. The scheme consists of three basic steps which are carried out for each grain orientation in the material: 1) prediction of the slip pattern in a grain from its current crystallographic orientation and dislocation microstructure, 2) updating of the grain orientation with a lattice rotation derived from the slip pattern and 3) updating of the dislocation microstructure with new dislocations which have their burgers vectors defined by the active slip systems and are generated in quantities depending on the shear amplitude of each slip system.

As illustrated in Fig. 1 the yield stress also depends on both grain orientation and dislocation structure and the yield stress is directly obtainable from the slip pattern. The coupling of textural and microstructural evolution and calculation of the yield stress at each updating step will therefore give the work hardening.

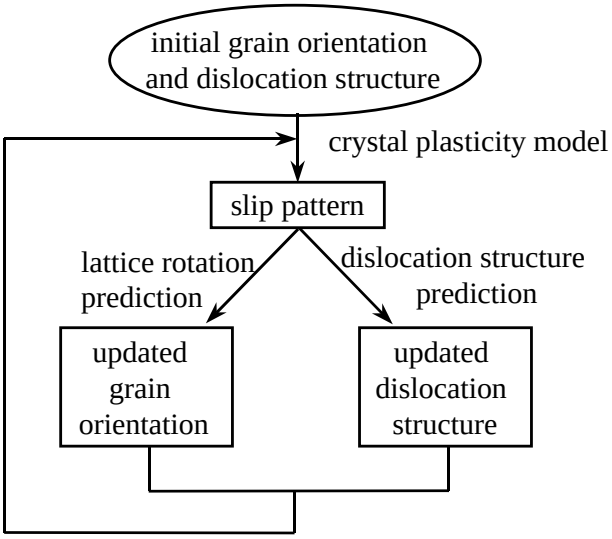

Fig. 1: Modelling scheme for the coupling between evolution of texture and dislocation microstructure.

5 Current implementation

The status of the three basic components is considered, leading to a currently realistic implementation of the modelling scheme outlined in Fig. 1.

Slip pattern prediction

The framework of the standard polycrystal plasticity models which are widely used for prediction of slip patterns without consideration of the dislocation microstructure has been extended to predict the effect of the dislocation boundaries.

The geometric effect of boundaries causing different slip patterns on the two sides of the boundaries has been modelled from a given boundary orientation assuming that each material volume deforms according to full constraints (Driver and Winther 1997) or relaxed constraints boundary conditions (Leffers 1994).

The resistance to slip offered by the boundaries has been modelled by assigning a critical resolved shear stress given by a Hall-Petch relation to the individual slip systems (Winther et al. 1997). The spacing between the boundaries in the slip plane is taken as the distance parameter in the Hall-Petch relation, and this distance depends on the relative orientation of the slip system and the boundary. So far this model has only been applied to predict the slip pattern in a grain after strain path changes, i.e. prediction of yield anisotropy, but the method is equally applicable to all models that are based on critical resolved shear stresses.

It is therefore concluded that models which take the microstructure into account when predicting the slip pattern are available. The strong correlation between grain orientation and microstructure type can be used in further evaluation of these models. The models must predict similar slip patterns for grain orientations with similar microstructures and different slip patterns for grain orientations with different microstructures.

Updating of grain orientation

Standard derivations of the lattice rotation from the slip pattern assuming that certain planes and directions are kept constant are available (see e.g. (Kocks and Chandra 1982) for a general description). The fact that the two volumes of material with different slip patterns on each side of a boundary must still meet at the boundary plane complicates the calculations but the problem can still be handled within the framework of the standard lattice rotation calculations (Leffers 1994).

Updating of dislocation microstructure

Unfortunately, the current understanding of the formation and evolution of the dislocation microstructure is definitely inadequate to allow formulation of general updating schemes for the dislocation structure based on the slip pattern and the deformation history, i.e. the arrow labelled ‘dislocation structure prediction’ in Fig. 1 cannot be realised at present.

The on-going microstructural studies are, however, beginning to establish sufficient experimental information on the dislocation microstructure that may serve as a database in which the necessary updating steps can be looked up. This implementation is presented in Fig. 2.

For example, the grain orientation dependence of the microstructure type in tensile deformed aluminium within moderate strain ranges suggests the following updating scheme: It is checked whether the grain has rotated to a new orientation with a different microstructure and if so the old microstructure is replaced with the proper type for the new orientation. To model the evolution over large strains, it is necessary to have several maps of the correlation between grain orientation and microstructure, each giving information on a specific strain range.

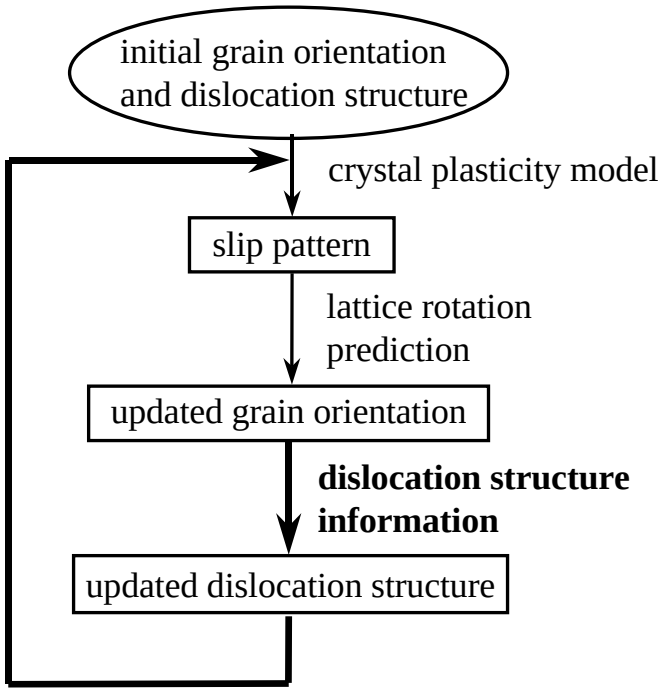

Fig. 2: Implementation with the current status of the basic components. Modifications to the modelling scheme in Fig. 1 are marked in bold.

6 Conclusion

A modelling scheme for the coupling of textural and microstructural evolution has been proposed. The model is based on the dependence of the slip pattern on both texture and dislocation microstructure combined with the importance of the slip pattern for the evolution of both texture and microstructure. A full implementation of this model is not possible at present – primarily due to insufficient theoretical understanding of the evolution of the dislocation microstructure. However, this understanding may be substituted by experimental characterisation of the microstructure, which is at a much more advanced state.

7 Acknowledgement

The author wishes to thank Dr. Niels Hansen for inspiring discussions and constructive criticism.

8 References

Vasudévan, A.K., Przystupa, M.A. and Fricke, W.G. (1996) Effect of composition on crystallographic texture in hot-rolled Al-Li-Cu alloys. *Materials Science and Engineering*, Vol. A208, No. pp. 172-180.

Leffers, T. (1996) The Brass-type texture once again. *Proc. of ICOTOM 11*. pp. 299-306.

Hansen, N. and Juul Jensen, D. (1992) Flow stress anisotropy caused by geometrically necessary boundaries. *Acta Metallurgica et Materialia*, Vol. 40, No. 12. pp. 3265-3275.

Huang, X. and Hansen, N. (1997) Grain orientation dependence of microstructure in aluminium deformed in tension. *Scripta Materialia*, Vol. 37, No. 1. pp. 1-7.

Huang, X. (1998) Grain orientation effect on microstructure in tensile strained copper. *Scripta Materialia*, Vol. 38, No. 11. pp. 1697-1703.

Liu, Q. and Hansen, N. (1995) Deformation microstructure and orientation of FCC crystals. *Phys. Stat. Sol. (a)*, Vol. 149, No. pp. 187-199.

Liu, Q., Juul Jensen, D. and Hansen, N. (1998) Effect of grain orientation on deformation structure in cold-rolled polycrystalline aluminium. *Acta Materialia*, Vol. 46, No. 16. pp. 5819-5838.

Driver, J.H. and Winther, G. (1997) Microtextures et hétérogénéités de deformation. *La Revue de Metallurgie-CIT/Science et Genie des Materiaux*, Vol. No. pp. 1021-1028.

Leffers, T. (1994) Lattice rotations during plastic deformation with grain subdivision. *Materials Science Forum*, Vol. 157-162, No. pp. 1815-1820.

Winther, G., Juul-Jensen, D. and Hansen, N. (1997) Modelling flow stress anisotropy caused by deformation induced dislocation boundaries. *Acta Materialia*, Vol. 45, No. 6. pp. 2455-2465.

Kocks, U.F. and Chandra, H. (1982) Slip geometry in partially contrained deformation. *Acta Metallurgica*, Vol. 30, No. pp. 695-709.

A2: Critical comparison of dislocation boundary alignment studied by TEM and EBSD: Technical issues and theoretical consequences by G. Winther, X. Huang, A. Godfrey and N. Hansen, Acta Materialia, 2004.

Available online at www.sciencedirect.com
SCIENCE DIRECT®
Acta Materialia 52 (2004) 4437–4446
Acta MATERIALIA
www.actamat-journals.com

Critical comparison of dislocation boundary alignment studied by TEM and EBSD: technical issues and theoretical consequences

G. Winther [a,*], X. Huang [a], A. Godfrey [b], N. Hansen [a]

[a] *Center for Fundamental Research: Metal Structures in 4D, Materials Research Department, Risø National Laboratory, P.O. Box 49, DK-4000 Roskilde, Denmark*
[b] *Department of Materials Science and Technology, Tsinghua University, 100084 Beijing, PR China*

Received 26 March 2004; accepted 22 May 2004
Available online 15 July 2004

Abstract

The plane of extended deformation induced boundaries (geometrically necessary boundaries) determined by transmission electron microscopy (TEM) has previously been found to be grain orientation dependent so that some grains have boundaries aligned with slip planes while others do not. However, in both types of grains the boundaries are aligned with macroscopic planes. A recently published analysis by electron backscattered diffraction (EBSD) found no evidence for alignment of boundaries with slip planes or any other simple crystallographic plane, i.e. only macroscopic alignment. This discrepancy is discussed based on a critical comparison of the TEM and EBSD based techniques and TEM observations of boundary planes in grains of selected orientations in cold-rolled aluminium. The latter clearly show that the EBSD finding is incorrect. The present analysis thereby confirms that grain orientation-dependent boundary planes is a general phenomenon.

Keywords: Dislocation boundaries; Transmission electron microscopy; Electron backscattering diffraction; Grain orientation dependence

1. Introduction

Microstructural characterisation and modelling of a variety of metals deformed by different thermomechanical processes have shown a universal structural evolution. Dislocations are generated during deformation and they accumulate in dislocation boundaries; typically extended dense dislocation walls and microbands, considered as geometrically necessary boundaries (GNBs) and short cell boundaries termed incidental dislocation boundaries (IDBs) [1,2].

The observed universal structural evolution has been related to general principles and processes that apply to the formation and storage of dislocations during plastic deformation. One such principle is that the dislocations organize in low-energy dislocation structures [3]. Constraining factors for such organisations are for example the number of active slip systems, three-dimensional dislocation mobility and frictional stress. These factors establish a connection between the deformation microstructure and the slip pattern, which is determined by the grain orientation and the external load conditions.

The connection between the microstructure and the orientation of the crystal in which the structure evolves has been demonstrated for single crystals [4–9] deformed in rolling, channel die compression and tension. About 5–10 years ago, it was also demonstrated for polycrystals monotonically deformed in tension and rolling [10–14]. These studies have been based on a quantitative characterisation of boundary parameters by transmission electron microscopy (TEM). Recently, grain orientation-dependent dislocation structures after cyclic deformation of polycrystals have also been observed, although the morphology of these structures differs from those formed by monotonic deformation [15–17].

The orientation of the plane of the extended GNBs has been given special attention. The boundary plane orientation has been analysed in two different co-ordinate

* Corresponding author. Tel.: +45-46-77-57-92; fax: +45-46-77-57-58.
E-mail address: grethe.winther@risoe.dk (G. Winther).

1359-6454/$30.00 © 2004 Acta Materialia Inc. Published by Elsevier Ltd. All rights reserved.
doi:10.1016/j.actamat.2004.05.050

systems, namely (a) the macroscopic sample system defined by the deformation axes [1,18–20] and (b) the crystallographic system defined by the axes of the crystallographic lattice [10–12,14,21]. This analysis has shown that although most of the GNBs have a macroscopic orientation, e.g. inclined about 45° with the rolling plane at small to medium rolling reductions, the boundary orientation in the crystallographic lattice strongly depends on the grain orientation [14]. This finding has several implications both for analysis of microstructural evolution and for establishment of relations between microstructure and mechanical properties, e.g. flow stress anisotropy [22]. The finding is also important for modelling of deformation textures as a pronounced effect of grain orientation suggests that texture evolution is less influenced by grain interaction.

In a recent paper by Hurley et al. [23], alignment of GNBs in an Al–0.13% Mg alloy cold-rolled to a reduction of 20% was studied using electron back scattered diffraction (EBSD) and scanning electron microscopy. They concluded that "no evidence was found for boundary alignment with slip planes or any other simple crystallographic elements". They also found that the boundary planes did not vary in a systematic way with grain orientation, i.e. no dependence on grain orientation.

In the present paper, both of these conclusions will be addressed. In the first part of the paper, the EBSD and TEM techniques and associated data analysis are discussed in order to point at possible reasons for the disagreeing results. In the second part of the paper, TEM images of grains of selected orientations also investigated by Hurley et al. [23] demonstrate that boundary planes depend on the grain orientation and that certain orientations have slip plane aligned boundaries. These data are part of a more complete investigation of the grain orientation dependence of dislocation boundary planes in commercial aluminium (AA1050) cold-rolled to a reduction of 25%, which will be presented in a forthcoming paper. Finally, correlations between grain orientation, boundary plane and slip pattern are discussed and it is demonstrated that studies of grain orientation-dependent dislocation boundary planes contribute to the understanding of polycrystalline plasticity.

2. Technical issues and data analysis

Studies of boundary alignment inevitably fall into three stages: selection of the experimental technique employed to visualise the boundaries, selection of the sample section(s) to be investigated and analysis of the data.

2.1. Experimental techniques

Due to the different physical principles behind the TEM and EBSD techniques, the two techniques do not reveal dislocation boundaries in exactly the same manner. In a bright field TEM image, traces of dislocation boundaries are revealed directly as dark lines with an observable width. By contrast, the EBSD technique samples points on a square or hexagonal grid, resulting in a map of how the orientations are distributed. Consequently, the trace of extended planar dislocation boundaries is not seen directly but appears as a combination of lines between points of different crystallographic orientation.

As will be demonstrated below, TEM may be used to determine the boundary plane by observation of one trace in a single sample section while data from two sample sections must be combined to determine a boundary plane by EBSD. Such combinations of data from two sample sections are of course also possible using TEM.

2.1.1. Determination from one boundary trace by TEM

A full determination of the boundary plane from a single boundary seen in one sample section is only possible by TEM. The fact that the boundaries are seen directly in TEM images makes it possible to tilt the sample and observe the changes in the width of well-defined boundaries, from which the boundary plane can be deduced [24,25]. The angular precision of this technique is better than 5° [26].

Fig. 1 shows an example of the detailed analysis for identification of the crystallographic plane of a boundary. Fig. 1(a) is the image when the beam is directed along the [1 2 1] direction in the crystallographic lattice. The boundary trace image is very narrow and sharp, indicating that the boundary plane is parallel to the beam. The trace of the boundary is parallel to the trace of the $(\bar{1}\,1\,\bar{1})$ plane containing the [1 2 1] beam direction. These two observations strongly suggest that the boundary is aligned with the $(\bar{1}\,1\,\bar{1})$ plane. This is further proved by tilting the sample around two axes: (i) substantial tilting (30°) about an axis perpendicular to the boundary trace to make the beam parallel to the [0 1 1] direction does not change the observed boundary width (see Fig. 1(b)), i.e. edge-on conditions are maintained and (ii) tilting around an axis parallel to the boundary trace results in a clearly increasing boundary width, as seen in Fig. 1(c), i.e. the boundary is no longer observed edge-on. The second tilt bringing the beam from the [1 2 1] direction to [1 1 1] was 19° as shown in Fig. 1(d) but for well-defined boundaries, the effect is clear already at smaller tilts. Note that the boundary trace direction changes with sample tilting but it follows the $(\bar{1}\,1\,\bar{1})$ trace as marked by a dashed line in each micrograph of Fig. 1. The $(\bar{1}\,1\,\bar{1})$ traces were determined based on the grain orientation and the sample tilting as described in [24]. As a further proof, the observed boundary spacing, which may also be changed by tilting, is the same in Fig. 1(a) and (b), where the boundaries are

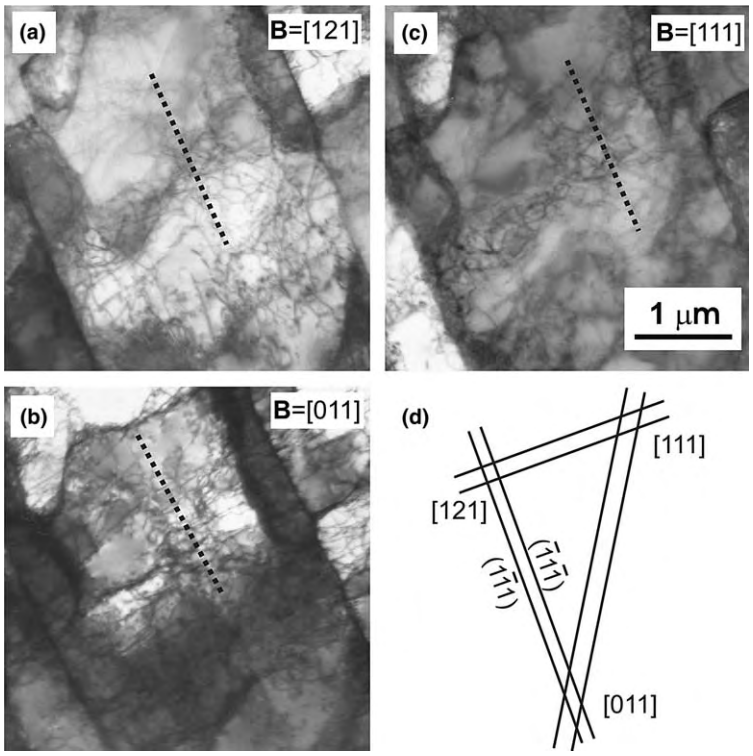

Fig. 1. TEM images of the same $(\bar{1}\,1\,\bar{1})$ aligned boundaries in a grain in 25% cold rolled AA1050. The images (a)–(c) are taken at different tilts, i.e. with the beam parallel to different crystallographic directions as indicated in the Kikuchi pattern in (d). (a) The boundary traces are sharp, i.e. the boundaries are seen edge-on, (b) tilting around an axis perpendicular to the boundary plane still gives a very sharp trace, i.e. edge-on conditions are maintained, and (c) after tilting around an axis parallel to the boundary plane, edge-on conditions no longer apply resulting in a very wide trace. During the sample tilting the boundary trace follows the changes of the $(\bar{1}\,1\,\bar{1})$ trace as marked on the micrographs.

edge-on, but about 7% larger in Fig. 1(c). It can therefore be concluded that the boundary definitely is parallel to the $(\bar{1}\,1\,\bar{1})$ plane.

This technique is of course also applicable to boundaries aligned with other crystallographic planes than $\{1\,1\,1\}$ planes. It has for example been used to determine that some of the boundaries in an aluminium single crystal of copper orientation deformed by channel die compression align with a $\{0\,0\,1\}$ plane even though the boundary trace in the observed sample section is parallel to the coincident traces of two $\{1\,1\,1\}$ planes [8].

2.1.2. Boundary trace determination in EBSD

Automated sampling by EBSD of a digitised image with well-defined lines representing misorientations above a pre-selected threshold makes boundary trace determination by digital image analysis attractive. Hurley et al. [23] devised an analysis method using the Radon transformation to detect the boundary trace directions in such images.

Application of the Radon transform is based on evaluating the expression

$$R(\rho,\theta) = \int\int f(x,y)\delta(r - x\cos\theta - y\sin\theta)\,\mathrm{d}x\,\mathrm{d}y, \qquad (1)$$

where $f(x,y)$ is the image intensity at the spatial co-ordinates (x,y), θ the inclination angle of and r the distance to a reference point of all possible linear traces in the image. To assist in distinguishing between traces that are approximately parallel (i.e. occurrence of lines with the same angles but different r-values in the total image), the Radon transform is evaluated on a small test-grid, which is swept over the image. At each position of the test-grid, the maximum value of the transform is recorded together with the corresponding value of the angle. The dominant trace angle is then obtained from the summed distribution of all these maxima.

One important complication when applying the Radon transform to EBSD misorientation maps is the inherent stepped nature of boundaries in the image. Smoothing operations may be applied to the misorientation map in the form of a Gaussian filter [23]. The amount of blurring required to remove step effects will, however, depend upon the direction of the boundary traces. As this direction approaches either 0° or 90° the traces will be represented by a mixture of long and short steps. Heavier blurring will be needed to remove the long segments than the short segments. The effect of stepped boundary representation is strongly affected by a number of factors, including the choice of EBSD step-size, the noise level in the orientation measurements, the choice of test-grid size and of the Radon space discretisation. A detailed analysis of the interdependency between these parameters will be published elsewhere.

The combination of a small test-grid relative to the step length and the occurrence of fragmented boundary traces, e.g. due to sampling of a boundary with a misorientation angle close to the detection limit, provides a particularly challenging situation. A good test to determine whether such effects contaminate a given data set would be to repeat the experimental measurement with the sample rotated 45° about the sample normal direction.

After having used the Radon transform to obtain a trace distribution from the EBSD data, it was found necessary to fit this to a Fourier series [23]. The need for this additional filtering step further demonstrates the non-trivial character of the problem.

2.2. Selection of sample sections

Independent of the experimental technique used, it is of course important that the investigated sample section reveals the boundary trace. The boundary trace is the intersection line between the boundary plane and the sample section. When the boundary planes are almost parallel to the sample section, the intersection lines become very widely spaced and they are therefore often not the dominant feature in the sampled image. For example, the rolling plane (RDTD section) in samples rolled to high strains and the torsion plane in samples deformed by high pressure torsion are useless in this respect [27].

For TEM, there is an additional reason to concentrate on sample sections to which the boundary planes are highly inclined. As illustrated in Section 2.1.1, boundaries are most clearly revealed in TEM when they are parallel to the electron beam, a condition which is most easily fulfilled when the boundary plane is steeply inclined to the sample section investigated. The tilting capacity of standard TEM sample holders is, however. rather large, meaning that also boundaries with smaller inclinations may be revealed after tilting. Due to the different nature of EBSD data, the visibility of a boundary trace in EBSD does not depend on the boundary inclination to the sample section but merely on the misorientation angle of the boundary.

In many cases, two sets of intersecting boundaries are formed in a grain. If the sampling step in EBSD is incommensurate with the spacing of the boundary traces, the misorientation map obtained may become very complicated. This is especially the case when the trace angles of the two boundary sets are almost the same. Also for TEM, boundaries with almost the same trace angles can be difficult to resolve.

The optimum sample section studied should therefore reveal a large difference in the trace angles of intersecting boundaries and it should be somewhat inclined to the boundary planes. The latter requirement is, however, most critical for TEM. In the following all possible sample sections for rolled samples are evaluated to identify the sample sections suitable for studies of boundary planes according to these criteria. In this investigation boundaries are assumed to lie on the idealised planes inclined ±45° to the rolling direction and parallel to the transverse direction (see Fig. 2).

Fig. 3 shows three figures, each representing all possible sample sections as defined by the rolling, transverse and normal directions. Fig. 3(a) shows the angle between the traces from the two boundary planes while Figs. 3(b) and (c) show the inclination angle of each of these boundary planes, respectively, to the sample sec-

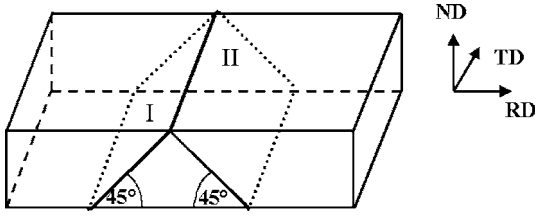

Fig. 2. The typical boundary planes in rolling are marked I and II.

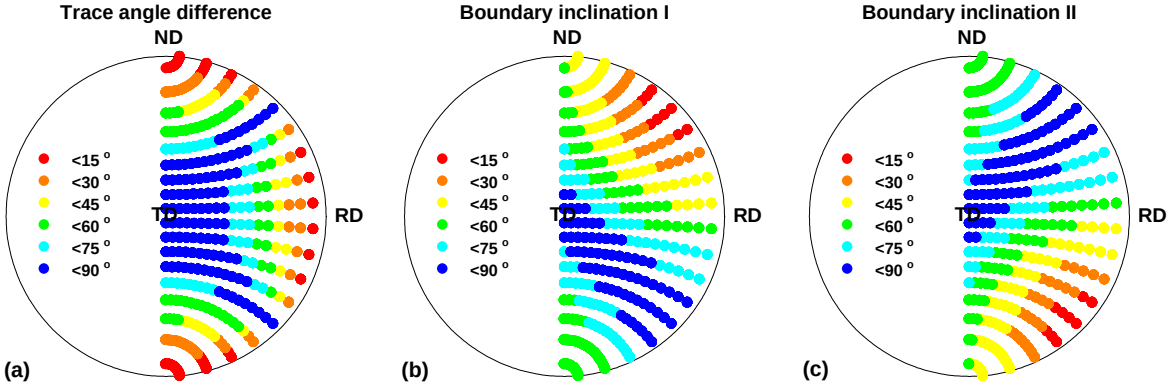

Fig. 3. Figures covering all possible sample sections defined by RD, TD and ND. Each figure shows properties of the two sets of boundaries (I and II) shown in Fig. 2 as a function of sample section: (a) difference in trace angles, (b–c) inclination angle of boundary set I and II, respectively.

tions. In these figures, blue represent the best conditions while red marks the poorest conditions. It is clearly seen that the sample section perpendicular to the transverse direction, i.e. the RDND or longitudinal section, is the optimum section in all cases. Also, the RDTD and TDND sections perpendicular to the normal and rolling directions, respectively, are the worst. These sections are also often referred to as the rolling and transverse sections.

A section inclined 45° to the rolling direction and parallel to the transverse direction also fulfills the criteria as seen in Fig. 3 but only for one of the two sets of boundaries. This section is roughly parallel to one of the expected boundary planes and perpendicular to the other and only the latter set of boundaries is clearly revealed because the spacing between the traces of the former set becomes very large due to its low inclination. Use of this sample section is therefore not straightforward.

The RDND section is therefore in general the optimum sample section for investigation of boundary planes in rolled samples. As demonstrated in Section 2.1.1, the boundary plane can be determined from this section alone, using TEM and the tilting technique. By contrast, EBSD relies on a combination of observations from two sample sections, which is difficult when only one sample section provides good viewing conditions.

2.3. Analysing for grain orientation dependence

Any co-ordinate system may of course be employed in boundary plane analysis but the two obvious ones are the sample system defined by the deformation axes and the system defined by the crystallographic axes. The crystallographic grain orientation of course relates the two systems.

Analysis carried out solely in the sample system has established that boundaries lie on a narrow range of planes in this system (see e.g. [20] for tension and [28] for rolling), which lie in the vicinity of the most stressed sample sections. By contrast, analysis purely in the crystallographic system shows that boundaries may lie on virtually all crystallographic planes (see e.g. [28,29]).

The grain orientation dependence of dislocation boundary planes should manifest itself in both the sample and crystallographic systems. However, it is clear that the highest resolution is obtained when analysing in the crystallographic system, where the range of boundary planes have been seen to be largest. Investigations of grain orientation-dependent boundary planes are therefore best carried out in the crystallographic system.

2.3.1. Subdivision of orientation space

The concept of grain orientation-dependent structures implies a subdivision of orientation space into subspaces so that grains within each subspace have some common characteristics which differ from the characteristics of grains in other subspaces. Definition of these subspaces is a very critical step, which must be motivated either directly by the data itself or by postulating a hypothesis which is then proved or disproved. Analysis of grain orientation-dependent phenomena and the associated subdivision of the orientation space is of course most easily accomplished when the relevant orientation space is small, the data points are plenty and cover the entire orientation space.

Ideally, the subspaces should reveal themselves in a plot of the grain orientations observed to have the various types of structures. This has for example been the case for tensile deformed aluminium and copper where three subspaces have been identified, having GNBs aligned with slip planes, GNBs not aligned with slip planes or no GNBs, respectively [11,12]. In the more detailed classification of the same data according to the detailed geometric relationship between slip planes and GNBs [14] and characterisation of cyclically deformed materials [15–17], the subspaces were also defined based on the structures observed.

In the case of less complete coverage of the orientation space, hypotheses for prediction of certain characteristics may be tested against the available data. This has for example been done for the occurrence of deformation twins in rolled brass [30] and features causing surface roughness in rolled aluminium [31], which were both related to the Schmid factors, and the slip plane alignment of GNBs in rolled aluminium [32,33], which was related to the slip concentration. In all of these cases, the predictions were based on grain orientation dependence of the expected slip patterns.

Selection of subspaces merely consisting of all orientations within an arbitrary distance of some ideal orientation, e.g. within 20° of typical rolling texture components as in [23], does not ensure a good choice, especially not when the chosen distance is large. The risk is that the selected orientation range spans more than one type of structure and furthermore does not cover the entire range of each type. If this is the case, detection of an existing grain orientation dependence becomes virtually impossible.

It is important that the grain orientation is retained in the data also after a grain has been assigned to an orientation subspace. As demonstrated later in this paper (Section 4.1, Table 1), the angles between the trace of a fixed crystallographic plane and for example the rolling direction may vary substantially within such a subspace. Conclusions based on comparison of boundary trace distributions in the sample co-ordinate system for the entire subspace and the trace of a crystallographic plane in a reference orientation within this subspace as done in [23] may therefore easily become erroneous. The exact grain orientation is also needed in

Table 1
Boundary trace directions in the RDND sample section in five grains within 15° of the ideal Brass orientation

Grain	Boundary trace to RD	{1 1 1} trace to RD	Deviation from {1 1 1} trace[a]
1	25°	20.4°	4.6°
	−33°	−35.0°	−2.0°
2	26°	21.4°	4.6°
	−40°	−37.6°	2.3°
3	38°	40.1°	−2.1°
	−28°	−24.8°	3.2°
4	44°	42.3°	−1.7°
	−26°	−29.2°	−3.2°
5	38°	37.3°	0.7°
	−31°	−33.1°	−2.1°
Ranges	25° to 44°		−3.2° to 4.6°
	−26° to −40°		

In all cases it has been confirmed by tilting in the TEM that the boundary truly aligns with the {1 1 1} plane.
[a] Negative signs indicate boundary traces closer to RD than the {1 1 1} trace.

order to detect systematic variations within a subspace, as e.g. done in [14].

2.3.2. Use of symmetry

Symmetry may be employed to reduce the orientation space considered. The smaller the orientation space considered the easier this is covered with good statistics. In tension, for example, uniaxial sample symmetry combined with cubic crystal symmetry has been used to convert all grain orientations to the standard stereographic triangle. All observations of boundary traces and planes must naturally also be converted to a grain orientation in this triangle [14].

For rolling, orthorhombic sample symmetry is usually assumed, meaning that the entire orientation space is reduced by a factor of 4. In practice, this conversion typically involves changing the sign of the observed trace angle with respect to the sample axes. Keeping track of the sign is a very efficient way of separating two sets of intersecting sets of boundaries in the trace distributions. If the sign is ignored, two otherwise rather distinct peaks in the trace distribution may be combined in a broad peak, leading to erroneous conclusions. Even when only one set of boundaries is observed, the sign conveys vital information when comparing with the trace angles of certain crystallographic planes, e.g. slip planes, which also have a sign. It is therefore important that the sign is transformed correctly and not simply disregarded as in the EBSD study presented in [23].

3. Boundary plane alignment in rolled samples

A comparison of the results obtained by TEM and EBSD for rolling is shown in Fig. 4 where the previously published TEM results [13] are shown as symbols and the orientations investigated by EBSD in [23], i.e. those within 20° of ideal orientations, are marked by different colours. Please note that the colour designates the nearest ideal orientation since the orientation subspaces defined around each ideal orientation overlap substantially. The TEM results are separated into two groups, namely grain orientations with at least one set of slip plane-aligned boundaries (solid symbols) and grain orientations having boundaries on other planes (open symbols). The TEM results show that the grains within 20° of the Goss, Copper, Brass and S orientations all had at least one set of slip plane-aligned boundaries, except in a very few cases, which is in clear conflict with the EBSD results, which only found boundaries aligned with slip planes near the Goss orientation. About one third of the TEM data within 20° of the P orientation had slip plane-aligned boundaries while the rest did not, showing that this orientation subspace contains different types of structures. In both studies, boundaries in grains within 20° of the Cube orientation were found not to align with slip planes.

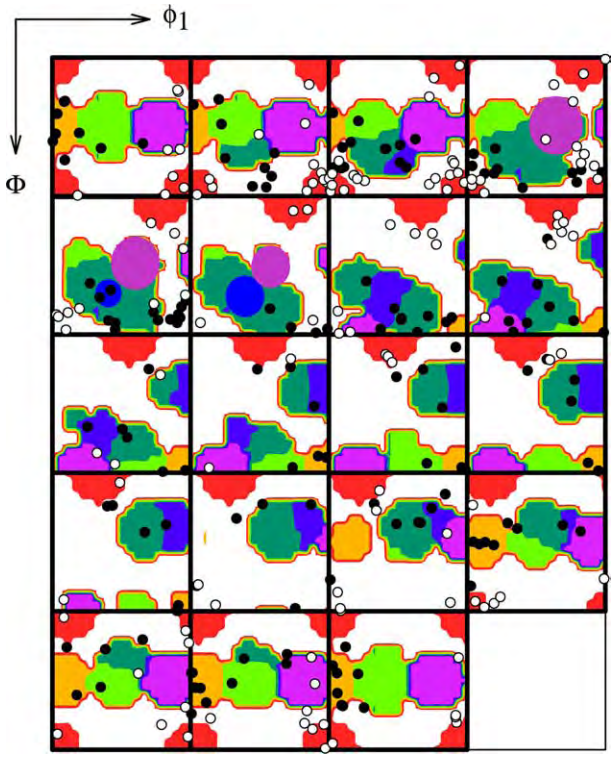

Fig. 4. ODF showing TEM data from Liu et al. [13] classified as having slip plane-aligned boundaries (solid symbols) or not slip plane-aligned boundaries (open symbols). Orientations within 20° of the ideal crystallographic orientations investigated by EBSD by Hurley et al. [23] are shown as coloured areas (red: Cube, green: Brass, orange: Goss, dark green: S, blue: Copper, pink: P).

In order to resolve the conflicting results in the two studies, detailed TEM data for the Brass and S orientations in 25% cold rolled AA1050 with a grain size of

about 100 μm are presented here. The Brass orientation was selected because it constitutes a very critical test: the two slip planes with which boundaries have been observed to align in this orientation deviate substantially from the macroscopic planes as illustrated in Fig. 5, especially the trace in the rolling plane is far from being parallel to TD. The S orientation was selected to allow direct comparison with the images shown in [23], albeit these images are electron channelling contrast images and not misorientation maps.

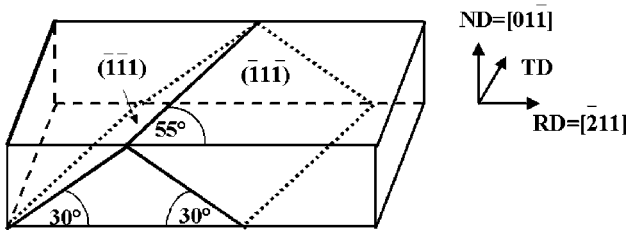

Fig. 5. Sketch showing the orientation of the two sets of slip plane-aligned boundaries in the ideal Brass orientation.

3.1. The Brass orientation – a critical test

Fig. 6 shows a TEM image of a grain near the ideal Brass orientation in the RDND sample section. Two sets of boundaries aligned with the trace of {1 1 1} planes are seen. The tilting technique described in Section 2.1.1 was employed to establish that also in three dimensions these boundaries definitely align with the $(\bar{1}\,1\,\bar{1})$ and $(\bar{1}\,\bar{1}\,1)$ planes.

Although the boundary planes are fully determined by these TEM observations, additional observations were made for another Brass oriented grain in the RDTD sample section to make a very thorough investigation of this critical case. The TEM image of the RDTD section in Fig. 7(a) clearly shows a more complicated morphology than the one seen in the RDND section due to the lower visibility in this section as discussed in Section 2.2. However, extended boundaries are still easily identified. For clarity, a tracing of these are shown in Fig. 7(b). It is obvious that they are not aligned with the transverse direction but deviate substantially from this. Most of the boundary traces align with the trace of the $(\bar{1}\,1\,\bar{1})$ plane but segments aligned with the $(\bar{1}\,\bar{1}\,1)$ trace occur occasionally. This

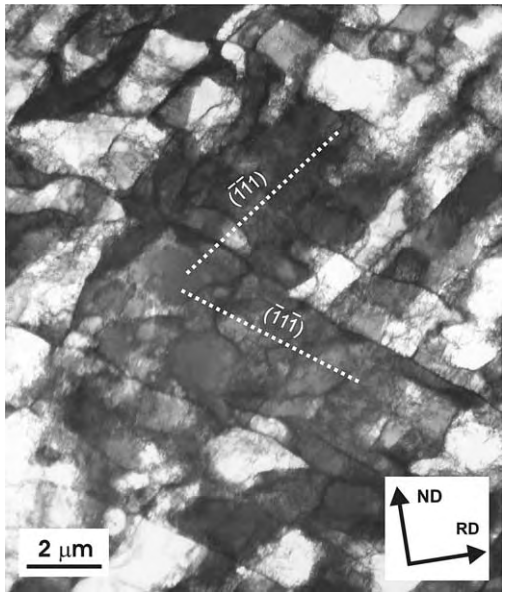

Fig. 6. TEM image of the RDND sample section of a Brass oriented grain in 25% cold rolled AA1050. The exact orientation is (0.02,0.65,−0.76)[−0.87,0.38,0.31]], i.e. about 7° from the ideal Brass orientation. The beam direction is parallel to [0 1 1], which is parallel to both the $(\bar{1}\,1\,\bar{1})$ and $(\bar{1}\,\bar{1}\,1)$ planes. The sharpness of the boundary traces shows that the boundaries are viewed edge-on, i.e. the boundaries align with the $(\bar{1}\,1\,\bar{1})$ and $(\bar{1}\,\bar{1}\,1)$ planes.

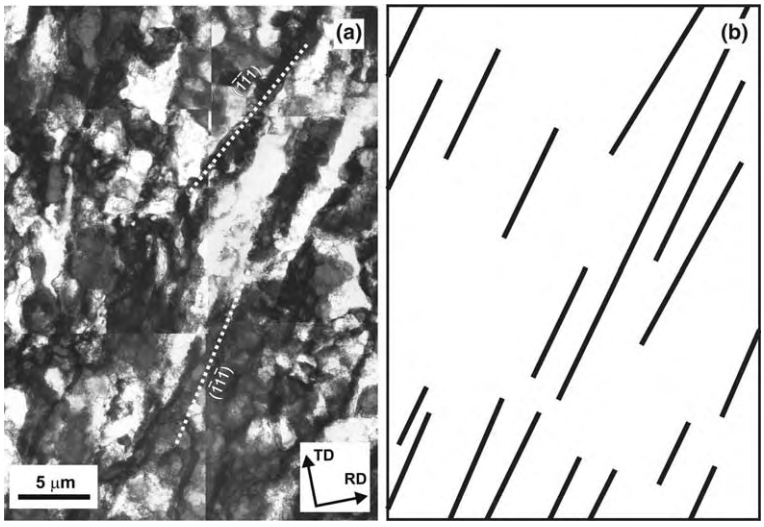

Fig. 7. (a) TEM image of the RDTD sample section of a Brass oriented grain in 25% cold rolled AA1050. The exact orientation is (0.01, 0.63, −0.78) [−0.75, 0.52, 0.41], i.e. about 9° from the ideal Brass orientation. (b) Tracing of the extended GNBs in (a).

observation in the RDTD section is in full agreement with the observations in the RDND section, meaning that the boundaries beyond any doubt align with the slip planes in the Brass oriented grains. This result is, however, in clear disagreement with the EBSD result in [23].

3.2. The S orientation – image comparison

Fig. 8 shows a TEM image of a grain 6° away from the ideal S in the RDND section. Two sets of intersecting boundaries are seen. Both of these are aligned with traces of {1 1 1} planes. However, tilting has established that only one of these is slip plane aligned (alignment is with the $(\bar{1}\,\bar{1}\,1)$ plane). The other boundary set does not align with the (1 1 1) plane but deviates about 25° from this.

This image may be compared with the electron channelling contrast images of two S oriented grains in both the RDTD and RDND sections shown in [23], although the exact orientation of these grains are not stated. The electron channelling contrast images show only one clear set of boundaries, although very weak indications of a second set may be present also. The clearly revealed boundary set apparently corresponds to the set not aligned with the slip plane in the TEM image in Fig. 8, which is also the more closely spaced boundary set. With respect to the stated clear differences between the two grains investigated by electron channelling contrast especially when seen in the RDTD section, this may be due to interference between the two boundary sets which is most severe in this section as was discussed in Section 2.2.

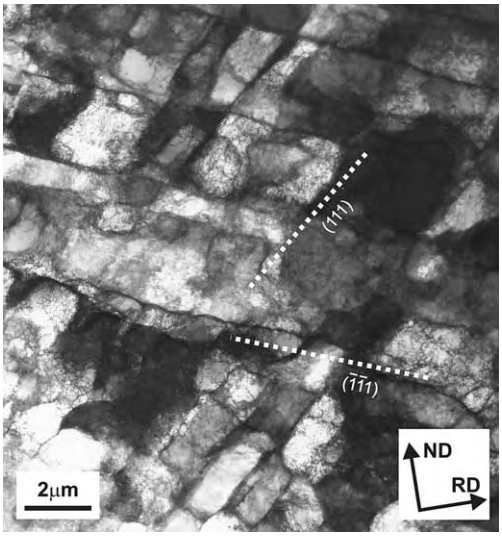

Fig. 8. TEM image of the RDND sample section of an S oriented grain in 25% cold rolled AA1050. The exact orientation is $(0.77, 0.60, -0.22)$ $[-0.49, 0.33, -0.80]$, i.e. about 6° from the ideal S. Two sets of boundaries are aligned with the traces of (1 1 1) and $(\bar{1}\,\bar{1}\,1)$ planes, respectively. Tilting, however, shows that only one of the boundary sets is slip plane-aligned (parallel to $(\bar{1}\,\bar{1}\,1)$) while the other set deviates from (1 1 1) by approximately 25°.

4. Discussion

4.1. Macroscopic vs. grain orientation-dependent crystallographic alignment

In the EBSD study in [23], it was concluded that boundaries in all the orientations investigated have the same macroscopic alignment and therefore do not exhibit any dependence on the grain orientation. The finding that boundaries in the Goss orientation were aligned with {1 1 1} planes was considered incidental since the slip planes in this orientation almost coincide with the most stressed sample planes.

The present authors, of whom one was among the first proposers of the macroscopic boundary alignment principle [1,28], certainly agree that there is a general tendency for boundaries to align with the most stressed sample planes. This has been shown for several deformation modes, including rolling [1,18,19], torsion [34] and tension [14,20]. However, this reflects the general directionality of the activated slip systems [33,35]. The exact boundary plane in a grain depends on these slip systems and therefore on the grain orientation as discussed further in the next section.

A truly objective study of whether boundaries preferentially align with certain sample planes or with crystallographic planes should include investigation in both co-ordinate systems. If the spread of crystallographic boundary planes in grains with almost similar crystallographic orientations is smaller than the spread of boundary planes in the sample system, the crystallographic preference must be stronger than the preference seen in the sample co-ordinate system and vice versa. The occurrence of a smaller spread in the crystallographic lattice was demonstrated for tension [14].

For the 25% rolled AA1050 sample, the variation of boundary planes in five grains within 15° of the ideal Brass orientation was investigated in the crystallographic as well as in the sample co-ordinate systems. By tilting in the TEM, it was established that the boundaries were very close to the slip planes. Subsequently, the deviation of the boundary trace from the slip plane trace as well as the angle between the boundary trace and the rolling direction as seen in the TEM image of the RDND sample section were measured, resulting in the data presented in Table 1. It is seen that the variation in the crystallographic co-ordinate system where boundaries lie within 5° of a slip plane is much smaller than in the sample system where the boundaries lie within 12° of the mean trace. In a forthcoming paper, it will be demonstrated that the variations in crystallographic boundary plane are systematic and follows the grain

orientation. These results on Brass oriented grains combined with the significantly different crystallographic boundary plane seen in the grain of the S orientation in Fig. 8 strongly suggest that also for rolling, crystallography is the stronger factor controlling the exact boundary plane.

4.2. Correlation with slip pattern

Previous papers on the alignment of boundary planes in the crystallographic lattice have established correlations between deformation mode, boundary alignment and slip pattern. In particular, the slip concentration, i.e. the fraction of the total slip in the grain occurring on one slip plane, is an important factor controlling the alignment with slip planes. High-slip concentrations (above about 45%) have been shown to correlate reasonably well with the occurrence of slip plane-aligned boundaries in both rolled and tensile deformed aluminium polycrystals [32,33].

A crucial step in establishing such correlations is of course prediction of the slip pattern. The fact that the boundary plane has been established as grain orientation dependent shows that the effect of grain interaction on the slip pattern is too small to significantly alter the boundary plane. Orientation-based models for slip pattern prediction should therefore be appropriate. The slip concentrations predicted by the Taylor model proved relatively successful in relation to the available data for rolled samples but less so for tension. Slip concentrations predicted for tension by the Taylor model using a particular solution to the inherent slip ambiguity problem associated with this model, however, improved the prediction somewhat [33]. This slip prediction is furthermore in better agreement with the lattice rotations of individual bulk grains observed by three-dimensional X-ray diffraction during tension [36]. Nevertheless, the slip patterns predicted with this model were clearly neither in full agreement with the observed rotations during tension nor the occurrence of slip plane-aligned boundaries, assuming the hypothesis of slip concentration as a controlling factor is correct. Also for deformation by rolling, the slip patterns and corresponding slip concentrations predicted by the Taylor model do not always agree with the experimental data on slip plane-aligned boundaries. For example, the Brass orientation is not predicted to have a high-slip concentration on the two-slip planes with which the boundaries have been seen to align in Fig. 6.

Correlations between the boundary plane and slip pattern have also been devised for boundaries which are not aligned with any slip plane. By considering the geometry of the deformation mode, a model based on equivalent slip planes has been devised [35]. This model correctly predicted the planes of boundaries in a number of highly symmetric crystal orientations. In analogy with the model outlined above based on slip patterns predicted by the Taylor model, this model does also not predict the slip plane alignment of the boundaries observed in the Brass oriented grains.

Although the factors and mechanisms controlling the plane of dislocation boundaries have obviously not been fully understood, it is clear that the origin of the grain orientation-dependent boundary planes must lie in a correlation with the slip pattern. In fact, the grain orientation dependence of dislocation boundary planes may be used as a tool to identify the slip pattern, i.e. to improve polycrystalline plasticity models [37]. In a study relating the different types of dislocation structures in tensile deformed aluminium polycrystals with variations in the expected slip patterns, better agreement was found when the slip pattern was deduced from Schmid factors instead of the Taylor model [14,37]. The present TEM data for the Brass oriented grains in rolled aluminium is an analogous example since the boundaries align with the two slip planes with the largest Schmid factors.

4.3. Boundary alignment studies by EBSD and TEM

TEM and EBSD based techniques to determine the plane of dislocation boundaries have been discussed in the previous sections, focusing on the inherent differences of the two types of microscopy as well as the pitfalls associated with data analysis and interpretation.

This leads to the following statements concerning the technical capabilities:

- TEM with appropriate tilting of the sample may be used to determine the plane of boundaries by observation in only one sample section. EBSD requires observation of two sample sections.
- Evaluation of all possible sample sections for rolling has shown that generally the boundaries are by far the best revealed in the RDND section, regardless of the technique used. It is, in fact, difficult to find an additional sample section, which is a requirement for the EBSD technique.
- For studies of a given sample section, the main limitation of TEM is the requirement of a relatively large inclination of the boundary plane to the sample section. For EBSD, the main limitation lies in the smaller angular and spatial resolution. Both techniques have difficulties in resolving two sets of boundaries with almost the same trace angles in the sample section observed.

EBSD certainly has advantages in the form of easier sample preparation and automated sampling of data ready for digital analysis. The disadvantages listed above are, however, severe and may render the technique unreliable. Part of the conflicting results obtained with the two techniques may be ascribed to these fundamental technical issues.

The argument put forward that TEM realistically only covers a small area compared to EBSD and that TEM results therefore are based on poor statistics has some truth to it. However, TEM can cover entire grains. More importantly in this context, the consistent TEM results shown in Section 4.1. for five Brass oriented grains clearly show a statistically valid tendency, especially because these grains were selected at random and observed in TEM foils from different parts of the sample. In other words, few data of high quality are better than plenty of data of dubious character.

The TEM technique is well established and indisputably well suited for determination of dislocation boundary planes. The present EBSD technique and associated data analysis is not yet sufficiently mature to allow definite conclusions on its future potential in this field.

5. Conclusion

1. TEM and EBSD based techniques to determine the plane of dislocation boundaries have been discussed, focusing on the inherent differences of the two types of microscopy as well as the pitfalls associated with data analysis and interpretation.
   - With appropriate sample tilting, the boundary plane may be determined from one sample section using TEM while EBSD requires two sample sections. This is particularly important for applicability of the techniques to rolled samples where only one good sample section exists, namely the RDND section.
2. The conclusion by Hurley et al. [23] based on EBSD data that boundary planes do not depend on the grain orientation has been proven incorrect. TEM studies of selected grain orientations in 25% cold rolled AA1050 confirm previous findings that:
   - Grain orientation-dependent dislocation boundary planes are a general phenomenon.
   - Some grain orientations have boundaries aligned with slip planes while others do not.
3. The boundary plane is linked with both crystallography and the macroscopic deformation mode but more closely with the former. This is due to a correlation between macroscopic deformation mode, slip pattern and boundary plane.

Acknowledgements

We thank Prof. B. Ralph and Dr. D. Juul Jensen for scientific discussions and Dr. G. Wu for help with experimental work. We also gratefully acknowledge the Danish National Research Foundation for supporting the Center for Fundamental Research: Metal Structures in Four Dimensions, within which this work was performed.

References

[1] Bay B, Hansen N, Kuhlmann Wilsdorf D. Mater Sci Eng A 1992;158:139–46.
[2] Hansen N, Juul Jensen D. Philos Trans R Soc Lond A 1999;357:1447–69.
[3] Hansen N, Kuhlmann Wilsdorf D. Mater Sci Eng 1986;81:141–61.
[4] Kawasaki Y. J Phys Soc Jpn 1974;36:142–8.
[5] Kawasaki Y, Takeuchi T. Scripta Metall 1980;14:183–8.
[6] Becker R, Butler JF, Hu H, Lalli LA. Met Trans A 1991;22A:45–58.
[7] Ferry M, Humphreys FJ. Acta Mater 1996;44:1293–308.
[8] Godfrey A, Juul Jensen D, Hansen N. Acta Mater 1998;46:835–48.
[9] Godfrey A, Juul Jensen D, Hansen N. Acta Mater 1998;46:823–33.
[10] Liu Q, Hansen N. Phys Stat Sol (a) 1995;149:187–99.
[11] Huang X, Hansen N. Scripta Mater 1997;37:1–7.
[12] Huang X. Scripta Mater 1998;38:1697–703.
[13] Liu Q, Juul Jensen D, Hansen N. Acta Mater 1998;46:5819–38.
[14] Winther G, Huang X, Hansen N. Acta Mater 2000;48:2187–98.
[15] Buque C, Holste C, Schwab A. In: Proceedings of 20th Risø International Symposium on Materials Science. Roskilde, Denmark: Risø National Laboratory; 1999. p. 277–82.
[16] Buque C, Bretschneider J, Schwab A, Holste C. Mater Sci Eng A 2001;300:254–62.
[17] Feaugas X, Gaudin C. Mater Sci Eng A 2001;309–310:382–5.
[18] Wilson DV, Bate PS. Acta Metall Mater 1994;42:1099–111.
[19] Akbari GH, Sellars CM, Whiteman JA. Acta Mater 1997;45:5047–58.
[20] Zhu Q, Sellars CM. Scripta Mater 2001;45:41–8.
[21] Liu Q, Hansen N. Proc R Soc Lond A 1998;454:2555–91.
[22] Winther G. In: Proceedings of 19th Risø International Symposium on Materials Science. Roskilde, Denmark: Risø National Laboratory; 1998. p. 185–99.
[23] Hurley PJ, Bate P, Humphreys FJ. Acta Mater 2003;51:4737–50.
[24] Huang X, Liu Q. Ultramicroscopy 1998;74:123–30.
[25] Hirsch P, Howie A, Nicholson R, Pashley D, Whelan M. Electron microscopy of thin crystals. Malabar, FL: Krieger; 1977.
[26] Edington J. Practical electron microscopy in materials science. Eindhoven: Philips Technical Library; 1975. p. 57.
[27] Huang X, Winther G, Hansen N, Hebesberger T, Vorhauer A, Pippan R, Zehetbauer M. In: Proceedings of Thermec 2003, Madrid; 2003. p. 2819–24.
[28] Bay B, Hansen N, Kuhlmann Wilsdorf D. Mater Sci Eng A 1989;113:385–97.
[29] Gil-Sevillano J, Torrealdea FJ. In: Proceedings of 2nd Risø International Symposium on Metallurgy and Materials Science. Roskilde, Denmark: Risø National Laboratory; 1981. p. 185–90.
[30] Leffers T, Ananthan VS. Texture Microstruct 1991;14–18:971–6.
[31] Choi YS, Piehler HR, Rollett AD. Metall Mater Trans A 2004;35:513–24.
[32] Winther G, Juul Jensen D, Hansen N. Acta Mater 1997;45:5059–68.
[33] Winther G. Acta Mater 2003;51:417–29.
[34] Hughes DA, Hansen N. Mater Sci Technol 1991;7:544–53.
[35] Wert J, Huang X. Philos Mag 2003;83:969–83.
[36] Winther G, Margulies L, Schmidt S, Poulsen HF. Acta Mater 2004;52:2863–72.
[37] Winther G. Mater Sci Eng A 2001;309–310:486–9.

A3: Crystallographic and macroscopic orientation of planar dislocation boundaries – correlation with grain orientation by G. Winther, X. Huang and N. Hansen, Acta Materialia, 2000

PERGAMON

Acta mater. 48 (2000) 2187–2198

Acta MATERIALIA

www.elsevier.com/locate/actamat

CRYSTALLOGRAPHIC AND MACROSCOPIC ORIENTATION OF PLANAR DISLOCATION BOUNDARIES—CORRELATION WITH GRAIN ORIENTATION

G. WINTHER†, X. HUANG and N. HANSEN

Materials Research Department, Risø National Laboratory, DK-4000 Roskilde, Denmark

(Received 8 November 1999; accepted 18 January 2000)

Abstract—A novel geometric analysis method for determination of the three-dimensional orientation of extended planar dislocation boundaries in polycrystals based on TEM measurements is presented. The analysis is applied to data for tensile deformed aluminium, revealing that the boundaries have a strong preference for certain crystallographic planes, depending on the crystallographic orientation of the grain. The crystallographic boundary planes are distributed around, but do not coincide with, the most stressed macroscopic planes inclined 45° to the tensile axis. The strong correlation between the crystallographic boundary planes and the grain orientation shows that the boundary orientation is closely linked to the active slip systems. The observed correlation can be explained by a Schmid factor analysis assuming activity on the five most stressed slip systems. © *2000 Acta Metallurgica Inc. Published by Elsevier Science Ltd. All rights reserved.*

Keywords: Microstructure; Dislocations; Transmission electron microscopy (TEM); Structural behaviour; Crystallographic grain orientation

1. INTRODUCTION

Deformation microstructures typically consist of extended planar dislocation boundaries and short cell boundaries arranged in a three-dimensional network. The extended planar dislocation boundaries have preferred macroscopic orientations, i.e. preferred orientations with respect to the deformation axes. The macroscopically preferred boundary planes generally coincide with the most stressed planes in the sample. At low and intermediate strain ($\varepsilon < 1$) this macroscopic preference has been observed in rolled f.c.c. [1] and b.c.c. metals [2, 3], and in f.c.c. metals deformed in torsion [4]. In rolling, the boundaries are inclined approximately 45° to the rolling direction in the longitudinal plane and are roughly perpendicular to the rolling direction in the rolling plane, and in torsion they are parallel and perpendicular to the shearing plane.

Recent studies of planar dislocation boundaries in f.c.c. polycrystals deformed in tension [5, 6] and rolling [7, 8] to strains less than 0.7 have also established a relationship between the crystallographic grain orientation and the orientation of the dislocation boundaries. In some grain orientations the boundaries are aligned with the slip planes, in other grain orientations the boundaries lie on planes far from the slip planes, and finally equiaxed cells are formed in certain grain orientations instead of extended planar boundaries. Results for tensile deformed aluminium are shown in Fig. 1. These findings suggest that the boundaries have preferred orientations in the crystallographic lattice, i.e. lie on planes with certain crystallographic indices, and that the crystallographically preferred orientation depends on the grain orientation. In a recent study on cyclically deformed polycrystalline nickel, grain orientation dependent dislocation structures were also observed [9].

In the following, the boundary orientation in the crystallographic lattice will be termed the "crystallographic orientation" to distinguish it from the "macroscopic orientation" defined with respect to the deformation axes.

The orientation of the planar dislocation boundaries is believed to be an important structural parameter relating deformation at the grain scale and the macroscopic scale. In this context the correlation between boundary orientation and grain orientation is particularly interesting. This corre-

† To whom all correspondence should be addressed.

PII: S1359-6454(00)00027-6

lation is investigated in this paper concentrating on the crystallographic orientation of the boundaries. For this purpose a novel geometric analysis method has been developed that allows determination of the three-dimensional orientation of the boundary planes. Results from application of the analysis to data for tensile deformed aluminium are presented, leading to a more detailed characterisation of the crystallographic boundary planes and subdivision of the triangle in Fig. 1 into more than three regions with different dislocation structures.

In order to investigate the apparent conflict between the existence of both crystallographic and macroscopic preferred orientations, the macroscopic orientation of the boundary planes is also calculated and the origin of preferred boundary orientations is discussed.

Finally, the determined crystallographically preferred boundary planes are compared with the boundary orientations reported for single crystals because previous studies of the boundary orientations have indicated a similarity between the boundaries in single and polycrystals [5–7].

2. GEOMETRIC ANALYSIS OF BOUNDARY PLANES

Determination of the three-dimensional orientation of boundaries is based on transmission microscopy observations of the boundary traces. In some cases, e.g. when the boundary orientation is close to a crystallographic plane of low index, the boundary orientation can be determined directly by tilting the sample until the boundary appears sharpest [10]. However, often the boundaries are away from low index planes and this technique is not easy to use. Other experimental techniques based on multiple measurements of each boundary at different tilts are available [11, 12], but these involve tedious procedures at the microscope and subsequent calculations to derive the boundary orientation.

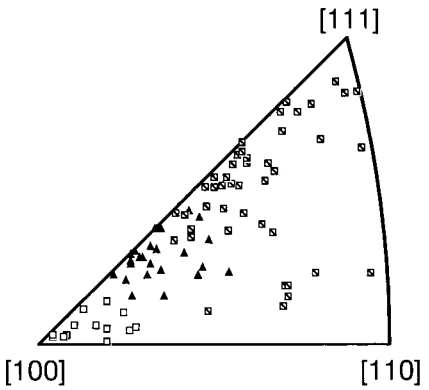

Fig. 1. Subdivision of the triangle into regions with boundaries having traces deviating less (triangles) and more (crossed squares) than 5° from the nearest slip plane trace and a region with equiaxed cells (open squares) instead of extended planar boundaries (from Ref. [5]).

The geometric analysis proposed in this paper is based on a single observation of the boundary in the microscope to obtain the angle between the boundary trace and the macroscopic deformation axis. Subsequent analysis of the boundary traces measured in many grains allows determination of the three-dimensional boundary orientation. It should be noted that the analysis assumes that the boundaries have preferred crystallographic orientations. Verification of this basic assumption is, however, an inherent feature of the analysis as no result can be obtained in the absence of such a preference.

2.1. Principle

The analysis is inspired by the method used for single crystals in which the boundaries can be observed in several inspection planes. Analysis of the angle between the trace and the macroscopic deformation axes in different inspection planes leads to an exact crystallographic plane represented as a point in an inverse pole figure, as illustrated in Fig. 2(a).

For polycrystals, however, investigation of the same grain in several inspection planes is virtually impossible. Only the set of possible boundary planes with the same trace in, but different inclinations to, the inspection plane can be determined. This set is represented by an arc in an inverse pole figure [Fig. 2(b)]. However, in axisymmetric tension, grains with the same crystallographic direction of the tensile axis are expected to be identical and these grains can be oriented differently with respect to the inspection plane. Observation of many grains with similar orientations of the tensile axis and analysis of the sets of possible boundary planes are therefore as close as one can get to observation of the same grain in many inspection planes. For deformation modes without uniaxial symmetry, observations of grains in several sample planes are needed to obtain this, but the rest of the analysis method still applies (Rolled samples may, for example, be investigated in the longitudinal and transverse planes). When the arcs representing the possible sets of boundaries in the different grains are drawn in the same inverse pole figure, the true boundary plane reveals itself as the point that all the arcs go through [Fig. 2(c)].

2.2. Practical implementation

Before looking for arc intersections, the sets of possible boundary planes for the observed grains must be calculated. Furthermore, the symmetry of both the crystal structure and the deformation should be considered before the arcs are drawn to

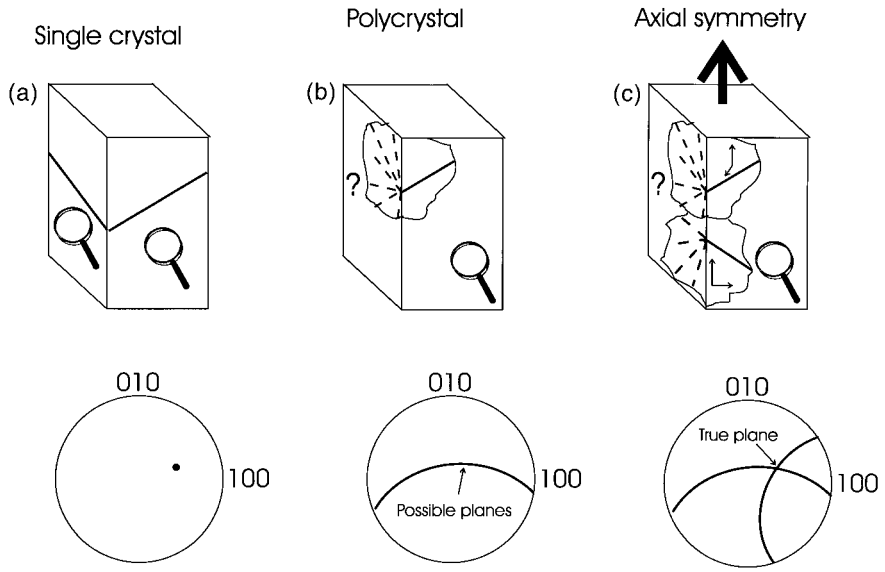

Fig. 2. Sketch of boundary determination from trace analysis in single and polycrystals. (a) Determination of the boundary plane in single crystals; (b) determination of the set of possible boundary planes in a grain in a polycrystal; (c) determination of the true boundary plane by inspection of grains with similar tensile axes, but oriented differently with respect to the inspection plane.

facilitate identification of the boundary planes. Finally, the geometric relation between the determined boundary plane and the nearest slip plane is introduced as a means to characterise and compare the boundary planes in grains with different orientations.

2.2.1. Calculation of possible boundary planes. For each grain, the set of possible boundary planes, $n(\beta)$, where β is the unknown inclination of the boundary to the inspection plane, is calculated based on the measured grain orientation and boundary trace angle, α. $n(\beta)$ is defined in the crystallographic lattice and given by the following equation, where the symbols are defined in Fig. 3.

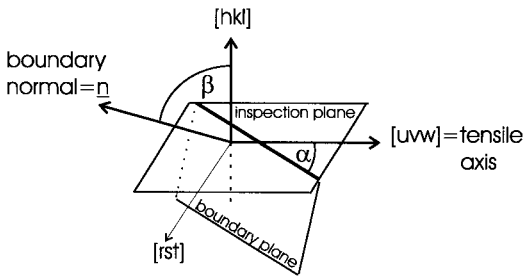

Fig. 3. The grain orientation is defined by the crystallographic directions of the tensile axis, [*uvw*], and the inspection plane normal, [*hkl*]. α is the measured angle between the tensile axis and the trace of the boundary plane in the inspection plane. β is the unknown inclination angle between the boundary plane with normal n, and the inspection plane.

$$n(\beta) = \begin{pmatrix} h & r & u \\ k & s & v \\ l & t & w \end{pmatrix} \begin{pmatrix} \cos(\beta) \\ \sin(\beta)\cos(\alpha) \\ -\sin(\beta)\sin(\alpha) \end{pmatrix};$$

$$\beta \in [-90^\circ, 90^\circ].$$

Inclination angles, β, ranging all the way from -90° to 90° are only a theoretical possibility because a boundary almost parallel to the inspection plane ($\beta \approx 0^\circ$) is practically invisible in TEM, while boundaries steeply inclined ($|\beta| \approx 90^\circ$) to the inspection plane are clearly visible. Consequently, only a limited range of orientations of the inspection plane gives good TEM images, where the boundary trace angles can be measured.

The decreasing visibility of the boundaries with decreasing inclination to the inspection plane can, however, be used to distinguish between intersections representing true boundary planes and incidental intersections between arcs representing boundaries with two different orientations. Intersections of arc segments that represent boundary planes steeply inclined to the inspection plane are more likely to represent true boundary planes. In addition to the plots shown below, plots of arc segments representing boundaries steeply inclined to the inspection plane only were made. In doing so, a steeply inclined boundary was arbitrarily defined as a boundary inclined more than 45° to the inspection plane, i.e. $|\beta| > 45^\circ$. These plots are not presented here, but in all cases the arc segments passed through or ended close to the identified boundary plane (in the latter case, the true boundary inclination is slightly lower than the arbitrarily defined 45°). This shows that the inclination of the ident-

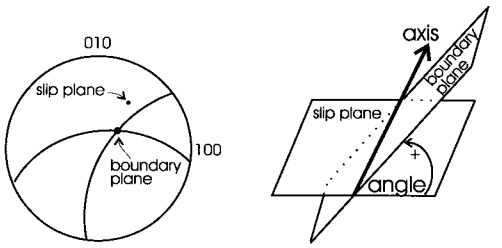

Fig. 4. Left: The boundary planes are characterised by their geometric relation to the nearest slip plane. Right: The relation is given by the angle between the slip plane and the boundary plane and the axis around which the boundary plane is rotated away from the slip plane. Anticlockwise rotations when looking in the axis direction are taken as positive.

ified boundary plane to the inspection plane is high and presumably sufficient to make the boundary visible.

2.2.2. Symmetry. The cubic crystal symmetry combined with the uniaxial sample symmetry gives 24 symmetrically equivalent crystallographic tensile axes [*uvw*], if axes pointing in the positive and negative direction are considered identical. In the analysis, all the measured grain orientations are converted to the symmetrically equivalent orientation lying in the stereographic triangle, where $u \geq v \geq w \geq 0$ (or $u \leq v \leq w \leq 0$). The symmetry operator invoked for conversion of the grain orientation is also applied to the set of possible boundary planes, $n(\beta)$, so that all sets refer to a crystallographic lattice with the tensile axis lying in the triangle, i.e. all arcs will intersect in the true boundary plane defined in this lattice.

The results of the two applications of the symmetry operator are thus (i) reduction of the grain orientation space considered from a full inverse pole figure to the stereographic triangle and (ii) an increased number of arcs representing possible boundary planes defined in the same crystallographic lattice and therefore easier identification of their intersection.

2.2.3. Boundary orientation description. In this paper the crystallographic orientation of the boundaries is described by their geometric relation to the nearest slip plane, which is marked in all the inverse pole figures presenting the results. The angle between the boundary and the slip plane, and the axis around which the boundary is rotated away from the slip plane describe the boundary orientation as shown in Fig. 4. Note that this angle/axis pair merely describes the orientation of the boundary plane relative to the slip plane. It has thus no relation to the misorientation between material volumes separated by the boundary or lattice rotations during deformation.

3. APPLICATION TO TENSILE DEFORMED ALUMINIUM

The geometric analysis is applied to transmission electron microscopy results on polycrystalline aluminium deformed in uniaxial tension to four strains in the range 0.05–0.34. These data were also the basis for the previous characterisation of grain orientation dependent dislocation structures in Ref. [5] where more details on material, deformation and transmission electron microscopy investigation can be found. Grains with the tensile direction in the vicinity of [100] are not considered because they do not form extended planar boundaries but have a structure consisting of equiaxed cells.

3.1. Grain orientation dependent crystallographic boundary planes

When arcs representing the possible boundary planes for all of the grains are drawn as described above in the same inverse pole figure, which is not shown here, the arcs do not go through a common point. This means that the grains do not all have dislocation boundaries with the same crystallographic orientation. Common points appear when only the arcs representing grains with similar orientations of the tensile axis, i.e. from the same region of the stereographic triangle, are drawn. It is therefore concluded that the crystallographic boundary orientation is grain orientation dependent.

Four different boundary orientations are found in regions labelled A to D.† The regions are somewhat overlapping, the overlap being especially pro-

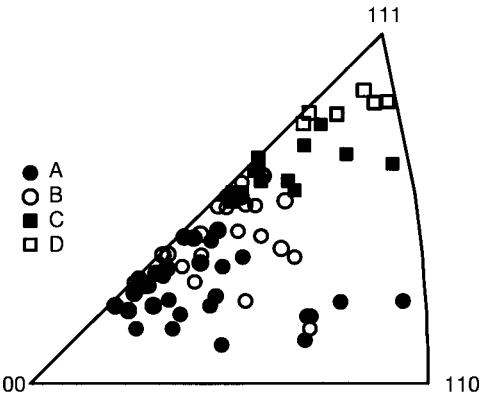

Fig. 5. The investigated grains cover four regions of the stereographic triangle (labelled A–D) where the formed dislocation boundaries have different preferred orientations.

† Note that the regions labelled A and B in Ref. [13] have been combined to region A in this paper and the labelling of the remaining regions changed accordingly (C to B, etc.).

Table 1. Summary of the rotations of the boundaries from the nearest slip planes in the different regions. The rotations are stated as angle/axis pairs

Region	Primary slip plane $(11\bar{1})$	Conjugate slip plane $(1\bar{1}1)$	Cross slip plane $(\bar{1}11)$	Critical slip plane (111)
A	0° to −10°/$[1\bar{2}\bar{1}]$	0° to -10°/$[\bar{1}12]$		Occasionally seen ?
B	0° to 10°/$[1\bar{2}\bar{1}]$	0° to 15°/$[\bar{1}12]$		Occasionally seen
C	10° to 35°/$[1\bar{2}\bar{1}]$ to $[2\bar{1}1]$		15° to 35°/$[\bar{1}1\bar{2}]$ to $[12\bar{1}]$	
D		10° to 35°/$[\bar{1}12]$ to $[\bar{2}\bar{1}1]$	15° to 35°/$[\bar{1}1\bar{2}]$ to $[12\bar{1}]$	

nounced for regions A and B. As described in more detail below, the boundaries in each region are rotated away from the slip planes around preferred crystallographic axes in preferred directions (positive or negative). The difference between the four regions lies in:

1. the slip planes to which the boundaries are related;
2. the axis around which the boundaries are rotated away from the slip plane;
3. the magnitude and sign of the angle between the boundary plane and the slip plane. This angle varies systematically with the grain orientation throughout each region, whereas no strain dependence could be detected.

Table 1 summarises the boundary orientations in each region and the extent of the different regions is shown in Fig. 5.

3.2. *Individual regions*

3.2.1. Region A. In region A, the arcs come close to the primary $(11\bar{1})$ or conjugate $(1\bar{1}1)$ slip planes. It is seen in Fig. 6(a) that the arcs close to the primary slip plane all pass through points representing planes rotated 0°–10° away from the primary slip plane around the $[1\bar{2}\bar{1}]$ axis in the negative direction [the circle in the inverse pole figure in Fig. 6(a) marks the plane rotated 10°]. The angle between the boundary plane and the slip plane increases when moving away from the [100] corner and up through the region. The grains with these boundaries are shown as circles in the triangle in Fig. 6(a).

The boundaries related to the conjugate slip plane are rotated less than 10° away from the slip plane in the negative direction around the $[\bar{1}12]$ axis. Again the highest angles are found in the upper part of the region. The plane rotated 10° is shown as a square in the inverse pole figure and the grains with these boundaries are marked with squares in the triangle in Fig. 6(a). The grains with boundaries related to the conjugate slip plane are only found in the vicinity of the [100]–[111] line and in many cases they also have a set of boundaries related to the primary slip plane.

Finally, the arcs from two of the grains are either rotated further away (10°–15°) from the primary slip plane in the opposite direction or lie close to the critical slip plane (111). These arcs are not shown in the inverse pole figure. The two grains with these boundaries lie in two different parts of the region—one is close to the [100]–[111] line and the other is far from it. They are marked with triangles in the stereographic triangle in Fig. 6(a).

3.2.2. Region B. In region B, most of the boundaries lie on planes rotated up to 10° away from the primary slip plane around the $[1\bar{2}\bar{1}]$ axis in the positive direction, as shown in Fig. 6(b) where the plane rotated 10° from the slip plane is marked with a circle. The deviation from the slip plane clearly increases with the distance from the [100] corner of the triangle like in region A. The $[1\bar{2}\bar{1}]$ axis is the same axis found in region A, but the rotation is in the opposite direction. The orientations of the grains with these boundaries are shown as circles in the triangle in Fig. 6(b).

Boundaries related to the conjugate slip plane are also seen, again sometimes as a second set and mostly in grains close to the [100]–[111] line. Determination of the rotation axis is not as easy as in the previous cases, but the rotation axis most consistent with the arcs is the same $[\bar{1}12]$ axis as in region A. However, in contrast to region A, the boundaries are rotated away from the conjugate slip plane in the positive direction. The magnitude of the positive rotations is less than 15° and increases with increasing distance from the [100] corner. The plane rotated 15° from the slip plane is marked with a square in the inverse pole figure in Fig. 6(b). The grain orientations are also marked with squares in the stereographic triangle.

Two boundaries are clearly rotated away from the critical slip plane, although the arcs are not shown. The grain orientations are marked with black triangles. No conclusions about the exact boundary plane can be drawn, but the deviation from the critical slip plane is larger than for the two grains in region A, possibly having boundaries related to the critical slip plane.

3.2.3. Region C. In this region, the arcs related to the primary slip plane do not intersect in a well-defined point, but follow approximately the same path in the lower and left part of the inverse pole figure [Fig. 6(c)]. Only one arc deviates from this path. The intersection between this arc and the rest gives boundaries rotated away from the primary slip plane around an axis close to $[2\bar{1}1]$, i.e. an axis different from the previous regions. Unfortunately, determination of the axis from the intersection

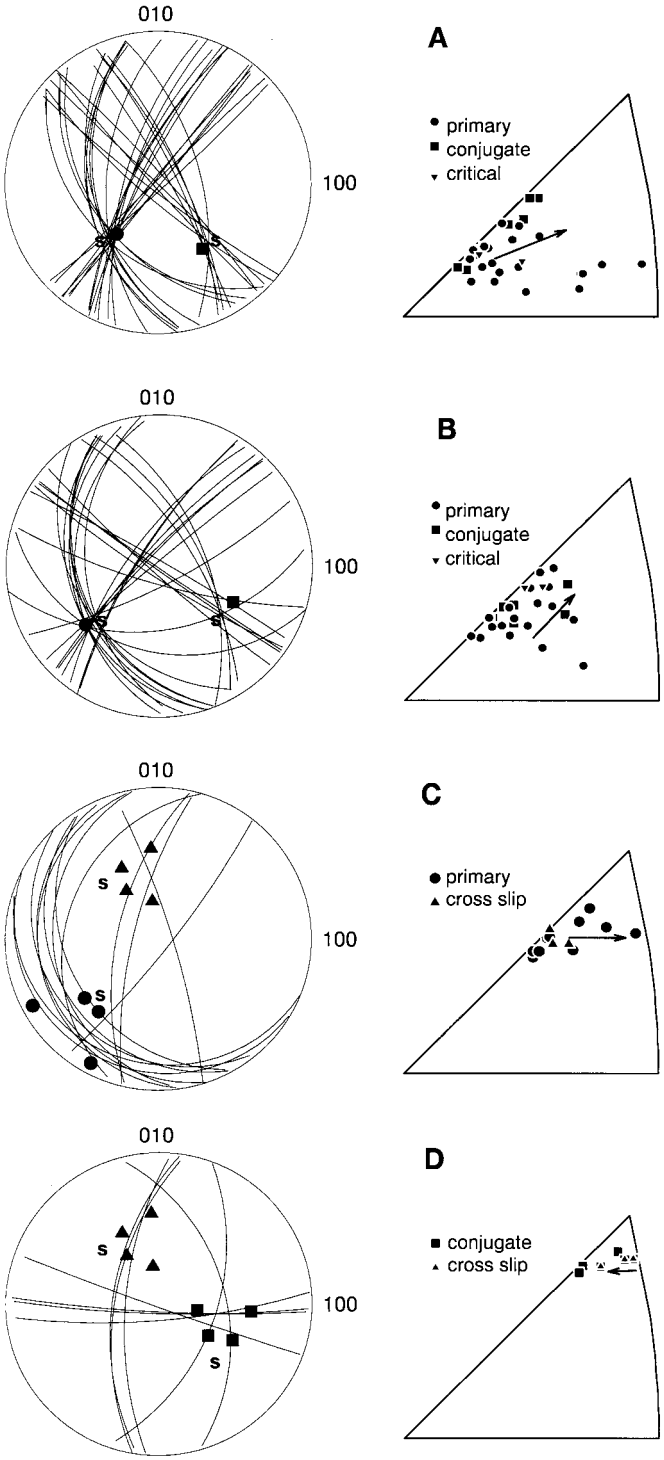

Fig. 6. Figures (A–D) show the four inverse pole figures with the arcs representing the possible boundary planes in regions A–D in Fig. 5. The arcs meet at the true boundary planes which are rotated differently from the nearest slip planes. The nearest slip planes are marked with the letter "s" and the symbols mark the boundary planes furthest from the slip plane. For each inverse pole figure, the orientation of the grains is shown in a stereographic triangle. The symbol used to mark a grain orientation indicates which slip plane that is closest to the boundary. Note that these symbols have no relation to the symbols used in the rest of the figures to represent grains in different regions. The tendency for increasing rotation angles from the nearest slip plane throughout the regions is illustrated with arrows.

between a single arc and all the rest is somewhat unreliable. One may, however, safely assume that the boundaries are rotated between 10° and 35° around axes between $[1\bar{2}\bar{1}]$ and $[2\bar{1}1]$. The four planes obtained from these axes and angles are marked with circles in the inverse pole figure and similarly the orientations of the grains with these boundaries are marked with circles in the stereographic triangle. The angle decreases with increasing distance from the [100]–[111] line.

In contrast to regions A and B, no boundaries related to the conjugate or critical slip planes are seen in this region. Instead, boundaries rotated 15°–35° away from the cross slip plane $(\bar{1}11)$ around an axis between $[\bar{1}1\bar{2}]$ and $[12\bar{1}]$ in the positive direction are found. The number of data points is insufficient to detect any system in the axis/angle variation. The four boundary planes obtained from these axes and angles are marked with triangles in the inverse pole figure and these symbols also mark the grain orientations in the stereographic triangle in Fig. 6(c).

3.2.4. Region D. Closest to the [111] corner, no boundaries related to the primary slip plane are seen. All the boundaries are related to the conjugate and cross slip planes. The boundaries related to the cross slip plane resemble those in region C. The orientation of grains with these boundaries are marked with triangles in the stereographic triangle in Fig. 6(d).

The arcs representing the boundaries rotated away from the conjugate slip plane do not cross in a well-defined point, but lie on planes rotated around axes between $[\bar{1}12]$ and $[\bar{2}\bar{1}1]$. There is almost certainly a spread of the axis in this region. The deviation angles are positive and lie between 15° and 35°, apparently with a tendency for larger angles with increasing distance from the [100]–[111] line, i.e. opposite to the tendency in region C. The four boundary planes obtained from these axes and angles are marked with squares in the inverse pole figure in Fig. 6(d) and the grain orientations are also marked with squares in the triangle.

4. CRYSTALLOGRAPHIC VS MACROSCOPIC ORIENTATION

As stated in the beginning of Section 2, the presented analysis would not have resulted in intersecting arcs at specific crystallographic planes if the boundaries did not have crystallographically preferred orientations.

A preferred macroscopic boundary orientation in analogy with observations in rolling and torsion would give boundaries lying on the most stressed planes, which are inclined 45° to the tensile axis and are tangents to a cone around this axis. In an inverse pole figure, these planes form a ring around the tensile axes and the arcs from grains with similar tensile axes would intersect this ring in different places, instead of intersecting in a point. As seen in Fig. 6, this is clearly not the case and it must therefore be concluded that the boundaries do not just form on the macroscopically most stressed planes, but have strong preferences for certain planes in the crystallographic lattice.

It is, however, possible that the preferred crystallographic planes are highly stressed, so that the

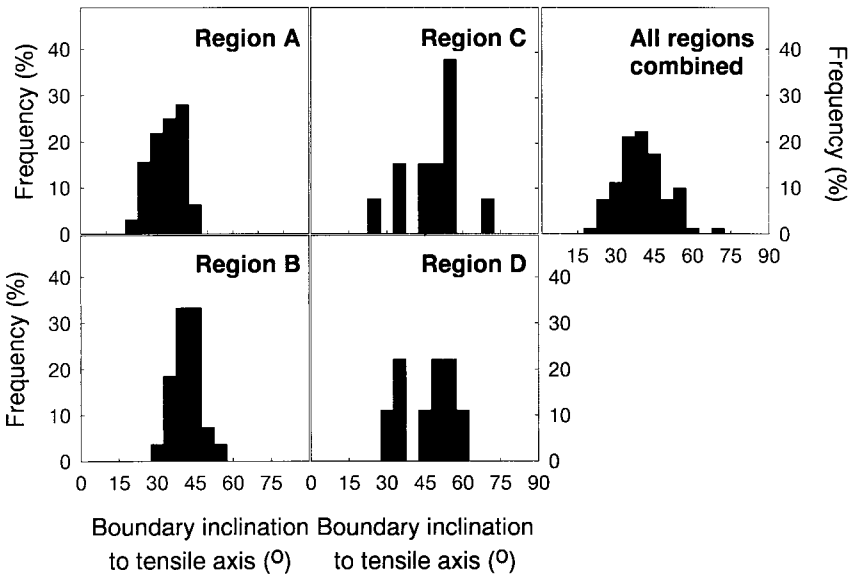

Fig. 7. Distributions of the inclination of the boundary planes to the tensile axis for the grains in regions A–D in Fig. 5 and the combined distribution for all grains.

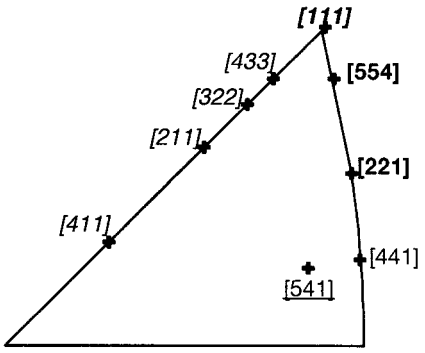

Fig. 8. Single crystal orientations investigated in Refs [16–20]. Crystals with similar boundary orientations are marked with the same font.

boundaries also have a preferred macroscopic inclination, although they do not exhibit rotational symmetry around the tensile axis. In order to investigate this, the inclination of the determined boundary planes to the tensile axis has been calculated. In regions C and D, where the axis around which the boundary planes are rotated away from the slip planes has only been determined as lying between two ⟨112⟩ axes (see Table 1), the boundary plane has been determined using the ⟨110⟩ axis lying in the middle of this axis range. Use of other axes within the range changes the macroscopic orientation distributions somewhat, but does not alter the conclusion of this section. The distributions of macroscopic inclination angles are shown in Fig. 7.

It is seen that there is considerable variation between the different regions. In regions A and B, the distributions form broad peaks where the majority of the boundaries are inclined slightly less than 45° to the tensile axis. The distributions of the boundaries related to the primary and conjugate slip planes overlap strongly, although the latter are ~5° less inclined to the tensile axis. The spread of the macroscopic boundary orientations is ~25°, i.e. twice the spread observed in the crystallographic co-ordinate system. This further demonstrates that the crystallographic orientation preference is much stronger than the macroscopic.

In regions C and D, the boundaries related to the cross slip plane are inclined about 30° to the tensile axis, while the boundaries related to the other slip planes (primary and conjugate, respectively) lie in the peaks with maxima around 50°. The macroscopic inclination of the two different crystallographic boundary orientations in each region is therefore not the same. This again shows that the crystallographic boundary orientation is more important than the macroscopic, even though the spreads in the macroscopic and crystallographic co-ordinate systems are comparable in these regions (~15–20°).

The final conclusion is therefore that the macroscopic preference is much weaker than the crystallographic. It is, however, noteworthy that the inclination to the tensile axis for the boundaries in all the regions forms a broad irregular peak centred slightly below 45°, as also shown in Fig. 7. This combined distribution resembles the distribution of the macroscopic boundary planes in rolled materials [14, 15]. A closer study of the boundary orientation in materials subjected to other deformation modes than tension will probably reveal that these boundaries also have preferred crystallographic orientations, depending on the grain orientation, and

Table 2. Boundary orientations for single crystals lying in the polycrystal regions A–D defined by Fig. 5. Differences between boundary orientations in single and polycrystals (see Table 1) are underlined

Poly-crystal region	Single crystal orientation	Nearest slip plane in single crystals	Single crystal boundary rotation axis/direction	Ref.
A	[541]	primary	$[2\bar{1}1]/\pm$	[17, 18]
	[441]	primary	$[1\bar{1}0]/-$	[20]
	[411][a]	primary, conjugate	p: $[2\bar{1}1]/\pm$ c: $[\bar{2}\bar{1}1]/\pm$	[20]
B	[411][a]	primary, conjugate	p: $[2\bar{1}1]/+$ c: $[\bar{2}\bar{1}1]/+$	[20]
	[211][a]	primary, conjugate, sometimes cross slip	p: $[2\bar{1}1]/+$ c: $[\bar{2}\bar{1}1]/+$ cross: ?	[16–18]
C	[211][a]	primary, conjugate sometimes cross slip	p: $[2\bar{1}1]/+$ c: $[\bar{2}\bar{1}1]/+$ cross: ?	[16–18]
	[322][a]	primary, conjugate	p: $[2\bar{1}1]/+$ c: $[\bar{2}\bar{1}1]/+$	[20]
	[221]	primary	$[1\bar{1}0]/+$	[20]
D	[322][a]	primary, conjugate	p: $[2\bar{1}1]/+$ c: $[\bar{2}\bar{1}1]/+$	[20]
	[433]	primary, conjugate	p: $[2\bar{1}1]/+$ c: $[\bar{2}\bar{1}1]/+$	[20]
	[111][b]	primary, conjugate, cross slip	p: $[2\bar{1}1]/+$ c: $[\bar{2}\bar{1}1]/+$ cross: $[01\bar{1}]/+$	[19]
	[554]	primary	$[1\bar{1}0]/+$	[20]

[a] Crystal orientation on the border between two regions.
[b] Primary, conjugate and cross slip planes are symmetrically equivalent.

that the large spread of the macroscopic boundary orientations reflects a stronger preference for specific crystallographic boundary orientations in grains with different orientation. The fact that some grain orientations in rolled aluminium polycrystals have been found to have boundaries that preferentially align with the slip planes [7, 8] supports this expectation.

5. COMPARISON WITH SINGLE CRYSTALS

Previous studies of the angle between the boundary trace and the trace of the nearest slip plane as observed directly in transmission electron microscopy have indicated a similarity between the boundaries formed in polycrystals (Al, Cu) and single crystals (Cu) [5–7] for strains less than approximately 1. The new determination of the boundary orientations in polycrystals allows a more detailed comparison with the single crystal results reported in Refs [16–20].

The single crystal orientations are shown in Fig. 8, where crystal orientations with similar boundary orientations are marked with the same font. It is seen that the subdivision of the triangle in Fig. 5 determined for polycrystalline aluminium does not apply to single crystals. In contrast to the polycrystals, the difference between single crystals on the ⟨100⟩–⟨111⟩ and the ⟨110⟩–⟨111⟩ lines, i.e. when moving horizontally in the triangle, is larger than the vertical differences between the ⟨100⟩–⟨110⟩ line and the ⟨111⟩ corner.

The general tendency for macroscopic boundary planes inclined about 45° to the tensile axis is found in both single and polycrystals. The detailed crystallographic boundary orientations in single crystals are compared with the polycrystal boundaries in Table 2, where the differences between the single and polycrystal boundaries are underlined. The comparison leads to the following conclusions:

- Dislocation boundaries in single and polycrystals are generally related to the same slip planes, except for a lack of boundaries related to the conjugate and primary slip planes in regions C and D, respectively, for the polycrystals.
- The angle between the boundary plane and the nearest slip plane is of similar magnitude in single and polycrystals for all regions.
- The degree of similarity between the rotations relating the boundary plane and the nearest slip plane differs from region to region:
  - In regions A–B, the polycrystal boundaries are rotated away from the slip planes in directions and around axes that differ from those in the single crystals.
  - In regions C–D, the polycrystal boundaries resemble those in single crystals. The direction of the rotation is the same in both types of crystals. The spread of rotation axes found in the polycrystals covers the axes seen in the single crystals but, in contrast to the single crystal observations, no systematic axis variation could be detected in the polycrystal when going from the [100]–[111] line to the [110]–[111] line. The fact that no systematic variation of the axis was detected for the polycrystal in regions C–D might, however, be ascribed to an insufficient number of observed grains.
- Comparison of the strain dependence of the boundary orientation in the two types of crystals is somewhat inconclusive:
  - In the polycrystals no strain dependence was detected. Instead, the angle between the boundary planes and slip planes in the polycrystals varies fairly systematically with the grain orientation.
  - In the single crystals, a strain dependence of the angle was observed in a [211] single crystal, which maintained its orientation during the deformation [18]. However, no change in the crystallographic boundary orientation was seen in a [541] crystal, although it rotated substantially towards the [211] crystal orientation [18].

6. DISCUSSION

6.1. Subdivision of the stereographic triangle

The analysis presented above focused on the orientation of the extended planar boundaries and the grains with equiaxed cells were therefore not included. These grains, which lie in the [100] corner of the triangle, may however be added to Fig. 5, as shown in Fig. 9(a). The stereographic triangle is thus really divided into five regions with different dislocation structures—four with extended planar boundaries and one with equiaxed cells.

The subdivision of the triangle into the five regions is based on the same TEM data used to obtain the subdivision shown in Fig. 1 (see Ref. [5]). In that study, the triangle was subdivided into only three regions: the region with equiaxed cells, and two regions where the trace of the boundary deviated less than or more than 5° from the trace of the nearest slip plane. However, when remembering the different subdivision criteria, the two subdivisions in Figs 1 and 9 agree. The region in Fig. 1 with boundaries aligned with the slip planes covers the part of region A close to the ⟨100⟩–⟨111⟩ line and the lower part of region B, which are also the parts of the triangle in Fig. 9(a) where the boundaries are closest to the slip planes. The previous subdivision in Fig. 1 did, however, not take the detailed geometric relation between boundary and slip planes into account and therefore the difference

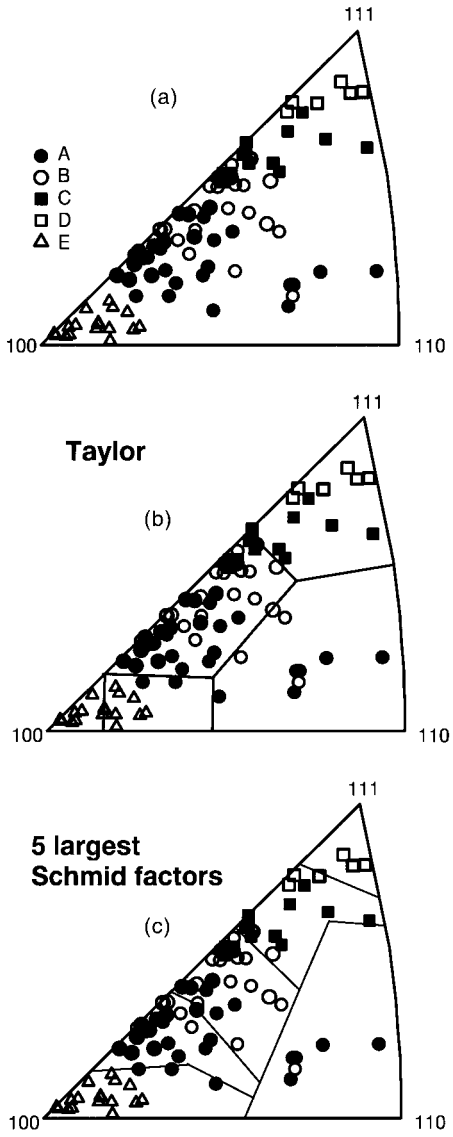

Fig. 9. Subdivision of the triangle according to (a) dislocation microstructure (repetition of Fig. 5 with the addition of region E, where the grains form equiaxed cells), (b) slip patterns predicted by the Taylor model and (c) the five most stressed slip systems.

between the boundary orientation in regions A and B was not detected. For the same reason, the wide extent of region A towards the [110] corner and the different orientations of the boundaries lying further from the slip plane (regions C and D) were not revealed. Figure 9(a) is therefore not in conflict with the previous subdivision, but an improvement obtained through a more detailed analysis.

It is possible that the triangle should be subdivided into even more regions, since the boundary orientation is only one parameter characterising the boundary. Boundaries with the same orientation may, for example, accommodate different misorientations between the material volumes they separate. Likewise, the grains in the four regions with extended boundaries in Fig. 9(a) may differ in more ways than by having boundaries of different crystallographic orientation. The previous study [5], for example, showed that the dislocation density in the boundaries is lower and the boundaries generally sharper in certain parts of the triangle. Investigations clarifying these points are currently in progress.

In contrast to the subdivisions in Figs 1 and 9(a), the subdivisions for single and polycrystals [Figs 8 and 9(a)] are different, but in both types of crystals the boundaries definitely have preferred crystallographic orientations, depending on the crystal/grain orientation.

6.2. Origin of preferred boundary orientations

The existence of a strong correlation between the grain orientation and the crystallographic boundary orientation, together with the dependence of the dislocation structure on the deformation mode, shows that the slip pattern is an important factor controlling boundary formation. The slip pattern depends on the grain orientation with respect to the deformation axes and the slip generates the dislocations forming the boundaries.

Regions of grain orientations with different preferred crystallographic boundary orientations consequently correspond to regions with qualitatively different slip patterns, presumably activation of different systems. The tendency for a systematic variation of the angle between the boundary plane and the nearest slip plane throughout each region reflects minor variations in this pattern with grain orientation, presumably different shear strains on each system. Overlap between regions may be attributed to strain effects (see discussion below) or to interaction between neighbouring grains which alters the slip pattern. The existence of grain orientation dependent boundary orientations does, however, show that grain interaction is of minor importance.

The importance of the slip pattern also explains the weaker macroscopic preference for boundary orientations with a similar relation to the deformation mode (boundaries on most stressed planes), irrespective of the deformation mode (rolling, torsion and tension) and the crystal structure (f.c.c. or b.c.c.). All grain orientations tend to slip on systems that are highly stressed and all boundaries should therefore have similar relations to the most stressed planes. It is, however, not clear exactly why the boundaries should be aligned with these macroscopic planes, except that boundaries aligned with the general slip direction may obstruct the slip the least. It is noteworthy that the preferred crystallographic boundary planes exhibit a similar tendency for alignment with slip planes that are highly active [7, 21].

The observed differences between single and polycrystals can also be explained by the slip pattern. Single crystals generally deform by slip on only one or a few slip systems, while multislip is dominant in polycrystals. This interpretation is consistent with the observation that the difference between the orientation of single and polycrystal boundaries is largest in the lower part of the stereographic triangle, i.e. in regions A–B, and smaller in regions C–D where multislip is more likely also for the single crystals.

6.3. Strain dependence of boundary orientations

The facts that the crystallographic boundary orientation correlates so strongly with the grain orientation, even within a region, and that the crystallographic boundary orientation apparently is independent of the strain, imply that the immediate grain orientation and not the history of the grain controls the crystallographic boundary orientation. On the other hand, the misorientation across the boundaries increases with strain, indicating that the dislocations accumulate in the boundaries during deformation. When the grain orientation rotates during deformation, the slip pattern also changes and dislocations with different Burgers vectors are generated in varying amounts at different states of the deformation. One would therefore expect that the boundary characteristics, including the crystallographic orientation, would be a function of the history, rather than of the immediate orientation. A mechanism for such a boundary reorientation in a rolled cube single crystal with increasing strain based on the slip pattern and maintenance of the boundary as a low energy dislocation structure has been proposed [22].

The preferred macroscopic boundary orientation has been observed [23] not to rotate away from the most stressed planes in the same way grain boundaries do, due to geometric effects induced by the change in the macroscopic shape of the sample. This also indicates that the boundaries somehow maintain preferred orientations. Evolution of the preferred macroscopic boundary orientations is, however, a combination of the evolution of both the stronger crystallographic boundary orientation and the texture. Analysis of the strain dependence of macroscopic boundary orientations is therefore even more complicated.

Further studies of the strain dependence of the boundary characteristics (orientation, misorientation across the boundaries, dislocation contents) are needed to understand the evolution of dislocation boundaries during deformation. Single crystal results in both tension [18] and rolling [24] suggest that at least some crystal orientations have strain dependent preferred crystallographic boundary orientations and this may also be found in polycrystals when larger strain ranges than applied here and more grain orientations at each strain are considered.

6.4. Slip pattern determination

The conclusion that the crystallographic boundary orientation reflects the slip pattern in the grain means that studies of the dislocation microstructure also give information on the slip pattern: The regions in Fig. 9(a) with different dislocation structures thus correspond to regions with different slip patterns. Comparison of Fig. 9(a) with slip pattern predictions obtained with polycrystal plasticity models is therefore an important tool when these models are evaluated.

The regions predicted to have the same sets of active slip systems with the classic Taylor model are shown in Fig. 9(b). It is seen that the Taylor model predicts a change in the slip pattern between some of the regions in Fig. 9(a). However, the changes between regions A/B and C/D are not predicted. Furthermore, the Taylor model predicts a change in the slip systems operating throughout regions A and E. This might reflect a change in other boundary characteristics than the orientation as described above. It is also possible that two different slip patterns may produce practically identical boundaries.

The Taylor model assumes full strain compatibility between the grains and slip on the systems that fulfil this while minimising the work. A better agreement between the regions in Fig. 9(a) with different microstructures and regions with different slip patterns is found with a Schmid factor analysis, where it is assumed that slip occurs on the most stressed slip systems, like in single crystals, but that multislip is induced in all grains to enforce some degree of strain compatibility. In Fig. 9(c) the triangle is subdivided into regions which have the same five most stressed slip systems. It is seen that, in addition to the regions correctly predicted by the Taylor model, the new subdivision also predicts the changes between regions A/B and C/D. All of region E is now predicted to have the same slip systems, while region A still is split up into two different slip patterns. Considering the wedge formed by region B and effectively bisecting region A, it is not unlikely that region A should indeed be subdivided into two regions.

The potential subdivision of region A, as well as the consequences of activity on the five most stressed systems for strain compatibility, work, texture development, etc., will be addressed in a subsequent paper. The fact that the boundaries once formed may also influence the slip pattern will also be considered in a coupled modelling of textural and microstructural evolution, following the lines suggested in Refs. [13, 25, 26].

7. CONCLUSION

- A geometric analysis method for determination of the three-dimensional orientation of extended planar dislocation boundaries in deformed polycrystals has been developed. The analysis is based on the angle between the trace of the boundary and the deformation axes as observed for a number of grains by TEM.
- The analysis has been applied to extended planar dislocation boundaries in tensile deformed polycrystalline aluminium ($0.05 < \varepsilon < 0.34$) leading to identification of preferred boundary planes in the crystallographic lattice and a weaker preferred boundary orientation with respect to the macroscopic tensile axis:
  - The preferred crystallographic boundary planes correlate with the grain orientation so that the stereographic triangle representing all possible grain orientations in axisymmetric tension is divided into five (possibly six) regions. One region only forms equiaxed cells, while the rest contains extended planar dislocation boundaries with different preferred crystallographic orientations. The existence of a strong crystallographic preference and the grain orientation dependence shows that the orientation of the extended planar boundaries is closely linked with the active slip systems in the grain.
  - The preference for macroscopic boundary orientations close to the most stressed planes, i.e. inclined about 45° to the tensile axis, is weaker than the crystallographic preference. The macroscopic preference is attributed to the general tendency of all grain orientations for slip on highly stressed slip systems, while the details of the slip in each grain determines the exact boundary orientation.
- The work is relevant to structure characterisation, but also has implications for future modelling efforts. The different dislocation structure in grains with different orientation shows that different slip systems are active. The correlation between the dislocation structure and the grain orientation therefore provides an experimental tool to validate the predictions of slip system activity obtained with polycrystal plasticity models.

REFERENCES

1. Bay, B., Hansen, N., Hughes, D. A. and Kuhlmann-Wilsdorf, D., *Acta metall. mater.*, 1992, **40**, 205.
2. Wilson, D. V. and Bate, P. S., *Acta metall. mater.*, 1994, **42**, 1099.
3. Akbari, G. H., Sellars, C. M. and Whiteman, J. A., *Acta mater.*, 1997, **45**, 5047.
4. Hughes, D. A. and Hansen, N., *Mater. Sci. Technol.*, 1991, **7**, 544.
5. Huang, X. and Hansen, N., *Scripta mater.*, 1997, **37**, 1.
6. Huang, X., *Scripta mater.*, 1998, **38**, 1697.
7. Liu, Q. and Hansen, N., *Phys. Stat. Sol. (a)*, 1995, **149**, 187.
8. Liu, Q., Juul, Jensen D. and Hansen, N., *Acta mater.*, 1998, **46**, 5819.
9. Buque, C., Holste, C. and Schwab, A., in *Proc. 20th Risø International Symposium on Materials Science*, ed. J. Bilde-Sørensen, J. V. Carstensen, N. Hansen, D. Juul Jensen, T. Leffers, W. Pantleon, O. B. Pedersen and G. Winther. 1999, pp. 277–282.
10. Huang, X. and Liu, Q., *Ultramicroscopy*, 1998, **74**, 123.
11. Liu, Q., *J. appl. Crystallogr.*, 1994, **27**, 762.
12. Young, C. T., Steele, J. H. and Lytton, J. L., *Metall. Trans.*, 1973, **4**, 2081.
13. Winther, G., in *Proc. 20th Risø International Symposium on Materials Science*, ed. J. Bilde-Sørensen, J. V. Carstensen, N. Hansen, D. Juul Jensen, T. Leffers, W. Pantleon, O. B. Pedersen and G. Winther. 1999. Risø National Laboratory, Roskilde, Denmark, pp. 541–546.
14. Falk, J., Bay, B. and Hansen, N., in *Proc. 16th Risø Symposium*, ed. N. Hansen, D. Juul Jensen, Y. L. Liu and B. Ralph. 1995. Risø National Laboratory, Roskilde, Denmark, pp. 351–357.
15. Christoffersen, H. and Leffers, T., *Scripta mater.*, 1997, **37**, 2041.
16. Anongba, P. N. B., Bonneville, J. and Martin, J. L., *Acta metall.*, 1993, **41**, 2907.
17. Kawasaki, Y., *J. Phys. Soc. Jap.*, 1974, **36**, 142.
18. Kawasaki, Y., *Jap. J. Appl. Phys.*, 1979, **18**, 1429.
19. Kawasaki, Y. and Takeuchi, T., *Scripta met.*, 1980, **14**, 183.
20. Kawasaki, Y., in *Strength of Materials*, ed. H. Oikawa. The Japan Institute of Metals, 1994, pp. 187–190.
21. Winther, G., Juul, Jensen D. and Hansen, N., *Acta mater.*, 1997, **45**, 5059.
22. Pantleon, W. and Hansen, N., in *Proc. 19th Risø International Symposium on Materials Science*, ed. J. V. Carstensen, T. Leffers, T. Lorentzen, O. B. Pedersen, B. F. Sørensen and G. Winther. 1998. Risø National Laboratory, Roskilde, Denmark, pp. 405–410.
23. Christoffersen, H. and Leffers, T., *Acta mater.*, 1998, **46**, 4093.
24. Liu, Q. and Hansen, N., *Proc. Roy. Soc. Lond. A*, 1998, **454**, 2555.
25. Winther, G., in *Proc. 19th Risø Symposium*, ed. J. V. Carstensen, T. Leffers, T. Lorentzen, O. B. Pedersen, B. F. Sørensen and G. Winther. 1998. Risø National Laboratory, Roskilde, Denmark, pp. 185–199.
26. Winther, G., in *Proc. ICOTOM 12*, ed. J. Szpunar. 1999. NRC Research Press, Ottawa, pp. 387–392.

A4: Dense dislocation walls and microbands aligned with slip planes – theoretical considerations by G. Winther, D. Juul Jensen and N. Hansen, Acta Materialia, 1997

Pergamon

Acta mater. Vol. 45, No. 12, pp. 5059–5068, 1997

Printed in Great Britain
PII: S1359-6454(97)00168-7
1359-6454/97 $17.00 + 0.00

DENSE DISLOCATION WALLS AND MICROBANDS ALIGNED WITH SLIP PLANES—THEORETICAL CONSIDERATIONS

G. WINTHER, D. JUUL JENSEN and N. HANSEN
Materials Department, Risø National Laboratory, DK-4000 Roskilde, Denmark

(Received 29 December 1996; accepted in revised form 12 May 1997)

Abstract—Some of the dislocation boundaries in cold deformed f.c.c. metals at low and intermediate strains lie on crystallographic slip planes and others have a macroscopic direction with respect to the sample axes (i.e. they are non-crystallographic). A model for the occurrence of the former type of dislocation boundaries is proposed. The model combines slip pattern analysis and dislocation theory. It is assumed (i) that the dislocations in the boundaries are generated by slip, (ii) that the deformation temperature is low enough to exclude dislocation climb and (iii) that the driving force for formation of boundaries is minimisation of the energy stored in the boundaries. Formation of crystallographic boundaries is predicted if two active slip systems in the same slip plane account for a large fraction of the total slip. For single crystals the agreement between predicted and experimentally observed crystallographic and non-crystallographic boundaries is excellent. For different grain orientations in poly crystalline aluminium specimens, the agreement between prediction and experiment is satisfactory in view of the complexity of polycrystal studies compared to studies of single crystals. © *1997 Acta Metallurgica Inc.*

1. INTRODUCTION

Significant progress has been made recently in the characterisation of microstructural development during plastic deformation (for an overview, see [1]), and a framework common to f.c.c. metals of medium to high stacking fault energy has been suggested [2]. It has been shown that the original grains subdivide by dislocation boundaries. At low and medium strain, dense dislocation walls (DDWs), microbands (MBs) and ordinary cell boundaries are dominating, whereas at high strain lamellar boundaries and subgrain boundaries develop. These dislocation structures, together with the crystallographic textures are key elements controlling important material properties [3–5].

In the literature, DDW/MBs as planar structures in f.c.c. single crystals have been reported to coincide with $\{111\}$ planes [6–12]. However, DDW/MBs which are not aligned with a $\{111\}$ plane have also been observed [11, 13]. In recent studies of polycrystalline aluminium deformed in rolling [14] and tension [15] both types of DDW/MBs have been observed. In the following these two types of boundaries will be termed crystallographic boundaries and non-crystallographic boundaries, respectively. A DDW/MB is normally taken to be crystallographic if its trace in the plane of observation deviates less than 5° from that of a $\{111\}$ plane.

The effect of grain orientation on the direction of DDW/MBs has been correlated with the distribution of Schmid factors for the individual slip systems in the grains. It was observed [14] that crystallographic DDW/MBs formed if the high Schmid factors were concentrated in two slip planes. If the high Schmid factors were distributed over several slip planes, the DDW/MBs were non-crystallographic. Kawasaki and Takeuchi [16] also observed that an increase in the number of slip systems caused an increasing deviation of the dislocation boundaries from the slip plane.

The aim of this paper is to analyse the occurrence of crystallographic DDW/MBs theoretically by combining dislocation theory and slip pattern predictions. The dislocations needed to form a boundary coinciding with a crystallographic plane are found from dislocation theory by considering both geometric and energetic relations. Assuming that the dislocations in the boundaries are generated by slip during deformation, slip patterns obtained from crystal plasticity calculations are analysed in order to identify grain orientations which form crystallographic DDW/MBs. The theoretical results are compared with experimental observations for both single crystals and aluminium polycrystals and a criterion for crystallographic DDW/MB formation is formulated.

2. THEORETICAL ANALYSIS

The analysis focuses on f.c.c. materials with $\{111\}\langle 011\rangle$ slip systems and it is based on the following assumptions:

1. The boundary dislocations are generated by slip

in the active slip systems, i.e. they have Burger's vectors given by the slip directions.

2. The number of generated dislocations from a particular slip system is proportional to the slip in that system.

3. The dislocations do not climb on a macroscopic scale, i.e. the analysis is only valid for deformation at low temperatures.

4. Dislocations assemble into boundaries to minimise their energy.

2.1. Formation of dislocation boundaries when considering both geometry and energy factors

A number of geometrical restrictions applies to dislocation boundary construction. First of all the dislocations in the boundary must have dislocation lines which lie in the boundary plane. The way the dislocations move to form the boundary must also be considered. Dislocations may move in three different ways:

- By slip, i.e. in the slip plane (edge and screw dislocations).
- By cross slip, i.e. into another slip plane (screw dislocations).
- By climb, i.e. out of the slip plane (edge dislocations).

In the absence of climb as stated in the third assumption above, the dislocations can only form the boundary through motion in slip planes and the dislocation lines must therefore lie in both the boundary plane and a slip plane. Recently, Wert *et al.* [13] utilised these geometrical relations to analyse the boundaries in a single crystal of cube orientation.

When dislocations assemble into a DDW/MB, their stress fields become screened by the other dislocations and DDW/MBs have therefore been characterised as low energy dislocation structures [17]. A low energy dislocation boundary with no long range stresses obeys Frank's law [18]:

$$\mathbf{V} \times \mathbf{a} = \sum_i \mathbf{b}_i \left\{ \frac{1}{2D_i \sin(\theta/2)} (\mathbf{n} \times \boldsymbol{\xi}_i) \cdot \mathbf{V} \right\}, \qquad (1)$$

for all vectors $\mathbf{V}$ in the boundary with normal $\mathbf{n}$ and consisting of dislocations with Burgers vectors $\mathbf{b}_i$ spacing D_i and dislocation line unit vectors $\boldsymbol{\xi}_i \cdot \mathbf{a}$ and θ are the misorientation axis and angle of the boundary, respectively.

Frank's law [equation (1)] imposes additional restrictions on the boundaries which can be constructed from a given set of dislocations. These restrictions have been investigated in general by Hirth and Lothe [18] and the results have been used to explain the boundaries formed in aluminium grains of ⟨120⟩ orientation during tensile deformation [19].

Application of the general results by Hirth and Lothe to the specific case of crystallographic boundaries leads to the following conclusions:

- A crystallographic boundary in f.c.c. materials contains at least two sets of dislocations (Frank's law does not allow a crystallographic boundary with a single set of dislocations).
- A boundary containing two sets of dislocations with Burgers vectors in the same slip plane and non-parallel dislocation lines is crystallographic (the two dislocation lines must lie both in the slip plane and in the boundary plane which is only geometrically possible if the slip plane is also the boundary plane).
- A crystallographic boundary containing just two sets of dislocations with Burgers vectors in the same slip plane is a pure twist boundary. If additional dislocation sets are incorporated into the boundary this restriction of the boundary misorientation axis is relaxed.

Two sets of dislocations with Burgers vectors in the same slip plane will be generated when there are two active slip systems in the same slip plane, i.e. *coplanar slip*. It seems intuitively reasonable that the crystal/grain will only form a DDW/MB from the dislocations generated by the coplanar systems if they are available in significant quantities. According to the second assumption above this means that a significant part of the slip takes place in the coplanar systems.

2.2. Formation of crystallographic boundaries. Effect of grain orientation

The present study is concentrated on finding crystal/grain orientations which are likely to form crystallographic boundaries in view of the considerations above, i.e. orientations where a boundary relates to a slip plane because it contains two sets of dislocations from that slip plane and where the shears on the slip systems generating these dislocations are large.

It is therefore proposed that a crystallographic DDW/MB forms if a large fraction of the shear in the crystal/grain occurs in two slip systems in the same slip plane. The total slip in the crystal/grain is given by the M-factor. The slip occurring on two slip systems in the same slip plane is quantified by the coplanar slip fraction:

$$\text{coplanar slip fraction} = \begin{cases} \dfrac{\Sigma \gamma_i}{M} & i \text{ runs over two active slip systems in the same slip plane} \\ 0 \quad , & \text{if there are less than two active systems in the same slip plane} \end{cases} \qquad (2)$$

where γ_i is the shear on slip system i.

Some grain orientations have a second slip plane

with coplanar slip. These grains may form two sets of crystallographic DDW/MBs.

It is difficult to quantify the term a "high" $\Sigma\gamma_i/M$ value theoretically. Instead a survey of the orientation space is made to obtain the $\Sigma\gamma_i/M$ values for grains with different orientations. The deformation considered is plane strain compression. Thereafter the term will be quantified through comparison with calculated slip patterns for grain orientations experimentally observed to have either crystallographic or non-crystallographic DDW/MBs.

3. COPLANAR SLIP FRACTIONS

Calculations of coplanar slip fractions have been made for grain orientations on a grid in Bunge's Euler space where φ_1, Φ and φ_2 were varied in 5° steps. The slip pattern in plane strain compression has been predicted with the Taylor model using full constraints (FC) and relaxed constraints (RC) [where ε_{13} and ε_{23} may be non-zero (RD = 1, ND = 3)] as boundary conditions. In the case of slip ambiguity the predicted slip pattern was taken as the average of all possible solutions. For each of the four slip planes in f.c.c. crystals the coplanar slip fractions [equation (2)] were calculated and the largest value for that grain orientation selected.

Figures 1 and 2 are ODF contour plots showing the obtained coplanar slip fractions. It is seen that different boundary conditions result in quite different coplanar slip fractions. RC generally gives higher fractions than FC because the coplanar slip involves two slip systems and the M-factor is the total slip in three or five systems, respectively.

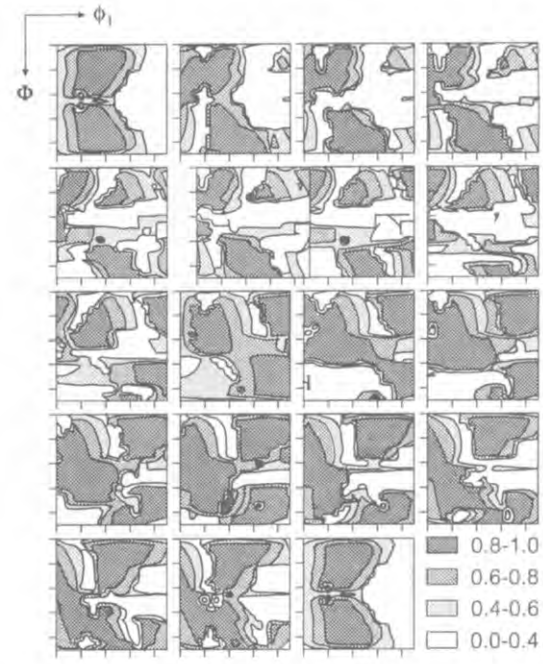

Fig. 2. ODF showing the largest coplanar slip fractions in RC plane strain compression.

Figure 3 shows an ODF of the second largest coplanar slip fractions in FC plane strain compression, i.e. the slip fractions which may result in

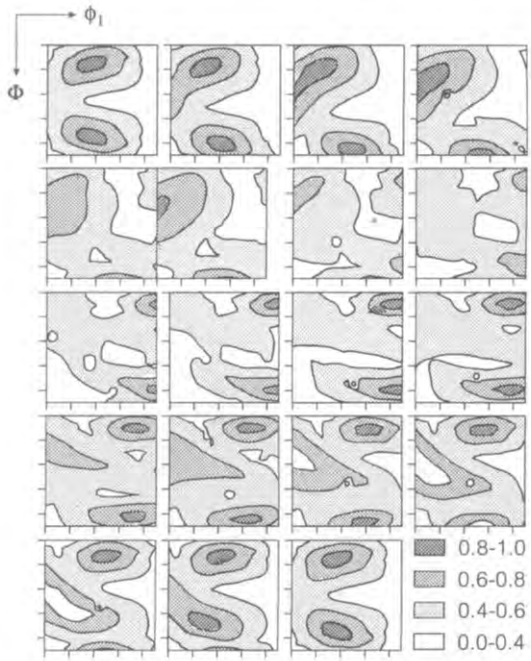

Fig. 1. ODF showing the largest coplanar slip fractions in FC plane strain compression.

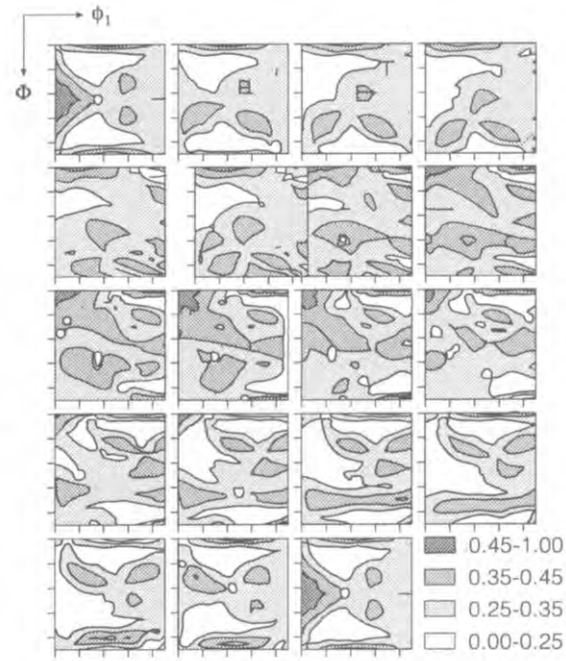

Fig. 3. ODF showing the second largest coplanar slip fractions in FC plane strain compression.

Table 1. Summary of microstructure observations in rolled and channel die compressed single crystals of f.c.c. metals. The observed structures are separated into three categories: structures with two, one or no DDW/MBs along traces of {111} slip planes. For each observation the material studied, the sample planes in which the structures were studied, and the reference number are given

Orientation	Deformation	2 along {111}	1 along {111}	Not along {111}
Goss	Rolling	Al–3% Mg (long) [8] Cu (long) [10] (MB2s) Cu (long) [7] Cu (long) [22]		
	Channel die		Al (long) [23]	
Brass	Rolling	Al (rol + long + trans) [12] Cu (long + trans) [6] Cu (long) [10] Cu (long) [22] Ni (long) [24]		
	Channel die		Al (long) [23]	
Copper	Rolling	Ni (long) [24]	Al (long) [9] Al–3% Mg (long + trans) [8] Cu (long + trans) [10] Al no line shift (rol + long + trans) [11]†	Al no line shift (rol + long + trans) [11]†
	Channel die		Al (long) [23]	
S	Rolling			
	Channel die		Al (long) [23]‡ (S-bands) Al (rol + long + trans) [25]‡ (S-bands)	
Cube	Rolling	Cu (long + trans) [6] (MB2s)		Al (long) [13] Cu (long) [22]
	Channel die			

†Crystallographic DDW/MBs were found in volumes of the crystal with coplanar slip, and non-crystallographic where slip occurred in two systems with the same slip direction but different slip planes.

‡One set of S-bands along a {111} and one set of non-crystallographic DDW/MBs were found.

the formation of a second set of crystallographic boundaries. Although the second largest coplanar slip fractions are of course lower than the largest in Fig. 1, some grain orientations exhibit fairly high values.

The direction of the predicted crystallographic DDW/MBs is given by the direction of the slip planes which experience much coplanar slip. These slip planes have been demonstrated to have a macroscopic direction [20]. They are distributed around the direction $(\alpha, \beta, \delta) = (90°, \pm 45°, 0°)$ (see Fig. 4). This is also the direction of maximum shear stress in the material during plane strain compression. It is interesting to note that this is also the direction around which the non-crystallographic DDW/MBs are found [2].

4. COMPARISON WITH EXPERIMENT

4.1. *Single crystals*

Table 1 summarises DDW/MB data on single crystals from literature for five texture components which are often used to describe rolling textures in f.c.c. metals [21]. The experimental data include crystals deformed in rolling and channel die compression and the DDW/MBs were observed in the rolling, longitudinal or transverse sample planes (see Fig. 4). Most of the investigations have been made in the longitudinal plane where the angle β

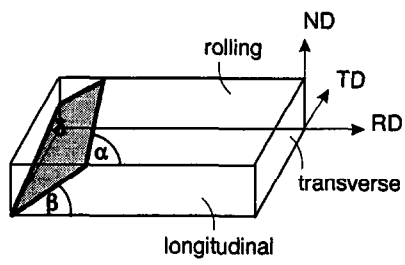

Fig. 4. Sketch of sample showing the traces of DDW/MBs in the rolling, longitudinal and transverse sample planes. The direction of a DDW/MB is given by the three angles (α, β, δ).

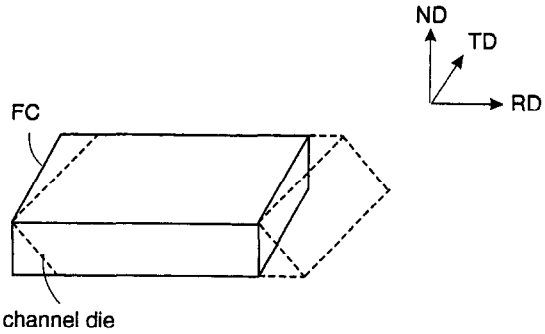

Fig. 5. Sketch of FC and channel die plane strain compression.

between the observed crystallographic DDW/MB traces and the rolling direction typically lies between 30 and 45°. The three-dimensional direction of slip planes and DDW/MBs are however not completely determined by the trace angle in a single sample plane. Note that coinciding traces of a DDW/MB and a $\{111\}$ plane in a single sample plane have therefore not been taken as evidence of crystallographic DDW/MBs in all of the references cited.

The idealised deformation which resembles rolling most is FC plane strain compression where all five strain components are fixed and five slip systems are needed to realise the deformation. In channel die compression the two shear components ε_{12} and ε_{13} are not restricted [see Fig. 5 (RD = 1, ND = 3)]. This means that only three strain components are fixed and that only three slip systems need to be active. In case of slip ambiguity, the deformation can be realised by several equivalent slip patterns. Any of these slip patterns or a mixture of them may be the actual slip pattern in the crystal. Table 2 shows the coplanar slip fractions predicted with FC and channel die plane strain compression for the single crystal orientations in Table 1. In case of slip ambiguity the coplanar slip fractions for the average slip pattern are stated.

Table 2 shows that for the Goss orientation all slip is concentrated in two sets of coplanar systems in both FC plane strain and channel die compression, i.e. Goss oriented crystals are predicted to form two sets of crystallographic DDW/MBs. Here it must, however, be noted that there is slip ambiguity for channel die deformation and that the deformation can also be realised by slip patterns with one or no coplanar slip systems. This probably explains why the Goss crystal deformed in channel die deformation only exhibits one set of crystallographic DDW/MBs while the rolled crystals all have two sets.

Brass oriented crystals in FC plane strain compression has some slip in one set of coplanar systems on a slip plane which is parallel to the longitudinal sample plane. However, two sets of crystallographic DDW/MBs are seen in the experiments in other directions, namely $(\alpha, \beta, \delta) = (-55°, \pm 30°, -22°)$ as defined in Fig. 4. In channel die deformation all slip is concentrated in two sets of coplanar systems with these directions. This may indicate that rolled brass oriented crystals do not deform according to FC boundary conditions. This explanation is supported by the dramatic reduction (25%) in the M-factor when the boundary conditions are relaxed. The solution for channel die deformation is again an average of two solutions each having one set of coplanar slip systems, perhaps explaining why only one set of crystallographic DDW/MBs is observed experimentally in channel die deformation. The reason why two sets are seen in rolling may be that the total shear strain of the crystal is lowered when the actual slip pattern is an average of the two equivalent solutions to the slip ambiguity problem.

Table 2. Fractions of coplanar slip. The angles (α, β, δ) define the direction of the slip planes (see Fig. 4). The total slip (the M-factor) is also given

Orientation	Deformation	Plane 1	Plane 2	M-factor
Goss (001)[100]	FC	0.50 (−90°, −35°, 0°)	0.50 (−90°, −35°, 0°)	2.45
	Channel die†	0.50 (−90°, −35°, 0°)	0.50 (−90°, −35°, 0°)	2.45
Brass (011)[−21−1]	FC	0.25 (−90°, −, 0°)	0.00	3.26
	Channel die†	0.50 (−55°, −30°, −22°)	0.50 (−55°, 30°, −22°)	2.45
Copper (112)[11−1]	FC	0.23 (−90°, −19°, 0°)	0.00	3.67
	Channel die	1.0 (−90°, −19°, 0°)	0.00	3.62
S (123)[63−4]	FC†	0.51 (42°, 41°, −44°)	0.27/0.23 (−4°, −13°, 72°)/ (78°, −21°, 5°)	3.49
	Channel die	0.98 (78°, −21°, 5°)	0.00	3.18
Cube (001)[100]	FC†	0.00	0.00	2.45
	Channel die†	0.00	0.00	2.45

†The stated slip pattern is an average of equivalent solutions.

The copper orientation has some coplanar slip in FC plane strain compression in the observed DDW/MB direction. When the boundary conditions are relaxed all slip takes place in these coplanar systems and although the M-factor does not change significantly one set of crystallographic DDW/MBs must be expected in this crystal orientation. This is also in good agreement with the experimentally observed microstructure. The model predictions gain further credibility by the observation of volumes with crystallographic and non-crystallographic DDW/MBs in the same crystal [11]. This could be correlated with the dominance of coplanar or non-coplanar slip systems.

For S oriented crystals one set of crystallographic DDW/MBs are predicted. However, there are two additional sets of coplanar slip systems which might give crystallographic DDW/MBs although their coplanar slip fractions are somewhat lower. Three sets of crystallographic DDW/MBs are hardly likely so it is difficult to predict the actual structure formed from this slip pattern. In channel die compression one of the coplanar slip systems becomes totally dominant and one set of crystallographic DDW/MBs is predicted. Experimentally, an S-band is observed with the upper trace parallel to the slip plane (α, β, δ) = (78°, −21°, 5°) which contains the large coplanar slip. S-bands are dislocation structures formed as a consequence of localised glide and the occurrence of a crystallographic S-band on a plane with much slip is therefore well explained.

Cube oriented crystals are not predicted to form crystallographic DDW/MBs which is in agreement with one of the experimental observations in Table 1 and in disagreement with the others. Further characterisation of the microstructure of this orientation is needed to clarify this. Unfortunately the cube orientation is unstable and therefore difficult to study.

The experimental microstructures are well explained from the coplanar slip fractions. One might, however, also suggest that a boundary related to a slip plane by cross slip receives dislocations formed in other slip planes. In that case a slip plane with no slip would be predicted to result in a crystallographic DDW/MB if there are two sets of dislocations that can cross slip to it even if there is no slip in the plane itself. Such planes might accumulate large dislocation populations. However, the direction of planes thus calculated to contain large dislocation populations does not agree with that of the experimentally observed crystallographic DDW/MBs.

4.2. *Polycrystals*

Liu and Hansen [14] investigated the microstructure of aluminium polycrystals with a grain size of 300 μm cold rolled to 5, 10, 30 and 50% by transmission electron microscopy in the longitudinal (RD/ND) plane. They observed grains with crystallographic and non-crystallographic DDW/MBs. The

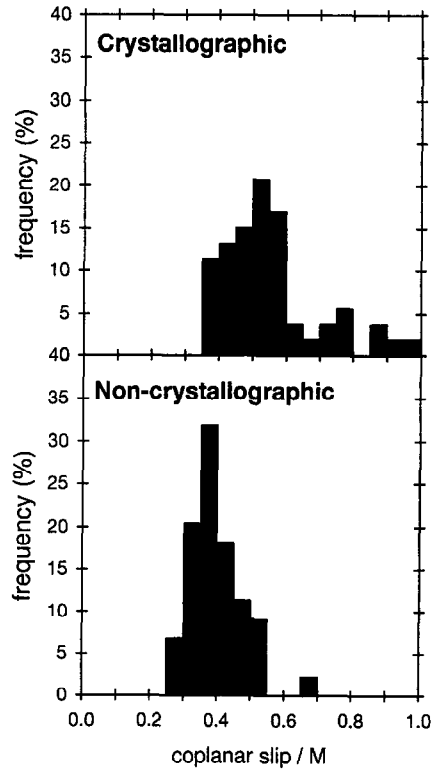

Fig. 6. Histograms for grains with crystallographic and non-crystallographic DDW/MBs showing the largest coplanar slip fractions. The deformation was FC plane strain compression.

three-dimensional direction of the DDW/MBs was determined by looking at the angle in fairly thick areas of foils taken from the longitudinal plane in transmission electron microscopy instead of just the angle of the DDW/MB trace [26]. DDW/MBs determined to lie within 5° of a slip plane were classified as crystallographic. The orientations of the 98 grains studied were fairly random though with some clustering around the cube and Goss orientations.

Calculations for these grains have only been made with FC boundary conditions due to the relatively low deformation degrees of the polycrystals. RC boundary conditions are not expected to be valid here because the grains are not sufficiently flat.

The largest coplanar slip fractions have been calculated for all of the grains in the two groups using the same procedure as for Fig. 1.

The two coplanar slip distributions for grains with crystallographic and non-crystallographic DDW/MBs in Fig. 6 obtained with FC boundary conditions have maxima at different coplanar slip fractions. However, the two distributions also overlap over a small range of coplanar slip fraction values. A coplanar slip fraction of 0.45 separates the two grain types best. This value was selected because 25% of the grains with crystallographic DDW/MBs have coplanar slip fractions below 0.45 and 23% of the

grains with non-crystallographic DDW/MBs have coplanar slip fractions above this value.

Figure 7 shows the orientations of the individual grains with the two microstructures on top of the predicted ODF from Fig. 1. Areas with coplanar slip fractions above 0.45 are grey. The experimental data are the same that were used for Fig. 6 from which the value of 0.45 was determined. It was therefore known in advance that a contour of this value would separate the two types of grains well. Due to the small overlap between the two coplanar slip fraction distributions observed in Fig. 6 the separation cannot be perfect. It is noted that there are areas where the experimental grain orientations with crystallographic and non-crystallographic DDW/MBs coincide (e.g. for $\varphi_2 = 10°$, $\varphi_1 \sim 10°$, $\phi \sim 70°$). This means that the two types of grains cannot be completely distinguished by their crystallographic orientation alone. This coincidence is however primarily found in the vicinity of a border between grey and white areas. Possible explanations for the coinciding grain orientations are discussed later in this paper.

Some grains had one and some two sets of crystallographic DDW/MBs. Histograms of the coplanar slip fractions occurring in a second slip system are shown for these two grain types in Fig. 8. It is seen that the distributions for grains with one or two sets of crystallographic DDW/MBs are not significantly different. Although not shown here, distributions calculated with contributions from cross slip do not yield a better separation of the two distributions. This type of calculation therefore cannot explain the occurrence of the two types of crystallographic microstructures. The reason for this is discussed later in the paper.

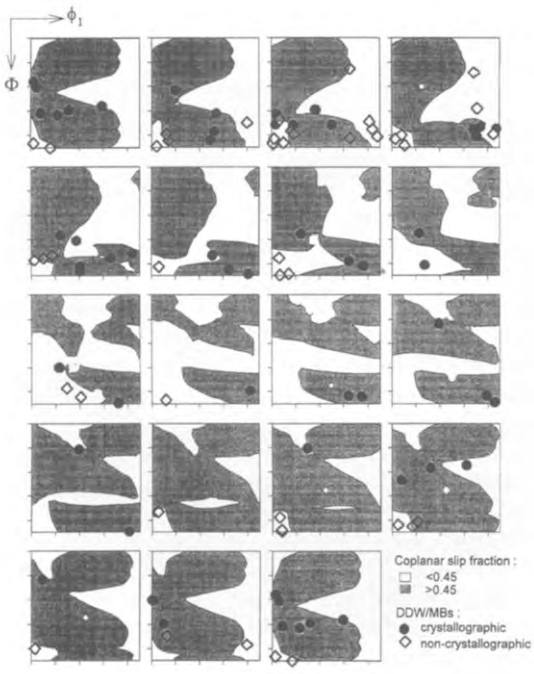

Fig. 7. ODF showing experimental grain orientations with crystallographic and non-crystallographic DDW/MBs on top of an ODF where the grey areas have coplanar slip fractions above 0.45 in FC plane strain compression.

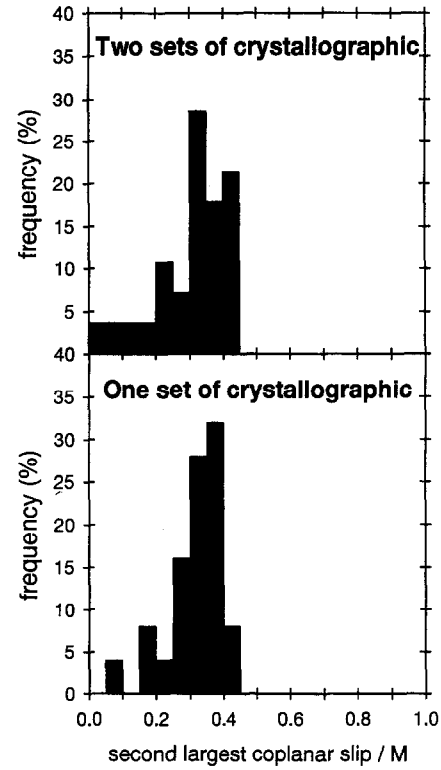

Fig. 8. Histograms showing the fractions of coplanar slip in a second slip plane with coplanar slip for grains with one and two sets of crystallographic DDW/MBs.

In another study of DDW/MBs in polycrystalline pure aluminium with a grain size of 130 μm [27] the angle between the trace of the nearest $\{111\}$ plane and a DDW/MB was recorded in grains of different orientation. Twenty-five grains were studied and the estimated standard deviation of the measured angles

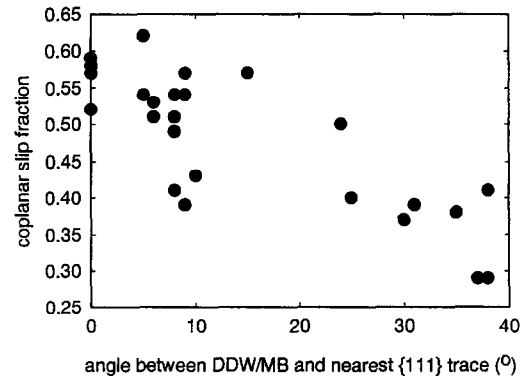

Fig. 9. Calculated coplanar slip fractions vs the angle between DDW/MBs and the nearest $\{111\}$ trace for the grain orientations studied in Ref. [27]. Some of the DDW/MBs were studied in the rolling plane and some in the longitudinal plane.

was 5°. The coplanar slip fractions in these grains have been calculated to provide a further test of the model. Figure 9 shows a plot of the calculated coplanar slip fractions for each orientation versus the recorded angle. It is seen that the DDW/MBs only deviate a little ($<10°$) from the $\{111\}$ trace when the coplanar slip fraction is high. Only three grain orientations have DDW/MBs less than 10° from a $\{111\}$ plane while the coplanar slip fraction is below 0.45. For the grains with larger angles between DDW/MBs and $\{111\}$ traces only two have coplanar slip fractions above 0.45. It is therefore concluded that the critical value of the coplanar slip fraction of 0.45 also seems valid here.

5. DISCUSSION

5.1. Mechanisms for dislocation motion

As pointed out previously cross slip may contribute to the formation of crystallographic boundaries. Slip planes with no or only one active slip system may receive additional sets of dislocations from other slip planes through cross slip and thereby become candidates for crystallographic boundary formation. Cross slip may also contribute additional dislocations to a slip plane which already has two sets of dislocations. Cross slip is relatively frequent in materials with high stacking fault energies, e.g. aluminium. However, calculations for the single crystals showed that inclusion of cross slip contributions lead to prediction of the wrong microstructures whereas the predictions were excellent when only the coplanar slip fractions were used. This does of course not rule out that cross slipping dislocations from other slip planes may also be incorporated in the boundary.

Cross slip may be essential for the mechanism of boundary formation. Jackson, de Lange and Young [28] proposed that cross slipping dislocations form pairs of dislocation arrays along the slip plane. In f.c.c. crystals secondary slip produces dislocations which form stable Lomer–Cottrell networks with the primary dislocations as long as the boundary plane stays within 25° of the primary slip plane [29].

5.2. Large coplanar slip fractions

In this study a large coplanar slip fraction has been assumed to be the parameter governing crystallographic DDW/MB formation. The earlier observations that few active slip systems lead to crystallographic DDW/MBs [14, 16] partly support this approach since each system accounts for a large fraction of the total slip when there are only few active systems. The importance of coplanar slip is also partly recognised in the observation that crystallographic DDW/MBs occurred when the four highest Schmid factors were concentrated on two planes [14]. There is also strong evidence for the importance of coplanar slip for crystallographic DDW/MB formation in the study of a crystal of copper orientation with both coplanar and codirectional slip patterns [11].

It has been assumed in this study that the fraction of coplanar slip in the grain is the important parameter. This has been confirmed by the obtained results. The coplanar slip fraction is a convenient measure of the generated dislocations but it is however possible that other factors such as the geometry and shear distribution of the remaining slip systems also have an influence. Further work is needed to investigate this.

A boundary consisting of just a single set of dislocations cannot be both a low energy boundary and crystallographic [18]. However as described by Kuhlmann-Wilsdorf and Comins [30] additional dislocations supplied by, e.g. unpredicted glide can contribute to the boundary formation and the DDW/MB thus becomes a crystallographic, low energy boundary consisting of more than one set of dislocations. Adding this possibility to the mechanisms for crystallographic boundary formation treated here means that a slip system which carries a lot of the total slip in the grain can also be expected to form crystallographic DDW/MBs. However, the slip system with most slip was one of the coplanar slip systems for 95% of the grain orientations investigated here. This means that the slip plane automatically contains the two sets of dislocations needed to form a low energy boundary. It also means that formation of the crystallographic boundaries at the onset of deformation where the grains may deform through single glide is expected to take place on the plane which at a later deformation step contains coplanar slip.

5.3. Comparison with experiment

5.3.1. Single crystals. The agreement between predicted and experimentally observed microstructures for the five investigated single crystal orientations was very good. The majority of the experimental findings could be explained by the occurrence of or lack of high coplanar slip fractions. Even some of the apparently conflicting experimental results regarding the occurrence of one or two sets of crystallographic DDW/MBs could be explained by differences in the actual slip patterns caused by slip ambiguity.

5.3.2. Polycrystals. For the polycrystal the model succeeds in separating grain orientations with crystallographic and non-crystallographic DDW/MBs. However, separation of grain orientations with one and two sets of crystallographic DDW/MBs could not be performed. One reason for the poorer prediction for the polycrystal is that the slip pattern is more difficult to predict for polycrystals due to grain interactions.

Another difficulty is that most of the grain orientations in a polycrystal are unstable, i.e. the grains change their orientation during deformation.

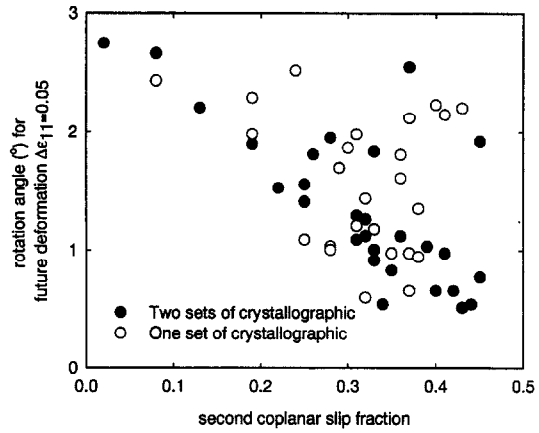

Fig. 10. Second largest coplanar slip fractions vs grain rotation angles for the grain orientations in Ref. [14].

The developed microstructure is expected to reflect the total deformation history of the grain and a snap shot of the slip pattern at a certain deformation stage is probably insufficient to predict the microstructure in all cases. In single crystal studies the initial orientation is at least known and most of the investigated single crystal orientations are furthermore stable.

Orientation instability may be the reason why the model proved incapable of predicting whether the grains formed one or two sets of crystallographic DDW/MBs. In order to get an impression of the instabilities, the rotation angles of the grains have been calculated for a single future deformation step with $\Delta\varepsilon_{11} = 0.05$. From these calculations it is of course not possible to find the orientation history but only an idea of the behaviour in future deformation. To a first approximation it is expected that grains with large future rotations also have a more unstable history. Their structure is therefore expected to deviate more from the predicted structure based on a given temporary orientation.

Figure 10 shows a plot of the calculated future rotation angles vs the second largest coplanar slip fractions in the grains with one or two sets of crystallographic DDW/MBs. It is seen that the grains with two sets of crystallographic DDW/MBs and small rotation angles have second highest coplanar slip fractions which generally exceed those of the grains with only one set of crystallographic DDW/MBs. Many of the unstable grains with only one set of crystallographic DDW/MBs also have high second coplanar slip fractions but the grains may not have been oriented for this second set of coplanar slip systems long enough to leave an impact on the microstructure.

The discrepancy between predicted and experimentally observed crystallographic DDW/MBs may also be caused by experimental problems in determining the exact direction of a DDW/MB with respect to its surroundings. Ideally, investigations should be made in not just one sample plane, i.e. rolling, longitudinal or transverse plane, but be supplemented by studies in at least one of the other planes. However, this is virtually impossible due to the need for either finding the same grain in different planes or making enough measurements for a statistical treatment of the data. In this respect single crystal studies are easier to deal with.

Furthermore, in a grain with a pronounced break up into subgrains and cell blocks the variation in grain orientation is rather large and the measured grain orientation becomes a function of position within the grain. Similarly, DDW/MBs are often wavy and consequently do not have an easily identifiable direction. Careful studies [11] of the spread of DDW/MB directions and crystallographic orientations are therefore needed to fully establish the crystallographic nature of a DDW/MB.

5.3.3. Boundary misorientation. A crystallographic DDW/MB which only contains two sets of dislocations from the same slip plane will be a pure twist boundary [18]. However, experimentally determined misorientation axes for crystallographic DDW/MBs are not restricted to boundary normals [11]. Incorporation of additional sets of dislocations allows other directions of the misorientation axes. It is therefore evident that crystallographic boundaries must receive additional dislocations from other slip systems. The model proposed here does not consider these slip systems but there is no conflict between a large coplanar slip fraction and contributions from other slip systems. These additional contributions may originate from e.g. cross slip or unpredicted glide. In its present form, the model therefore cannot predict the misorientation axis.

The misorientation angle cannot be predicted either. To obtain the misorientation angle from equation (1) the spacing D_i between the effective boundary dislocations must be known. Dislocations with opposite signs annihilate if they are close enough or form dipoles in which case they will not contribute to the misorientation across the boundary. The effective boundary dislocations are therefore the excess dislocations of one sign, a quantity which is difficult to determine.

Wert *et al.* [13] assumed that negative and positive dislocations are generated in equal amounts, which must be true on average, and the amount of excess dislocations of one sign from a given slip system was therefore related to the difference in slip amplitudes of that slip system in the material on the two sides of the boundary (dislocations moving towards the boundary from opposite sides have opposite signs). This approach requires information on the boundary misorientation which is needed to predict the differences in the slip pattern on the two sides of the boundary.

The excess of dislocations of one sign has also been attributed to local statistical fluctuations [31] which must be important at least at the onset of boundary

formation before the misorientation between the material on the two sides of the boundary has developed. Use of this method requires a model for the statistical fluctuations.

One of these two approaches may be useful in future expansions of the model but for the time being the model is only capable of predicting whether crystallographic or non-crystallographic DDW/MBs are to be expected.

6. CONCLUSION

A model which predicts the orientations of grains which form crystallographic DDW/MBs in plane strain compression has been defined. The model is based on a combination of dislocation theory and slip pattern predictions. It assumes that the boundary dislocations are generated by slip and that dislocations assemble into low energy boundaries.

Crystallographic DDW/MBs are predicted to form if two active slip systems in the same slip plane account for a large fraction of the total slip in the grain. The critical value of this coplanar slip fraction has been estimated to 0.45 for aluminium polycrystals by comparison with experimental data.

The agreement between predicted and experimental occurrences of crystallographic and non-crystallographic DDW/MBs was excellent for single crystals. The occurrence of one or two sets of crystallographic DDW/MBs could also be predicted.

For polycrystals there is reasonably good agreement between experimental observations and predictions. However, it was not possible to predict whether one or two sets of crystallographic DDW/MBs form. This is ascribed to the instability of the crystallographic orientations during deformation which means that the DDW/MBs may have been formed when the grains had another crystallographic orientation and also that the DDW/MBs may not yet have formed in a new crystallographic orientation.

Acknowledgements—The authors wish to thank Professor J. A. Wert, Dr J. B. Bilde-Sørensen and Dr T. Leffers for helpful discussions and Dr Q. Liu and Dr A. Godfrey for access to their data. This work is performed within the Engineering Science Centre for Structural Characterisation and Modelling of Materials.

REFERENCES

1. Hughes, D. A., *Proc. of 16th Risø International Symposium on Materials Science*, (ed. N. Hansen *et al.*), 1995, 63.
2. Bay, B., Hansen, N., Hughes, D. A. and Kuhlmann-Wilsdorf, D., *Acta metall.*, 1992, **40,** 205.
3. Juul Jensen, D. and Hansen, N., *Acta metall.*, 1990, **38,** 1369.
4. Hansen, N. and Juul Jensen, D., *Acta metall.*, 1992, **40,** 3265.
5. Winther, G., Juul Jensen, D. and Hansen, N., *Acta Mater.*, 1997, **45,** 2455.
6. Malin, A., Huber, J. and Hatherly, M., *Z. Metallk.*, 1981, **72,** 310.
7. Wróbel, M., Dymek, S., Blicharski, M. and Gorczyca, S., *Textures and Microstructures*, 1988, **10,** 9.
8. Morii, K., Mecking, H. and Nakayama, Y., *Acta metall.*, 1985, **33,** 379.
9. Morii, K. and Nakayama, Y., *Scripta metall.*, 1985, **19,** 185.
10. Nakayama, Y. and Morii, K., *Transactions of the Japan Institute of Metals*, 1982, **23,** 422.
11. Godfrey, A., Juul Jensen, D. and Hansen, N., submitted for publication.
12. Godfrey, A., Juul Jensen, D. and Hansen, N., submitted for publication.
13. Wert, J. A., Liu, Q. and Hansen, N., *Acta Mater.*, 1997, **45,** 2565.
14. Liu, Q. and Hansen, N., *Phys. Stat. Sol. (a)*, 1995, **149,** 187.
15. Huang, X. and Hansen, N., *Scripta Mater.*, 1997, **37,** 1.
16. Kawasaki, Y. and Takeuchi, T., *Scripta metall.*, 1980, **14,** 183.
17. Hansen, N. and Kuhlmann-Wilsdorf, D., *Mat. Sci. Eng.*, 1986, **81,** 141.
18. Hirth, J. P. and Lothe, J., *Theory of Dislocations*, 1968.
19. Bilde-Sørensen, J. B., *Mat. Sci. Eng.*, 1986, **81,** 211.
20. Winther, G. and Juul Jensen, D., *Comput. Mater. Sci.*, (in press).
21. Lücke, K., *Proc. of 6th ICOTOM*, ed. S.-I. Nagashima, 1981, 14.
22. Wróbel, M., Dymek, S., Blicharski, M. and Gorczyca, S., *Z.Metallkd.*, 1994, **85,** 415.
23. Driver, J. H., Juul Jensen, D. and Hansen, N., *Acta metall.*, 1994, **42,** 3105.
24. Feller-Kniepmeier, M. and Wanderka, N., *Proc. of ICOTOM 8*, ed. J. S. Kallend *et al.*, 1988, 517.
25. Godfrey, A., private communication.
26. Liu, Q., *J. Appl. Cryst.*, 1994, **27,** 762.
27. Bay, B., Hansen, N. and Kuhlmann-Wilsdorf, D., *Mat. Sci. Eng.*, 1989, **A113,** 385.
28. Jackson, P. J., de Lange, O. L. and Young, C. J., *Acta metall.*, 1982, **30,** 483.
29. Jackson, P. J. and Siedersleben, M., *Scripta metall.*, 1984, **18,** 749.
30. Kuhlmann-Wilsdorf, D. and Comins, N. R., *Mat. Sci. Eng.*, 1983, **60,** 7.
31. Pantleon, W. and Klimanek, P., *Comput. Mater. Sci.*, 1994, **3,** 223.

A5: Slip patterns and preferred dislocation boundary planes by G. Winther, Acta Materialia, 2003

Available online at www.sciencedirect.com
SCIENCE DIRECT®
Pergamon
Acta Materialia 51 (2003) 417–429
Acta MATERIALIA
www.actamat-journals.com

Slip patterns and preferred dislocation boundary planes

G. Winther *

Center for Fundamental Research: Metal Structures in 4D, Materials Research Department, Risø National Laboratory, P.O. Box 49, DK-4000 Roskilde, Denmark

Received 7 August 2002; received in revised form 7 August 2002; accepted 16 September 2002

Abstract

The planes of deformation induced extended planar dislocation boundaries are analysed in two different co-ordinate systems, namely the macroscopic system defined by the deformation axes and the crystallographic system given by the crystallographic lattice. The analysis covers single and polycrystals of fcc metals in three deformation modes (rolling, tension and torsion). In the macroscopic system, boundaries lie close to the macroscopically most stressed planes. In the crystallographic system, the boundary plane depends on the grain/crystal orientation. The boundary planes in both co-ordinate systems are rationalised based on the slip. The more the slip is concentrated on a slip plane, the closer the boundaries lie to this. The macroscopic preference arises from the macroscopic directionality of the slip. The established relations are applied to (a) prediction of boundary planes from slip patterns and (b) prediction of slip patterns from boundary planes.

Keywords: Forming processes; Metal and alloys; Microstructure; Deformation structure; Dislocation boundaries

1. Introduction

Plastic deformation of metals and alloys of medium to high stacking fault energy to moderate strain levels results in formation of a microstructure consisting of extended planar dislocation boundaries and short cell boundaries [1]. It is generally observed that cell boundaries lie on randomly distributed planes while the planes with which extended planar boundaries align still are debated [2–5].

Determination of preferred boundary planes is obviously of interest in research aimed at understanding the fundamental principles governing formation of deformation induced dislocation structures. However, such relations also have more direct technological perspectives.

Formation and evolution of dislocation boundaries during deformation have an impact on mechanical properties. Prediction of relations between forming processes and boundary characteristics is therefore essential for subsequent successful modelling of mechanical properties. In particular, the preferred planes of extended planar dislocation boundaries give rise to mechanical anisotropy [6–9]. From a micromechanical point of view, it is expected that channels with easy slip may arise along boundaries aligned with slip planes. Bound-

* Tel.: +45-46-77-57-92; fax: +45-46-77-57-58.
E-mail address: grethe.winther@risoe.dk (G. Winther).

1359-6454/03/$30.00
doi:10.1016/S1359-6454(02)00423-8

aries lying far from slip planes should obstruct the slip process more.

Extended planar dislocation boundaries have been reported to align with the macroscopically most stressed planes [1,3,4], which are given by the macroscopic deformation mode. In other studies the boundary plane has been related to low index crystallographic planes [5,10]—mostly slip planes, which are the planes on which deformation takes place at the crystallographic level. Recently, a strong correlation between the orientation of a grain and the orientation of the boundaries in the crystallographic lattice has been reported [11–13]: some grain orientations have boundaries close to slip planes while other grain orientations have boundaries far from slip planes but still related to these [14].

The observations strongly indicate that the orientation of extended planar dislocation boundaries is closely linked to the deformation processes at both the macroscopic and crystallographic levels. The aim of the present paper is to explore and rationalise these links. Most of the previous work in this field has focused on a single deformation mode. These efforts have established the necessary background for the present work, which unifies observations from three deformation modes, namely rolling, tension and torsion.

The first part of the paper gives a brief overview of the experimental evidence for preferred boundary planes in the macroscopic and crystallographic co-ordinate systems. In particular the relation of preferred boundary planes to both macroscopically most stressed planes and slip planes is investigated in detail.

The established grain orientation dependence of the boundary planes strongly indicates that a major factor controlling boundary plane orientations is the slip pattern, i.e. the ensemble of active slip systems and the magnitude of their shear strains. The second part of the paper therefore concentrates on tracing the origin of preferred boundary planes in both the macroscopic and crystallographic co-ordinate systems to the slip pattern. The result of this effort is relations which allow prediction of (a) boundary planes from assumed slip patterns and (b) slip patterns from determined boundary planes.

2. Preferred boundary planes

In the following, evidence supporting the existence of preferred macroscopic and crystallographic boundary planes is summarised for a number of deformation processes. Only boundaries in fcc metals of medium to high stacking fault energy deformed to moderate strains ($\varepsilon < 1$) are considered.

2.1. Preferred macroscopic boundary planes

The plane of a dislocation boundary cannot be determined directly by current experimental techniques. Only the trace of a boundary on the plane of inspection can be observed. Unfortunately inspection of a boundary in different planes is only relatively easy in single crystals. Various experimental techniques to obtain the three-dimensional plane of boundaries in polycrystals have been developed [14–18] but these are all time consuming. For practical reasons studies of polycrystals have therefore been mostly limited to studies of many grains in one inspection plane. These studies have shown that boundaries generally align with the macroscopically most stressed planes. Observations for rolling, tension and torsion are summarised below.

2.1.1. Rolling

There are two perpendicular macroscopically most stressed planes in plane strain compression, which is the ideal deformation mode usually assumed for homogeneous rolling. These are inclined ±45° to the rolling direction in the longitudinal plane and are perpendicular to the rolling direction in the rolling plane. Boundaries are predominately found in the vicinity of these two planes [19–21] but the mean trace angle in the longitudinal sample plane varies somewhat between 30 and 45°. Also the spread of boundary planes around these macroscopic planes is typically more than 20° as seen in Fig. 1.

2.1.2. Tension

The macroscopically most stressed planes are tangents to a cone inclined 45° to the tensile axis and the number of most stressed planes is infinite.

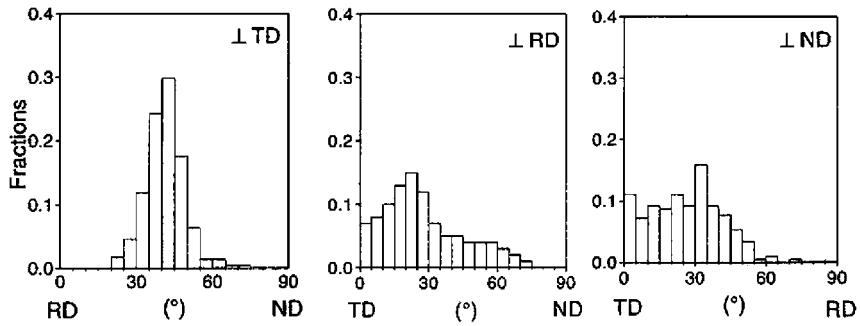

Fig. 1. Histograms showing the angle between boundary traces and macroscopic sample axes in the three sample planes for polycrystalline copper 11% cold rolled (from Ref. [20]).

Experimental data have been found to agree well with boundaries lying close to this cone although with a mean inclination to the tensile axis of 35° and a standard deviation of 5° [4]. Application of a different analysis technique gave comparable results [14].

2.1.3. Torsion

The macroscopically most stressed planes are the shearing plane perpendicular to the torsion axis and all planes parallel to the torsion axis because the stress tensor is symmetric. Boundaries are found to scatter around these planes [22].

2.2. Preferred crystallographic boundary planes

Especially for rolled and tensile deformed single crystals, where the crystallographic boundary plane is more easily determined than in polycrystals, boundaries have been reported to align with slip planes [23–31]. Many of these studies have established that the boundaries are not exactly on slip planes but deviate a few degrees from these [23–25]. Boundaries lying far from slip planes have, however, also been observed in many single crystals [31–33]. Even for single crystals, there is thus no unique crystallographic plane with which dislocation boundaries preferentially align.

For polycrystals, it has recently been found for both rolling and tension that there is a strong correlation between the crystallographic plane of the boundaries and the crystallographic orientation of a grain. Some grain orientations have boundaries close to slip planes and other orientations have boundaries lying far from slip planes [11–13]. This was first realised for rolled aluminium polycrystals [11].

A more detailed investigation of the crystallographic orientation of dislocation boundaries as a function of grain orientation has so far only been carried out on a tensile deformed aluminium polycrystal [14]. It was found that the crystallographic planes on which extended planar dislocation boundaries lie, have very well-defined geometric relations to the slip planes. This is also the case when the boundaries lie far from the slip planes. In fact there is a systematic deviation so that boundaries deviate more and more (up to 35°) from the slip plane as a function of grain orientation. Geometrically this deviation can be characterised as a rotation of the boundary plane away from the slip plane about specific crystallographic axes. At certain points in grain orientation space the rotation direction is reversed.

Although studies of crystallographic boundary planes have only been carried out in this detail for tension, boundaries in rolled materials have many of the same characteristics: boundaries roughly aligned with slip planes are more straight and have smaller misorientation angles than boundaries far from slip planes [12,34]. It is therefore expected that boundaries in metals deformed by rolling and torsion will exhibit the same type of systematic geometric relations to the slip planes as boundaries in tensile deformed metals. This expectation is further supported by the examples given later in this paper where the boundary plane is related to the slip pattern.

2.3. Comparison of macroscopic and crystallographic preferences

Boundaries clearly tend to cluster around certain macroscopic planes, which are generally close to the macroscopically most stressed planes. The detailed study of the exact crystallographic boundary planes in tension has allowed a closer evaluation of the importance of the macroscopically most stressed planes: it has been investigated whether boundary planes deviate from the slip plane to approach the macroscopically most stressed planes [35]. It was found that boundaries do not always deviate from the slip plane to get nearer to the macroscopically most stressed plane but may also get further away from this plane. Even when the macroscopically most stressed plane coincides with a slip plane the boundary plane can deviate about 10° from this plane. This finding shows that macroscopically most stressed planes (in analogy with slip planes) are not per se preferred boundary planes.

The scatter of the boundary planes around the macroscopic preferred planes has also been compared to the scatter in the crystallographic lattice [14]. The conclusion was that, when different, the scatter around the macroscopic planes was always larger than the scatter in the crystallographic lattice. Furthermore, the boundaries in tension are randomly distributed about the tensile axis in the macroscopic co-ordinate system. The planes of the observed boundaries are, however, fixed in the crystallographic lattice where there is no rotational symmetry about the tensile axis. These findings show that crystallography is a more important factor controlling boundary plane orientation than macroscopic stress.

The conclusion is that boundaries have both macroscopic and crystallographic preferred orientations but that the macroscopic preference is weaker than the crystallographic:

- In the macroscopic sample co-ordinate system, boundaries cluster around the most stressed planes. However, there is a significant spread around these macroscopic planes and no clear geometric relation between these planes and boundary planes.
- In the crystallographic lattice, there is an unambiguous geometric relationship between boundary planes and slip planes. The deviation of a boundary plane from the nearest slip plane varies systematically with the grain orientation.

3. Relations between preferred boundary planes and slip pattern

The strong correlation between crystallographic boundary plane and crystallographic grain orientation indicates that the origin of preferred boundary planes can be traced to the slip pattern. The different active slip systems contribute dislocations with different Burgers vectors. Interaction of these dislocations causes them to assemble into boundaries with preferred orientations. The following analysis of the relations between the slip pattern and the occurrence of both crystallographic and macroscopic preferred boundary planes is a significant contribution to the knowledge on which theories for fundamental boundary formation mechanisms are to be based.

3.1. Crystallographic relations

For both single and polycrystals of aluminium and copper deformed in rolling and tension the degree of slip concentration on a slip plane has been found to correlate with the alignment of dislocation boundaries with slip planes.

When a large fraction of the slip in a grain occurs on one or two slip planes, boundaries lie close to these planes. This is for example the case for rolled single crystals of the stable orientations [20–25,27]. An empirical quantitative relation was determined for rolled aluminium polycrystals. It was found that boundary traces deviate less than 5° from the slip plane trace when the fraction of slip exceeds approximately 45% [36].[1] In tensile

[1] In Ref. [36] the fraction of coplanar slip (i.e. slip on two systems in the same slip plane) was considered. Relaxing the requirement for coplanar slip to include only one system in a plane, however, makes practically no difference for rolling but is important for e.g. tension. In the present paper, the fraction of slip on a plane has been evaluated on this relaxed basis.

deformation, single crystals oriented for single or double slip, i.e. where all slip is predicted to occur on one or two slip planes, have boundaries almost parallel to these planes [23–25]. Grains of these orientations in a polycrystal also have boundaries lying within 10° of the primary slip plane [14].

Turning to the opposite case, i.e. to crystals with highly distributed slip, boundaries deviate much from the slip planes. For example, rolled single crystals of cube orientation {001}⟨100⟩ have four equally active slip systems on four different slip planes. Boundaries in these crystals lie about 35° from the nearest slip plane [33]. Grains of similar orientation in polycrystals have also been observed to form boundaries far from slip planes [11]. In tension, copper single crystals with ⟨111⟩ in the tensile direction slip on six equally active systems on three slip planes. They have boundaries on planes that deviate 25° from the slip planes [32]. In ⟨111⟩ oriented grains in polycrystalline aluminium they deviate up to 35° [14].

The most distributed slip occurs in tensile deformed grains/crystals with [100] in the tensile direction where eight systems on four slip planes may be equally active. These grains/crystals do not form extended planar dislocation boundaries [12,13]. A possible explanation for the lack of extended planar boundaries is that many combinations of these eight slip systems are able to produce the same strain. The slip in individual grains/crystals may therefore be highly heterogeneous, suppressing formation of a well-ordered deformation structure dominated by extended planar boundaries. A comparable structure consisting of only cells has been observed in the vicinity of particles where slip heterogeneities must also be expected [37].

3.2. Macroscopic relations

It is seen above that the crystallographic preference is tightly linked to the slip pattern. The fact that the macroscopic preferred planes are the most stressed planes suggests that the macroscopic preference can also be traced to the slip pattern as the slip pattern depends on the macroscopic deformation mode.

The fraction of macroscopic stress that is transmitted to an individual slip system is given by its Schmid factor, which is the product of two cosines, one to the angle between macroscopic stress and slip plane and the other to the angle between macroscopic stress and slip direction. Assuming that the active slip systems have high Schmid factors, it is clear that these must have preferred relations to the macroscopic stress: either slip plane, slip direction or both of these must be approximately aligned with the macroscopically most stressed planes.

Consideration of the relative orientation of slip planes and macroscopically most stressed planes in grain orientations with highly concentrated and highly distributed slip gives a hint on the origin of the preferred macroscopic boundary planes and its relation to the slip pattern:

- When slip is concentrated on one or two slip planes these planes always lie close to the macroscopically most stressed planes. As boundary planes in these cases lie close to the active slip planes, boundary planes must therefore also lie close to the macroscopically most stressed planes.
- When slip is highly distributed among many slip planes none or all of these lie close to the macroscopically most stressed planes:

  -When none of the slip planes lie close to macroscopically most stressed planes, the boundary planes must deviate much from the slip plane to align approximately with the macroscopically most stressed planes. This is in good agreement with the crystallographic conclusions in Section 3.1.
  -When all of the slip planes lie close to the macroscopically most stressed planes the macroscopic deformation mode must be highly symmetric with many ($\geq$4) most stressed planes. In tension, where the number of macroscopically most stressed planes is infinite, boundaries may lie close to a macroscopically most stressed plane while being either close to or far from a slip plane.

This relation between slip concentration and the macroscopic orientation of slip planes is illustrated

for three deformation modes (rolling, tension and torsion) in Fig. 2. The slip pattern has been calculated using the Taylor model for grains lying on a $5° \times 5° \times 5°$ grid in Euler space. For tension, grains with more than four slip patterns with five active systems as solutions to the Taylor calculation were excluded from the calculation as they do not form extended planar dislocation boundaries. If not otherwise stated the average of the different possible slip patterns was used. When the fraction of slip occurring on a single slip plane was above 45% (as determined empirically as the best value for a rolled aluminium polycrystal [36]), the grain was classified as having concentrated slip. When no slip plane had a slip concentration of this magnitude the grain was classified as having distributed slip. For all active slip systems in each grain, the angle between slip plane and the nearest macroscopically most stressed plane was calculated. This angle was then weighted with the fraction of slip occurring on that slip system as well as the volume fraction of grains of that orientation in a random texture. The histograms in Fig. 2 thus show the fraction of slip occurring on planes with different inclinations to macroscopically most stressed planes in a randomly textured sample. The same was done for the slip directions in Fig. 3.

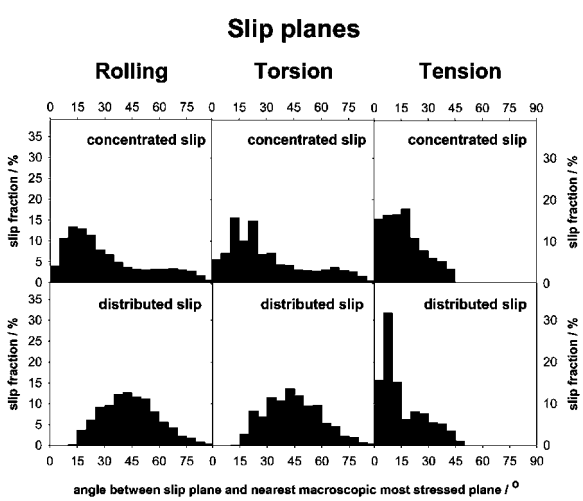

Fig. 2. Histograms showing the fraction of slip on slip planes with different angles to the nearest macroscopically most stressed plane for grain orientations with concentrated and distributed slip in a randomly textured sample.

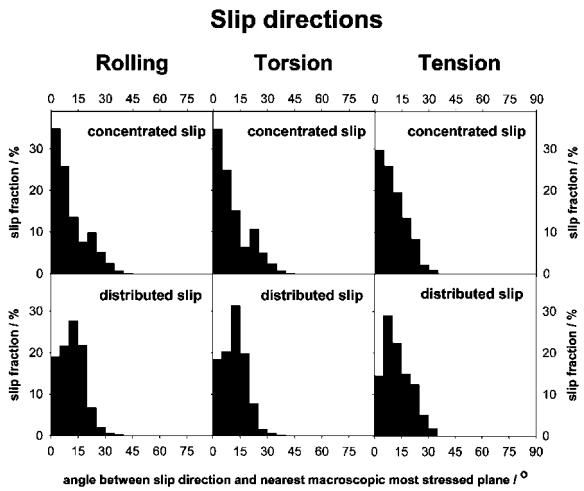

Fig. 3. Histograms showing the fraction of slip in slip directions with different angles to the nearest macroscopically most stressed plane for grain orientations with concentrated and distributed slip in a randomly textured sample.

It is clear from Fig. 2 that the grains classified as having concentrated slip have their most active slip planes aligned approximately with the macroscopically most stressed planes for all three deformation modes. As also seen in Fig. 2, grains with distributed slip do not have active slip planes in the vicinity of macroscopically most stressed planes in rolling and torsion. For the distributed slip in tension, however, most of the slip takes place on planes close to the macroscopically most stressed planes. The peak between 0 and 15° is reduced to a size equal to the peak around 25° if the slip pattern with most slip on the primary slip system is selected among the possible Taylor solutions. The reason for introduction of this calculation becomes clear in Section 4. For both concentrated and distributed slip in all three deformation modes, the slip directions are roughly aligned with the macroscopically most stressed planes as shown in Fig. 3.

These results show that there is a macroscopic directionality of the slip systems. The Burgers vectors of the dislocations which are generated and accumulated into boundaries during deformation depend on the slip system on which they are generated. For both highly concentrated slip and highly distributed slip the Burgers vectors are aligned with the macroscopically most stressed planes

because slip plane and/or the slip direction are/is aligned with it. The macroscopic directionality of slip therefore also implies a macroscopic directionality of the generated dislocations. Although the mechanism behind assembly of dislocations into boundaries is not clear, it appears that this directionality of the Burgers vectors is maintained in a common macroscopic directionality of the dislocation boundaries. It is also at present difficult to tell whether the directionality of slip directions or slip planes is more important. The directionality of the slip directions seems to be more alike for all grain orientations than that of slip planes. However, the systematic geometric relationship between boundary planes and slip planes observed for tension implies some influence of the slip plane. For some highly symmetric crystal orientations in rolling an influence of both slip plane and slip direction has been found [38].

Comparison of the crystallographic and macroscopic relations leads to the following conclusions: The macroscopic directionality of dislocation boundaries reflects the macroscopic directionality of crystallographic slip. In the crystallographic lattice, the macroscopic directionality is linked to the slip concentration; when slip is concentrated on a few slip planes these lie close to macroscopically most stressed planes. When slip is distributed, the slip planes in most cases lie far from the macroscopically most stressed planes so that only the slip directions align with these. It should be emphasised that there is thus no conflict between the existence of macroscopic and crystallographic preferred boundary planes.

4. Predictions from boundary plane/slip pattern relations

The established relations between boundary planes and the slip pattern may be used in both directions, i.e. to predict either boundary planes or slip patterns provided the other can be predicted by other means or directly observed.

4.1. Prediction of boundary planes

As described in Section 3.1 boundaries approximately line up with slip planes with high concentrations of slip. Slip planes with high slip concentration can therefore readily be identified, provided good models for slip pattern prediction are available. The exact deviation of the boundary from the slip plane is harder to predict. It must be related to further details of the slip pattern which have not yet been clarified. However, for many practical purposes, e.g. when modelling the mechanical effects of boundaries, it is probably sufficient to know that the boundaries lie in the vicinity of a slip plane.

Prediction of the approximate orientation of the boundaries lying far from slip planes is more difficult as there are many crystallographic planes which do so. As demonstrated in Section 3, there seems to be a relation to the slip directions but the nature of this relation is still undisclosed. Presently, the best prediction is therefore obtained by combining the crystallographic and macroscopic relations; from the concentration of slip it can be determined whether boundaries lie close to slip planes or not. If they do, the slip plane with which they align can also be determined among the four possible {111} planes. If it is determined that boundaries lie far from slip planes, the best option is to assume that they lie close to a macroscopically most stressed plane.

4.1.1. Grain orientations with slip plane aligned boundaries

The slip patterns predicted by the Taylor model, while still averaging over the possible solutions to the ambiguity problem, form the basis for prediction of grain orientations with slip plane aligned boundaries in this section. Figs. 4–6 show the orientation of grains with concentrated slip (i.e. more than 45% of the slip on one slip plane) for the three deformation modes considered in this paper. In the following these predictions are compared with experimental data available from literature.

A complication when comparing different data sets is that quantification of slip plane alignment is somewhat arbitrary. Ideally, one should also consider the three-dimensional orientation of the boundary plane but for practical reasons most studies have been limited to trace investigations in a single sample plane. In these studies, a boundary

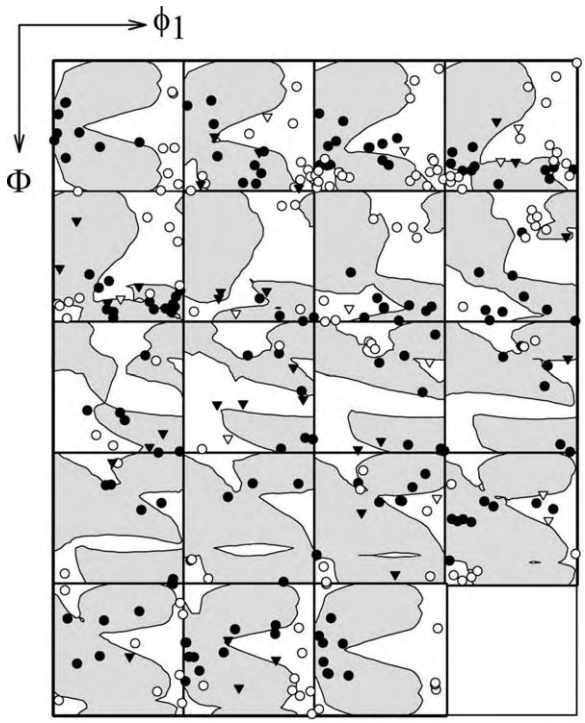

Fig. 4. Orientation distribution function showing grain orientations predicted to have concentrated slip in rolling as grey areas. Filled symbols are grain orientations experimentally observed to have slip plane aligned boundaries. Open symbols are grain orientations observed to have boundaries lying far from slip planes. Circles and triangles are for cold [11] and hot rolled aluminium [39], respectively.

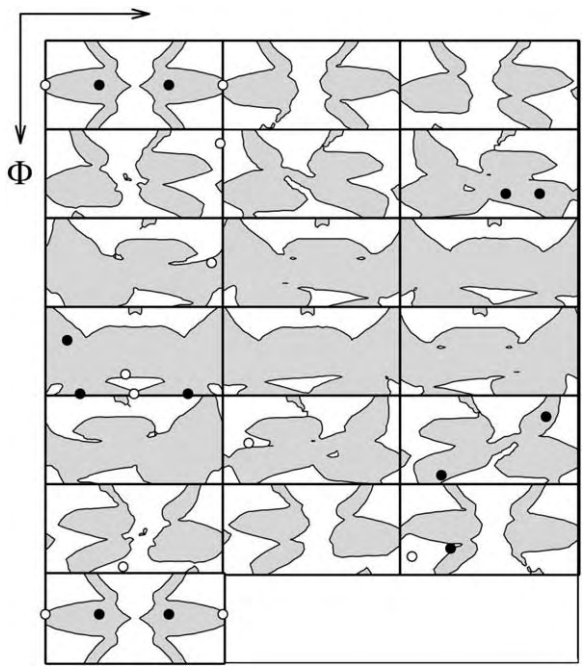

Fig. 5. Orientation distribution function showing grain orientations predicted to have concentrated slip in torsion as grey areas. Filled and open symbols are orientations of grains experimentally observed to have slip plane aligned boundaries or boundaries far from slip planes, respectively, in nickel. The data are from conventional torsion (Refs. [22] and [41] where only approximate orientations are given) and from high pressure torsion (Ref. [40], precise orientations used).

has mostly been classified as slip plane aligned if its trace deviates less than 5° from a slip plane trace [12,34,39,40]. Taking this angle as 7° instead was done for tensile deformed copper resulting in a somewhat different classification [13].[2] Determination of the three-dimensional planes of boundaries has so far been carried out only for tensile deformed aluminium [14]. The result of this investigation indicates that a total deviation less than 10° from a slip plane is a more practical and consistent criterion. For this discussion the experimental data for rolling and torsion are based on a trace deviation of 5° while a three-dimensional deviation of 10° is used for tension. In the comparison of the different deformation modes it is assumed that a three-dimensional deviation of 10° also applies to rolling and torsion. Use of a different value would however, not affect the conclusions.

Fig. 4 shows the prediction for rolling where grey areas mark the grain orientations predicted to have slip plane aligned boundaries. Data for cold rolled polycrystalline aluminium [11] are included as circles. These were the data from which the threshold of 45% slip concentration was determined [36]. New data for an aluminium alloy (AA 3104) plane strain compressed at 510°C [39] are included as triangles. It is seen that there is indeed very good agreement between the grey areas in the ODF and the filled symbols, which represent grain orientations predicted and experimentally observed

[2] That the differences in classification were largely due to the different criterion and not real structural differences between different materials was checked with the author of Ref. [13].

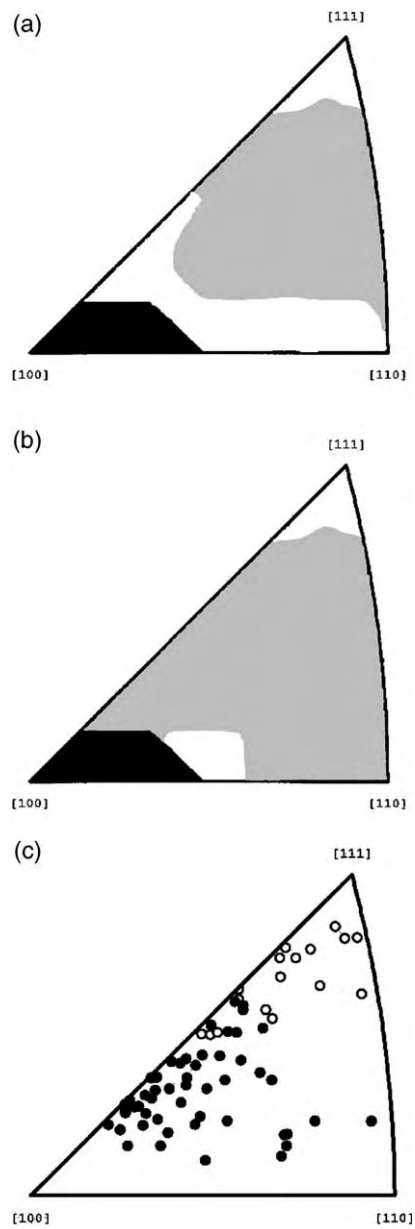

Fig. 6. Stereographic triangles showing the orientation of the tensile axis for grains with (a) concentrated slip predicted from the average Taylor solution (grey areas), (b) concentrated slip predicted from the Taylor solution with most primary slip (grey areas), and (c) experimentally observed slip plane aligned and not slip plane aligned boundaries (filled and open symbols, respectively) for tensile deformed polycrystalline aluminium [14]. Black areas in the ⟨100⟩ corners are grain orientations which do not form extended planar boundaries.

to have slip plane aligned boundaries, respectively. The open symbols represent grain orientations with boundaries lying far from slip planes and it is seen that these dominate in the white areas of the ODF. Although the data are not shown, similar agreement was obtained for cold rolled copper. It is noteworthy that the deviation angles between boundary traces and slip plane traces for grains lying just outside the grey areas were only slightly larger than 5° both for the hot rolled aluminium and the cold rolled copper. The magnitude of the deviation for the cold rolled aluminium sample is unfortunately not available. This indicates that the transition from slip plane aligned to not slip plane aligned boundaries is not well defined. It is also seen that open and filled symbols are found on both sides of the line separating grey and white areas so that this transition is not completely quantitatively predicted. However, these uncertainties in the prediction are limited to this transition region.

For torsion, experimental data on boundary planes are extremely scarce. A few data points for polycrystalline nickel where the approximate grain orientation was stated have been extracted from literature [22,41]. Additionally, three data points for high pressure torsion of nickel at a pressure of 4 GPa were included [40]. All these data are shown in Fig. 5 on top of an ODF marking grain orientations predicted to form boundaries close to slip planes as grey areas. It is seen that there is good agreement. All open and filled symbols, which are experimental data with slip plane aligned boundaries and not slip plane aligned boundaries, respectively, lie within or close to the areas in the ODF predicted to have that type of boundaries. Considering the uncertainty in some of the experimental grain orientations, this is encouraging but there are too few data points to allow solid conclusions.

For tension, grain orientations predicted to have high slip concentrations are marked as grey areas in the stereographic triangle in Fig. 6(a). Again grain orientations, which do not have extended planar dislocation boundaries, are excluded (black area in triangle). Comparison with the triangle in Fig. 6(c) showing experimental data for polycrystalline aluminium reveals that the prediction in Fig. 6(a) is correct near the ⟨111⟩ corner and in the

middle of the triangle but fails in other parts of the triangle. As shown in Fig. 6(b) these discrepancies are almost eliminated if the slip pattern with the highest shear on the primary slip plane is selected among the possible Taylor solutions instead of the average solution. This solution obviously gives more concentrated slip at the ⟨100⟩ − ⟨111⟩ and ⟨100⟩ − ⟨110⟩ lines. Due to the lack of experimental data it is impossible to judge whether the remaining white area near the ⟨100⟩ corner is a correct prediction. The transition between crystal orientations with slip plane aligned and not slip plane aligned boundaries near the ⟨111⟩ corner is qualitatively but not quantitatively predicted.

These comparisons between prediction and experimental data show that slip plane alignment is definitely associated with slip concentration. Overall the predictions for all three deformation modes are good. Quantitatively accurate prediction of the transition between slip plane aligned and not slip plane aligned boundaries is a little difficult. There are probably several reasons for this. One problem is that boundaries always deviate from the slip plane and that classification of slip plane aligned and not slip plane aligned boundaries is somewhat arbitrary. Furthermore, the full slip pattern and not just the most active systems must have an effect on the boundary plane. Predictions based on a single value characterising the slip concentration can therefore hardly be expected to capture all features of these boundaries.

4.2. Prediction of slip patterns

The crystallographic plane of dislocation boundaries can be used to deduce something about the slip. From the discussions above it is clear that this plane gives information on the concentration of slip. However, information on the similarity of slip in different grains or crystals can also be extracted.

4.2.1. Slip concentration

The closer the boundary is to the slip plane, the more the slip is concentrated on that plane. That the closeness of a boundary to a slip plane can be used to deduce information about the slip pattern has already been demonstrated above. It was seen that slip concentrations based on the average of the slip patterns predicted by the Taylor model did not match the observed boundary planes. Use of the solution with most primary slip gives a much better agreement. That this solution is more correct is supported by in situ observations of lattice rotations of individual grains deeply embedded in a polycrystal during tension by three-dimensional X-ray diffraction microscopy [42].

To assist in this type of analysis, a plot of the expected slip concentration versus the experimentally observed angle between slip plane and boundary plane is shown in Fig. 7. The possible range of these angles extends from 0–35° and possible slip concentrations range from 100–25% when slip is evenly distributed among the four {111} slip planes, corresponding to the most distributed slip possible. As illustrated in the previous section an estimated slip concentration above 45% roughly matches a deviation angle of 10°. Finally, the determined crystallographic boundary planes in tension show that deviation angles between 10° and 35° also occur so that the function is continuous [14].

The fact that relatively large variations in slip concentration (45–100%) only give deviations up to 10° may seem surprising. One should, however, bear in mind that the calculated concentration is the concentration on a single slip plane. In many cases practically all slip occurs on two slip planes (i.e. each has a slip concentration close to 50%). This is for example the case for rolled or channel die deformed crystals of Goss [27,31,43,44] and brass [26,31,44,45] orientations and ⟨211⟩ crystals deformed in tension [46,47]. However, a drastic change occurs when the slip is evenly distributed on three planes as boundaries in tensile deformed ⟨111⟩ crystals deviate very much from any slip plane [32].

4.2.2. Slip in single crystals and polycrystals

Comparison of dislocation boundary planes in different crystals/grains in view of the considerations above yields information on the similarities and differences between the active slip systems. A particularly interesting example is comparison of single crystals oriented for single slip in tension with grains of similar orientation in a polycrystal, where single slip is not expected as grains in a

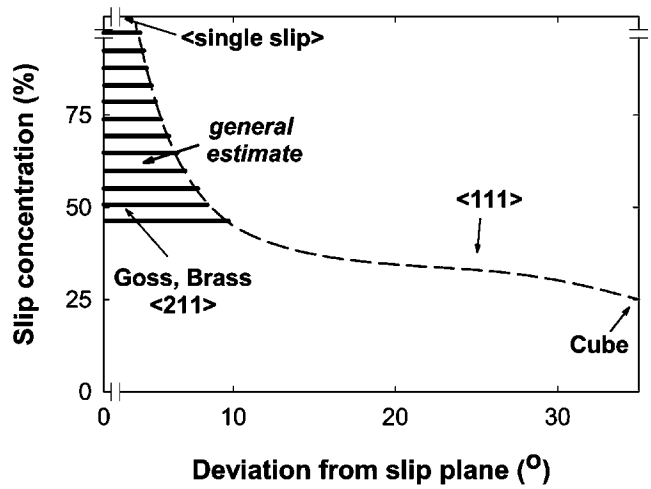

Fig. 7. Increase in observed deviation angles between dislocation boundary planes and nearest slip plane with decreasing slip concentration, i.e. the largest fraction of slip occurring on a single slip plane. The hatched area marks the range of slip concentration generally estimated to give boundaries within 10° of a slip plane. Experimentally observed deviations are included for a number of cases. Tensile data include ⟨111⟩, ⟨211⟩ and single slip oriented single crystals. Rolled and channel die deformed single crystals encompass Goss, brass and cube orientations. Broken axes illustrate that boundaries do not coincide exactly with a slip plane and a slip concentration of 100% probably does not occur either.

polycrystal must maintain strain compatibility with the surroundings.

Dislocation boundary planes in single crystals oriented for single slip and grains of similar orientation in polycrystals have both similarities and differences. In both cases the extended planar boundaries are rotated away from the primary slip plane about similar crystallographic axes, although possibly not exactly the same axis [14,48]. During deformation of the single crystals the direction in which the boundary plane is rotated away from the slip plane is reversed as the orientation of the tensile axis rotates [48]. The reversal occurs at a crystal orientation around the line in the stereographic triangle in Fig. 8 which marks a similar reversal for grains in a polycrystal. The difference is that boundaries in single crystals maintain a constant angle of a few degrees to the slip plane [24,48] while the angle between boundary plane and slip plane increases systematically with grain orientation in the polycrystal as also indicated in Fig. 8 [14].

Based on the considerations above it is concluded that in both cases slip is concentrated on the primary slip plane but more so in the single crystal. The systematic increase of the angle

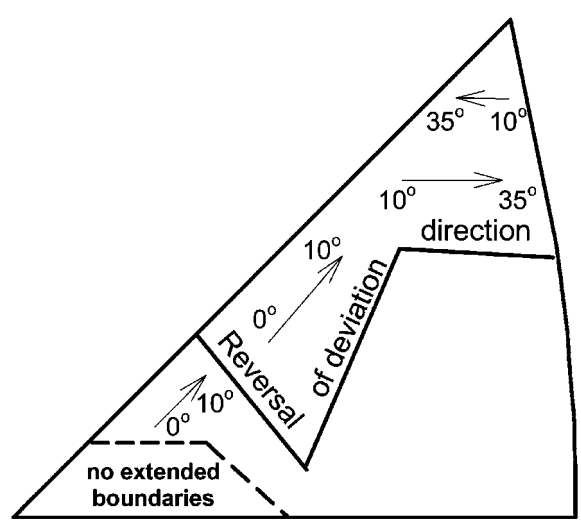

Fig. 8. Stereographic triangle showing the orientation of the tensile axis. The arrows and numbers illustrate the systematic variation of the boundary deviation from slip planes for tensile deformed polycrystalline aluminium. The solid line marks the line at which the direction in which the boundaries deviate from the slip plane is reversed.

between boundary plane and slip plane in the polycrystal as a function of grain orientation shows that secondary systems gradually become more and more active. This is in good agreement with the requirement for strain compatibility in a polycrystal. To obtain strain compatibility more secondary slip is needed and the magnitude of the secondary slip must be grain orientation dependent.

Concerning the identity of the secondary systems it is concluded that they are practically the same in the single crystals and the grains. Otherwise the geometric relations between boundary planes and slip planes would not be so similar. It must also be concluded that in both cases new secondary slip systems are activated when the tensile direction crosses the line in Fig. 8 causing reversal of the direction in which boundaries are rotated away from slip planes.

5. Conclusions

The planes of extended planar dislocation boundaries formed in fcc metals of medium to high stacking fault energy during deformation to low and moderate strains have been analysed for three deformation modes. The main conclusions are:

1. Extended planar dislocation boundaries lie on preferred planes:
   - In the macroscopic sample co-ordinate system, boundaries cluster around planes close to the most stressed planes. However, there is a significant spread around these macroscopic planes and no clear geometric relation between these planes and boundary planes.
   - In the crystallographic lattice, there is an unambiguous geometric relationship between boundary planes and slip planes, which varies systematically with the grain orientation. Deviations of boundary planes from the nearest slip planes range from a few degrees to 35°.
2. Both crystallographic and macroscopic preferred boundary planes are traced to the slip pattern. Relations between specific features of the slip pattern and boundary planes are established:
   - The macroscopic preference is linked to a macroscopic directionality of crystallographic slip. This arises because slip planes and/or slip directions are roughly parallel to the macroscopically most stressed planes.
   - The crystallographic preference is linked to the degree of slip concentration. Boundary planes lie close to slip planes when the slip is concentrated on one or two slip planes. When slip is distributed among many slip planes, boundary planes lie far from slip planes.
3. There is no conflict between the existence of macroscopic and crystallographic preferred boundary planes. When the slip is concentrated on a few slip planes these lie close to macroscopically most stressed planes. When the slip is distributed, no slip plane is close to a macroscopically most stressed plane in most cases. Instead the slip directions align with the macroscopically most stressed planes.
4. Relations between dislocation boundary planes and slip are established. These relations are employed to predict boundary planes from slip patterns and slip patterns from boundary planes. Scientifically, these relations are important because they provide information on which models for boundary formation mechanisms can be based. Technologically, they provide the tool needed for prediction of boundary planes for further evaluation of their mechanical effects. The preferred planes of the boundaries give rise to mechanical anisotropy; boundaries aligned with a slip plane obstruct the slip on these planes less than boundaries lying far from the slip plane (i.e. intersecting the slip plane more frequently).

Acknowledgements

The author gratefully acknowledges the Danish National Research Foundation for supporting the Center for Fundamental Research: Metal Structures in Four Dimensions, within which this work was performed. The author also thanks Dr D.A. Hughes, Dr W. Pantleon and especially Dr N. Hansen for enlightening discussions and Dr D. Juul Jensen for valuable comments on the manuscript.

References

[1] Bay B, Hansen N, Hughes DA, Kuhlmann-Wilsdorf D. Acta Metall Mater 1992;40:205–19.
[2] Christoffersen H, Leffers T. Scr Mater 1997;37:2041–6.
[3] Christoffersen H, Leffers T. Acta mater 1998;46:4093–102.
[4] Zhu Q, Sellars CM. Scr Mater 2001;45:41–8.
[5] Peeters B, Bacroix B, Teodosiu C, Van Houtte P, Aernoudt E. Acta mater 2001;49:1621–32.
[6] Juul Jensen D, Hansen N. In: Proceedings of ICSMA 9, Haifa. 1991. p. 179–86.
[7] Winther G, Juul Jensen D, Hansen N. Acta mater 1997;45:2455–65.
[8] Wilson DV, Bate PS. Acta mater 1996;44:3371–83.
[9] Peeters B, Seefeldt M, Teodosiu C, Kalidindi SR, Van Houtte P, Aernoudt E. Acta mater 2001;49:1607–19.
[10] Gil Sevillano J, Torrealdea FJ. In: Proceedings of the Second Risø International Symposium on Metallurgy and Materials Science: Deformation of Polycrystals: Mechanisms and Microstructures, Risø, Denmark. 1981. p. 185–90.
[11] Liu Q, Hansen N. Phys Status Solidi A 1995;149:187–99.
[12] Huang X, Hansen N. Scripta Mater 1997;37:1–7.
[13] Huang X. Scripta Mater 1998;38:1697–703.
[14] Winther G, Huang X, Hansen N. Acta mater 2000;48:2187–98.
[15] Young CT, Steele JH, Lytton JL. Metall Trans 1973;4:2081–9.
[16] Liu Q. J Appl Crystallogr 1994;27:762–6.
[17] Huang X, Liu Q. Ultramicroscopy 1998;74:123–30.
[18] Randle V. Scr Mater 2001;44:2789–94.
[19] Juul Jensen D, Hansen N. Acta Metall Mater 1990;38:1369–80.
[20] Leffers T, Christoffersen H. Mater Sci Forum 1998;273–275:77–86.
[21] Bay B, Hansen N, Kuhlmann-Wilsdorf D. Mater Sci Eng, A 1989;113:385–97.
[22] Hughes DA, Hansen N. Mater Sci Technol 1991;7:544–53.
[23] Basinski ZS, Basinski SJ. Philos Mag 1964;9:51–80.
[24] Kawasaki Y. Jpn J Appl Phys 1979;18:1429–38.
[25] Steeds JW. Proc R Soc A 1966;292:343–73.
[26] Malin A, Huber J, Hatherly M. Z Metallkd 1981;72:310–7.
[27] Wróbel M, Dymek S, Blicharski M, Gorczyca S. Textures Microstuct 1988;10:9–19.
[28] Driver JH, Juul Jensen D, Hansen N. Acta Metall Mater 1994;42:3105–14.
[29] Godfrey A, Juul Jensen D, Hansen N. Acta mater 1998;46:823–33.
[30] Morii K, Nakayama Y. Scr Metall 1985;19:185–8.
[31] Wróbel M, Dymek S, Blicharski M, Gorczyca S. Z Metallkd 1994;85:415–25.
[32] Kawasaki Y, Takeuchi T. Scr Metall 1980;14:183–8.
[33] Liu Q, Hansen N. Proc R Soc London, A 1998;454:2555–91.
[34] Liu Q, Juul Jensen D, Hansen N. Acta mater 1998;46:5819–38.
[35] Winther G. In: Proceedings of 21st Risø International Symposium on Materials Science: Recrystallization—Fundamental aspects and relations to deformation microstructure, Risø, Denmark. 2000. p. 653–8.
[36] Winther G, Juul Jensen D, Hansen N. Acta mater 1997;45:5059–68.
[37] Barlow CY, Hansen N. Acta mater 1991;39:1971–9.
[38] Wert J, Huang X, submitted for publication.
[39] Liu W. Materials Research Department. Roskilde: Risø National Laboratory; 1998. p. 51.
[40] Winther G, Hansen N, Hebesberger T, Huang X, Pippan R, Zehetbauer M. In: Proceedings of 22nd Risø International Symposium on Materials Science: Science of metastable and nanocrystalline alloys: Structure, properties and modelling, Risø, Roskilde. 2001. p. 435–40.
[41] Hughes DA, Lebensohn RA, Wenk HR, Kumar A. Proc R Soc London, A 2000;456:921–53.
[42] Winther G, Margulies L, Poulsen HF, in preparation.
[43] Morii K, Mecking H, Nakayama Y. Acta Metall 1985;33:379–86.
[44] Nakayama Y, Morii K. Trans Jpn Inst Metals 1982;23:422–31.
[45] Feller-Kniepmeier M, Wanderka N. In: Proceedings of ICOTOM 8. 1988. p. 517–23.
[46] Kawasaki Y. J Phys Soc Jpn 1974;36:142–8.
[47] Anongba PNB, Bonneville J, Martin JL. Acta Metall 1993;41:2907–22.
[48] Winther G, Huang X, Nielsen SF, Wert J. In: Proceedings of Material Instabilities and Patterning in Metals, MRS Spring Meeting, San Francisco. 2001. BB1-8.

A6: Dislocation structures. Part II. Slip system dependence by G. Winther and X. Huang, Phil. Mag., 2007

Philosophical Magazine,
Vol. 87, No. 33, 21 November 2007, 5215–5235

Taylor & Francis
Taylor & Francis Group

Dislocation structures. Part II. Slip system dependence

G. WINTHER* and X. HUANG

Center for Fundamental Research: Metal Structures in Four Dimensions, Materials Research Department, Risø National Laboratory, Technical University of Denmark, DK-4000 Roskilde, Denmark

(*Received 21 March 2007; in final form 10 July 2007*)

Part I established, via extensive transmission electron microscopy investigations, that the type of dislocation structure formed in metals of medium-to-high stacking fault energy upon deformation in tension or rolling to moderate strain levels ($\leq$0.8) depends strongly on crystallographic grain orientation. This paper analyzes the grain orientation-dependent structures in terms of the active slip systems, focusing on the crystallographic plane of extended planar boundaries (geometrically necessary boundaries). The analysis establishes slip systems as the factor controlling the dislocation structure. Five fundamental slip classes, consisting of one to three active slip systems, have been identified. Multiple activation of these slip classes is also considered. The slip classes give rise to different types of dislocation structure, of which all except one contains geometrically necessary planar boundaries aligning with unique crystallographic planes (not necessarily slip planes). A slip class leads to the same type of structure, irrespective of the macroscopic deformation mode, as also demonstrated by successful predictions for shear deformation.

1. Introduction

Part I [1] established that dislocation structures in fcc metals of medium-to-high stacking fault energy, cold-deformed to intermediate strains ($0.05 < \varepsilon < 0.8$) in tension and rolling, depend on crystallographic grain orientation. The aim of the present paper is to identify the factors underlying the grain orientation dependence of the dislocation structures and to generalise the findings to a state where they can be used predictively, e.g. on other deformation modes. The strong effect of crystallographic grain orientation on the dislocation structure must originate from the physical phenomena behind dislocation boundary formation, namely interaction between the available dislocations. More specifically, the available dislocations are generated by crystallographic slip on a number of systems, which, in the present fcc case, are $\{111\}\langle 1\bar{1}0\rangle$. The grain orientation dependence of the dislocation structure, therefore, reflects an underlying dependence on the slip systems. Previous work only considered geometrically necessary boundaries (GNBs) aligned with a slip plane [2, 3] or was limited to a few crystal orientations [4, 5], while the present paper establishes universal relations between slip systems and dislocation structure.

*Corresponding author. Email: grethe.winther@risoe.dk

Philosophical Magazine
ISSN 1478–6435 print/ISSN 1478–6443 online © 2007 Taylor & Francis
http://www.tandf.co.uk/journals
DOI: 10.1080/14786430701591505

From a purely scientific perspective, relations between slip systems and dislocation structure characteristics open up a new avenue of research on boundary formation and evolution mechanisms by identifying a well-ordered basis for studies of interactions between the available dislocations. From a technological perspective, the interest in such relations lies in their predictive capacity. More specifically, the different dislocation structures, which are revealed by post-mortem studies of the deformed sample, give evidence of the active slip systems during deformation and can, therefore, contribute to research on deformation textures. In addition, the ability to predict the dislocation structure based on the slip systems is an essential part of modelling the effect of structure on the mechanical properties [6].

2. Methods and terminology

2.1. *Grain orientation and slip system terminology*

Following Part I and to facilitate the analysis, the direction of the tensile axis for all grains is reduced to the stereographic triangle shown in figure 1, where the primary system is $(11\bar{1})[101]$. The figure also summarizes the standard terminology for the double slip configurations activated at the edges of the triangle. Codirectional slip systems may be oriented for either obtuse or acute cross slip, i.e. cross slip, which is either assisted or inhibited by the externally applied force (see, e.g. [7]). The two processes are henceforth referred to as easy and difficult cross slip, respectively.

The rolling plane and rolling direction for all grains are referred to in the general notation $\{hkl\}\langle uvw\rangle$. To make a direct comparison with tension, the slip systems are referred to in terms of their relative geometry, using the terms coplanar and codirectional slip, etc. It should, however, be noted that the identity of the actual slip systems behind these terms in the rolled grain orientations are not always those shown in figure 1.

2.2. *Slip system determination*

Care has been taken to only consider cases where the slip systems are unambiguously determined. The focus is, therefore, on grain or crystal orientations where a Schmid factor analysis and the Taylor model predict the same systems, as these two methods represent two extreme sets of boundary conditions. Although not always stated in the paper, the shape change and lattice rotations of single crystals have also been considered, when available, to verify the slip systems. In all cases, it is assumed that rolling corresponds to plane strain compression.

The need to know the slip systems rules out a number of commonly considered grain orientations, e.g. the Brass orientation in rolling, where the Taylor model and the Schmid factors predict different slip systems. The Brass orientation is considered separately towards the end to illustrate how the results obtained in this paper can be used to predict the slip systems based on the dislocation structure.

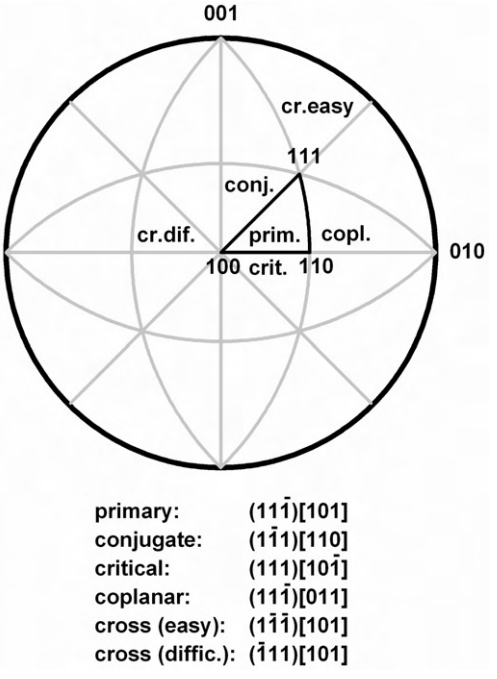

Figure 1. Stereogram showing the triangle used to present the orientation of the tensile axis (the same used in Part I [1]). The primary slip system in this triangle is listed as well as the terminology used to describe the dominant systems in some of the neighbouring triangles.

Table 1. Summary of the considered slip systems, deformation modes and crystal/grain orientations. Note that the analysis shows that some of the slip systems listed may be decomposed into simpler classes. These fundamental slip classes are listed in table 2.

Slip systems	Deformation mode	Crystal/grain orientation
Single slip	Tension	Middle of triangle
	Rolling	{$\bar{1}$13}⟨741⟩
Double slip		
Conjugate slip	Tension	[100]–[211]
Critical slip	Tension	[100]–[110]
Coplanar slip	Tension	[110]–[221]
	Rolling	Goss, 45°ND rotated Cube
Codirectional slip	Rolling	Cube, Copper, S
Symmetric multislip		
Four to six systems	Tension	[211]–[111]–[221]
Eight systems	Tension	[100]

2.3. *Slip classes*

To make the investigation of the relations between slip systems and dislocation structures systematic, the simplest situation, namely single slip, is investigated first, followed by an increasing number of active slip systems in different configurations

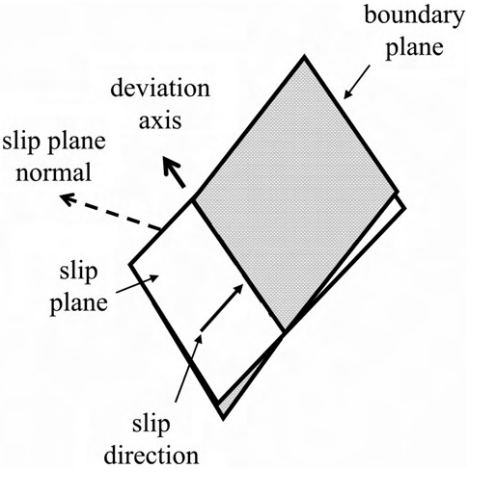

Figure 2. Sketch illustrating the marking of slip plane, slip plane normal, slip direction, boundary plane and deviation axis in figures 3–5 and 8. The example takes the slip plane to the boundary plane by counter-clockwise rotation when looking in the direction of the deviation axis. This is defined as a negative rotation.

described using the terminology of figure 1. An overview of the investigated slip configurations, crystal/grain orientations and deformation modes is given in table 1.

During the analysis, it is shown that some of the considered slip system configurations can be decomposed into simpler cases. A combination of slip systems, which leads to a unique alignment of the dislocation structure is termed a *slip class*. In some cases, a specific slip class is activated by both uniaxial tension and rolling, although for different crystallographic orientations of the grain/crystal with respect to the deformation axes. These cases serve to prove that the slip class controls the dislocation structure.

2.4. *Relation between slip class and boundary planes*

Following Part I, the geometric relationship between a slip class and the boundary plane is defined in terms of the deviation axis around which the boundary plane is rotated away from the nearest slip plane, i.e. the intersection line between slip plane and boundary plane. The positive sign of the deviation angle is chosen so that a clockwise rotation takes the slip plane to the boundary plane when looking in the direction of the axis. The slip class/boundary plane relationship is furthermore illustrated in a number of figures. Figure 2 gives an introduction to these figures, showing how slip plane, slip plane normal, slip direction, boundary plane and deviation axis are marked.

3. Single and double slip

This section considers the single and double slip configurations activated by tension and rolling in the crystal/grain orientations listed in table 1. During the analysis,

these five cases are demonstrated to represent only three fundamental slip classes, as some of the cases represent multiple activation of the same slip class or independent activation of two different slip classes, resulting in two sets of coexisting dislocation boundaries with the characteristics of their respective slip classes.

3.1. *Single, conjugate and critical slip*

Plenty of data on the dislocation boundaries formed in single crystals oriented for single slip in tension are available in the literature. Most of this work is on copper, demonstrating that the boundaries align with the primary slip plane [8–10]. Normally, single slip is not associated with rolling; however, some crystal orientations are predicted to deform by single slip in rolling under relaxed boundary conditions. One such orientation is $\{\bar{1}13\}\langle 741\rangle$, when ε_{13} is allowed to take non-zero values. In a rolled copper single crystal of this orientation, which was deformed by single slip as evidenced by its lattice rotation, the boundaries were found to align with the active slip plane [11], exactly as in tension.

Although these single crystal boundaries are reported as aligning with the slip plane, they typically do not coincide exactly with the slip plane but deviate a few degrees ($<10^\circ$) from it [8, 9, 12]. In all cases, the axis around which the boundary plane is rotated slightly away from the slip plane is of the $\langle 211\rangle$ type. The variant of the $\langle 211\rangle$ axis as well as the deviation direction, however, varies between studies: one study of copper single crystals [10] reported positive deviation around $[2\bar{1}1]$, which is inclined 30° to the primary [101] slip direction (see figure 3a). Another copper single crystal study [13] found an axis of $[1\bar{2}\bar{1}]$, which is perpendicular to the slip direction as illustrated in figure 3b. The latter axis was also found in a study [14] of deformation bands with dominant single slip in a tensile-deformed aluminium crystal of initial [110] orientation, with the sign of the deviation reversing during deformation as the crystal orientation rotated.

Although not expected to be a pure single slip case, the boundaries in tensile-deformed polycrystals for grains with the tensile axis lying in the middle of the triangle and near the [100]–[111] line exhibit the same characteristic alignment with the primary slip plane with a $[1\bar{2}\bar{1}]$ deviation axis, i.e. perpendicular to the primary slip direction (Part I and [15, 16]). The majority of these boundaries are rotated in the negative direction, while positive rotations are found in a certain range of grain orientations (see figure 4 in Part I and also [15] for details).

In copper single crystals ideally oriented for conjugate double slip, i.e. on the [100]–[111] line, two sets of boundaries are seen [5] in the range [411]–[211]. They align with the primary and conjugate slip planes, respectively. This is also the case in aluminium and copper polycrystals for grains near this part of the [100]–[111] line. The deviations from the conjugate slip plane have the same characteristics as for the primary slip plane, i.e. the deviation axis is either the $[\bar{1}12]$ axis perpendicular to the conjugate slip direction [110] or the [211] axis inclined 30° to the conjugate slip direction. Closer to [111], i.e. in the approximate range [211]–[111], boundaries lying much further away from any slip plane are seen. These are considered in a subsequent section and are indicative of activation of another slip class.

Table 2. Summary of the relations between the deduced fundamental slip class and experimentally verified dislocation boundary plane. The slip system terminology is defined in figure 2 and the indices of boundary planes and deviation axes refer to the same reference frame.

Fundamental slip class	Approximate boundary plane	Approximate deviation from slip plane Axis/angle	Illustration
Single slip	$(11\bar{1})$	$[2\bar{1}1]$ or $[1\bar{2}\bar{1}]$*/<±10°	figure 3
Coplanar slip	$(11\bar{1})$	$[1\bar{1}0]$/<−10°	figure 4
Codirectional slip			
Symmetric			
Easy cross slip	(101)	[101]/35°	figure 5a
Difficult cross slip	(010)	[101]/55°	figure 5b
General ($a\gamma_{11\bar{1}} = \gamma_{\bar{1}11}$)			
Easy cross slip	$(1-a, 1+a, a-1)$	[101]/Closer to more active	
Difficult cross slip	$(1+a, 1-a, -a-1)$	[101]/Closer to more active	figure 5c
Two-fold activation of easily cross slipping systems	Equiaxed cells only		
Dependent coplanar and codirectional slip	$(35\bar{1})$	$[2\bar{1}1]/29°$	
3 systems, with one being coplanar and codirectional, respectively, to the others			figure 8a
Two-fold activation:			
4 systems on 2 slip planes	$(35\bar{1})$; $(3\bar{1}5)$	$[2\bar{1}1]/29°$;$[\bar{2}\bar{1}1]/29°$	figure 8b
4 systems on 3 slip planes	$(44\bar{1})$	$[1\bar{1}0]/29°$	figure 8c
6 systems on 3 planes	(115)	$[\bar{1}10]/-39°$**	figure 8d

*Conflicting data on the identity of the ⟨211⟩ axis.
**Angle to closest slip plane, which is the critical plane (111). Experimentally {115} closer to other slip planes are also found.

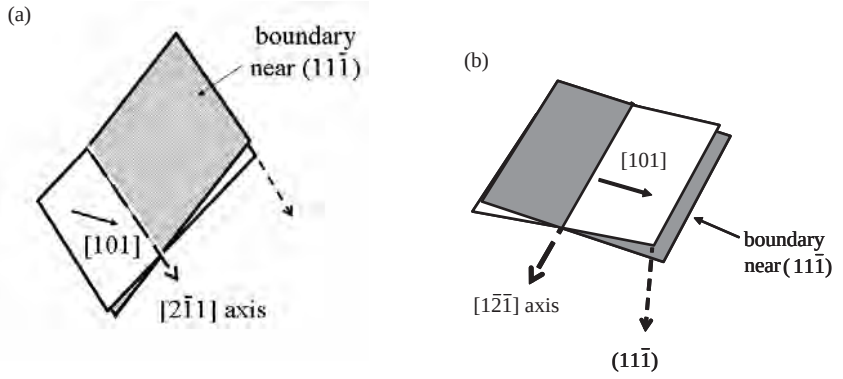

Figure 3. The relationship between slip system and the boundary plane for the single slip class. The boundary is rotated away from the slip plane around a ⟨211⟩ axis. The detailed relationship varies between studies: a) tensile deformed single crystal [10], where the boundary is rotated away from the slip plane in the positive direction, and b) tensile deformed single crystal [13] and polycrystals (Part I, [15] [16]). The sign of the deviation direction (negative in b) has been observed to change systematically with grain orientation in the polycrystals (Part I, [15]).

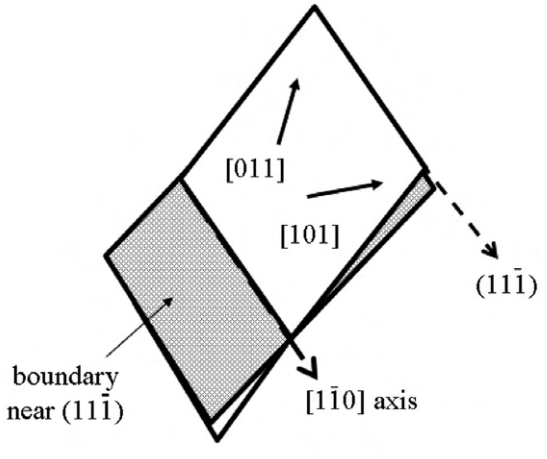

Figure 4. The relationship between two equally active coplanar slip systems and the boundary plane (e.g. rolled Goss and 45° ND rotated Cube, tension on the [110]-[211] line [5]).

Observations of boundaries in grains of warm-deformed aluminium [17] and cold-deformed copper (Part I, figure 11) with the tensile axis near the [100]–[110] line, i.e. grains where the primary and critical slip systems are both expected to be highly active, reveal a similar picture: the boundaries are rotated away from both the primary and critical slip planes. The deviation angle between boundary and slip plane is, however, often larger than in the case of conjugate double slip.

In conclusion, single slip gives rise to boundaries very close to the slip plane but rotated slightly away from this around a ⟨211⟩ axis. The exact identity of this axis varies between different studies. Possible reasons for this will be discussed later.

Single slip is the first fundamental slip class identified here and the relation between slip class and boundary plane is summarized in the first row of table 2. Conjugate and critical double slip result in boundaries with the same alignment characteristics and are, therefore, considered as two-fold activation of the single slip class.

3.2. *Coplanar slip*

The Schmid factors for single crystals with the tensile axis on the [110]–[111] line suggest two equally activated systems on the same slip plane. Kawasaki [5] investigated a number of copper single crystals on this line. In the range [441]–[221], the boundaries aligned with the coplanar slip plane but deviated slightly from this slip plane by negative rotation around the $[1\bar{1}0]$ axis, inclined 60° to both slip directions (see figure 4). The deviation geometry between boundary and slip plane is, therefore, different from the single slip case and coplanar slip is, thus, a new slip class. Between [221] and [111], boundaries deviating substantially from the slip planes were found, which, in analogy with the conjugate slip case, indicate the onset of another slip class as will be considered in a subsequent section.

Rolling does not activate only one set of coplanar systems but two-fold activation of this class occurs in the stable $\{011\}\langle 100\rangle$ orientation (Goss) and the metastable $\{100\}\langle 011\rangle$ (45° ND rotated Cube) orientation. These crystal orientations form boundaries, which align closely with $\{111\}$ slip planes, as indicated by the boundary traces in a number of single crystal studies [11, 18–21] and fully established by tilting in the TEM for a number of near-Goss-oriented grains in polycrystalline aluminium (Part I and [22]).

Single crystals of the metastable $\{100\}\langle 011\rangle$ orientation break up during rolling into bands where one set of the coplanar slip systems is more active. Each band of a crystal of this orientation [23, 24] contained boundaries closely aligned with the coplanar slip plane, which was the more active as evidenced by the lattice rotation of the band. The deviation axis around which the boundary was rotated from the slip plane was the same as for the tensile-deformed single crystals. Other studies of the same crystal orientation [4, 23, 24] found the sign of the deviation from the slip plane to be negative as for tensile-deformed single crystals on the [441]–[221] line. Polycrystal studies of grains of near $\{100\}\langle 011\rangle$ orientation also found boundaries closely aligned with the coplanar slip planes (Part I and [22]).

On the basis of the above observations, coplanar slip is included as a fundamental slip class in table 2. The coplanar slip class leads to boundaries closely aligned with the slip plane, but deviating slightly from this by rotation around a $[1\bar{1}0]$ axis in the negative direction.

3.3. *Codirectional slip*

The rolled Cube orientation, i.e. $\{100\}\langle 001\rangle$, is metastable and easily breaks up into bands, within which two codirectional slip systems oriented for easy cross slip dominate [25]. TEM studies of such deformation bands in rolled Cube-oriented aluminium single crystals [26] show boundaries aligned with two $\{101\}$ planes. Similar boundary planes are found in rolled polycrystalline aluminium of near-Cube

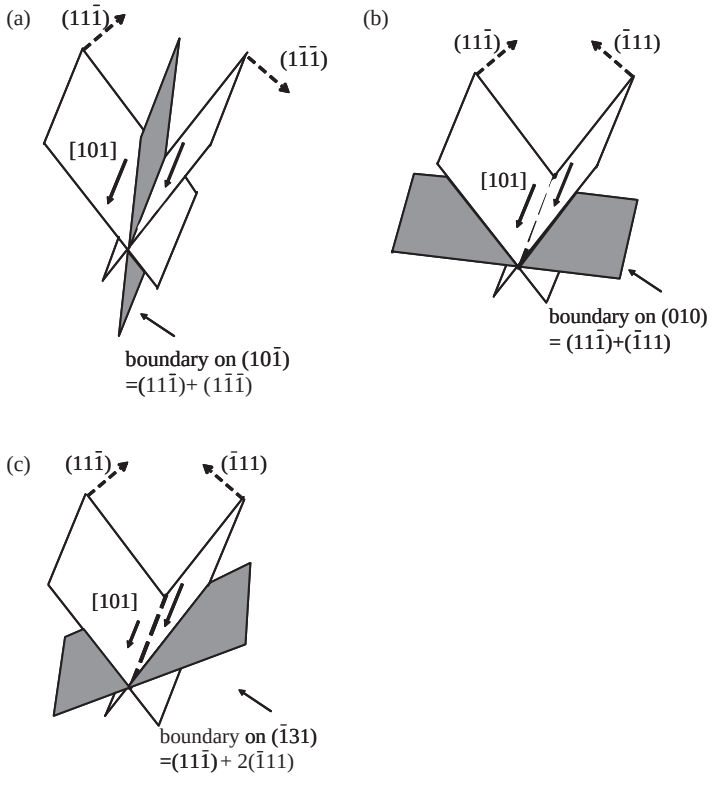

Figure 5. The relationship between slip systems and boundary plane for codirectional slip. a) symmetric codirectional slip oriented for easy cross slip (e.g. rolled Cube), b) symmetric codirectional slip oriented for difficult cross slip (e.g. rolled Copper), c) asymmetric codirectional slip oriented for difficult cross slip, with the system on ($\bar{1}$11) being twice as active as the one on (11$\bar{1}$) (e.g. rolled S).

orientation (Part I, table 4 and [22]). Each {101} plane contains the common slip direction and lies in between the two slip planes of the codirectional systems, thus bisecting the acute angle between the two slip planes (see figure 5a). This angle is 70.5°.

A corresponding example of isolated codirectional slip oriented for difficult cross slip could not be found. The rolled Copper and S orientations, i.e. {112}⟨$\bar{1}\bar{1}$1⟩ and {213}⟨$\bar{3}\bar{6}$4⟩, have four active systems, of which two codirectional systems oriented for difficult cross slip are the most active. The two other systems are coplanar. As established in Part I, it is characteristic for these orientations, as well as the orientations between them along the rolling texture β-fibre, that they may have two sets of boundaries, one of which is close to a slip plane and can be traced to the coplanar slip class as described above in section 3.2. The other set of boundaries must originate from the codirectional slip.

The two codirectional systems in the Copper orientation are equally activated. The corresponding boundaries in the Copper orientation (Part I and [27]) align with the {010} plane. In analogy with the boundaries in the Cube orientation, this plane

contains the common slip direction and bisects the angle between the two active slip planes (see figure 5b). However, by contrast to the Cube orientation, the bisected angle is the obtuse angle between the slip planes, i.e. 109.5°. This difference is attributed to the difference in the codirectional slip geometry, leading to easy and difficult cross slip. As also illustrated in figure 5, the boundary planes are, in both cases, linear combinations of the slip planes, when taking the different signs of the slip plane normals resulting from the two types of cross slip geometry into account.

In the S orientation, one of the codirectional systems is twice as active as the other. The resulting boundary plane is very close to the $\{\bar{1}31\}$ plane (Part I, table 4), deviating about 25° from the more active codirectional slip plane by a rotation around the codirectional slip direction (see figure 5c). This $\{\bar{1}31\}$ plane is the linear combination of the two codirectional slip planes weighted by their respective slip activities (2:1), as also illustrated in figure 5c.

Generalizing the findings, the existence of the codirectional slip class is deduced leading to a boundary plane which is a linear combination of the two active slip planes weighted with their respective slip activities (see table 2 for the general equations). This boundary plane is aligned with the codirectional slip direction. Note that two-fold activation of the codirectional slip class oriented for easy cross slip is a special situation which will be considered in section 4.1.

4. Symmetric multislip cases

It was demonstrated in section 3.3 that the coplanar and codirectional slip classes may be activated independently, resulting in two sets of independent boundaries having the characteristics typical for the respective slip classes. This section is

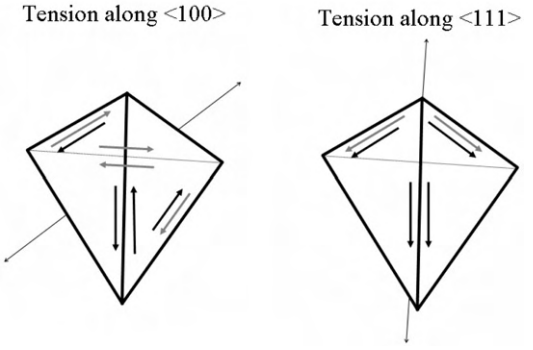

Figure 6. The two stress states considered, represented by perspective views of Thompson tetrahedra. Configurations with 8 equally activated systems for tension along ⟨100⟩ and 6 equally activated systems for tension along ⟨111⟩. The thin arrows mark the tensile directions. The slip plane normals of the three planes active for tension along ⟨111⟩ point towards the centre of the tetrahedron, while the last slip plane normal (the critical slip plane at the base of the tetrahedron) points outwards. This means that by contrast to figure 5, slip systems oriented for difficult cross slip are represented by parallel slip directions while those oriented for easy cross slip are anti-parallel.

concerned with the situation where the coplanar and codirectional slip systems are not independent, i.e. when the coplanar systems are also codirectional with other active systems. The ultimate slip system configurations of this type are multislip cases with six and eight equivalent slip systems. Five such cases are possible for fcc crystals [28], but only three are activated in tension and rolling. However, due to the lack of data for the rolling case, this paper only considers the two cases possible in tension, as illustrated in figure 6. Treatment of these cases is complicated by the fact that all six or eight systems do not necessarily have to be active for the crystal/grain to deform as prescribed by the deformation mode.

Tension along [100] leads to definition of two-fold activation of the codirectional slip oriented for easy cross slip as a new slip class. Tension along [111] also leads to a new slip class, termed dependent coplanar and codirectional slip, to be added as the last class to table 2, together with specialties concerning two-or-more-fold activation of this class.

4.1. *Tension along [100]*

Tension along [100] ideally equally activates eight slip systems, which are all coplanar, codirectional (oriented for easy cross slip) and critical to other systems. As described in Part I, grains in polycrystalline copper [30] and aluminium [31] tensile deformed along [100] have a dislocation structure dominated by cells (termed Type 2 in Part I), and this structure is also found in single crystals [29].

The cell structure was also seen in Part I in rolled copper grains of Cube orientation. Cells – and no GNBs – in Cube-oriented rolled single crystals have also previously been reported in certain layers of both aluminium [26] and copper [11] single crystals, where the Cube orientation remained stable, indicating equal activity of the two sets of codirectional systems.

The finding of the same cell structure in both tension and rolling indicates activation of the same slip class. The slip systems in the rolled Cube orientation constitute two-fold activation of the codirectional slip class oriented for easy cross slip. The idealized eight equally active systems in the tensile deformed [100] orientation may be seen as four-fold activation of the same slip class. It is, therefore, concluded that two-or-more-fold activation of codirectional slip oriented for easy cross slip produces a dislocation structure, which is special by not containing any GNBs, only cells. As a unique dislocation structure is produced, a new slip class is added to table 2.

4.2. *Tension along [111]*

Tension along [111] ideally equally activates six slip systems, which are all coplanar, codirectional (oriented for difficult cross slip) and conjugate to another active system. According to both the Taylor model and the Schmid factors, these six systems may be expected in the entire region spanned by [211]–[111]–[221].

A tensile-deformed single crystal of the ideal [111] orientation had three sets of boundaries deviating about 25° from the active slip planes [29]. Two of these boundary sets were rotated away from the slip planes around ⟨211⟩ axes and lie close

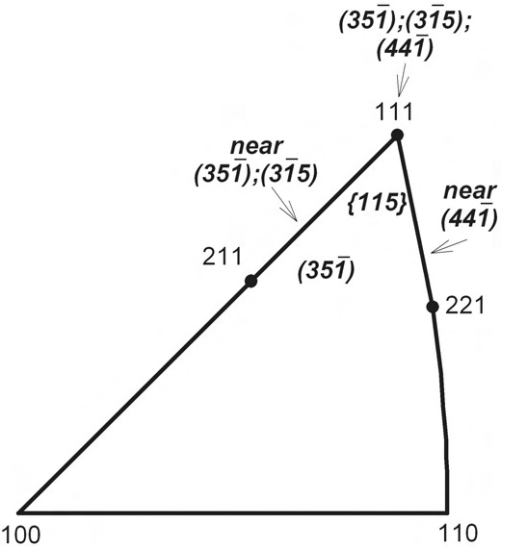

Figure 7. Illustration of the boundary planes in the part of the stereographic triangle spanned by [211]-[111]-[221].

to the (35$\bar{1}$) and (3$\bar{1}$5) planes. The third boundary set was rotated around a ⟨110⟩ axis and was close to (44$\bar{1}$). Single crystals on the [211]–[111] line have boundaries deviating more than 10° from the primary and conjugate slip planes by rotation around the same ⟨211⟩ axes, while large deviations around the ⟨110⟩ axis are found in single crystals on the [221]–[111] line (Note that these orientations were excluded from the analysis of conjugate and coplanar double slip owing to the substantially larger deviation angles and, for the [221]–[111] line also, a change in the deviation direction, which indicated that the slip was not pure double slip).

Part I investigated grains of tensile-deformed polycrystalline aluminium in the part of the triangle spanned by [211]–[111]–[221]. Near the [111] orientation, the boundaries were close to {115} planes but spanned a range of planes from {115} to {001}, in most cases. Further away from [111], only boundaries near {351} were found. Figure 7 summarizes the experimental observations of boundaries on {351}, {441} and {115} planes.

4.2.1. {351} Boundaries. On the [211]–[111] line both the Taylor model and the Schmid factors predict that the two most active systems are the primary and conjugate systems, followed by two codirectional systems, which are coplanar with the primary and conjugate systems, respectively (see figure 8b for a sketch of these slip systems and the (35$\bar{1}$) and (3$\bar{1}$5) boundary planes). The fact that two sets of boundaries are seen means that the slip class behind the {351}-boundary type is two-fold activated. The {351}-boundary plane obviously differs from the boundary planes considered so far. It is, therefore, concluded that a new fundamental slip class is identified. This new slip class must consist of three systems, one of which is

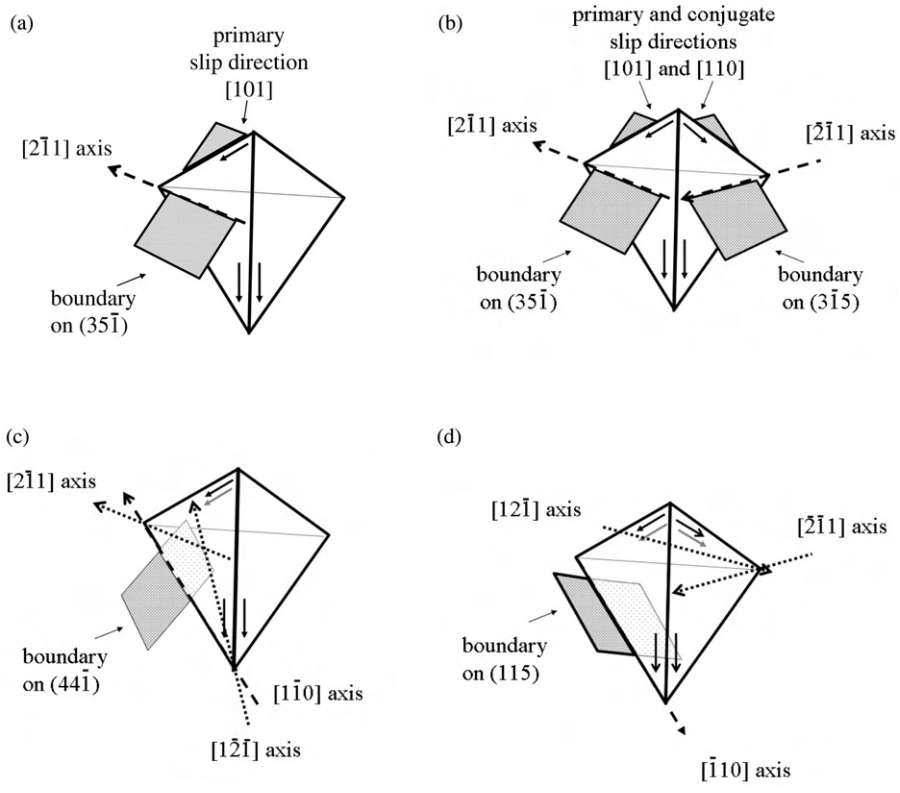

Figure 8. Perspective views of Thompson tetrahedra illustrating the dependent coplanar and codirectional slip class: a) definition of the fundamental slip class consisting of a slip system which is coplanar and codirectional, respectively, with two other slip systems. The boundary on [3$\bar{5}$1] is rotated 29° away from the coplanar slip plane around the [2$\bar{1}$1] axis perpendicular to the slip direction, which is coplanar and codirectional with the others (e.g. in polycrystals away from the line near [211] (Part I)); b) Two-fold activation of the class involving four systems on two slip planes (primary and conjugate), resulting in two sets of boundaries (e.g. tension on [211]-[111] line [5]; in polycrystals also away from the line near [211] (Part I)); c) Two-fold activation of the class involving four systems on three slip planes. The boundary on [44$\bar{1}$] is rotated 25° away from the coplanar slip plane around the [1$\bar{1}$0] axis, which is the sum of the two ⟨211⟩ axes marked as dotted arrows (e.g. tension around [221]-[111] [5]); d) Two-fold activation of the class involving six systems on three planes. The different arrow heads on the slip directions indicate that the slip systems may be viewed as distributed in two sets of dependent coplanar and codirectional slip configurations. The boundary contains the [$\bar{1}$10] axis, which is the sum of the two ⟨211⟩ axes associated with the two configurations (dotted arrows) (e.g. in polycrystals near [111] (Part I)).

coplanar and codirectional, respectively, with the other two (see figure 8a). The new slip class is termed 'dependent coplanar and codirectional slip'.

4.2.2. {441} Boundaries. Moving to the [221]–[111] line, the Taylor model and the Schmid factors do not agree on the four most active systems. The difference between

the third, fourth, fifth and sixth largest Schmid factors is, however, rather small (at most 30% at [221]). It is further noted that the slip systems based on the four largest Schmid factors correspond to independent activation of the coplanar and codirectional slip class, which according to the analysis in section 3.3 should give two independent sets of boundaries on the $(11\bar{1})$and (001) planes, which are obviously not in agreement with the observed $(44\bar{1})$-boundary plane. The slip systems from the Taylor model represent a two-fold activation of the dependent coplanar and codirectional slip class in such a way that four systems on three slip planes are involved (see figure 8c). The observed $(44\bar{1})$-boundary plane is rotated away from the slip plane around the $[1\bar{1}0]$ axis, which is the sum of the two $\langle 211\rangle$ axes (see figure 8c) associated with the two-fold activation of the slip class. The {441}-type boundary is, therefore, a linear combination of two {351}-type boundaries, i.e. $(35\bar{1}) + (53\bar{1}) = (44\bar{1})$.

4.2.3. {115} Boundaries. Finally, turning to the {115}-boundary plane, it is observed that {115} is also a linear combination of two {351} planes, as $(3\bar{1}5) + (\bar{1}35) = (115)$. The {115} boundaries may, therefore, also be attributed to two-fold activation of the dependent coplanar and codirectional slip class. In this case, there are six slip systems on three slip planes involved (see figure 8d). This figure illustrates how the six systems may be divided into two sets of three systems, marked in the figure by the different types of arrow heads. Each of these sets represents the dependent coplanar and codirectional slip class and – if operating alone – would give rise to a {351} boundary rotated away from the slip planes around a $\langle 211\rangle$ axis. The observed spread of the boundary planes towards boundaries on {001} probably reflects an influence of the third set of codirectional systems, since this codirectional set, if operating alone, would result in boundaries on {001}. It is, therefore, proposed that the span of boundary planes observed may be the result of activation of different slip classes, all giving rise to boundaries containing the observed $\langle \bar{1}10\rangle$ axis.

Three configurations of the type shown in Figure 8d may be constructed from the six slip systems, giving rise to boundaries on (115), (511) and (151), respectively. These boundaries are all closer to the critical slip plane than to any of the active slip planes.

4.2.4. Dependent coplanar and codirectional slip class. In conclusion, the multislip case with six systems has been decomposed, leading to identification of a new fundamental slip class, involving three systems, of which one is coplanar and codirectional, respectively, to the two others. This slip class is termed dependent coplanar and codirectional slip. When only activated once, it gives rise to boundaries on a {351} plane rotated around the $\langle 211\rangle$ axis, which is perpendicular to the codirectional slip direction and lies in the coplanar slip plane. Multiple activation of this slip class may involve four systems on two planes, four systems on three planes and six systems on three planes. Such multiple activation results in boundary planes which are linear combinations of {351}-type boundaries (see table 2).

5. Discussion

5.1. *Universality*

Universal relations between the crystallographic boundary plane and the slip class have been established, as listed in table 2. The slip class has been established as the dominant factor controlling the crystallographic alignment of the dislocation structure by the findings that the three slip classes, which are induced by both tension and rolling, result in the same boundary types:

- Single slip in single crystals deformed in tension and rolling results in boundaries closely aligned with the slip plane.
- Coplanar slip systems result in boundaries aligned with the active slip planes but rotated slightly away from this around a ⟨101⟩ axis, as found along the [110]–[211] line in tension and in the Goss and 45° ND rotated Cube orientations in rolling.
- Two or more sets of codirectional slip systems oriented for easy cross slip lead to cell structures when activated in either tension along [100] or rolling of the exact Cube orientation.

It has also been seen that more complex slip system configurations may be broken down into multiple activation of the slip classes listed in table 2. This is, for example, the case for conjugate and critical double slip, which represent a two-fold activation of the single slip class. Examples of simultaneous activation of two different slip classes are the rolled Copper and S orientations, in which the independent activation of the coplanar and codirectional slip classes leads to two sets of boundaries with the characteristics listed in table 2 for coplanar and codirectional slip, respectively.

The number of slip systems involved in a slip class apparently controls the variation in the boundary plane observed within a grain/crystal. Boundaries arising from single or double slip show little variation, while boundaries originating from the dependent coplanar and codirectional slip class consist of straight segments, which are, however, less parallel. The most extreme case is for six active systems where the boundary plane varies between {115} and {001} but notably contains the same $\langle \bar{1}10 \rangle$ axis.

5.2. *Predictive capacity*

The relations in table 2 may be used both forwards and backwards in a predictive manner, i.e. either to deduce the slip systems from the observed dislocation structure or the dislocation structure from the slip systems. This predictive capacity can only be convincingly proven on an independent data set, which has not been used in the present derivation of the relations. The prediction of slip systems based on an observed dislocation structure is demonstrated for the rolled Brass orientation and the prediction of dislocation structures from slip systems is illustrated on data from a new deformation mode, namely shear/torsion.

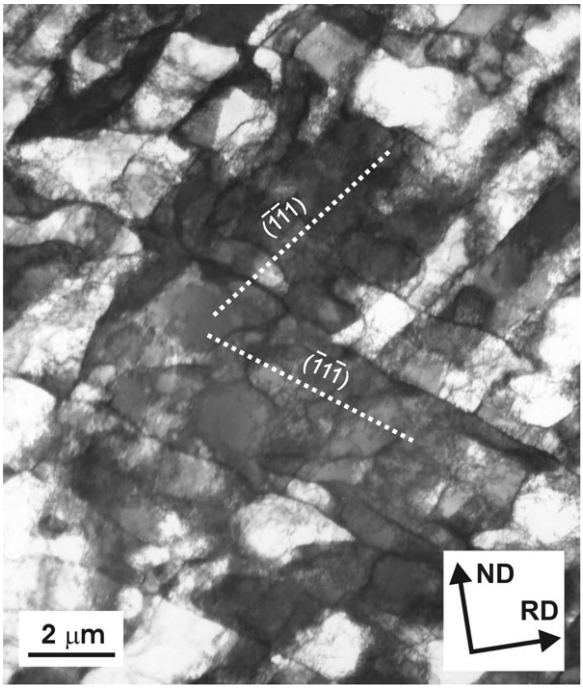

Figure 9. TEM image of the longitudinal sample section of a Brass oriented grain in AA1050 cold-rolled to a strain of 0.33. The exact orientation is (0.02,0.65,-0.76) [-0.87,0.38,0.31], i.e. about 7° from the ideal Brass orientation. The sharpness of the boundary traces shows that the boundaries are viewed edge-on, i.e. the boundaries align with the $(\bar{1}1\bar{1})$ and $(\bar{1}\bar{1}1)$ planes. The beam direction is parallel to [011], which is parallel to both the $(\bar{1}1\bar{1})$ and $(\bar{1}\bar{1}1)$ planes, and must also be the deviation axes for both sets of boundaries. From [35].

Table 3. Schmid factors and shear amplitudes predicted by the Taylor model for rolling of the (0.02, 0.65, −0.76)[−0.87, 0.38, 0.31] orientation (7° from the ideal Brass orientation). Based on the TEM image of the dislocation structure seen in figure 9, the four systems with the highest Schmid factors (in bold) are deduced active.

Plane	(111)	$(11\bar{1})$	$(\bar{1}11)$	$(1\bar{1}1)$
Direction	$[01\bar{1}]$ $[\bar{1}01]$ $[1\bar{1}0]$	$[0\bar{1}\bar{1}]$ [101] $[\bar{1}10]$	$[01\bar{1}]$ [101] $[\bar{1}\bar{1}0]$	$[0\bar{1}\bar{1}]$ $[\bar{1}01]$ [110]
Schmid	0.05 −0.11 0.06	0.16 **0.61 −0.77**	0.13 -0.40 0.27	0.33 **−0.90 0.57**
Taylor	0.00 0.27 -0.29	0.00 0.00 −0.96	0.00 0.00 0.00	0.00 −1.45 0.00

Table 4. Active slip systems predicted for the three stable shear texture components. The Taylor model and the Schmid factors predict the same systems. The slip class and predicted boundary plane are also listed, together with the angle between the boundary plane trace and the shear direction in the plane containing both the shear direction and the shear plane normal.

Orientation	Slip systems	Slip class	Boundary plane	Trace angle to shear direction
(001)[110]	$(\bar{1}11)[110]$,$(1\bar{1}1)[110]$	Codirectional	(001)	0°
(111)[11$\bar{2}$]	$(111)[01\bar{1}]$,$(11\bar{1})[10\bar{1}]$	Coplanar	(111)	0°
(111)[1$\bar{1}$0]	$(111)[1\bar{1}0]$	Single	(111)	0°

Table 5. Active slip systems predicted by the Taylor model and the Schmid factors for the orientation (−0.34, −0.69, 0.64)[−0.93, 0.14, −0.34] deformed by shear. The slip classes and predicted boundary planes are also listed, together with the angle between the boundary plane trace and the shear direction in the plane containing both the shear direction and the shear plane normal. Figure 10 shows a TEM image of this orientation.

	Slip systems	Slip class	Boundary plane	Trace angle to shear direction
Taylor	$(111)[01\bar{1}]$,$(1\bar{1}\bar{1})[01\bar{1}]$; $(11\bar{1})[\bar{1}0\bar{1}]$,$(11\bar{1})[\bar{1}10]$	Codirectional; Coplanar	(100); $(11\bar{1})$	−70°; −15°
Schmid	$(111)[01\bar{1}]$,$(11\bar{1})[01\bar{1}]$; $(11\bar{1})[\bar{1}01]$,$(11\bar{1})[\bar{1}10]$	Coplanar; Coplanar	(111); $(11\bar{1})$	−71°; −15°

5.2.1. Slip systems from dislocation structures. Figure 9 shows a TEM image of a grain of near Brass orientation $(01\bar{1})[\bar{2}11]$. Two sets of GNBs align with the $(11\bar{1})$ and $(1\bar{1}1)$ slip planes, respectively. Both sets deviate from the slip planes by small rotations about the [011] axis. From table 2 and figure 4 it is seen that these boundary planes originate from two-fold activation of the coplanar slip class, more specifically systems $(11\bar{1})[101]$, $(11\bar{1})[1\bar{1}0]$ and $(1\bar{1}1)[10\bar{1}]$, $(1\bar{1}1)[110]$.

The slip systems predicted for the Brass orientation above are in good agreement with the stability of the Brass orientation in the sense that the net lattice rotation produced by these systems is zero if they are equally activated. The resulting strain, however, deviates somewhat from the ideal plane strain compression condition.

Having obtained the active systems from the dislocation structure they may be compared with the predictions of the standard models. As seen from table 3, the four active systems have the highest Schmid factors. However, two of the systems have significantly higher Schmid factors than the two others. Activation of only the two systems with the highest Schmid factors would also have given rise to GNBs aligned with $(11\bar{1})$ and $(1\bar{1}1)$, but the deviation axes would be of the $\langle 211\rangle$-type instead of the measured [011].

The slip systems predicted by the Taylor model represent two-fold activation of the dependent coplanar and codirectional slip class in the configuration involving four systems on three slip planes. According to the relations in table 2, one set of GNBs on (144) should be expected, which is obviously not in agreement with the experimental observations in figure 9.

It is noteworthy that the relations have succeeded in resolving the slip systems for the Brass orientation since the failure of the Taylor model to predict the intensity of this texture component has been the subject of many modelling efforts, typically involving assumed relaxation of the imposed strain components. This example fully establishes the relations as an efficient tool to evaluate and improve models for deformation texture prediction.

5.2.2. Dislocation structures from slip systems. For all of the three orientations representing the major shear texture components, namely (001)[110], $(111)[11\bar{2}]$ and $(111)[1\bar{1}0]$, the Taylor model and the Schmid factors predict the same active slip systems, as listed in table 4. As also seen in the table, three slip classes are

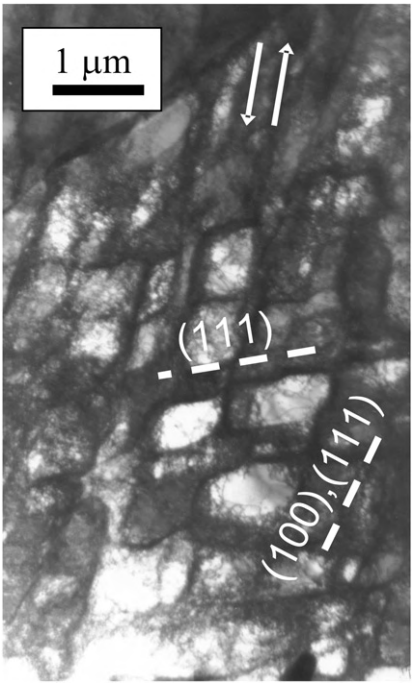

Figure 10. TEM image of a section parallel to the torsion axis of a grain of (−0.34, −0.69,0.64)[−0.93,0.14,−0.34] orientation, i.e. near $(\bar{1}\bar{2}2)[\bar{6}1\bar{2}]$, in Nickel subjected to high pressure torsion at 4 GPa to a strain of 0.5. The image is taken at zero tilt. Two sets of boundaries are seen with traces parallel to the trace of $[11\bar{1}]$ and the common trace of [100] and [111]. The sharpness of the boundaries confirms that the boundaries align with $[11\bar{1}]$ and [100].

represented, namely symmetric codirectional slip, symmetric coplanar slip and single slip. The boundary planes predicted based on the relations in table 2 are (001), (111) and (111), respectively, in the crystallographic lattice. In the coordinate system defined by the macroscopic deformation mode (shear plane normal and shear direction), these planes are all parallel to the shearing plane. This is in perfect agreement with the general observation that the boundary traces align with the shear direction, especially at higher strain, where the shear texture is well-developed [32, 33].

As a further evaluation of the predictions, an experimentally investigated grain with an orientation near $(\bar{1}\bar{2}2)[\bar{6}1\bar{2}]$ in nickel deformed by high pressure torsion to a strain of 0.5 at 4 GPa is investigated. The slip systems predicted by the Taylor model and the Schmid factors are not identical as seen in table 5. The Taylor model predicts independent symmetric codirectional slip and coplanar slip, meaning that two sets of boundaries aligned with (100) and $(11\bar{1})$, respectively, is predicted. The Schmid factors predict two-fold activation of the coplanar slip class, i.e. boundaries aligned with (111) and $(11\bar{1})$.

Figure 10 is a TEM image of this orientation. It is seen that the predicted boundary traces, which are indicated in the image, match the experimental observations (Note that the traces of (100) and (111) coincide). Furthermore, both

the observed traces are fairly sharp, showing that the boundaries are close to being viewed edge-on. The boundary plane, therefore, truly aligns with $(11\bar{1})$, which is 5° from being parallel to the beam. It also resolves that the second set of boundaries align with (100) as predicted based on the slip systems from the Taylor model. The (100) plane is only inclined 5° to the beam while the inclination of the (111) plane is 47°.

Prediction of the dislocation structure alignment is of practical importance in the modelling of mechanical anisotropy where the parallelism of the GNBs makes an important contribution. It has been demonstrated that modelling based on the precise GNB alignment in the individual grains is greatly superior to modelling based on the average GNB alignment in the sample [6].

5.3. *Unresolved issues*

With the establishment of the relations between dislocation structure type and slip class, most of the available data have been explained. However, two subtle issues are still left unresolved: (i) the identity of the deviation axis and the sign of the deviation for the single slip class and (ii) the variant of the {115} plane with which the boundaries align for multiple activation of the dependent coplanar and codirectional slip class.

5.3.1. Deviation axis for the single slip class. While agreeing that the deviation axis for the boundaries closely aligned with the primary slip plane $(11\bar{1})$ is of the ⟨211⟩-type, different studies [10, 13, 14, 15, 16] disagree on the exact variant of this axis, reporting either $[2\bar{1}1]$ or $[1\bar{2}\bar{1}]$. Also the sign of the deviation is debated.

It is well established from analyses of slip line traces, as well as of the Burgers vectors of the dislocations observed in tensile deformed single crystals, that secondary slip systems are almost always activated. These secondary slip systems may be the parameter responsible for the observed discrepancies. For example, slip trace analysis [34] of a single crystal tensile deformed along [311] found activation of dependent coplanar and codirectional slip rather than pure conjugate double slip, which, together with the fact that the conjugate systems were by far the most active, may explain the observations in a [411] crystal of boundaries almost aligned with the slip planes but with a deviation axis and sign characteristic of the dependent coplanar and codirectional slip class [5].

5.3.2. Variant of {115} boundaries. Assuming only the six systems normally expected for the [111] orientation three variants of {115}–{001} spans are expected from the analysis in section 4.2.3. The boundaries presented in figure 4 of Part I span four different variants of {115}–{001} planes, of which only two are among those predicted. An unpublished trace analysis using a geometric method [14, 15] for grains near [111] of tensile-deformed copper is in agreement with having boundaries on the three {115} planes closest to the critical slip plane but also indicated that some boundaries aligned with other {115} planes. The origin of these other variants is at present unexplained but may be related to the general complexity of the slip in the

[111] orientation, which may be seen as six-fold activation of the dependent coplanar and codirectional slip class.

6. Conclusions

Dislocation structures in single crystals and polycrystals in fcc metals of medium to high stacking fault energy deformed to moderate strains ($0.05 < \varepsilon < 0.8$) exhibit a strong dependence on the crystal/grain orientation. Detailed data on the crystallographic plane of extended boundaries after tension and rolling have been determined in Part I. These planes are not always slip planes and a structure type consisting only of equiaxed cells has also been observed. The crystallographic alignment of the dislocation boundaries has been analysed in terms of slip systems. The following conclusions were made:

- The slip systems control the grain orientation dependence of dislocation structures.
- The slip system configurations in tension and rolling have been decomposed into fundamental slip classes. Each slip class leads to a unique dislocation structure.
- The same slip class activated in different deformation modes, including shear deformation, leads to the same dislocation structure.
- The predictive capacity of the slip class/dislocation structure relations, which is their technological motivation, is demonstrated by (i) deduction of slip systems based on experimentally observed dislocation structures and (ii) prediction of dislocation structures from the slip systems.

Acknowledgements

The authors are grateful to Dr. N. Hansen for enthusiastically contributing to discussions on the subject over many years. Dr. A. Godfrey, Dr. D. Juul Jensen, Dr. T. Leffers, Professor B. Ralph and Professor J. Wert are also thanked for their valuable comments. The authors also gratefully acknowledge the Danish National Research Foundation for supporting the Center for Fundamental Research: Metal Structures in Four Dimensions, within which this work was performed.

References

[1] X. Huang, G. Winther, Phil. Mag., this issue.
[2] G. Winther, D. Juul Jensen and N. Hansen, Acta Mater. **45** 5059 (1997).
[3] G. Winther, Acta Mater. **51** 417 (2003).
[4] J. Wert and X. Huang, Phil. Mag. **83** 969 (2003).

[5] Y. Kawasaki, in *Strength of Materials*, edited by H. Oikawa, K. Maruyama, S. Takeuchi, *et al*. (The Japan Institute of Metals, Tokyo, 1994).
[6] G. Winther, Scripta Mater. **52** 995 (2005).
[7] L. Kubin, B. Devincre and T. Hoc, Phil. Mag. **86** 4023 (2006).
[8] J.W. Steeds, Proc. R. Soc. A **292** 343 (1966).
[9] Z.S. Basinski and S.J. Basinski, Phil. Mag. **9** 51 (1964).
[10] Y. Kawasaki, J. Phys. Soc. Jpn **36** 142 (1974).
[11] M. Wróbel, S. Dymek, M. Blicharski, *et al*., Z. Metallkd. **85** 415 (1994).
[12] Y. Kawasaki, Jpn. J. Appl. Phys. **18** 1429 (1979).
[13] Z.S. Basinski, Disc. Faraday Soc. **93** 38 (1964).
[14] G. Winther, X. Huang, S.F. Nielsen, *et al*., in *Proceedings of Material Instabilities and Patterning in Metals*, edited by P. Spätig, R. Schäublin, M. Victoria. MRS Spring Meeting, (2001).
[15] G. Winther, X. Huang and N. Hansen, Acta Mater. **48** 2187 (2000).
[16] X. Huang, Mater. Sci. Technol. **21** 1379 (2005).
[17] Y. He, X. Huang, N. Hansen, *et al*., Mater. Sci. Technol. **21** 1471 (2005).
[18] Y. Nakayama and K. Morii, Trans. Jpn Inst. Metals **23** 422 (1982).
[19] M. Wróbel, S. Dymek, M. Blicharski, *et al*., Textures Microstuct. **10** 9 (1988).
[20] K. Morii, H. Mecking and Y. Nakayama, Acta Metall. **33** 379 (1985).
[21] K. Morii and Y. Nakayama, Scripta Metall. **19** 185 (1985).
[22] Q. Liu, D. Juul Jensen and N. Hansen, Acta Mater. **46** 5819 (1998).
[23] R. Becker, J.F. Butler, H. Hu, *et al*., Metall. Trans. A **22A** 45 (1991).
[24] Z.J. Li, A. Godfrey and Q. Liu, Scripta Mater. **45** 847 (2001).
[25] Q. Liu, J. Wert and N. Hansen, Acta Mater. **48** 4267 (2000).
[26] Q. Liu and N. Hansen, Proc. R. Soc. A **454** 2555 (1998).
[27] A. Godfrey, D. Juul Jensen and N. Hansen, Acta Mater. **46** 835 (1998).
[28] J. Bishop, Phil. Mag. **44** 51 (1953).
[29] Y. Kawasaki and T. Takeuchi, Scripta Metall. **14** 183 (1980).
[30] X. Huang, Scripta Mater. **38** 1697 (1998).
[31] X. Huang and N. Hansen, Scripta Mater. **37** 1 (1997).
[32] D.A. Hughes and N. Hansen, Mater. Sci. Technol. **7** 544 (1991).
[33] D.A. Hughes, R.A. Lebensohn, H.R. Wenk, *et al*., Proc. R. Soc. Lond. A **456** 921 (2000).
[34] D. Kramer, M. Savage and L. Levine, Acta Mater. **53** 4655 (2005).
[35] G. Winther, X. Huang, A. Godfrey, *et al*., Acta Mater. **52** 4437 (2004).

A7: Modelling flow stress anisotropy caused by deformation induced dislocation boundaries by G. Winther, D. Juul Jensen and N. Hansen, Acta Materialia, 1997

Pergamon

PII: S1359-6454(96)00345-X

Acta mater. Vol. 45, No. 6, pp. 2455–2465, 1997

Published by Elsevier Science Ltd

1359-6454/97 $17.00 + 0.00

MODELLING FLOW STRESS ANISOTROPY CAUSED BY DEFORMATION INDUCED DISLOCATION BOUNDARIES

GRETHE WINTHER†, DORTE JUUL JENSEN and NIELS HANSEN

Materials Department, Risø National Laboratory, DK-4000 Roskilde, Denmark

(Received 2 July 1996; accepted 18 September 1996)

Abstract—Models have been developed for the combined effect of texture and microstructure on the flow stress anisotropy of metals containing dislocation boundaries with a macroscopic orientation with respect to the sample axes. These are the Taylor and the Sachs models modified to include the anisotropic critical resolved shear stress from the dislocation boundaries. The model predictions have shown that the presence of dislocations in an idealized configuration has a significant effect on the anisotropy caused by the crystallographic texture. These model predictions have been tested for a number of materials parameters. Modelling results have finally been compared with measurements of flow stress anisotropy in aluminium sheets cold rolled 18%, and good agreement has been found. © *1997 Acta Metallurgica Inc.*

1. INTRODUCTION

Mechanical anisotropy of metals has been studied extensively due to its importance in industrial forming [1, 2], and also because it is a macroscopic property reflecting the texture and structure of a metal [3, 4]. Many studies have demonstrated the importance of crystallographic texture [5–7] and that crystal plasticity models, e.g. the Taylor model, are useful in describing textural anisotropy [5]. It has, however, also been shown [4] that texture alone cannot explain many experimental observations of anisotropy and other causes have been suggested, e.g. the effect of (i) latent hardening [4, 8]; (ii) grain shape [9, 10]; and (iii) precipitates [3, 11, 12]. In recent years [4, 13–17] the effect of deformation induced dislocation boundaries has been added to this list.

The mechanical anisotropy caused by dislocations accumulating in high density boundaries has been related to a combined effect of their resistance to slip and their macroscopic orientation with respect to the sample axes [4, 15, 16]. For instance, it has been suggested [15, 18] that dislocation boundaries in the form of dense dislocation walls (DDWs) and microbands (MBs) resist slip like ordinary grain boundaries. The macroscopic orientation of the dislocation boundaries depends on the deformation pattern, e.g. in rolling [19] it has been observed that DDW/MBs on average form at angles of approximately 45° and 90° to the rolling direction in the longitudinal and rolling plane, respectively. Figure 1 shows a typical microstructure observed in the longitudinal plane and Fig. 2 is a schematic illustrating the typical three-dimensional orientation of DDW/MBs. In presenting these figures it must be added that other orientations may also be seen and that DDW/MBs of different orientation may exist in separate regions of a grain. Intersection of bands is also observed, but not often at low strain [20].

The mechanical anisotropy caused by dislocation boundaries (DDW/MBs) has been considered in a model where the effects of texture and microstructure are treated separately. In this so-called conical slip model [15] it is assumed that all slip takes place in a cone inclined at 45° to the tensile direction, i.e. on planes that experience the highest shear stress. Predictions based on this model have agreed well with experimental observations for pure aluminium and commercially pure aluminium tested in tension after cold rolling [15]. The conical slip model is based on simple assumptions which must be expanded in order to model the behaviour of materials realistically. A more realistic model could be based on crystal plasticity calculations and take the following phenomena into account: (i) the simultaneous effect of texture and microstructure leading to an anisotropic critical resolved shear stress; (ii) the occurrence of slip at different angles to the loading direction; and (iii) the possibility that the presence of dislocation boundaries affects the slip pattern.

A model based on these ideas has previously been proposed [16]. However, the formulation of the anisotropic critical resolved shear stress is of a qualitative nature with no direct physical interpretation and the importance of the model parameters has not been investigated.

In the following, a new model approach using parameters with direct physical meaning is presented including investigation of the sensitivity of the flow stress anisotropy to (i) the resistance to slip by dislocation boundaries; (ii) the macroscopic orien-

†To whom correspondence should be addressed.

Fig. 1. TEM micrograph from a longitudinal (RD/ND) plane of 30% cold-rolled aluminium (99.996%). The micrograph shows a well-developed set of microbands (A) and one very weak set (B) (Fig. 7 from Ref. [21]).

tation of these boundaries; and (iii) variations in the crystallographic texture. In all these studies the dependence on the number of active slip systems has also been investigated by using, in parallel, the Taylor model [22] and the Sachs model [23]. Finally, model predictions have been compared with experimental observations of cold-rolled aluminium tested in tension at different angles to the rolling direction in the rolling plane.

2. TWO MODELS

Several models for the deformation of polycrystalline materials through slip are available. A widely used model is the Taylor model [22], where it is assumed that all grains deform with the same strain as the sample itself. This ensures strain compatibility between neighbouring grains. It has been shown that realization of this deformation pattern requires at least five active slip systems in each grain. Another model is the Sachs model, according to which each grain only has a single active slip system [23]. The two models represent extreme cases and have therefore been selected in the present study to establish bounds for the mechanical anisotropy. The new models presented in the following are termed the T-model and the S-model, respectively.

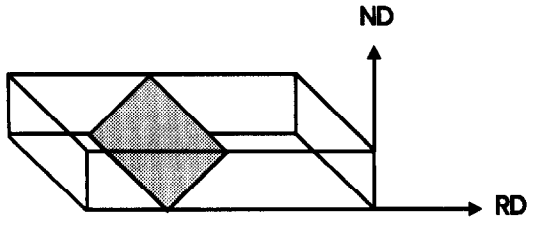

Fig. 2. Schematic illustrating the typical three-dimensional orientation of DDW/MB formed in cold-rolling.

The anisotropic strengthening effect of dislocation boundaries (DDW/MBs) is introduced through the critical resolved shear stress which is given by the Petch–Hall relation, i.e. the critical resolved shear stress

$$\tau_{\mathrm{crss},i} = \tau_0 + x d_i^{-0.5}, \tag{1}$$

where d_i is the distance between the dislocation boundaries experienced by the ith slip system and τ_0 and x are assumed common to all slip systems. τ_0 is the isotropic frictional stress and x characterizes the resistance to slip offered by the DDW/MBs. The ratio x/τ_0 defines the relative importance of the anisotropic and isotropic part of the critical resolved shear stress. The macroscopic orientation of the dislocation boundaries and their spacings are introduced in the model through d_i, which is the distance between the dislocation boundaries. In the conical slip model [15] this distance is taken equal to the distance in the slip plane between the boundaries (see Fig. 3), i.e.

$$d_{\text{slip plane}} = \frac{K}{\sin(\arccos(n_{\mathrm{sp}} \cdot n_{\mathrm{MB}}))}, \tag{2}$$

where n_{sp} and n_{MB} are unit vectors normal to the slip plane and the plane of the DDW/MBs, respectively. K is the spacing between the boundaries in the normal direction. Alternatively, d_i has been calculated as the

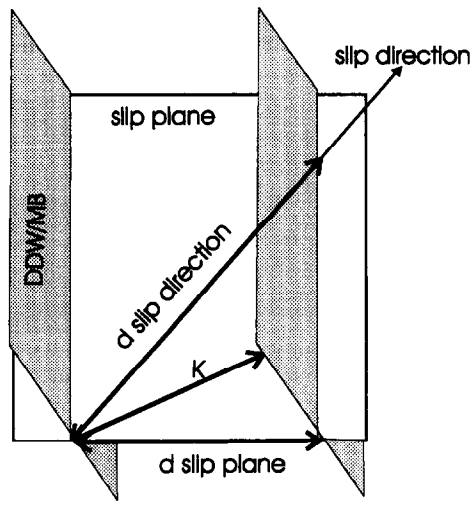

Fig. 3. Schematic illustrating the two ways of calculating the distance between DDW/MBs. The figure shows a slip plane (in the plane of the paper) intersected by the planes of two DDW/MBs (coming out of the paper). The distances taken in the slip plane and the slip direction have been marked. K is the perpendicular spacing between DDW/MBs taken in the direction of the DDW/MB boundary normal.

distance between boundaries in the slip direction, following a suggestion in Refs [9, 10] where the effect of grain shape on Lankford parameters has been modelled. From Fig. 3 it follows that

$$d_{\text{slip direction}} = \frac{K}{|u_{\text{sd}} \cdot n_{\text{MB}}|}, \tag{3}$$

where u_{sd} is a unit vector in the slip direction.

The spacing K is an important structure parameter. A variation in K mathematically corresponds to a variation in x in equation (1) as K can be extracted from equations (2) and (3) and be incorporated in x. It is seen that a decrease in the K-value, i.e. smaller spacing, corresponds to larger x-values, i.e. increasing anisotropy.

The model calculations have been carried out with a program that is based on one described in Ref. [24]. This program has been modified to yield predictions for the new models T and S as described in detail in the Appendix.

The models described in this section are of a general nature and can be used for different geometrical arrangements of dislocation boundaries with respect to the loading direction. In the following only one case is considered, namely modelling of the effect of dislocation boundaries (DDW/MBs) formed by cold-rolling on the flow stress in uniaxial tension as a function of the angle α in the rolling plane between rolling and tensile directions as shown in Fig. 4.

3. SENSITIVITY TO MODEL PARAMETERS

The model approach described in Section 2 has been used to calculate the effect of model parameters on the flow stress anisotropy. The following parameters have been investigated: (i) resistance to slip by DDW/MBs, (ii) macroscopic orientation of DDW/MBs, and (iii) crystallographic texture. For each parameter the flow stress has been calculated as a function of α (see Fig. 4) for four different cases:

1. T model, d_i measured in the slip plane (equation (2))
2. T model, d_i measured in the slip direction (equation (3))
3. S-model, d_i measured in the slip plane (equation (2))
4. S-model, d_i measured in the slip direction (equation (3))

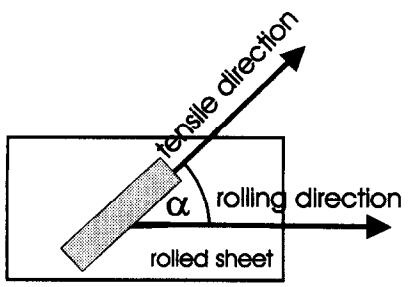

Fig. 4. Tensile samples were cut from the rolled sheets. The angle α between the rolling and tensile direction was varied.

The absolute value of the predicted flow stress calculated with model T is higher than the value calculated with model S. Measuring d_i in the slip plane yields higher flow stress values than measuring it in the slip direction. In order to facilitate comparison of the anisotropy predicted by the different models, which is the subject of this paper, all flow stress values have been normalized in the predicted flow stress for $\alpha = 0$, i.e. coinciding tensile and rolling directions.

3.1. *Resistance of DDW/MBs*

To investigate the effect of the resistance to slip by the dislocation boundaries, the ratio x/τ_0 has been selected as the parameter in an idealized case. In this case the trace of the typical DDW/MBs in the longitudinal and rolling plane is inclined 45° and 90°, respectively, to the rolling direction (see Fig. 2). A spacing (K) of 3 μm has been used and it has been assumed that the crystallographic texture is random, i.e. in the absence of DDW/MBs there is no anisotropy.

Two values of the ratio x/τ_0 have been used, namely one and infinity. The first of these values corresponds to an equal contribution to the flow stress from the DDW/MBs (anisotropic) and from the matrix material between the DDW/MBs (isotropic). The second case ($x/\tau_0 = \infty$) corresponds to a situation where the matrix is very soft and the DDW/MBs thus completely control the flow stress of the individual grains.

The flow stress anisotropy with model T and the distance d_i taken both in the slip plane and the slip direction is shown in Fig. 5. There is a general increase in flow stress with the angle α—except for a shallow minimum around 30°. When the ratio x/τ_0 increases from one to infinity, i.e. the strength of the DDW/MBs increases, the flow stress anisotropy also increases. The way the distance d_i between the DDW/MBs is calculated has a small effect on the magnitude of the predicted anisotropy. Interpreting the distance in equation (1) as the distance in the slip direction gives more anisotropy than taking it in the slip plane.

The flow stress calculated with model S and presented in Fig. 5 also exhibits more anisotropy when the ratio x/τ_0 is infinite. In contrast to model T, the qualitative behaviour of the flow stress depends strongly on the interpretation of the distance d_i between DDW/MBs. When the distance in the slip plane is used the flow stress increases with the angle. However, there is a minimum around 45° when the

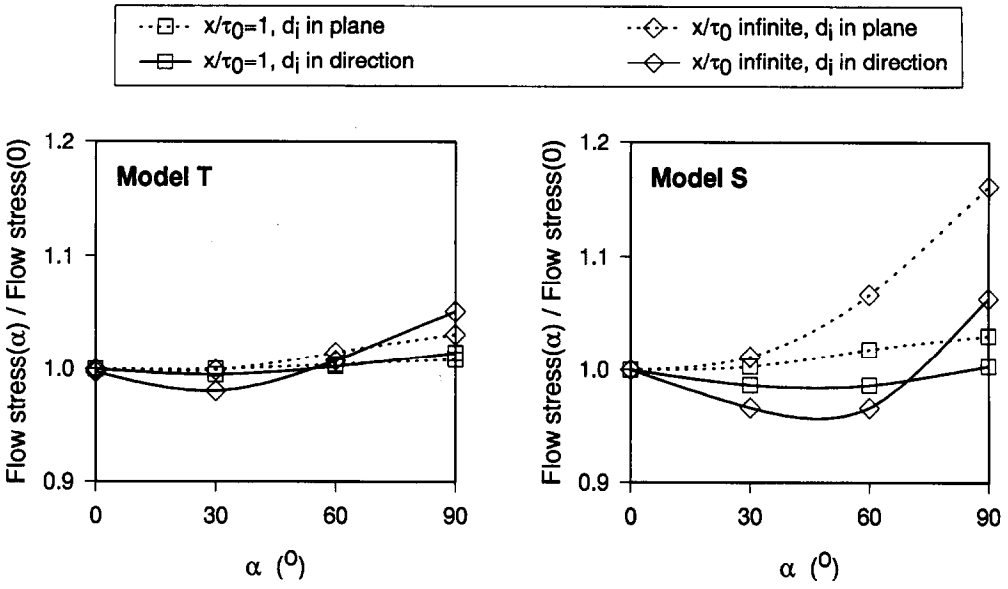

Fig. 5. Flow stress anisotropy for a random texture calculated with models T and S with x/τ_0 values equal to one and infinity and the distance calculated both in the slip plane and the slip direction.

distance is taken in the slip direction. It is noted that model S gives more anisotropy than model T.

3.2. *Macroscopic orientation of the DDW/MBs*

Real materials usually have DDW/MBs which are distributed around the idealized orientation shown in Figs 1 and 2. The sensitivity to relatively small orientation changes around the idealized orientation is explored by calculations with DDW/MBs sets i, ii and iii in Table 1. Another set of DDW/MBs with a completely different orientation (iv) is also included in the calculations. All calculations were made with a random texture and an infinite x/τ_0 ratio. The results are seen in Fig. 6.

It is seen that the curves fall into two groups for model T. For DDW/MBs sets i, ii and iii, which do not differ much from each other, the flow stress increases with the angle α, whereas set iv gives a decreasing flow stress. Similar observations hold for model S when the distance d_i is measured in the slip plane. However, when the distance is taken in the slip direction, the four DDW/MBs sets give anisotropies which cannot be classified into groups.

3.3. *Sensitivity to crystallographic texture*

The main deformation texture components found in rolled materials are Brass, Goss, Copper and S [25]. The Cube orientation is a typical recrystallization component and often found in the initial texture before deformation of the sample [25]. Calculations have therefore been carried out for these specific texture components to study the sensitivity of the anisotropy to the texture of the material.

Table 1. Orientations of the DDW/MB used

DDW/MB set	Angle (°) in the rolling plane	Angle (°) in the longitudinal plane
i	90°	45°
ii	90°	30°
iii	75°	45°
iv	15°	15°

The calculations have been made with $x/\tau_0 = 0$ and $x/\tau_0 = \infty$, i.e. no anisotropy and large anisotropy, respectively, caused by the DDW/MBs. The DDW/MBs have the idealized orientation used in Section 3.1. As an example, the results for the Brass component provided by models T and S with the distance d_i taken in both the slip plane and the slip direction are shown in Fig. 7. Comparison of the results calculated with the usual Taylor and Sachs models, which only take texture into account, and models T and S, which consider both texture and DDW/MBs, reveals the effect of DDW/MBs. When the distance is taken in the slip plane, both models T and S predict relatively small effects in the anisotropy of Cube and Copper components and large effects for Brass and Goss components. For the S component only model S gives a moderate effect. When the distance is taken in the slip direction, models T and S give very large effects for the Goss, Copper and Cube components and also large effects for the Brass component, whereas only model S gives a large effect for the S component.

There is a general anisotropic hardening effect due to the contributions from DDW/MBs to the critical shear stress on the active slip systems. These contributions may be of such magnitude that the deformation can be realized with less work with other slip system combinations than those active in the absence of DDW/MBs, i.e. slip pattern changes compensate for the hardening effect of DDW/MBs. The occurrence of such changes in the slip pattern is

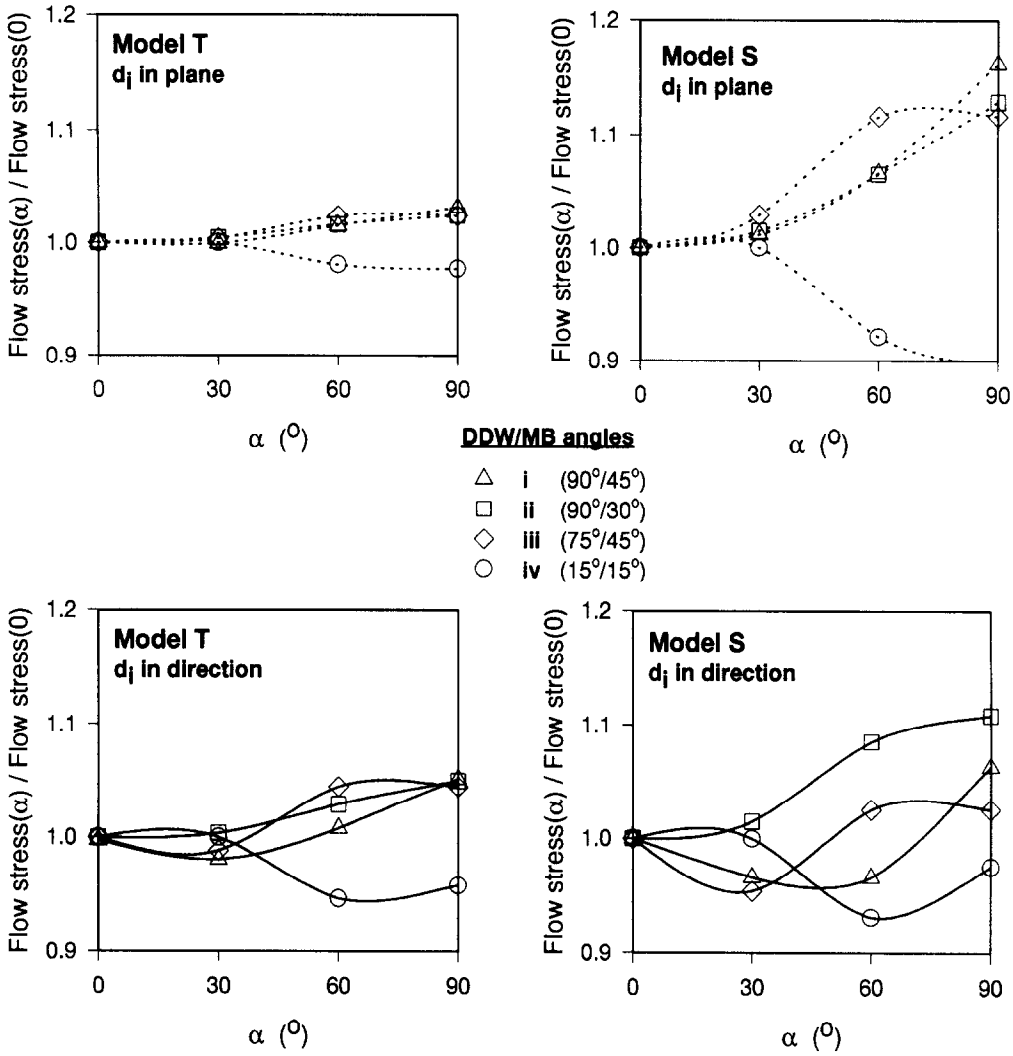

Fig. 6. Flow stress anisotropy for a random texture with DDW/MBs in the four different orientations in Table 1. The flow stress is calculated with models T and S using $x/\tau_0 = \infty$ and with the distance d_i measured in the slip plane and the slip direction.

illustrated in Table 2. The changes in the slip pattern and the magnitude of the hardening depend on the orientation of the slip systems relative to both the DDW/MBs and the tensile axis. Due to this dual dependency it is not easy to predict the effect of DDW/MBs on the flow stress of individual texture components intuitively. However, changes in the slip pattern must occur in such a way that more slip takes place in slip systems with lower critically resolved shear stresses. Geometrically this means that slip planes, which are more parallel to the DDW/MBs, must be more active when the distance d_i between the DDW/MBs is measured in the slip plane. Similarly, more slip must occur in directions which are more parallel to the DDW/MBs when the distance is taken in the slip direction.

4. COMPARISON WITH EXPERIMENTAL DATA

Experimental data in the form of measured textures and DDW/MB orientations and spacings for three 99.5% pure aluminium samples cold rolled to a true strain of 0.2 [4, 26] have been used as input to the models. The angles between the traces of observed DDW/MB planes and the rolling direction in the rolling and longitudinal planes are as stated in Table 3. It is seen that all materials had a majority of the DDW/MBs lying close to the idealized set used in previous calculations.

The textures of the three materials have been measured using neutron diffraction and are introduced in the calculations as described in the Appendix. To investigate the effects of texture alone, model calculations have been carried out with the traditional Taylor and Sachs models (models T and S with $x/\tau_0 = 0$). Calculations with $x/\tau_0 = \infty$ have also been carried out to obtain the upper limit of the anisotropy predicted by the models.

Intermediate ratios of x/τ_0 give anisotropies lying between these extremes. The ratio x/τ_0 may be used

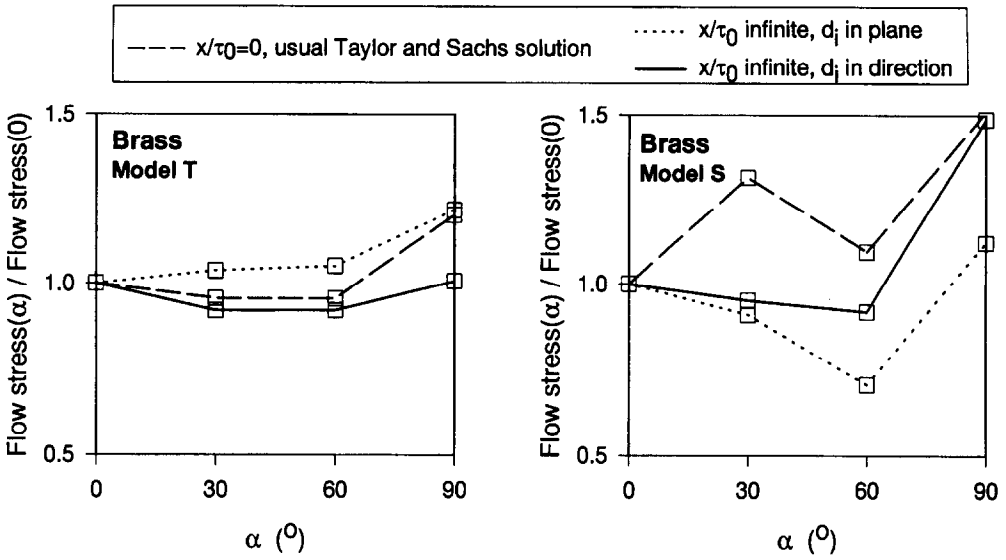

Fig. 7. Flow stress anisotropy of the Brass texture component calculated with models T and S using $x/\tau_0 = 0$ (the usual Taylor and Sachs solution) and for $x/\tau_0 = \infty$. The distance d_i has been measured both in the slip plane and the slip direction.

as a fitting parameter to obtain the best agreement between predicted and experimental anisotropy. However, such a procedure has not been attempted here due to the rather large scatter in the experimental data, and the apparent experimental anisotropy in the normalized plots depends on the accuracy of the data point to which the rest are normalized.

The flow stress predictions of the models and the experimental data ($\sigma_{0.2}$) are shown in Figs 8 and 9. It is seen that the traditional Taylor and Sachs solutions, which only account for the texture effects, exhibit flow stress anisotropies which are generally low compared with the experimental data.

The results for model T in Fig. 8 show that for material A the predicted anisotropies are comparable to the measured values. For material B it is evident that the predicted anisotropy is far too low compared with the experimental data. For material C calculations, with all values of x/τ_0—even the traditional Taylor solution ($x/\tau_0 = 0$)—gives a predicted anisotropy which is in good agreement with the experimental observations.

Considering the results from model S in Fig. 9, it is seen that here both measures for the distance d_i and a wide range of x/τ_0 ratios seem to fit the data equally well for material C. For materials A and B, the calculations with the distance d_i taken in the slip direction give an anisotropy which differs qualitatively from that experimentally observed. The experimental data and the model predictions agree qualitatively when the distance in the slip plane is used. For material A the x/τ_0 ratio which gives the best prediction lies somewhere between the lower ($x/\tau_0 = 0$) and upper ($x/\tau_0 = \infty$) bounds used here. An infinite x/τ_0 ratio provides a reasonable agreement with the experimental data for material B.

5. DISCUSSION

5.1. *Model approach*

The models (T and S) for flow stress anisotropy are based on the slip pattern assumptions characterizing the Taylor and the Sachs model. Thus, the main difference between model T and model S is the number of active slip systems. This is the reason why

Table 2. Changes in the slip pattern when the x/τ_0 ratio is changed from zero to infinity are marked with +. In the case of slip ambiguity all combinations giving the same work were considered and if these combinations were not the same, a change was registered

α (°)	Goss		Brass		Copper		S		Cube	
	plane	direct.	plane	direct.	plane	direct.	plane	direct.	plane	direct.
Model T										
0	+	+	−	−	+	−	−	−	+	+
30	+	+	+	+	−	+	−	−	+	+
60	+	+	+	+	−	+	−	−	+	−
90	+	+	−	+	−	−	−	−	+	+
Model S										
0	+	+	+	+	+	+	+	+	+	+
30	+	+	+	+	+	+	+	+	+	+
60	+	+	+	+	+	+	−	+	+	+
90	+	+	+	+	+	+	−	+	+	+

Table 3. Experimental observations of mean angles between the trace of the microbands and the rolling direction in the rolling and longitudinal planes (from Refs [4, 26])

Material	Frequency (%)	Angle (°) in rolling plane	Angle (°) in longitudinal plane
A	100	83	42
B	83	83	42
	17	20	14
C	38	83	32
	19	−20	−3
	43	83	−38

model S yields more anisotropy than model T. The final flow stress anisotropy reflects the orientations of all active slip systems relative to the DDW/MBs. As the five active slip systems in model T must be oriented differently to the DDW/MBs, the resulting macroscopic anisotropy will be an average of large and small contributions from DDW/MBs in the individual slip systems. In model S the macroscopic flow stress directly reflects the influence from DDW/MBs on the single active system.

This dependency on the number of active slip systems is in good agreement with the findings of the model [16] based on the same principles as models T and S that a reduced number of active slip systems is needed to give an effect of DDW/MBs on yield surfaces.

A similar averaging effect may also account for the fact that model T is relatively insensitive to the way the distance d_i in equation (1) is calculated, whereas the anisotropy calculated with model S changes qualitatively with the interpretation of d_i (see Fig. 5).

A Petch–Hall equation (equation (1)) has been used to model the effect of DDW/MBs on the flow stress anisotropy. d_i is the structural parameter in this equation, defining a distance between boundaries which stop moving dislocations. Taking this distance in the slip direction assumes that, in effect, all moving dislocations are edge dislocations. A screw dislocation moves perpendicular to this direction, and since a dislocation population is a mixture of edge and screw dislocations it is suggested that d_i will take some average value in the slip plane independent of the slip direction. The importance of the slip plane has been a basic assumption in previous models of

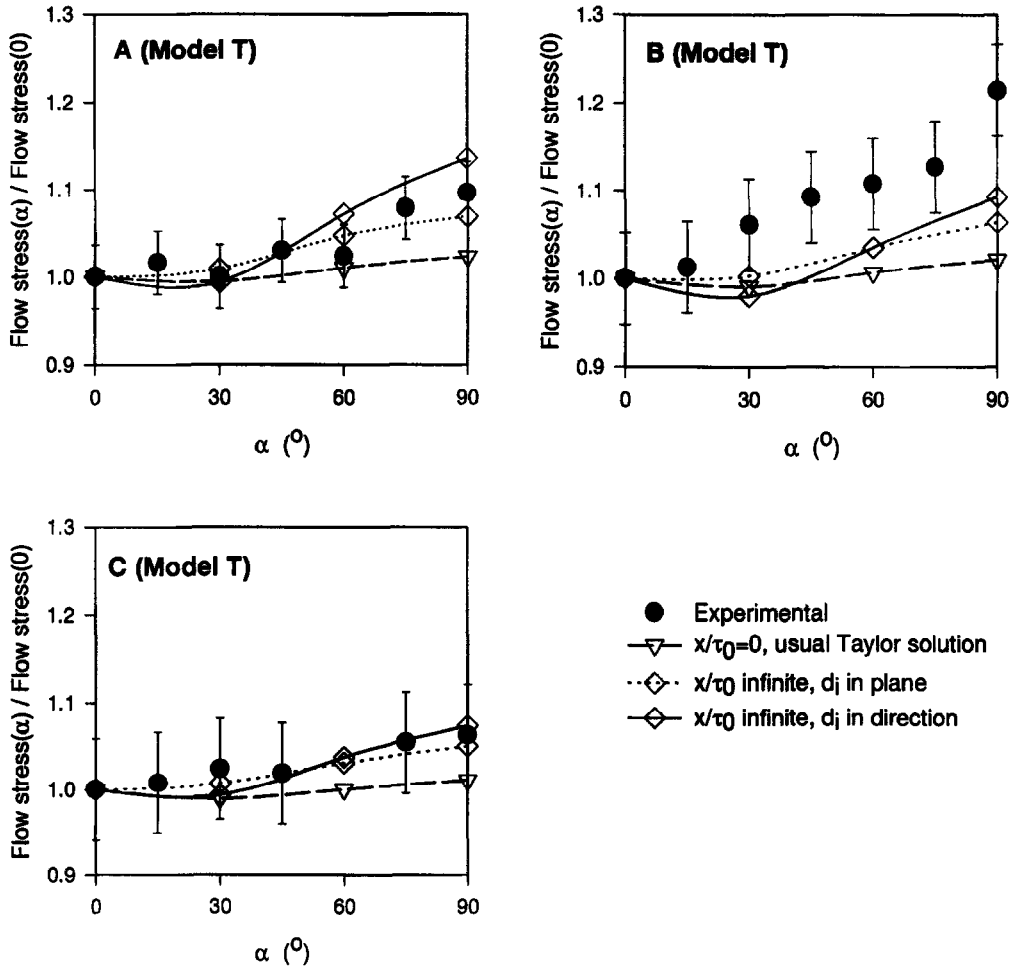

Fig. 8. Experimental data, the usual Taylor solution and model T solutions with $x/\tau_0 = \infty$ and the distance d_i calculated in the slip plane and the slip direction.

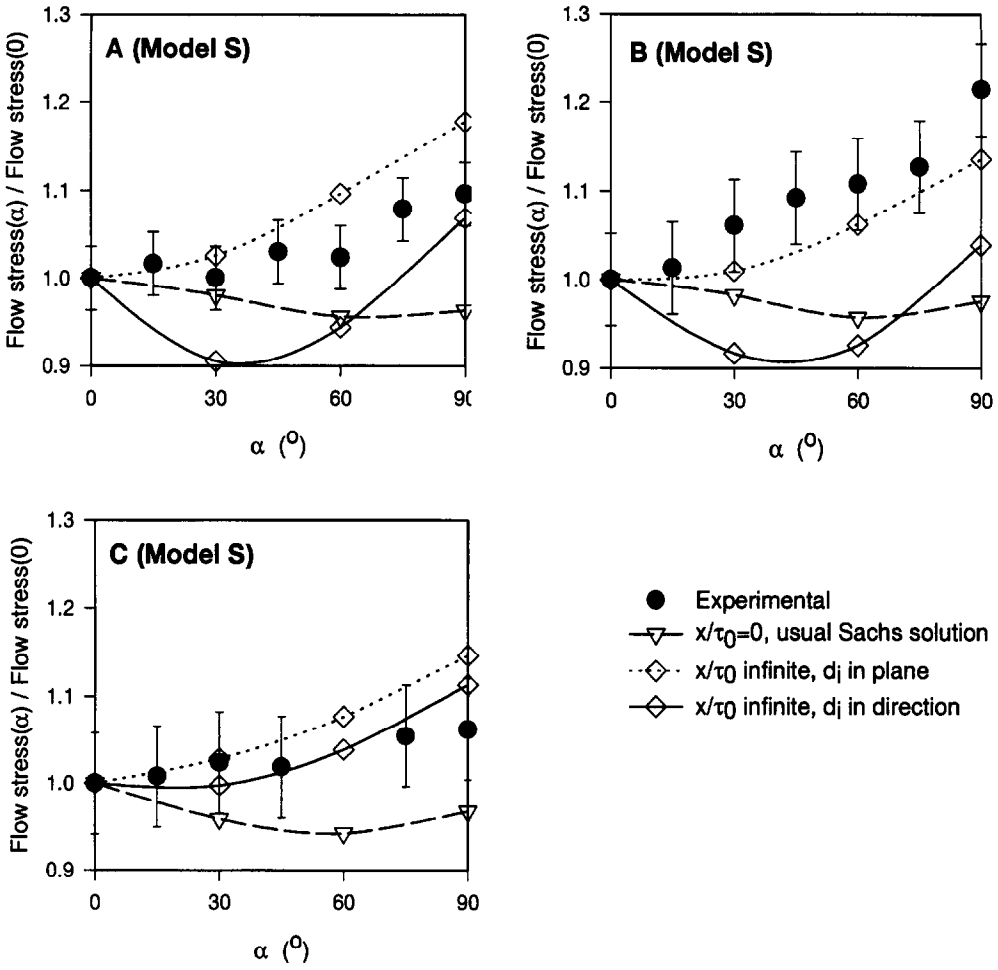

Fig. 9. Experimental data, the usual Sachs solution and model S solutions with $x/\tau_0 = \infty$ and the distance d_i calculated in the slip plane and the slip direction.

microstructural contributions [15, 16]. This leads to a preference for d_i being the distance determined in the slip plane. A comparison of model predictions with experimental findings gives no clear preference to either of the ways to calculate d_i, although somewhat better agreement with experimental data is observed when the distance in the slip plane is used (see Figs 8 and 9). This observation adds to studies [9, 10] of the effect of grain shape on Lankford parameters where the distance between grain boundaries has been calculated both as the distance in the slip direction and perpendicular to this direction. In these studies it was found that the first approach gives better agreement with experimental findings.

Application of equation (1) requires an estimate of x which is a measurement of the resistance to glide due to the presence of DDW/MBs. It has been assumed [15] that the resistance equals that of a grain boundary and x has been taken equal to the Petch–Hall slope when plotting the flow stress of a recrystallized material versus the reciprocal square root of the grain size. This has been modified in the present work where the effect of x has been examined through the parameter x/τ_0. The matrix is subdivided by ordinary cell boundaries which are not macroscopically oriented, i.e. they contribute to the flow stress, but not to the flow stress anisotropy. The strength contribution from the cell boundaries is proportional to the reciprocal cell size. This cell size decreases with the strain, i.e. τ_0 increases with strain. For a constant x this means that x/τ_0 decreases and it follows that the anisotropy should decrease with increasing strain. This is counteracted by a decrease in the spacing (K) between the DDW/MBs with increasing strain, leading to a decrease in d_i and an increase in anisotropy. Finally, it can be added that the assumption that dislocation boundaries have a resistance to slip propagation equivalent to that of grain boundaries requires that they have a sufficiently high misorientation angle. This angle increases with strain [27] reaching average values of 2–5° at strains between 0.1 and 0.4 [28]. Most boundaries of such angles are assumed to resist glide similar to the way high angle grain boundaries do. It must however be emphasized that x/τ_0 cannot be estimated with great precision.

The sample texture is important for the predicted anisotropy. The presence of DDW/MBs induces large changes in the anisotropy of samples with strong Brass and Goss textures for both models T and S, regardless of the measure used for the distance between DDW/MBs. The qualitative features of the anisotropy of these two orientations depend strongly on the number of active slip systems and the calculation of d_i. Studies of samples with strong Brass or Goss textures or single crystals may therefore be a good way to test the models further.

5.2. *Model predictions—experimental data*

As seen in Figs 8 and 9, inclusion of a contribution from DDW/MBs clearly improves model predictions compared with cases where only the texture effect is taken into account (i.e. results with the usual Taylor and Sachs models). This applies to both the T and the S-models. As regards the choice of d_i it appears that the distance in the slip plane gives somewhat better agreement with experimental data than taking the distance in the slip direction. This is especially so for the S-model.

Near quantitative predictions seem to be realized with model T for two (A and C) out of three materials when taking $x/\tau_0 = \infty$. For model S, good agreement is obtained for all three materials when calculating d_i in the slip plane and for $x/\tau_0 = \infty$. It appears, however, that for materials A and C, $x/\tau_0 = \infty$ is an overestimate; thus the predicted curves in Figs 8 and 9 must be considered upper bounds.

The model calculations have only been made for selected orientations of the DDW/MBs. In reality the DDW/MBs in materials A, B and C were distributed around the mean orientations used in these calculations. It has, however, been shown here (see Section 3.2 and Fig. 7) that variations of 15° in the trace of the DDW/MBs in the longitudinal and rolling plane, respectively, do not change the trend of the calculated flow stress (except when model S is used with d_i in the slip direction). The dependency on DDW/MB orientation is therefore not strong enough to explain the observed deviation between model predictions and experimental data. The weak orientation dependence also means that careful characterization of the distribution of DDW/MB orientations is not crucial for use of the models.

5.3. *Comparison with the conical slip model*

The conical slip model calculates an effective flow stress given as [15]

$$\sigma_{\text{eff}} = \frac{3.06}{M_{\text{Taylor}}}(\sigma_0 + K_2 Gb/C^n + K_1(Gb)^{0.5} D_{\text{MB}}^{-0.5}), \quad (4)$$

where the first term in brackets is a friction stress, the second is a contribution from ordinary cell boundaries and the third is the contribution from DDW/MBs. D_{MB} is the average distance between DDW/MB taken in planes inclined 45° to the tensile direction (see Ref. [15] for more details) and C is the cell diameter. $3.06/M_{\text{Taylor}}$ is the Taylor M-factor for a random texture divided by the M-factor for the material.

In order to compare the conical slip model to models T and S, the constants τ_0 and x in equation (1) have to be related to the constants in equation (4). τ_0 represents the isotropic part of the critical resolved shear stress and is therefore given by

$$\tau_0 = \frac{\sigma_0 + K_2 Gb/C^n}{M_m}, \quad (5)$$

where division by M_m converts from a macroscopic stress to a stress on an individual slip system. M_m is the M-factor for a random texture calculated with either the Taylor or the Sachs model. The parameter x is given by

$$x = \frac{K_1(Gb)^{0.5}}{M_m}. \quad (6)$$

The flow stress predicted by models T and S using τ_0 and x given by equations (5) and (6) is directly comparable to the experimental data but not to the effective flow stress predicted by the conical slip model (cf. equation (4)). For comparison the experimental data and the predictions of models T and S must be converted to an effective flow stress given as

$$\sigma_{\text{eff}} = \frac{3.06}{M_{\text{Taylor}}}\sigma_{\text{real}}. \quad (7)$$

Figure 10 shows the effective flow stress predicted by the different models for materials A and B. The following values [15] have been used for the constants in equations (4)–(6), $\sigma_0 = 20$ MPa, $K_1(Gb)^{0.5} = 70$ MPa μm$^{0.5}$ and $K_2 Gb = 56$ MPa μm and $n = 1$. The cell diameter (C) and the spacing (K) between DDW/MBs have been estimated as 1.6 μm and 4 μm, respectively.

It is seen that model S with the distance taken in the slip plane yields results which most resemble the results of the conical slip model. This is not surprising since the conical slip model assumes that the slip is concentrated on planes inclined 45° to the tensile direction, which is most comparable to using a single active slip system, and uses the average distance between DDW/MBs in these planes. For both materials A and B the conical slip model predicts the most anisotropy. One reason for this is the ability of the new models to compensate for the anisotropic hardening due to DDW/MBs through changes in the slip pattern as described in Section 3.3.

The conical slip model agrees better with the experimental data for material B, whereas the models described here give better results for material A. However, models T and S are preferred to avoid the assumptions of concentrated slip in a cone and no influence from the DDW/MBs on the slip pattern. The new models therefore have a better physical basis. Furthermore, the conical slip model cannot

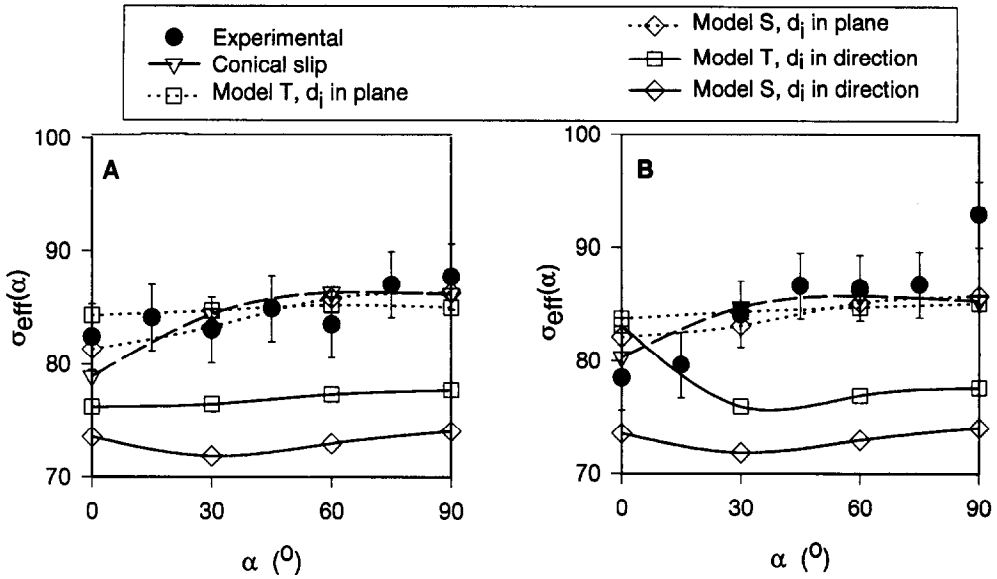

Fig. 10. Comparison of results obtained for materials A and B with the conical slip model and models T and S with d_i measured in the slip plane and the slip direction.

easily be extended to deformation other than by uniaxial tension, whereas models T and S can be used with more complicated deformation geometries.

6. CONCLUSIONS

- Models have been developed for the combined effect on the flow stress anisotropy of (i) dislocation boundaries with a preferential macroscopic orientation; and (ii) texture. These are the Taylor and the Sachs models modified to include an anisotropic critical resolved shear stress from dislocation boundaries, whose contribution to the flow stress is assumed to follow a Petch–Hall relation.
- Model predictions have shown that the presence of dislocation boundaries in idealized configurations has a significant effect on anisotropic yield. This effect of boundaries has been analyzed for changes in the macroscopic orientation and strength of boundaries and for changes in texture. The results show that a high level of anisotropy is to be expected in materials with strong boundaries in a relatively soft matrix material that deforms on few slip systems. Brass and Goss textured samples are predicted to be particularly anisotropic. The exact macroscopic orientation of the boundaries only has secondary influence.
- Model predictions have been compared with the behaviour of cold-rolled (18%) aluminium containing macroscopically oriented dense dislocation walls and microbands (DDW/MBs). The model predictions, in agreement with experiment, show that the flow increases with the angle between the rolling and the tensile direction. The predicted increase can be as high as 18% depending on the number of active slip systems and the choice of the distance parameter in the Petch–Hall relation.

Acknowledgements—The present work is performed under the Danish Materials Technology Development Programme financed by the Danish Agency for Development of Trade and Industry, the Danish Natural Science Research Council and the Danish Technical Research Council. The authors wish to thank Professor J. H. Driver for the source code for his crystal plasticity program.

REFERENCES

1. Sachdev, A. K. and Embury, J. D., *Formability and Metallurgical Structure*. TMS, Warrendale, 1987.
2. Boehler, J.-P. and Khan, A. S., *Anisotropy and Localisation of Plastic Deformation*. Elsevier, Amsterdam, 1991.
3. Hosford, W. F. and Zeisloft, R. H., *Metallurgical Trans.* 1972, **3,** 113.
4. Juul Jensen, D. and Hansen, N., *Acta metall.* 1990, **38,** 1369.
5. Bunge, H. J. and Roberts, W. T., *J. Appl. Crystallography* 1969, **2,** 116.
6. Kallend, J. S. and Davies, G. J., *J. Inst. Metals* 1971, **5,** 257.
7. Lequeu, P. and Jonas, J. J., *Metallurgical Trans. A* 1988, **19A,** 105.
8. Kocks, U. F., Franciosi, P. and Kawai, M., *Textures and Microstructures* 1991, **14–18,** 1103.
9. Bunge, H. J., Wagner, F., Welch, P. I. and Houtte, P. V., *J. Physique Lett.* 1985, **46,** L1109.
10. Wagner, F., Bunge, H. J. and Houtte, P. V., *Proc. of ICOTOM* 8 (edited by J. S. Kallend, *et al.*), 369, 1988.
11. Bate, P., Roberts, W. T. and Wilson, D. V., *Acta metall.* 1981, **29,** 1797.
12. Azari, H. N., Murty, G. S. and Upadhyaya, G. S., *Materials Chemistry and Physics* 1994, **37,** 349.
13. Raphanel, J. L., Schmitt, J.-H. and Baudelet, B., *Proc. of 8th Risø International Symposium on Materials Science* (edited by S. I. Andersen, *et al.*), 491, 1987.
14. Li, F. and Bate, P. S., *Acta metall.* 1991, **39,** 2639.
15. Hansen, N. and Juul Jensen, D., *Acta metall.* 1992, **40,** 3265.
16. Rollett, A. D., Juul Jensen, D. and Stout, M. G., *Proc.*

of 13th Risø International Symposium on Materials Science (edited by S. I. Andersen, *et al.*), 93, 1992.
17. Bate, P. S., *Proc. of 15th Risø International Symposium on Materials Science* (edited by S. I. Andersen, *et al.*), 231, 1994.
18. Kuhlmann-Wilsdorf, D. and Hansen, N., *Scripta metall. mater.* 1991, **25,** 1557.
19. Bay, B., Hansen, N., Hughes, D. A. and Kuhlmann-Wilsdorf, D., *Acta metall.* 1992, **40,** 205.
20. Hansen, N., *Materials Sci. and Technol.* 1990, **6,** 1039.
21. Bay, B., Hansen, N. and Kuhlmann-Wilsdorf, D., *Materials Sci. and Engng A* 1989, **113,** 385.
22. Taylor, G. I., *J. Inst. Metals* 1938, **62,** 307.
23. Sachs, G., *Z. VDI* 1928, **72,** 734.
24. Fortunier, R. and Driver, J. H., *Proc. of IUTAM/ICM Symposium* (edited by J. P. Boehler), 379, 1990.
25. Lücke, K., *Proc. of 6th ICOTOM* (edited by S.-I. Nagashima), 14, 1981.
26. Juul Jensen, D. and Hansen, N., *Strength of Metals* (edited by Oikawa, *et al.*), The Japan Institute of Metals, 1994.
27. Hughes, D. A., *Proc. of 16th Risø International Symposium on Materials Science* (edited by N. Hansen, *et al.*), 63, 1995.
28. Liu, Q. and Hansen, N., *Scripta metall. mater.* 1995, **32,** 1289.
29. Kocks, U. F., Kallend, J. S. and Biondo, A. C., *Textures and Microstructures* 1991, **14–18,** 199.
30. Kallend, J. S., Kocks, U. F., Rollett, A. D. and Wenk, H.-R., *Materials Sci. and Engng* 1991, **A132,** 1.

APPENDIX

The program described in Ref. [24] calculates the work needed to apply a given strain to a single crystal through slip on $\{111\}\langle 011\rangle$ systems. The number of imposed strain components determines the number of active slip systems so that five imposed strain components give the Taylor solution and one imposed component gives the Sachs solution. The unimposed strain components are allowed to take any value which minimizes the work.

The critical resolved shear stress in equation (1) has been introduced into this program with calculation of the distance d_i between DDW/MBs given by either equation (2) or (3).

In order to model the behaviour of a polycrystal, the program is modified to take a number of discrete grains which represent the texture of the material as input. The calculated flow stress for these individual grains is then averaged while taking their volume fractions into account. The input consists of 1152 grains distributed on a lattice in Kocks' Euler space [29]. For non-random textures the volume fractions of the grains have been adjusted to represent the desired texture by means of the popLA programming package [30] from experimental pole figures.

The lattice in Kocks' Euler space was originally constructed with the assumption of cubic crystal and monoclinic sample symmetry [29], i.e. it is assumed that deformation of each grain is indifferent to inversion of the normal direction of the sample. The number of grain orientations considered is, therefore, only half of what is needed in the absence of this symmetry element. However, rotating the tensile direction α° around the normal direction removes this symmetry element. This also applies when DDW/MBs with a specific orientation to the sample axes are introduced. To correct for the missing symmetry element, an additional calculation has been made for each grain where the grain was transformed from the orientation $(hkl)\ [uvw]$ to $(-h\ \ -k\ \ -l)\ [uvw]$ and the orientation of the DDW/MBs with respect to the sample axes was kept constant.

Each grain is rotated α° around the normal direction before application of the simulated tensile strain.

For the Taylor model, results have been calculated with different values of the parameter q in the strain tensor;

$$\epsilon = \begin{bmatrix} 1 & 0 & 0 \\ 0 & -q & 0 \\ 0 & 0 & -(1-q) \end{bmatrix}. \tag{A1}$$

It is assumed that the value of the q parameter which occurs in free uniaxial tension is the one which gives minimum work per unit volume. This work has therefore been taken as the flow stress.

The strain tensor for the Sachs model was

$$\epsilon = \begin{bmatrix} ? & ? & ? \\ ? & ? & ? \\ ? & ? & 1 \end{bmatrix}, \tag{A2}$$

where ? signifies an unimposed strain component. As only one strain component is imposed, only one slip system is active. Due to ease of implementation the tensile axis was not in the x-direction but in the z-direction so all grains had to be rotated to interchange these two directions before application of the simulated strain.

A8: Effect of grain orientation dependent microstructures on flow stress anisotropy modelling by G. Winther, Scripta Materialia, 2005

Available online at www.sciencedirect.com
SCIENCE DIRECT®
Scripta Materialia 52 (2005) 995–1000
Scripta MATERIALIA
www.actamat-journals.com

Effect of grain orientation dependent microstructures on flow stress anisotropy modelling

Grethe Winther *

Center for Fundamental Research, Metal Structures in Four Dimensions, Materials Research Department, P.O. Box 49, Risø National Laboratory, DK4000 Roskilde, Denmark

Received 14 September 2004; received in revised form 14 January 2005; accepted 20 January 2005

Abstract

The effect of introducing dislocation boundaries on crystallographic planes dependent on the grain orientation into the modelling of flow stress anisotropy of a rolled sheet is investigated. Use of grain orientation dependent boundary planes and constants derived from microstructural data gives good agreement with experimental data.

Keywords: Dislocation boundaries; Texture; Strain path change; Modelling; Aluminium

1. Introduction

Many metal properties important for industrial processing, including flow stress anisotropy of rolled sheets, depend on the anisotropic microstructure of the metal. Such anisotropic microstructures encompass crystallographic texture [1], grain shape [2], the shape and spatial distribution of particles [3] as well as deformation-induced dislocation boundaries [4–6]. This paper concentrates on the combined effects of texture and dislocation boundaries on the flow stress immediately after a strain path change.

The effect of texture is generally well predicted by polycrystal plasticity models [1]. The dislocation structure typical for monotonically cold-deformed metals of intermediate to high stacking fault energy consists of almost parallel extended planar dislocation boundaries (often termed 'geometrically necessary boundaries') which subdivide the grains on a micrometer scale. In between these, randomly oriented cell boundaries ('incidental dislocation boundaries') occur. The parallelism of the extended planar dislocation boundaries makes them a source of mechanical anisotropy. The effect of extended planar dislocation boundaries has been suggested to be somewhat analogous to the effect of grain boundaries and their contribution to the flow stress anisotropy was quite successfully calculated based on a Hall–Petch relation [7]. At first, the effects of the texture and the dislocation boundaries both calculated at the bulk level were simply added [7]. Subsequently, the model was refined to combine the two effects at the grain level by introducing anisotropic critical resolved shear stresses given by a Hall–Petch type relation into traditional polycrystal plasticity models [8,9].

Generally, extended planar dislocation boundaries align with certain macroscopic planes close to the most stressed sample planes, i.e. for rolling the planes inclined about 45° to the rolling direction in the longitudinal sample plane and perpendicular to the rolling direction in the rolling plane. It is, however, also clear from many studies that the boundary plane depends on the crystallographic orientation of the grain.

* Tel.: +45 46 77 57 92; fax: +45 46 77 57 58.
E-mail address: grethe.winther@risoe.dk

1359-6462/$ - see front matter
doi:10.1016/j.scriptamat.2005.01.029

Modelling of the effect of dislocation boundaries on the flow stress anisotropy in rolled aluminium has previously been based on the general macroscopic alignment of the boundaries. The aim of the present paper is to investigate the effect of using grain orientation dependent boundary planes. The first section of the paper briefly reviews the knowledge of grain orientation dependent boundary planes, subsequently the model approach used is outlined and a number of calculations on hypothetical cases are carried out to illustrate the effect of using grain orientation dependent boundary planes. Finally improvements compared to previous work are demonstrated by applying the model to experimental data and the results are discussed.

2. Grain orientation dependent boundary planes

The planes of extended planar dislocation boundaries may be determined by transmission electron microscopy as described in Refs. [10,11]. An extensive study [12] has been carried out for rolled aluminium, resulting in separation of the measured grain orientations into two groups, namely those with boundaries aligning with slip planes, i.e. within about 5° of a slip plane, and those with boundaries on other planes, which were not characterised further. In particular, it is found that grains near the Brass [11] and Goss [12] orientations formed two sets of slip-plane-aligned boundaries. In most cases, however, one of the two sets was more clearly developed than the other. Results from tensile deformation show that also boundaries which lie far from a slip plane lie on crystallographic planes which depend on the grain orientation [13]. Detailed characterisation of the boundaries not aligned with any slip plane has not been carried out yet. Boundaries aligned with the slip direction have been found in rolled single crystals of Cube [14] and Copper [15] orientations but it is still undetermined if this is a general phenomenon.

In order to calculate the flow stress anisotropy caused by the extended planar dislocation boundaries, one should know the boundary plane of all grain orientations. Ideally, these should be predicted based on the predeformation as originally suggested in Refs. [16,17]. The present status of the boundary plane prediction is that grain orientations which form boundaries aligned with slip planes are fairly well predicted as the grain orientations where most of the slip is concentrated on one slip plane [18]. The boundaries align with this highly active slip plane.

Concerning the boundaries not aligned with any slip plane, the modelling in this paper is based on the well-established facts, that (i) the boundaries not aligned with any slip plane cluster around the macroscopically most stressed planes and (ii) that within a grain the dominant boundaries are typically inclined either positively or negatively to the rolling plane.

3. Modelling approach

The model used to predict the flow stress anisotropy is the model proposed in Ref. [9] and outlined here. It is based on the full constraints Taylor model which has been extended to include anisotropic critical resolved shear stresses given by the relative orientation of the slip system and the plane of the dislocation boundaries. The critical resolved shear stress, $\tau_{\mathrm{crss},i}$ of the i th system is given as

$$\tau_{\mathrm{crss},i} = \tau_0 + x \cdot K^{-\frac{1}{2}} \cdot d_i^{-\frac{1}{2}}, \tag{1}$$

where τ_0 is the isotropic part, x characterises the resistance to slip offered by the boundaries and K is the boundary spacing measured perpendicular to the boundary plane. τ_0, x and K are assumed common to all slip systems. d_i is a geometric factor which accounts for the difference between the perpendicular boundary spacing K and the distance between boundaries calculated in the slip direction for the i th system, $u_{\mathrm{sd},i}$, as

$$d_i = \frac{1}{|u_{\mathrm{sd},i} \cdot n|}. \tag{2}$$

In Eq. (2), n is the boundary plane normal.

For each grain the critical resolved shear stress for each of the $\{1\,1\,1\}\langle 1\,1\,0\rangle$ slip systems is calculated from the predicted boundary plane normal and the grain orientation using Eqs. (1) and (2). These critical resolved shear stresses are then used instead of the conventional isotropic value in the Taylor model to calculate the flow stress. In these calculations the contraction ratio, i.e. the ratio of the strain components perpendicular to the tensile direction, is varied and the final value selected is the one giving the lowest flow stress for the bulk sample. Calculations are made for different angles between the tensile direction and the rolling direction, ranging from tension parallel to the rolling direction to tension perpendicular to the rolling direction. The texture of the material is introduced by assigning appropriate weights to 1152 individual grains covering the orientation space relevant for rolling.

4. Effect of grain orientation dependent boundary planes

Two series of calculations are made to investigate the effect of including grain orientation dependent boundary planes in the prediction of flow stress anisotropy. All of these calculations are made for hypothetical textures derived from a random texture. The texture used in the first series has a constant intensity for all grain orienta-

tions which are predicted to have boundaries aligned with highly active slip planes using the model proposed in Ref. [18]. The intensity of all other grain orientations is zero. This hypothetical texture termed A is used to focus on the effect of slip plane alignment. The hypothetical texture used for the second series has a constant intensity for all grains not predicted to have slip-plane-aligned boundaries and zero intensity everywhere else. This texture termed B is used to illustrate the importance of the sign of the inclination between boundary plane and rolling plane while still assuming that all boundaries lie on the macroscopically most stressed planes, i.e. are inclined 45° to the rolling plane. The detailed ODF showing the division of a random texture into the hypothetical textures A and B may be found in Ref. [18]. About 60% of the grains in a randomly textured sample belong to texture A. In both the first and second series of calculations the flow stress values are normalised to the value predicted for the case where the tensile direction is parallel to the rolling direction ($\alpha = 0°$). The parameters τ_0, x and K are arbitrarily set to 1 MPa, 1 MPa $\mu m^{1/2}$ and 1 μm, respectively.

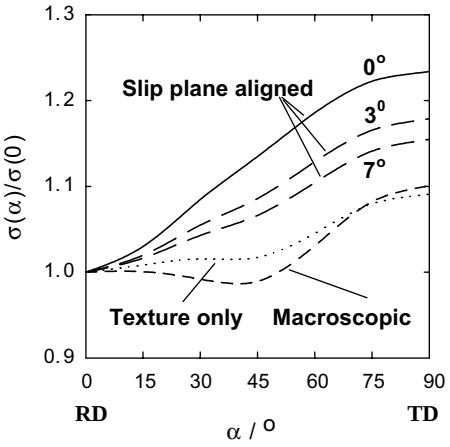

Fig. 1. Simulations for texture A of the normalised flow stress of a rolled sheet tested in tension with different angles, α, between tensile axis and the rolling direction, going from tension along RD ($\alpha = 0°$) to tension along TD ($\alpha = 90°$). The dotted and short dashed lines assumes no boundaries and all boundaries on the macroscopically most stressed planes, respectively. The three curves labelled 'slip plane aligned' assumes boundaries on (solid line) or slightly deviating from the slip plane (long dashes).

4.1. Slip plane alignment (texture A)

At first, two reference calculations are made illustrating the anisotropy predicted (i) from texture A alone, i.e. without any boundaries, and (ii) with an additional contribution from boundaries on the macroscopically most stressed planes. Here half of the boundaries in each grain are inclined +45° to the rolling plane while the other half of the boundaries are inclined −45°. The two sets of boundaries are not intersecting, meaning that the contribution from each set is calculated independently using Eqs. (1) and (2). The boundaries are thus the same in all grains, i.e. no grain orientation dependence is assumed. These two predictions are shown in Fig. 1 as the dotted and dashed line, respectively. They do not deviate much from each other.

The results of introducing grain orientation dependent dislocation structures in the form of slip-plane-aligned boundaries are also presented in Fig. 1. The solid line is the anisotropy for the case where the boundaries coincide exactly with the slip plane, which is seen to give a very big effect. It is, however, known from many studies that the boundaries rarely or never coincide exactly with the slip plane. They always deviate a few degrees, even in single crystals oriented for single slip [19]. Calculations have therefore been carried out for cases where the boundaries are tilted 3° and 7° away from the slip plane. The tilted boundaries lie on the plane with the same trace as the slip plane in the rolling plane of the sample but their trace deviates from the slip plane trace in the longitudinal sample plane. The effect of the small misalignment is to decrease the anisotropy somewhat as seen from the dashed lines. Still, even with this more realistic interpretation of the term 'slip-plane-aligned boundaries', the predicted anisotropy is significantly larger than the very small effect when only macroscopic alignment of the boundaries is considered.

4.2. Inclination angle of not-slip-plane-aligned boundaries (texture B)

For texture B representing the grains which do not form slip-plane-aligned boundaries, the exact plane of the boundaries is not known in general. The obvious choice is therefore to assume that the boundaries lie on the macroscopically most stressed planes. Assuming that a grain only has one set of such boundaries the effect of the sign of the inclination of the boundary to the rolling plane is investigated in Fig. 2. In analogy with the calculations in Section 4.1 the prediction based on texture B alone is included in the figure as the dotted line. The two solid lines show the effects of selecting the inclination in each grain orientation giving the larger or smaller effect, respectively. These curves thus represent the bounds on the flow stress predicted based on macroscopically oriented boundary planes. It is seen that one of the bounds practically coincides with the purely texture based prediction, i.e. the boundaries do not contribute to the anisotropy of the bulk sample although the effect on individual grains may be larger. The other bound shows a slightly smaller flow stress perpendicular to the rolling direction than parallel to this. It has previously been established that use of another inclination angle between boundary plane and rolling plane than 45° for all grains does not alter the prediction significantly [9]. The difference between flow stress

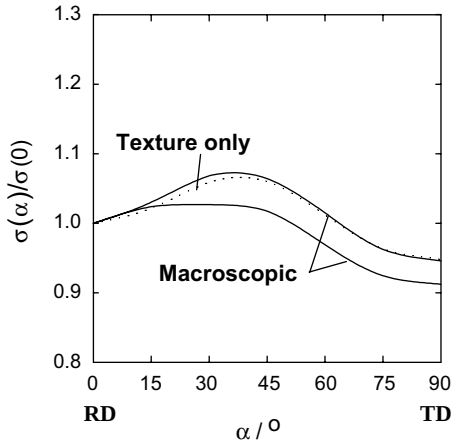

Fig. 2. Simulations for texture B of the normalised flow stress of a rolled sheet tested in tension with different angles, α, between tensile axis and the rolling direction. The dotted line assumes no boundaries. The two solid lines indicate the bounds on the anisotropy obtainable using boundaries on macroscopically most stressed planes inclined positively or negatively to the rolling plane (see text).

predictions using the two options for boundary planes in grains belonging to texture B is therefore relatively small.

4.3. Best available grain orientation dependent boundary planes

Based on the calculations above it is decided that the best available prediction of grain orientation dependent boundary planes is to assume that all the grains belonging to texture A have boundaries aligned with a highly active slip plane but tilted 3° away from this. This tilt angle is selected because boundaries within about 5° of the slip plane have been classified as slip-plane-aligned [12]. The grains belonging to texture B with boundaries not aligned with slip planes are assumed to have boundaries on the macroscopically most stressed planes with half of the boundaries inclined +45° to the rolling plane while the other half is inclined −45°. The latter is contradictory to the fact that typically only one set dominates within a grain but it gives an effect in between the two bounds established in Fig. 2.

Prediction of the boundary plane is based on the immediate grain orientation, i.e. with no consideration of the orientation history of a grain, which may have changed substantially during rolling. This is warranted by the fact that no strain dependence of the boundary plane has been detected in materials tensile deformed or rolled to strains below about 50% [12,20].

5. Comparison with experiment

This section applies the model to an experimentally measured texture and compares the predicted flow stress anisotropy using grain orientation dependent boundary planes to experimental data as well as previous predictions using only macroscopically aligned boundaries. The measured flow stress anisotropy of aluminium (AA 1050) prerolled to a true strain of 0.2, inducing a typical rolling texture and dislocation structure in the material [6] is shown in Fig. 3. The symbols in Fig. 3 indicate the $\sigma_{0.2}$ values for tensile testing in different directions. Previous modelling work using the experimentally determined texture and only macroscopically aligned boundaries, i.e. without grain orientation dependence, gave qualitatively acceptable predictions of the flow stress anisotropy but failed in producing quantitative agreement [9]. The degree of anisotropy was greatly underestimated. Taking the previous model to the extreme by using an infinite value of the ratio $x \cdot K^{-1/2}/\tau_0$ was not able to bring the anisotropy up to the experimentally observed level. This is illustrated in Fig. 3 where the value of τ_0 is set to 0 MPa and $x \cdot K^{-1/2}$ to 41 MPa. This gives good agreement with the predicted flow stress parallel to the rolling direction but not perpendicular to this. The prediction based on the new model using grain orientation dependent dislocation boundary planes as defined above in Section 4.3 and the measured texture is also shown in Fig. 3. The constants in Eq. (1) were $x = 33\ \text{MPa}\,\mu\text{m}^{1/2}$ and $\tau_0 = 20$ MPa [21]. These constants are based on measured microstructural parameters (boundary spacing and misorientation for both extended planar dislocation boundaries and the cell boundaries in between these). The perpendicular boundary spacing, K, was measured to

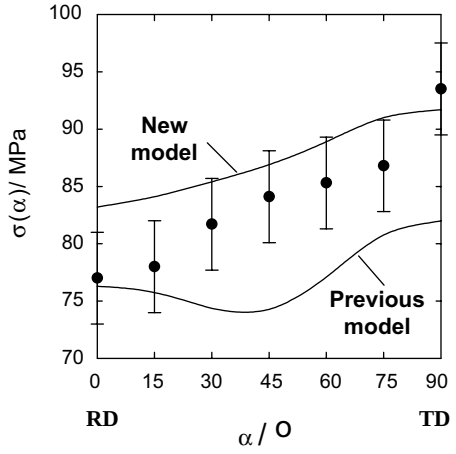

Fig. 3. Experimental data [6] and simulations of the normalised flow stress of an aluminium sheet rolled to a true strain of 0.2 and subsequently tested in tension with different angles, α, between tensile axis and the rolling direction. The line labelled 'new model' shows the result with grain orientation dependent boundary planes and modelling constants derived from measured microstructural parameters. The line labelled 'previous model' shows the best obtainable result based on macroscopically aligned boundaries only, even when allowing completely unrealistic modelling constants.

3 μm [6]. Good quantitative agreement of both the degree of anisotropy and the flow stress level is obtained. The effect of introducing grain orientation dependent boundary planes is thus enormous; not only giving better agreement with experiment but also doing so while using experimentally based modelling constants.

6. Discussion

It is encouraging that the big improvement in the flow stress anisotropy prediction has been made without a detailed experimental map of the dislocation boundary planes in all grain orientations. In other words, the present understanding of the grain orientation dependence is sufficiently advanced to allow predictions of boundary planes of a quality usable for subsequent prediction of material properties. It is discussed below to what extent refinement of our understanding of grain orientation dependent dislocation boundary planes may improve these predictions. This is done by analysing the origin of the effect of introducing slip-plane-aligned boundaries in more detail.

6.1. Effect of slip plane alignment

The origin of the large effect of slip-plane-aligned boundaries lies in the geometric expression of the distance between boundaries seen from the point of view of an individual slip system given by Eq. (2). For boundaries coinciding exactly with the slip plane this equation evaluates to infinity for all slip systems in the slip plane with which the boundaries align, meaning that the boundaries do not contribute to the critical resolved shear stress given by Eq. (1). The resolved shear stress on these systems must, however, still overcome the τ_0 value representing the friction stress and the isotropic contribution from the dislocation cells between the extended planar boundaries. The effect of tilting the boundaries slightly out of the slip plane is to lower the distance given by Eq. (2) from infinity to a finite but still large value. This lowers the anisotropy compared to coincidence with the slip plane but nevertheless still results in high anisotropy as seen in Fig. 1.

It is interesting to note that the increased anisotropy predicted from slip-plane-aligned boundaries arises from a lowering of the flow stress when a significant part of the slip occurs parallel—or roughly parallel—to the boundaries. In the present context this is the case for tension along RD while only very little slip occurs parallel to the boundaries for tension along TD. Introduction of slip-plane-aligned boundaries therefore increases the anisotropy by lowering the flow stress along RD rather than increasing the flow stress along TD.

According to Eq. (2), boundaries aligned with the slip direction but not with the slip plane will have a similar effect. As already mentioned in Section 2 boundaries aligned with the slip direction have been observed in rolled single crystals of special orientations. If it turns out that many of the boundaries not aligned with a slip plane align with the slip direction, the flow stress along RD will be lowered, most likely resulting in even better agreement between prediction and experiment for the data set in Fig. 3.

The suggestion that boundary alignment with slip directions in addition to alignment with slip planes induces large anisotropy is of course heavily based on Eq. (2), which assumes that it is the slip direction that determines the effect of a boundary. This is certainly reasonable if edge dislocations are responsible for the slip. However, screw dislocations move in a direction perpendicular to the slip direction and the distance relevant for them may therefore be in this direction instead.

6.2. Lankford coefficients

Lankford coefficients for rolled aluminium typically show values below 1 for tension along RD and above 1 for tension along TD (see e.g. Ref. [22]). Predictions with the Taylor model based on the rolling texture alone give roughly identical values below 1 in both directions, which is in fairly good agreement with experimental data for a recrystallised aluminium with a typical rolling texture, i.e. in the absence of a deformation-induced dislocation structure [23].

In parallel to the prediction of the flow stress anisotropy presented in Fig. 3, Lankford coefficients were predicted. The values predicted using grain orientation dependent boundary planes differed somewhat from those predicted based on texture alone but also had roughly identical values below 1 along both RD and TD. A very preliminary calculation assuming that many boundaries align with the slip direction, however, produced values considerably below 1 for tension along RD and very close to 1 for tension along TD, following the shape of the experimental curve reported in Ref. [22] for the same alloy at a higher rolling prestrain (50%) fairly well. The importance of this highly uncertain preliminary result should not be exaggerated. Nevertheless, it serves as a further incentive to continue the work on characterisation and understanding of dislocation boundary planes.

7. Conclusion

Using flow stress anisotropy as an example, the dependence of the plane of extended dislocation boundaries on the crystallographic grain orientation has been proven to influence the mechanical properties of the

material. Introduction of grain orientation dependent dislocation boundary planes in a previously proposed model has resulted in great improvements of the prediction for aluminium, with constants derived from experimentally determined microstructural parameters.

Acknowledgements

The author wishes to thank Dr Niels Hansen for scientific discussions. She also gratefully acknowledges the Danish National Research Foundation for supporting the Center for Fundamental Research: Metal Structures in Four Dimensions, within which this work was performed.

References

[1] Kocks UF, Tomé CN, Wenk H-R. Texture and anisotropy: preferred orientations in polycrystals and their effect on materials properties. Cambridge: Cambridge University Press; 1998. p. 375–6.
[2] Bunge HJ, Wagner F, Welch PI, Houtte PV. J Phys Lett 1985; 46:L1109–13.
[3] Hosford WF, Zeisloft RH. Metall Trans 1972;3:113–21.
[4] Li F, Bate PS. Acta Metall 1991;39:2639–50.
[5] Eardley ES, Coulet A, Court SA, Humphreys F, Bate P. Mater Sci For 2003;426–432:363–8.
[6] Juul Jensen D, Hansen N. Acta Metall Mater 1990;38:1369–80.
[7] Hansen N, Juul Jensen D. Acta Metall Mater 1992;40:3265–75.
[8] Rollett AD, Juul Jensen D, Stout MG. In: Proc of 13th Risø Symp, Denmark; 1992. p. 93–109.
[9] Winther G, Juul Jensen D, Hansen N. Acta Mater 1997;45:2455–65.
[10] Huang X, Liu Q. Ultramicroscopy 1998;74:123–30.
[11] Winther G, Huang X, Godfrey A, Hansen N. Acta Mater 2004;52:4437–46.
[12] Liu Q, Juul Jensen D, Hansen N. Acta Mater 1998;46:5819–38.
[13] Winther G, Huang X, Hansen N. Acta Mater 2000;48:2187–98.
[14] Liu Q, Hansen N. Proc R Soc A 1998;454:2555–91.
[15] Godfrey A, Juul Jensen D, Hansen N. Acta Mater 1998;46:835–48.
[16] Winther G. In: Proc of 19th Risø Symp, Risø, Denmark; 1998. p. 185–99.
[17] Winther G. In: Proc of ICOTOM 12, Montreal; 1999. p. 387–92.
[18] Winther G. Acta Mater 2003;51:417–29.
[19] Steeds JW. Proc R Soc A 1966;292:343–73.
[20] Huang X, Hansen N. Scr Mater 1997;37:1–7.
[21] Hansen N. Mat Sci Eng A., to be published.
[22] Takahashi H, Motohashi H, Tsuchida S. Int J Plast 1996;12:935–49.
[23] Peyrac C, Penelle R. In: Proc of ICOTOM 8; 1988. p. 977–83.

A9: Lattice rotations of individual bulk grains Part II: correlation with initial orientation and model comparison by G. Winther, L. Margulies, S. Schmidt and HF. Poulsen, Acta Materialia, 2004

Available online at www.sciencedirect.com
SCIENCE DIRECT®
Acta Materialia 52 (2004) 2863–2872
Acta MATERIALIA
www.actamat-journals.com

Lattice rotations of individual bulk grains Part II: correlation with initial orientation and model comparison

G. Winther [a,*], L. Margulies [a,b], S. Schmidt [a], H.F. Poulsen [a]

[a] *Center for Fundamental Research: Metal Structures in 4D, Materials Research Department, Risø National Laboratory, P.O. Box 49, DK-4000 Roskilde, Denmark*
[b] *European Synchrotron Radiation Facility, BP220, F-38043 Grenoble Cedex, France*

Received 30 September 2003; received in revised form 25 February 2004; accepted 26 February 2004
Available online 12 April 2004

Abstract

The lattice rotations of 95 individual bulk grains during 6% tensile elongation of aluminium have been analysed for correlations between the initial grain orientation and the rotation behaviour. Four distinct regions in orientation space with different rotation behaviour have been identified. The analysis shows that the grain orientation is the main factor controlling the rotations. Some variation within each region shows that other factors have a secondary effect, also depending on the grain orientation. The Taylor model using the solution to the ambiguity problem which maximises primary slip predicts the overall rotations reasonably well in some of the regions, however large discrepancies occur, especially in the ⟨1 0 0⟩ corner and in the middle of the stereographic triangle. Self-consistent modelling predicted the observed large variation in the ⟨1 0 0⟩ corner but did not predict the correct rotation directions.

Keywords: Plastic deformation; Aluminium; Texture; Modelling; Grain orientation dependence

1. Introduction

Polycrystal plasticity models are routinely employed to predict deformation textures. Conceptually very different models have been devised [1–6]. Their main difference lies in the assumed relative importance of the initial crystallographic grain orientation and grain interaction for slip and lattice rotation of individual grains. In spite of the wide application of polycrystal plasticity models, problems concerning both the orientation of the stable texture components and the evolving intensity of these still remain unsolved. To identify the modelling approach closest to physical reality, data on the lattice rotation of individual grains are needed.

The 3DXRD microscope developed by Risø and the European Synchrotron Radiation Facility has made studies of the behaviour of individual grains deeply embedded in the bulk of the material possible by use of high energy X-ray diffraction. Part I of this paper [7] presents the experimental procedures and the lattice rotation of 95 individual grains during tensile testing of polycrystalline aluminium with a grain size of 75 μm to a strain of 6%. This is the first comprehensive data set on the full rotation of individual grains, measured under conditions which undoubtedly are representative of bulk deformation. In Part I, it was concluded that the rotations exhibit orientation dependence and this is the basis for the present analysis, which aims at identifying quantitative correlations between crystallographic grain orientation and rotation path.

Since a strong grain orientation dependence is observed, the analysis includes comparison with the classical purely orientation-based predictions by Sachs [1] and Taylor [2]. Comparison with a prediction from a self-consistent model is also included with the emphasis on the observed experimental scatter of the rotation paths for grains with comparable orientations.

* Corresponding author. Tel.: +45-46-77-57-92; fax: +45-46-77-57-58.
E-mail address: grethe.winther@risoe.dk (G. Winther).

1359-6454/$30.00 © 2004 Acta Materialia Inc. Published by Elsevier Ltd. All rights reserved.
doi:10.1016/j.actamat.2004.02.045

2. Correlation with grain orientation

In uniaxial tension the crystallographic orientation of a grain is often only designated by the tensile direction. In the following analysis of the experimentally measured lattice rotations, rotation of the tensile direction is therefore first considered. Correlations between this rotation and the tensile direction are established, leading to division of the stereographic triangle into different regions with different main rotation trends. Rotation axes and angles are then further analysed to quantify the variation within each region.

2.1. Division of the stereographic triangle

Careful visual inspection of the stereographic triangle in Fig. 1 showing the rotation of the tensile direction for all grains revealed that it can be divided into four regions exhibiting different rotation trends:

- Grains in the ⟨1 1 0⟩ corner rotate towards the ⟨1 0 0⟩–⟨1 1 1⟩ line (region 1).
- Grains at the ⟨1 0 0⟩–⟨1 1 1⟩ line rotate along this line towards the ⟨1 1 1⟩ corner (region 2).
- Grains half way up the ⟨1 1 0⟩–⟨1 1 1⟩ line, i.e., close to ⟨2 2 1⟩, rotate directly towards the ⟨1 1 1⟩ corner (region 3).
- Grains in the ⟨1 0 0⟩ corner of the triangle rotate in widely different directions (region 4).

Simplicity and reproducibility of the separation of the regions was considered essential for its use in model evaluation. These criteria are fulfilled by basing the division on the relationship between the initial orientation and the distance from specific points in the triangle. In the division shown in Fig. 1, region 4 covers all orientations within 24.2° of ⟨1 0 0⟩, region 3 covers orientations within 8.0° of ⟨2 2 1⟩, region 1 covers remaining orientations within 24.0° of ⟨1 1 0⟩ and region 2 covers the rest of the triangle.

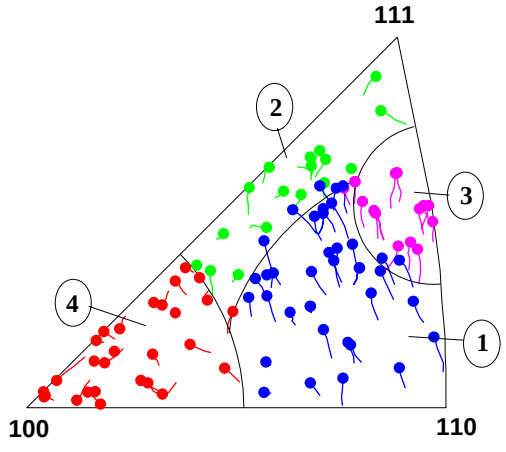

Fig. 1. Stereographic triangle showing the rotation of the tensile direction as lines. The symbols mark the final orientation of the tensile direction. The triangle is divided into regions (labelled 1–4 and with different colours) with different rotation behaviour. The line defining a region is drawn at a certain distance from a reference point as described in the text. The initial orientation of a grain determines the region to which the grain belongs.

Near the ⟨1 1 1⟩ corner the number of measured grains is too small to determine a general trend. The grain closest to ⟨1 1 1⟩ at the ⟨1 0 0⟩–⟨1 1 1⟩ line, however, indicates extension of region 2 with continued rotation along this line towards ⟨1 1 1⟩. The grain closer to the ⟨1 1 0⟩–⟨1 1 1⟩ line in the vicinity of ⟨1 1 1⟩ has a different rotation behaviour but it is impossible from data on one grain to conclude the possible existence of a fifth region. In the present paper the ⟨1 1 1⟩ corner is regarded as belonging to region 2. It should also be noted that the upper part of region 3 as defined by the distance to ⟨2 2 1⟩ covers a part of the triangle with no data points.

2.2. Quantitative analysis

The division presented in Fig. 1 was mainly derived based on visual inspection. In this section, the rotations are analysed quantitatively: the rotations are presented in terms of rotation axes and angles, the variation within each region is investigated, and finally the transition between regions are analysed. Per definition the rotation angle of the tensile direction is regarded positive. The rotation direction is given by the sign of the rotation axis so that rotations are always clockwise when looking along the axis. In contrast, the axis of rotation around the tensile direction is always taken equal to the tensile direction, meaning that positive and negative values of the rotation angles in this case designate clockwise and counter clockwise rotations, respectively.

The crystallographic axis around which the tensile direction of each grain rotates from the undeformed state to a strain of 6% is shown in the inverse pole figure in Fig. 2 where the same colouring scheme as in Fig. 1 is employed to indicate the orientation of the tensile direction. The triangle containing the tensile direction is also indicated in the figure. Note that the axis around which the tensile direction rotates must be perpendicular to the tensile direction. It is therefore confined to the band indicated in Fig. 2.

Fig. 3 shows the distribution of the angle of rotation of the tensile direction for each of the four regions. It is seen that on average grains in regions 1 and 3, i.e., grains closest to the ⟨1 1 0⟩–⟨1 1 1⟩ line, rotate about 1° more than those in regions 2 and 4. It is also clear that the smallest variation in the rotation angles is found in region 3. However, more than two thirds of the grains in region 1 also lie in the range spanned by region 3. The distribution in region 2 is rather flat while the distribution for region 4 is bimodal with about a third of the grains (8) rotating very little (<0.5°) and a second peak

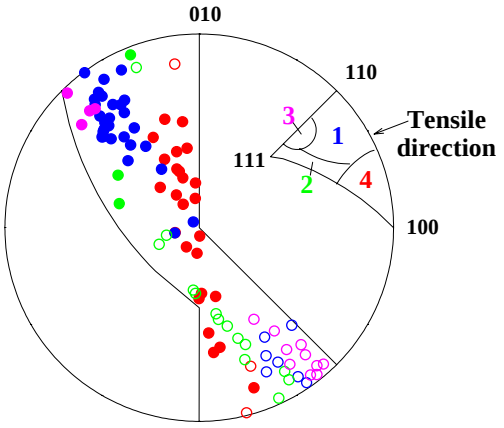

Fig. 2. Inverse pole figure showing the component of the rotation axis, which corresponds to rotation of the tensile direction. These components are perpendicular to the tensile direction and therefore lie within the indicated band. The colours refer to the crystallographic orientation of the grain in terms of the regions given in Fig. 1 and also sketched in the triangle showing the tensile direction in this figure. Filled symbols refer to rotation axes on the upper half of the unit sphere while open symbols represent axes on the lower half, and all rotations are clockwise.

containing a comparable number of grains (10) rotating about 2°.

Fig. 4 shows distributions of the angles for the rotation around the tensile direction for each region. The sign of this angle is selected so that positive angles correspond to rotations clockwise around the tensile direction when looking in the direction of the axis. All regions have both positive and negative angles. The rotation around the tensile direction is generally significantly smaller than the rotation of the tensile direction although the opposite is the case for a few grains. No relation was found between the rotation angles for the tensile direction and the magnitude or direction of the rotation around the tensile axis. In Part I [7] it was demonstrated that positive rotations mainly occur along the edges of the stereographic triangle. In view of the smaller magnitude and the apparent largely random character of the rotation around the tensile axis, the analysis is restricted to the rotation of the tensile direction.

2.2.1. Variation within each region

The variation within each region is further analysed for potential systematic trends, which may indicate that the region should be split in two. For this analysis, each region is further subdivided into two or three parts with different distances to the reference points on which the original division is based. For region 2, no reference point is defined so this region is instead divided into a lower and an upper part, each containing about half of the data points of the original region. The subregions are shown in Fig. 5. The analysis concentrates on the rotation axis rather than the angle because grains with

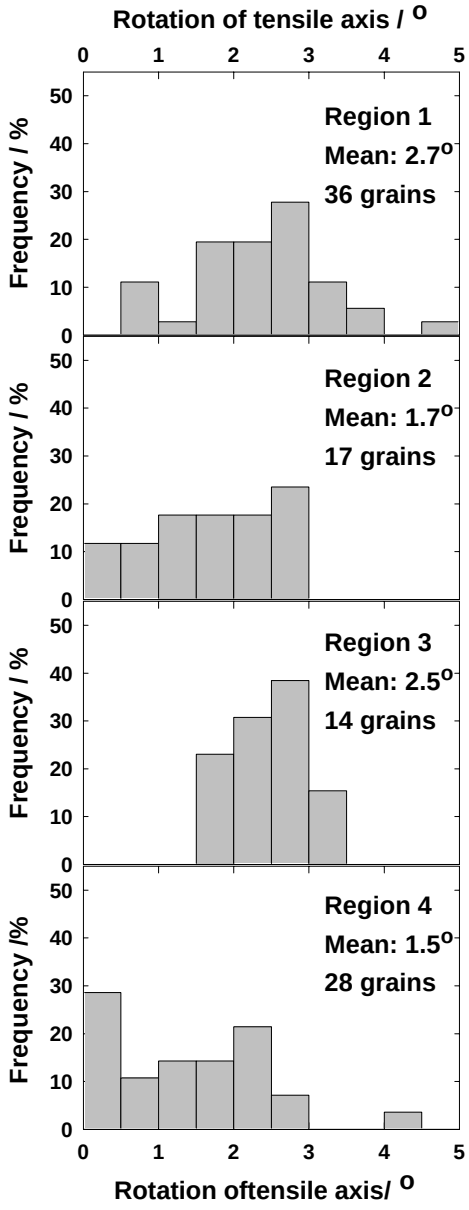

Fig. 3. Distribution of angles for rotation of the tensile direction in each of the regions in Fig. 1.

comparable orientations slipping on widely different slip systems are more likely to have very different rotation axes than rotation angles. As an estimate of whether the variation in rotation axes between grains of relatively close orientation reflect activation of significantly different slip systems, the angle between their rotation axes may be compared to the angle between the tensile directions. If the former significantly exceeds the latter, different slip systems must operate in the two grains. For each of the subregions in Fig. 5, the mean rotation axis is listed in Table 1 and also shown in Fig. 6. To estimate if the variation in rotation axes reflects large changes in the set of active slip systems, the mean deviation angles between the individual rotation axes and the mean axis

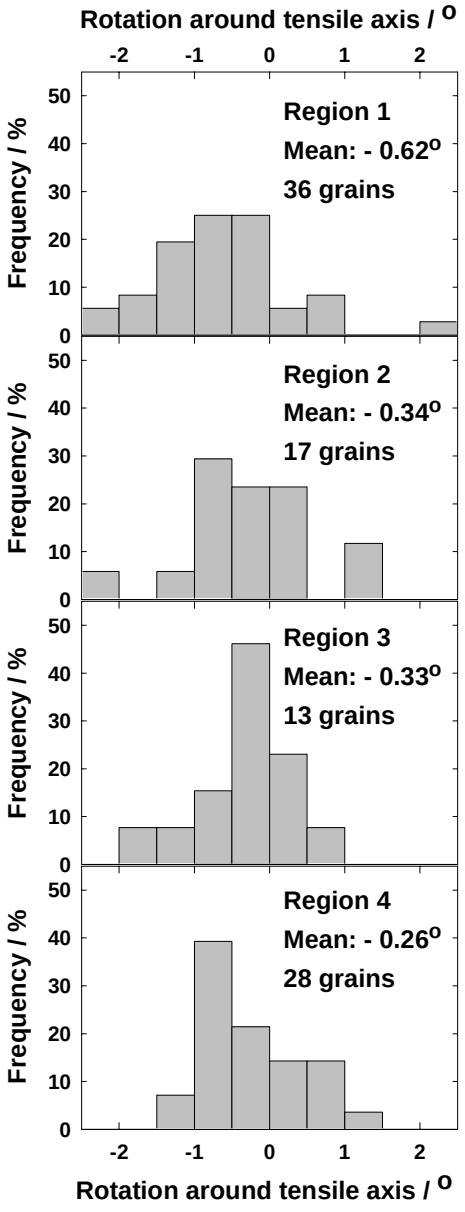

Fig. 4. Distribution of angles of rotation around the tensile direction for each of the regions in Fig. 1. Positive angles correspond to clockwise rotation when looking in the direction of the axis.

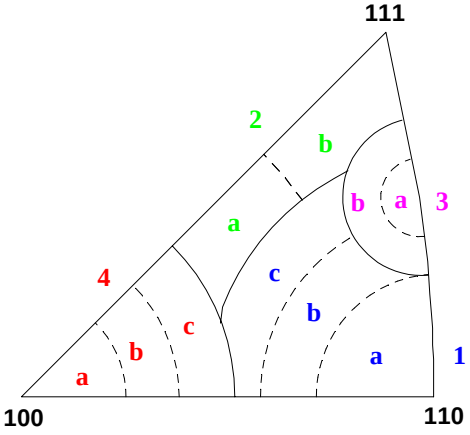

Fig. 5. Stereographic triangle showing how the regions from Fig. 1 are divided into subregions to analyse the variation within each region.

as well as the mean deviation of the corresponding tensile directions from the mean tensile direction in each subregion are also listed.

The mean rotation axes for region 1 exhibit a tendency for moving horizontally to the right in the inverse pole figure with increasing distance of the tensile axes from ⟨1 1 0⟩, i.e., in the direction expected when taking into account that the rotation axis must be perpendicular to the tensile direction. Also the magnitude of this horizontal variation (10° as calculated from the data in Table 1) is in agreement with that of the mean tensile direction (12°). The fact that the mean deviation of the rotation axis increases with the distance from ⟨1 1 0⟩ may partly be attributed to the larger variation in tensile direction with the distance of the subregion from ⟨1 1 0⟩ and is not considered significant. It is of more significance that the variation in rotation axis clearly exceeds the variation of the tensile direction. Nevertheless, both rotation axes and rotation angles exhibit the same main trends throughout the region.

For region 3, the angle between the mean rotation axes for the two subregions is very small, corresponding to the small range of tensile directions covered by this region. Again the variation in mean rotation axes exceeds that of the tensile direction but this variation is on the same order throughout the region. Noting that this region also has by far the narrowest distribution of rotation angles for the tensile direction (see Fig. 3), it is concluded that this region is very homogenous.

For region 4, it is seen that the variation from the mean rotation axes is large for all subregions. Remembering that the distribution of rotation angles for the tensile direction is bimodal with a peak below 0.5° and that the estimated precision of a single orientation measurement is 0.3° [7], the rotation axes are replotted in Fig. 7 but this time grains with rotations of the tensile axis less than 0.5° are excluded (Note that the only rotation axis lying on the upper half of the sphere (open symbol) is for the grain at the triple point between regions 1, 2 and 4). Two clusters of rotation axes (labelled 4I and 4II) now emerge with the mean rotation axes listed in Table 2. The two mean axes are inclined 94° to each other. The mean deviation from the mean axis of each cluster is on the same order as for region 1. With respect to rotation angles, the tensile direction of grains in cluster 4I rotates less than in cluster 4II (mean values of 1.72° and 2.24°, respectively). Taking the mean of the two mean rotations gives a resulting rotation of about 1.4° around an axis lying close to the centre of the inverse pole figure. Comparison of Figs. 2 and 7 shows that three of the eight grains with the tensile axis ro-

Table 1
Parameters calculated for each subregion defined in Fig. 5. The mean axis for rotation of the tensile direction is plotted in Fig. 6

Subregion of Fig. 5	Mean axis for rotation of tensile direction (Miller indices)	Mean deviation from mean rotation axis (°)	Mean rotation angle of the tensile direction (°)	Mean deviation from mean tensile direction (°)
1a	[0.64;−0.74;−0.19]	12.2	2.6	4.8
1b	[0.58;−0.76;−0.30]	17.0	2.16	5.8
1c	[0.55;−0.78;−0.29]	20.0	2.40	6.2
2a	[0.16;−0.80;0.57][a]	40.6[a]	1.78[a]	5.0
2b	[0.38;−0.84;0.38][a]	31.4[a]	2.04[a]	3.8
3a	[0.65;−0.75;0.12]	10.8	2.40	2.2
3b	[0.63;−0.77;0.09]	10.8	2.50	3.0
4a	[0.06;−0.03;−1.00]	37.4	1.22	3.4
4b	[0.11;−0.08;−0.99]	44.0	1.92	3.4
4c	[0.34;−0.63;−0.70]	50.8	1.38	3.8

[a] After exclusion of a grain with tensile rotation less than 0.5.

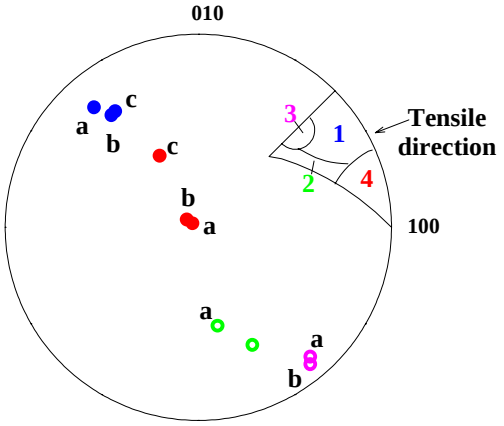

Fig. 6. Inverse pole figure showing the mean axis for rotation of the tensile direction. The mean axes are calculated for the different subregions shown in Fig. 5. Filled symbols refer to rotation axes on the lower half of the unit sphere while open symbols represent axes on the upper half, and all rotations are clockwise. Symbol colours mark the region as sketched in the triangle.

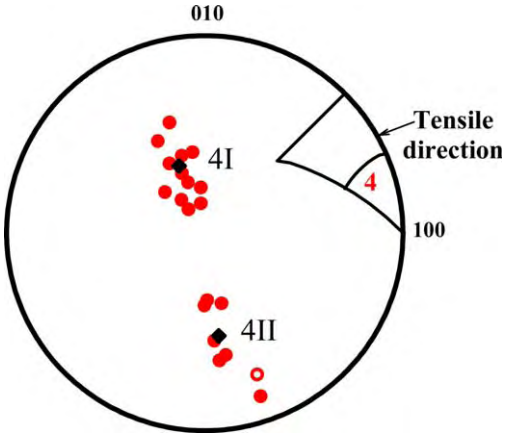

Fig. 7. Inverse pole figure showing the component of the rotation axis which corresponds to rotation of the tensile direction for grains in region 4. Grains where the tensile direction rotates less than 0.5° are excluded. Mean axes for the two clusters are shown as black diamonds. Filled symbols refer to rotation axes on the upper half of the unit sphere while open symbols represent axes on the lower half.

Table 2
Parameters calculated for the two clusters of rotation axis for region 4 seen in Fig. 7

	Mean axis for rotation of tensile direction	Mean deviation from mean rotation axis (°)	Mean rotation angle of the tensile direction (°)
4I	[0.23;−0.60;−0.77]	18.0	1.72
4II	[−0.12;0.81;−0.57]	14.6	2.24

tating less than 0.5° have rotation axes in this area. However, their rotation angles are only on the order of a third of the expected mean value. It is therefore unlikely although not impossible that the small rotations of the tensile axis reflect a linear combination of the rotations designated 4I and 4II, i.e., a third group of grains with a very small rotation of the tensile direction probably exists in this region. The rotations 4I and 4II are found in all of the three subregions whereas the practically non-rotating tensile directions are only observed in subregions 4a and 4c.

In the analysis of region 2, two grains with rotations of the tensile direction less than 0.5° are excluded from the analysis. However, the difference in mean rotation axes for the subregions 2a and 2b is still large as seen in Fig. 6. Quantitatively, the mean rotation axes lie 18° apart while the difference in mean tensile directions is smaller (13°). Furthermore, the mean deviation from the mean rotation axes listed in Table 1 for each subregion is large. The variation in the rotation angle of the tensile direction was investigated as a function of rotation axis to find out if different rotation trends may be discerned as for region 4. A tendency for a minimum angle of about 1° for the rotations most parallel to the ⟨1 0 0⟩–⟨1 1 1⟩ line in the lower subregion 2a was observed. These rotations may be the sum of two other rotation trends seen in this subregion, having components towards and away from the ⟨1 0 0⟩–⟨1 1 1⟩ line, respectively. However, the number of grains was insufficient for a detailed quantitative analysis. No such trend was found in the subregion 2b. From the analysis, it is clear that

region 2 is not as homogenous as regions 1 and 3 with respect to the variations within each subregion. The variation between subregions is also definitely larger than for the other regions but too ill-defined to justify splitting up region 2.

2.2.2. Transitions between regions

In the following the sharpness of the transition between neighbouring regions is investigated based on visual inspection of Fig. 1 as well as the quantitative parameters derived for each region.

Inspection of Fig. 1 shows that at the transition from region 1 to 2 the rotation paths change abruptly from being almost perpendicular to the ⟨1 0 0⟩–⟨1 1 1⟩ line to become roughly parallel to this line. Quantitative comparison of their two adjacent subregions 1c and 2a also reveals mean rotation axes deviating 28° from each other and differences in mean rotation angles. This transition therefore is very sharp.

The mean rotation axis for a zone including grains in region 1 within 2° of the transition to region 3 is almost identical to the mean axis for the entire region 1. However, considering grains in region 1 within 4° of the transition instead gives a mean rotation axis closer to that of region 3b. Close inspection of Fig. 1 shows that this transition involves an intermediate zone where grains with the characteristics of both regions coexist.

The transition between regions 1 and 4 is less well-defined. From Fig. 1 it is seen that the transition zone is characterised by a diverging rotation field with grains rotating little in the vicinity of the present transition in region 1 and rotations in different directions on the left side in region 4. The main rotation direction on each side of the present transition is however not very different, and depending on the criterion used, slightly different transition lines may be drawn.

The transition between regions 2 and 4 is characterised by an abrupt reversal of the rotation direction so that some of the grains in region 4 rotates downwards towards the ⟨1 0 0⟩ corner roughly parallel to the ⟨1 0 0⟩–⟨1 1 1⟩ line while all grains in region 2 have a component rotating upwards along this line towards ⟨1 1 1⟩. In the transition zone grains with practically no rotation of the tensile direction are observed in both regions but the transition line is well-defined.

2.3. Summary of experimental findings

The stereographic triangle is divided into four regions with different rotation behaviour. The existence of these four regions clearly shows that the crystallographic orientation of the tensile direction, i.e., grain orientation, dominates the rotation behaviour in the material and strain range investigated here. The variation of rotation axes within each region is however larger than the variation of tensile directions, indicating that the grain orientation difference alone is not enough to explain the variation in rotation axes. This is particularly the case for regions 2 and 4. In region 4, the large variation is due to the coexistence of probably three different rotation trends, each exhibiting a much smaller variation comparable to those of regions 1 and 3. In the lower part of region 2, the data indicate the existence of two different rotations and linear combinations of these but no definite conclusion could be drawn. Also the rotation angles exhibit significant variation within each region but nevertheless differences between the regions are clear.

The transitions between region 2 and its neighbouring regions are abrupt and their positions very well-defined. The transitions between regions 1 and 3 and 1 and 4 involve transition zones. For the transition between regions 1 and 3 the transition zone contains rotations characteristic of either region while the transition between regions 1 and 4 is ill-defined and involves a diverging rotation field.

3. Comparison with classical orientation-based models

The established division of the stereographic triangle into four regions with different lattice rotations shows that grain orientation is a major factor controlling the rotations. Comparison of the observed behaviour in each region with predictions of the classical purely orientation-based models, i.e., the Sachs [1] and Taylor [2] predictions is the obvious next step.

3.1. Sachs

Rotations of the tensile directions predicted by the Sachs model are shown in the stereographic triangle in Fig. 8. The rotations are calculated from the anti-symmetric part of the displacement gradient tensor, as normally done for polycrystal deformation, i.e., they do not correspond to those predicted for single crystals where the rotation is given by the fixed positions of the two crystal ends in the grips of the tensile testing machine. It is seen that the rotation direction of the tensile direction in most regions lies far from the prediction. Only the grains in region 1 rotate in the predicted direction.

The Sachs model generally overestimates the magnitude of the rotation of the tensile direction although a few grains in regions 1 and 4 rotate more than predicted. The variation of experimental rotations is larger than predicted in most regions. The model predicts negative rotations around the tensile direction for all regions except region 4 where all rotations are predicted to be positive. This is in contrast to the experimental data where all regions contain both negative and positive rotations, with the positive rotations mainly occurring close to the edges of the stereographic triangle.

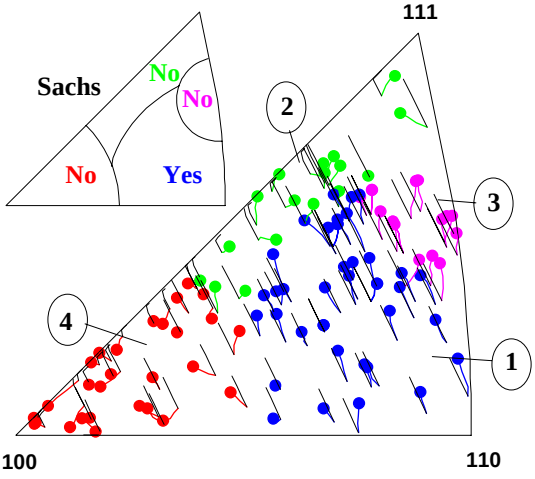

Fig. 8. Comparison with the Sachs model. Stereographic triangle showing prediction (black lines) on top of the experimental data (coloured lines, final orientation marked with symbol). The small triangle indicates whether acceptable agreement is found for each region.

3.2. Taylor

Rotations of the tensile direction predicted by the Taylor model are shown in Fig. 9(a). In this figure, the rotations are calculated from the average of the different solutions to the Taylor ambiguity problem, i.e., either six or eight slip systems are active. Overall, the predicted rotation field is quite homogenous with gradual transitions between different trends. This is not the case for the experimental rotations where rather abrupt changes are seen especially between regions 1 and 2.

A comparison between predicted and observed rotation paths for each of the identified regions shows that the model predicts the rotation path of the tensile direction for the grains in region 3 well. For region 2 the average of the experimental paths agrees fairly well with the predicted rotation path throughout the region but the experimental data scatter significantly around the prediction. In region 1 the predicted rotation is generally more directly towards ⟨1 1 1⟩ than the experimental one. In region 4 the predicted rotations do not at all match the experimental ones. The sign of the rotation around the tensile direction is predicted to be purely negative in regions 2 and 3 while regions 1 and 4 have a mixture of positive and negative rotations. The model generally underestimates the magnitudes of the rotation of both the tensile direction and around this axis.

Inspired by the success of the Sachs model with respect to the rotation of the tensile direction in region 1, the rotations were also calculated for the solution to the Taylor ambiguity problem that maximises slip on the primary slip system. Rotations of the tensile direction calculated with this solution are shown in Fig. 9(b). It is seen that the difference between this solution and the average solution to the ambiguity problem (Fig. 9(a)) is

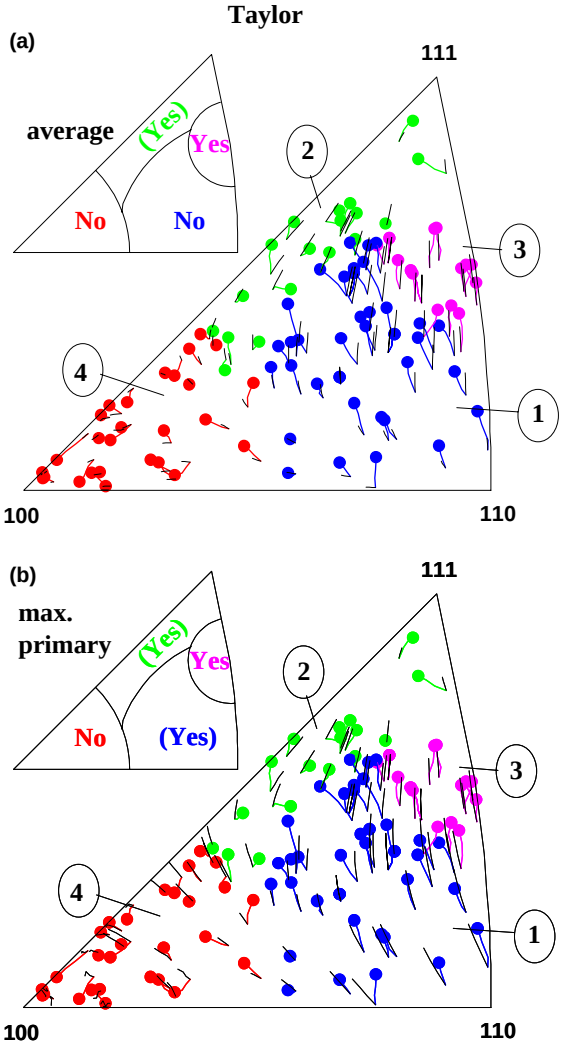

Fig. 9. Comparison with the Taylor model using (a) the average of the different solutions to the ambiguity problem and (b) the solution with maximum primary slip. Stereographic triangles showing the prediction (black lines) on top of the experimental data (coloured line, final orientation marked with symbol). The small triangles indicate whether acceptable agreement is found for each region.

large in regions 1 and 4 both with respect to rotation direction and rotation angles. Predictions of the rotation of the tensile direction in the other regions are marginally different. The predicted rotation paths for the part of region 1 closest to the ⟨1 1 0⟩ corner match the experimental rotations much better than the prediction in Fig. 9. However, in the part of region 1 furthest away from ⟨1 1 0⟩, the predicted rotation with maximum primary slip approaches that obtained using the average solution to the ambiguity problem and deviates from the experimental observations.

The magnitude of the predicted rotation of the tensile direction using this solution to the ambiguity problem agrees much better with the experimental data in regions 1 and 4 than that of the average solution while there is little or no difference in regions 3 and 2, respectively. For

the rotation around the tensile direction the magnitude predicted with maximum primary slip is also in better agreement with the experimental data. The predicted rotation direction around the tensile direction is negative for all grains except those in region 4 which are all positive while the sign of the experimentally observed rotations apparently does not depend on the regions defined here but more on the closeness of the grain to the edge of the triangle.

4. Comparison with self-consistent models

In the self-consistent models, each grain interacts with a matrix representing the average material. Grains of the same crystallographic orientation are predicted to behave identically but this behaviour depends on the bulk texture.

Detailed calculations for the present material have not been carried out. Instead the experimental rotation paths are compared with a prediction from the literature. Fig. 10 shows an example of predicted rotation direction of the tensile direction predicted by Lorentzen et al. [8] using a self-consistent model assuming plastic interaction between a grain and the matrix. Rate insensitivity and latent hardening slightly higher than self-hardening were employed. The modelled aluminium material had a random bulk texture. Please note that Fig. 10 only presents the rotation direction, i.e., the length of the arrows does not reflect the rotation angle.

A significant difference between this prediction and the Taylor predictions in Fig. 9 is seen in the ⟨1 0 0⟩ corner where a large variation in rotation direction is predicted by the self-consistent model. The region of the triangle predicted to exhibit these variations matches region 4 in Fig. 1 where the variation in rotation direction is large. However, closer analysis of the observed rotation paths reveals both similarities and differences: rotations along the ⟨1 0 0⟩–⟨1 1 1⟩ line towards ⟨1 0 0⟩ are found in both predicted and experimental data. The experimentally observed rotations directly towards the ⟨1 0 0⟩–⟨1 1 1⟩ line are however not predicted. Instead the model predicts rotations away from this line, i.e. in the opposite direction. In the rest of the triangle the agreement between prediction and experiment was at the same level as for the Taylor prediction. Direct application of the model to the experimental bulk texture as well as other self-consistent approaches may of course produce improved predictions but this is outside the scope of this paper. The main conclusion drawn here is that the self-consistent approach produces grain orientation dependence of the variation between grains in the same region. Furthermore, region 4, which exhibits the largest variation, is also the region for which the largest variation is predicted.

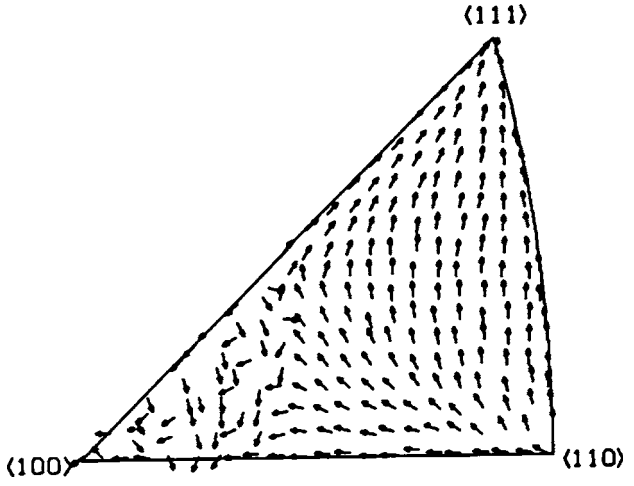

Fig. 10. Self-consistent prediction of the rotation of the tensile direction of aluminium from 3% to 5% tensile elongation. The arrows represent the rotation direction and not the angle. From [8].

5. Discussion

The results and conclusions from the present data are compared with those of other experiments addressing the same problems. Subsequently, the implications of the grain orientation dependence and rotation behaviour in the four regions identified here for crystal plasticity modelling are discussed.

5.1. Comparison with previous results

Bunge and Fuchs [9] investigated the rotations of an ensemble of surface and bulk grains within an aluminium wire with respect to the axis of the wire after about 1% elongation by an X-ray oscillating film method. The ⟨1 0 0⟩ corner is the only orientation region where comparison with the present data set is possible. Both studies observed a lack of dominant rotation towards ⟨1 0 0⟩, which is the observed minor component of bulk textures. However, Bunge and Fuchs report vanishing mean rotation angles in this region, while the present data show a bimodal distribution where about a third of the grains rotate very little and the rotation of the rest of the grains is roughly comparable to that found in the other orientation regions.

Panchanadeeswaran, Doherty and co-workers [10–12] studied the rotation of individual grains on the internal surfaces of a split aluminium sample deformed in channel die compression up to strains of 50%. They concluded that Taylor-type models failed to explain the observed rotations for the majority of the investigated grains. Although the grains rotated towards the traditional rolling texture components these were often not the ones predicted for each individual grain. Similar conclusions were drawn from a study of columnar

grains uniaxially compressed to a strain of 40% [13]. In the latter case, finite element-based models were significantly better than the Taylor model, indicating a relatively strong effect of grain interaction. These conclusions somewhat disagree with the above analysis based on the present data although grains in the ⟨1 0 0⟩ corner may rotate very differently and grains in the ⟨1 1 0⟩ corner do not rotate directly toward a stable bulk texture component.

The two main differences between these experiments and the present data are: (i) that the 3DXRD method undisputedly measures the rotation of grains deeply embedded in the bulk of the material while the other methods concerns grains at or near surfaces/interfaces and (ii) that this is the first detailed analysis covering the entire orientation space relevant for the deformation mode, resulting in quantitative identification of orientation regions with distinctly different rotation behaviour.

5.2. Modelling based on grain orientation

The present division of the stereographic triangle into four regions with clearly different rotation behaviour shows that the grain orientation is a very important parameter. Comparison with the classical models by Sachs and Taylor reveals that the traditional orientation-based models certainly do not explain the behaviour in all regions. Nevertheless the predictions for some regions are in reasonable agreement with the experimental observations, explaining why these models are still widely used to predict bulk textures.

Normally, the Taylor and Sachs models are considered to be upper and lower bound models, respectively. Please note that the terms upper and lower do not refer to the predicted rotation angle but to the work involved. The rotations predicted by the Sachs model are in fact larger than those of the Taylor model. Still, the data analysed here confirm that both rotation direction and rotation angle generally lie in between the predictions of these models. This is perhaps best illustrated by the fact that the version of the Taylor model which maximises primary slip is the best of the purely orientation-based models investigated here, although the prediction is not perfect. Especially, the behaviour in the middle of the triangle and in the ⟨1 0 0⟩ corner (region 4) is poorly accounted for.

One of the most challenging of the revealed deficiencies of the Taylor model is the prediction of too smooth transitions especially between regions 1 and 2. Abrupt transitions imply a major change in the active slip systems in contrast to the gradual changes predicted with the Taylor model. This problem is probably related to the other critical point in the middle of the triangle (at the transition between regions 1 and 2), namely that the rotations indicate so much primary slip that strain compatibility with neighbouring grains seems very difficult.

A much-debated problem in polycrystal plasticity is the ambiguity in the slip system selection [14]. The Taylor model, for example, predicts 6 or 8 active slip systems while strain compatibility may be achieved with only 5, leading to multiple solutions for the slip system activity with the same strain and stress conditions. Selection of one solution among these is not trivial. In fact, minimisation or elimination of the problem has been seen as a major advantage of other models derived from the Taylor model by incorporation of additional physically based criteria, e.g., relaxed constraint models [15], rate sensitive models [6] and other models considering hardening effects [16,17]. The experimental data reveal relatively small variation of the rotation axes within regions 1 and 3, larger and apparently continuous variation within region 2 and most likely three different rotation trends in region 4. These results indicate that the search for a unique solution is justified for regions 1 and 3 while it is difficult at this point to say whether the large variations within regions 2 and 4 originate from ambiguity or from grain interaction. It is noteworthy that the Taylor model predicts the largest effects of ambiguity in regions 1 and 4 and the smallest for region 2, i.e., not in agreement with the present experimental results.

5.3. Modelling grain interaction effects

In spite of the clear overall dependence on the initial grain orientation, the variation in rotation axes within each region is larger than those expected from the variation in grain orientations and also the rotation angles vary. It is however clear from the present data that the character and magnitude of the variations are also grain orientation-dependent. The variations are likely to originate from interaction with neighbouring grains.

Modelling the interaction between neighbouring grains may be done in different detail, ranging from self-consistent models considering interaction between a grain and a matrix representing the average material to finite element-based models where the detailed interaction between each grain and its neighbours is taken into account.

In fact, the strong correlations between grain orientation and rotation behaviour observed here may be seen as an argument for the self-consistent approach because deterministic correlations between grain orientation and rotation behaviour are inherent in these models with an additional dependency on the bulk texture.

A number of models take the effect of interaction between a grain and its nearest neighbour(s) into account. The Lamel model [18] is an example of these models. In relation to the present experimental data,

a major task for these models is to determine the sensitivity of different grain orientations to grain interaction effects, as e.g., done in [19]. Addition of either stochastic stress or stochastic strain contributions to the conditions experienced by individual grains as done by Leffers in the 'modified Sachs model' [20,21] is another way to address this problem.

Finite element-based models directly take the effect of interaction between all the grains in the sample into account. To the authors' knowledge, no finite element-based prediction of the effect of different neighbours on the rotation of individual grains with different orientations in tension is available in the literature. It has therefore not been possible to evaluate the capability of these models in relation to the present experimental data. A very important part of finite element-based modelling is of course the underlying orientation-based crystal plasticity model. The present analysis indicates that the traditional models are inadequate, at least in some orientation regions.

6. Conclusion

The lattice rotations of 95 individual bulk grains during 6% tensile elongation have been analysed. The analysis shows that

1. The grain orientation is the main factor controlling the rotations. Other factors, e.g., grain interaction, have a secondary effect, which is also grain orientation-dependent.
2. Four regions of the stereographic triangle with different rotation behaviour have been identified.
3. The transitions between the four regions are generally characterised by distinct changes in the rotation behaviour.
4. Comparison with traditional polycrystal plasticity predictions gave the following conclusions:
   - The classical predictions by Sachs and Taylor serve as reasonable estimates of the extreme rotations. The Taylor model using the solution to the ambiguity problem which maximises primary slip yields the best result. However, large discrepancies occur, especially in the $\langle 1\,0\,0\rangle$ corner and in the middle of the stereographic triangle.
   - Self-consistent modelling proved capable of predicting large variation in rotation behaviour in the $\langle 1\,0\,0\rangle$ corner but did not predict the correct rotation directions.

Acknowledgements

We thank Dr. N. Hansen and Dr. D. Juul Jensen for scientific discussions. We acknowledge the European Synchrotron Radiation Facility for provision of synchrotron radiation facilities and we thank the ID11 staff for their assistance. The authors also gratefully acknowledge the Danish National Research Foundation for supporting the Center for Fundamental Research: Metal Structures in Four Dimensions, within which this work was performed, and the Danish Natural Science Research Council via Dansync.

References

[1] Sachs GZ. Ver Deu Ing 1928;72:734–6.
[2] Taylor GJ. J Inst Met 1938;62:307.
[3] Kröner E. Acta Metall 1961;9:155.
[4] Hutchinson JW. Proc Roy Soc A 1970;319:247.
[5] Mika DP, Dawson PR. Mater Sci Eng A 1998;257:62–76.
[6] Kocks UF, Tomé CN, Wenk HR. Texture and anisotropy Preferred orientations in polycrystals and their effect on materials properties. Cambridge: Cambridge University Press; 1998. 375–376.
[7] Poulsen HF, Margulies L, Schmidt S, Winther G. Acta Mater 2003;51:3821–30.
[8] Lorentzsen T, Clausen B, Leffers T. In: Proceedings of the 19th Risø International Symposium on Materials Science: Modelling of Structure and Mechanics of Materials from Microscale to Product, Roskilde, Denmark, 1998, p. 345–54.
[9] Bunge HJ, Fuchs R. Phys Stat Sol 1969;32:169–77.
[10] Panchanadeeswaran S, Doherty RD. Scripta Metall Mater 1993;28:213–8.
[11] Panchanadeeswaran S, Becker R, Doherty RD, Kunze K. Mater Sci Forum 1994;157–162:1277–82.
[12] Panchanadeeswaran S, Doherty RD, Becker R. Acta Mater 1996;44:1233–62.
[13] Bhattachayya A, El-Danaf E, Kalidindi SR, Doherty RD. Int J Plasticity 2001;17:861.
[14] Leffers, T. In: Proceedings of the ICOTOM 8, Santa Fe, 1988. p. 273–84.
[15] Kocks, UF Canova GR. In: Proceedings of the 2nd Risø International Symposium on Deformation of Polycrystals: Mechanisms and Microstructures, Risø, Denmark, 1981. p. 35–44.
[16] Renouard M, Wintenberger MCR. Acad Sci Paris B 1981;292:385–8.
[17] Peeters B, Seefeldt M, Van Houtte P, Aernoudt E. Scripta Mater 2001;45:1349–56.
[18] Van Houtte P, Delannay L, Samajdar I. Textures Microstruct 1999;31:109–49.
[19] Delannay L, Van Houtte P, Samajdar I. J Phys IV 1999;9:43–52.
[20] Leffers, T. In: Proceedings of the 5th International Conference on Strength of Metals and Alloys, Aachen, 1979. p, 769–774.
[21] Winther G, Leffers T, Clausen B. In: Proceedings of the ICOTOM 12, Montreal, 1999. p. 399–404.

A10: Slip systems extracted from lattice rotations and dislocation structures by G. Winther, Acta Materialia, 2008

Available online at www.sciencedirect.com
ScienceDirect
Acta Materialia 56 (2008) 1919–1932
Acta MATERIALIA
www.elsevier.com/locate/actamat

Slip systems extracted from lattice rotations and dislocation structures

Grethe Winther *

Center for Fundamental Research: Metal Structures in Four Dimensions, Materials Research Department, Risø DTU – National Laboratory for Sustainable Energy, Technical University of Denmark, DK-4000 Roskilde, Denmark

Received 26 August 2007; received in revised form 11 December 2007; accepted 13 December 2007
Available online 26 March 2008

Abstract

Data on lattice rotations and dislocation structures induced in aluminium by tensile deformation are analysed together in order to extract the active slip systems. The analysis falls in two steps: (i) from the combination of lattice rotation and dislocation structure data, the grain orientation space represented by the stereographic triangle is subdivided into regions with the same active slip systems; and (ii) the active slip systems calculated from the lattice rotations are compared with those known to be active based on the dislocation structure. For the entire stereographic triangle active slip systems which are in good agreement with both lattice rotations and dislocation structures are identified, showing that the grain orientation is the primary factor controlling the slip systems.

Keywords: Plastic deformation; Slip; Dislocation boundaries; Texture; Aluminium

1. Introduction

Slip systems are normally predicted by polycrystal plasticity models. Classical models, like the Sachs [1] and Taylor/Bishop–Hill [2,3] models, consider a grain as an independent entity; self-consistent models consider the interaction between a grain and a matrix representing the rest of the material [4]; and finite element models take the detailed interaction between neighbouring grains into account [5]. Common to all of these models is that the active slip systems are calculated from the assumed or predicted stress and strain conditions of the grain and the crystallographic grain orientation.

An important aim of slip system predictions is to further calculate the lattice rotations of the individual grains to simulate deformation texture evolution. Until recently, these lattice rotation predictions could only be compared with experimental bulk textures, data from surface grains or experiments designed to mimic bulk behaviour while still investigating surfaces [6–8]. With the development of the three-dimensional X-ray diffraction technique (3DXRD), however, lattice rotations for a large number of individual grains deeply embedded in the bulk of the sample during tensile deformation can now be measured directly [9–11].

Previous comparison of the lattice rotations measured by 3DXRD with the results of standard polycrystal plasticity models has revealed disagreements which are related to deficiencies in the slip system prediction [12]. It has also been established that the lattice rotations depend strongly on the crystallographic grain orientation [12], which shows that the grain orientation must be an important factor controlling the slip systems. However, additional information is required to unambiguously determine the active slip systems.

Studies combining lattice rotations and local plastic strain measurements obtained from shape changes of individual grains have been carried out for plane strain compressed columnar grains for which the surface is assumed representative of the bulk [13]. For bulk grains, measurements of the local plastic strain is also becoming possible by means of marker techniques in X-ray tomography [14–16]. It has been proposed to combine the local plastic strain measured by this technique with lattice rotations

* Tel.: +45 4677 5792.
E-mail address: grethe.winther@risoe.dk

1359-6454/$34.00 © 2007 Acta Materialia Inc. Published by Elsevier Ltd. All rights reserved.
doi:10.1016/j.actamat.2007.12.026

obtained by the 3DXRD technique to determine the active slip systems in bulk grains, but such results have not yet been reported [17].

The present paper takes an alternative approach and combines the lattice rotation data with data on deformation-induced dislocation structures. Extensive transmission electron microscopy (TEM) studies of bulk grains have demonstrated that dislocation structures, like lattice rotations, depend on the grain orientation [18–24]. In particular, the crystallographic alignment of extended planar dislocation boundaries, also termed geometrically necessary boundaries (GNBs), has been investigated. The grain-orientation dependence of the GNB alignment has been traced to a dependence on the active slip systems [21,25]. Detailed studies of individual GNBs have revealed that the dislocations in the GNBs largely correspond to those generated by the expected active slip systems [26,27]. These observations are in agreement with calculations [28] assuming that the GNBs are low-energy dislocation structures (LEDS) [29]. However, the LEDS principle has not been generally successful in prediction of the GNB characteristics from slip systems, although evolution of GNBs has been modelled based on this principle [30]. By contrast, predictive relations between slip systems and the GNB alignment have recently been identified through a systematic study of the grain-orientation dependence of the structures formed in different deformation modes [31]. In this paper, these relations are exploited to determine the identity of the dominating active slip systems from the dislocation structure.

The first part of the paper summarizes and correlates the grain-orientation dependence of the lattice rotations measured by 3DXRD and the dislocation structures investigated by TEM to identify the grain-orientation dependence of the slip systems in tension. The second part compares the slip systems calculated from the experimental lattice rotations and those deduced from the dislocation structures to identify the systems which are in agreement with both sets of data.

2. Lattice rotations and dislocation structures

The stereographic triangle selected to represent the crystallographic orientation of the tensile axis is the one spanned by the [1 0 0], [1 1 0] and [1 1 1] zone axes, as illustrated in Fig. 1. The primary, conjugate, critical and cross-slip planes in this triangle are $(1\,1\,\bar{1})$, $(1\,\bar{1}\,1)$, $(1\,1\,1)$ and $(\bar{1}\,1\,1)$, respectively. The primary, conjugate, critical and cross-slip systems are −b2, d3, −a2 and −c2 in the Bishop–Hill notation (see Table 1). The latter three are

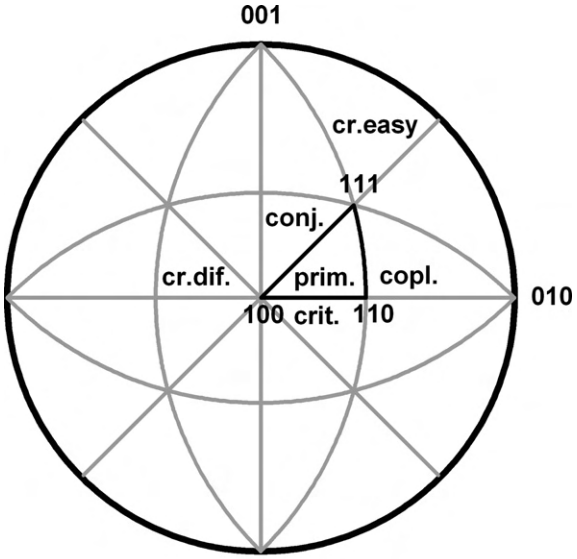

Fig. 1. Full stereogram identifying the triangle used throughout the paper, as well as the associated primary, conjugate, critical and cross-slip systems.

the primary systems in the neighbouring triangles, as indicated in Fig. 1.

2.1. Lattice rotations

The lattice rotations of about 100 individual bulk grains of aluminium (AA1050, grain size of 75 μm) have been measured by 3DXRD during tension to 6% elongation [11]. By means of a conical slit diffraction spots originating from a volume of 5 μm × 5 μm × ~300 μm located in the center of a sample with a cross-section of 4 × 8 mm^2 were recorded. Measurements were made in several positions along the tensile axis of the sample to monitor a large number of grains. The diffracting volume at each position does not contain an entire grain but several grains in parts which typically span over both the grain boundary region and the grain interior. The parts of the grain investigated at 0%, 2%, 4% and 6% strain were not exactly identical and also at each strain the volume changed due to rotation of the sample to obtain diffraction from other planes. However, the fact that the determined rotation paths in general are smooth indicates a relatively uniform behaviour of each

Table 1
Slip systems in Bishop–Hill notation

Plane	$(1\,1\,1)$	$(\bar{1}\,\bar{1}\,1)$	$(\bar{1}\,1\,1)$	$(1\,\bar{1}\,1)$
Direction	$[0\,1\,\bar{1}][\bar{1}\,0\,1][1\,\bar{1}\,0]$	$[0\,\bar{1}\,\bar{1}][1\,0\,1][\bar{1}\,1\,0]$	$[0\,1\,\bar{1}][1\,0\,1][\bar{1}\,\bar{1}\,0]$	$[0\,\bar{1}\,\bar{1}][\bar{1}\,0\,1][1\,1\,0]$
Notation	a1 a2 a3	b1 b2 b3	c1 c2 c3	d1 d2 d3

individual grain. Several positions investigated within one very large grain in a similar experiment on copper also showed the same rotation behaviour [10]. Averaged over many grains, the magnitude of the rotation is more than twice the magnitude of the developing internal orientation spread measured as the full-width-half-maximum value of the diffraction spots at 6% strain. Furthermore, the spread of the individual diffraction peaks is often in the form of weak tails trailing behind the main spot along the rotation direction, indicating activity of the same slip systems but with different activities. This observation is also in agreement with recent electron backscatter pattern studies of rolled metals, where orientation gradients in the direction of the expected lattice rotations were often seen [32]. For the purpose of this paper a grain is therefore considered an entity and the reported rotations represent changes in its mean orientation from 0% to 6% strain.

The rotations of the tensile axes are shown in Fig. 2, where the solid circles represent the final orientations. The triangle has been subdivided into four regions, labelled 1–4, with different dominant rotation behaviour of the tensile axis [12]:

1. Grains in the [1 1 0] corner rotate towards the [1 0 0]–[1 1 1] line.
2. Grains at the [1 0 0]–[1 1 1] line rotate along this line towards [1 1 1].
3. Grains half way up the [1 1 0]–[1 1 1] line, i.e. close to [2 2 1], rotate directly towards [1 1 1].
4. Grains near [1 0 0] exhibit three different trends: (4I) rotation towards the [1 0 0]–[1 1 1] line, (4II) rotation along the [1 0 0]–[1 1 1] line towards [1 0 0] and (4III) virtually no rotation of the tensile axis.

The transitions between regions 1 and 2 as well as between regions 2 and 4 are sharp. The remaining transitions are less well defined. The rotations around the tensile axis were small and did not exhibit any noticeable dependence on the grain orientation. It must, however, be emphasized that the calculations made in the following are based on the full rotation, not just that of the tensile axis.

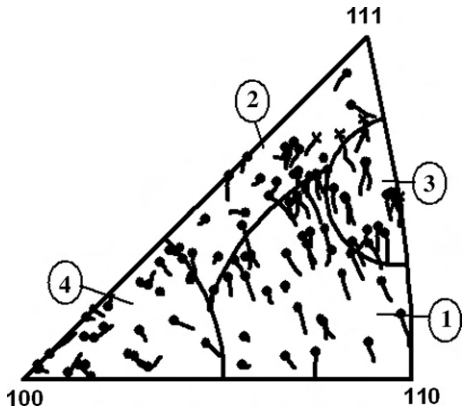

Fig. 2. Stereographic triangle showing the rotation of the tensile axis for individual grains during 6% tensile elongation of 99.5% pure aluminium with a grain size of 75 μm (circles) and 99% pure copper with a grain size of 35 μm (crosses). The respective symbols mark the final orientation after elongation. The triangle is subdivided into regions labelled 1–4, which exhibit different rotation behaviour. The figure is a combination of data from Refs. [10,12].

Two similar experiments were conducted on four grains in pure aluminium with a grain size of 300 μm deformed to 11% elongation [9] and seven grains in copper with a grain size of 35 μm to 6% elongation [10]. These data follow the same trend as in the AA1050. However, four of the copper grains lie in the upper part of rotation region 3, which is poorly covered in the AA1050 experiment. In order to get as complete coverage of the triangle as possible, the AA1050 data are combined with these four copper grains in this analysis. The copper rotations are shown in Fig. 2, with the final orientations marked as crosses.

2.2. Dislocation structures

The deformation-induced dislocation structure was investigated by TEM. In particular, the crystallographic plane of the GNBs was determined by recording the trace of the GNB with respect to the tensile axis and tilting the sample in the microscope until the trace is very sharp, showing that the GNB is viewed edge-on. From the trace angle, the tilt angle and the crystallographic orientation of the grain the crystallographic GNB plane is determined. It should be emphasized that the GNBs often consist of straight segments lying on closely spaced parallel planes, which may result in some curvature when connected over larger distances [24].

The grain-orientation dependence of the dislocation structure alignment has been shown to be the same for aluminium and copper [24] for a wide range of experimental parameters. Basically three main types of structures exist: Type 1, with GNBs aligned with {1 1 1} slip planes; Type 2, with no GNBs but only short, randomly oriented cell boundaries (also referred to as incidental dislocation boundaries (IDBs)); and Type 3, where the GNBs lie far from {1 1 1} slip planes. Examples of these structure types are shown in Fig. 3a–c. Their grain-orientation dependence is illustrated in Fig. 3d. The position of the transition between Type 1 and Type 3 structures has been clearly determined based on data from copper and aluminium samples of different purities [24] and grain sizes (down to 4 μm) [22], although there are occasional observations of Type 1 structures near this line in Type 3 region. The transition between Type 2 and Type 1 structures depends somewhat on the metal type, and the transition included in Fig. 4 is that determined for AA1050 [24]. The grain-orientation dependence of the dislocation structure types is remarkably insensitive to grain size [22] and strain level [18,19,24] in the investigated ranges (300 to 4 μm, and 5–30% elongation, respectively). Furthermore, the structure is uniform over the grain where the GNBs in general run straight up to the grain boundary [24], although changes

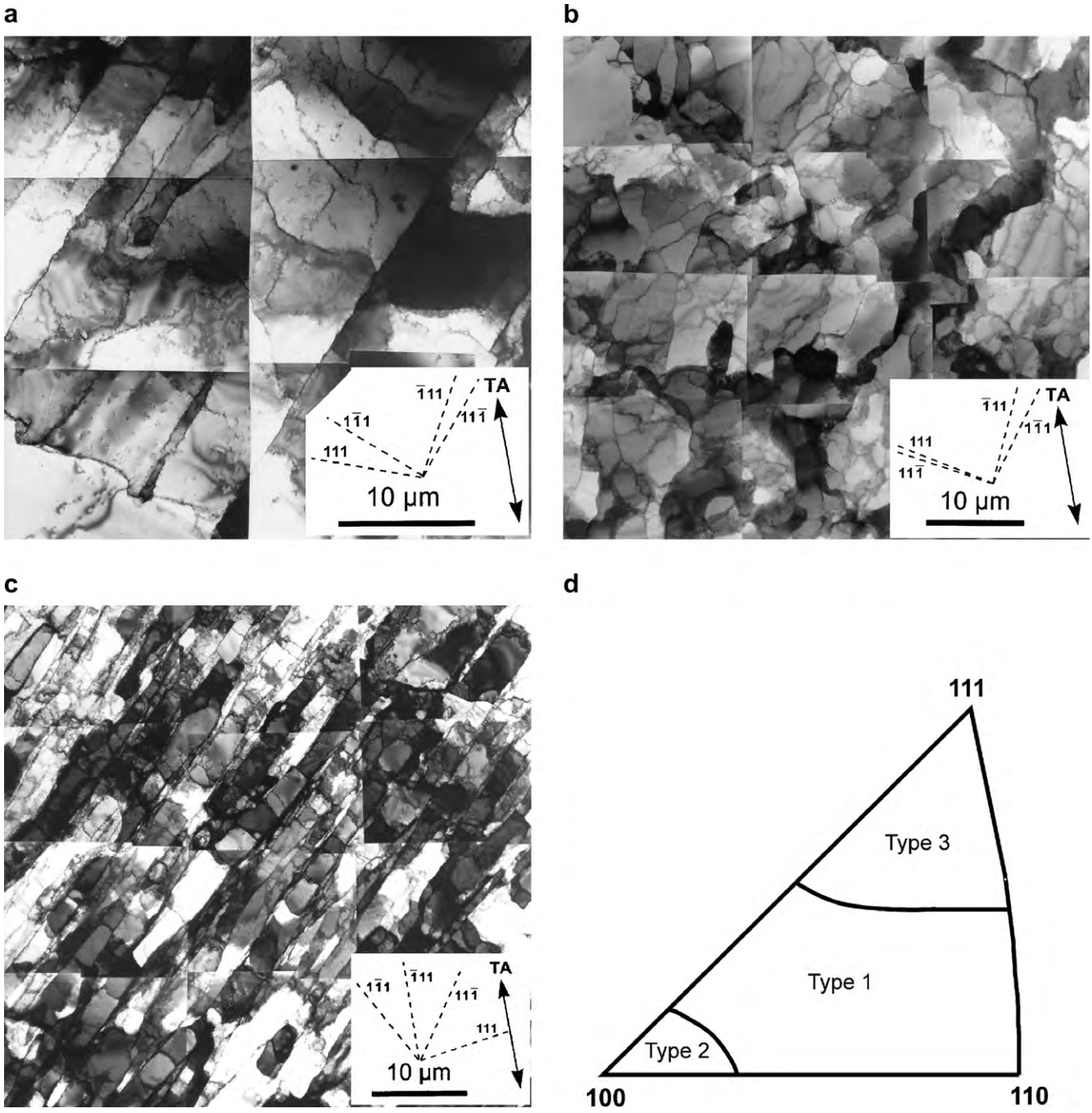

Fig. 3. (a–c) TEM images of dislocation structure Types 1, 2 and 3 in pure aluminium (from Ref. [18]). Traces of the {1 1 1} slip planes are marked on the images. For Type 1 the GNBs align with a slip plane, while this is not the case for Type 3. Type 2 contains no planar GNBs but only cells. (d) Stereographic triangle presenting the grain-orientation dependence of the three structure types.

especially in the vicinity of triple junctions are observed [33]. Although there is typically some orientation spread within the grain, this is not sufficient to change the dislocation structure. In analogy with the lattice rotations, a grain is therefore considered as an entity represented by a mean orientation.

Fig. 4 shows the results of even more detailed characterization of the planes of the GNBs, showing that the triangle is further subdivided according to the detailed crystallographic GNB plane [24]. In particular, Type 3 structures can be subdivided into GNBs aligning with $(3\,5\,\bar{1})$, $(3\,\bar{1}\,5)$ and variants of {1 1 5} planes, respectively. The dotted line representing the transition between {1 1 5} and {3 5 1} planes has been clearly determined [24]. As also indicated in Fig. 4, $(3\,\bar{1}\,5)$ planes are seen in the vicinity of the [1 0 0]–[1 1 1], line but the extension of this plane into the triangle has not been well determined. For polycrystals, the region around the [2 2 1] orientation has not been investigated in detail, as indicated by the question mark in Fig. 4, although it is clear that the GNBs are not aligned

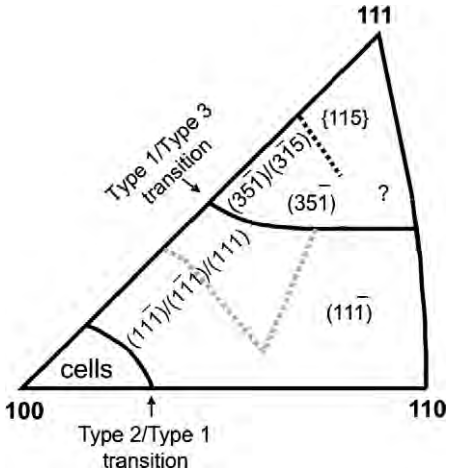

Fig. 4. Stereographic triangle showing the orientation dependence of the dislocation structure after tensile deformation. Solid lines mark the transition between Type 1 and Type 3 structures. Dotted lines mark further transitions between different crystallographic GNB planes. The grey dotted line indicates that the sign of small deviations from the {1 1 1} planes changes, but this transition is not well defined. The question mark designates that the exact GNB plane in this part of the triangle has not been determined in polycrystals. Single crystals on the [1 1 0]–[1 1 1] line have GNBs close to (4 4 $\bar{1}$).

with a {1 1 1} slip plane. Single crystals on the [1 1 0]–[1 1 1] line have boundaries deviating more and more from the slip plane and aligning with (4 4 $\bar{1}$) near [1 1 1] [34].

In Type 1 structures the GNBs most often align with the primary slip plane. GNBs aligned with the critical and conjugate slip planes are also found near the [1 0 0] corner. In all cases the GNBs deviate a little (<10°) from the exact slip plane by rotation around the ⟨1 1 2⟩ axis perpendicular to the primary, critical or conjugate slip direction (for more details see Refs. [21,24]). However, the sign of the deviation from the slip plane can be either negative or positive. The occurrence of these signs is grain-orientation dependent [21,24], but there is some overlap between grain orientations with negative and positive deviations. The grey dotted line in Fig. 4 therefore only represents the approximate location of the transition [21].

3. Grain-orientation dependence of the slip systems

As accounted for in Sections 2 and 3, the experimental observations are well documented and typical for face-centred cubic metals of medium to high stacking fault energy that are also not sensitive to the grain size. This warrants comparison of the two types of data in spite of the facts that the lattice rotations and dislocation structures have not been investigated for the exact same sample and that the two data sets do not cover exactly the same strain range: the rotation data are limited to elongation to 6%, which is comparable to the lowest strain (5%) for which the dislocation structure was characterized. The grain-orientation dependence of the dislocation structure alignment is, however, the same in the investigated strain range up to 30% elongation. It is therefore expected that the underlying grain-orientation dependence of the slip systems must be the same over the entire strain range, so that when a grain rotates into a new region of the triangle the slip systems change accordingly, leading to changes in both the dislocation structure and the course of the lattice rotation. Even though this has not been demonstrated experimentally, the different strain levels are neglected in the following analysis.

As the subdivisions of the triangle according to rotation behaviour (Fig. 2) and dislocation structure alignment (Fig. 4) reflect the underlying dependence of the slip systems, superposition of the two subdivisions must yield the subdivision according to slip systems. This superposition is shown in Fig. 5a, where the lines subdividing the triangle based on lattice rotations and dislocation structures are dashed and dotted, respectively. While some similarities are seen, many differences are also obvious. This shows that some changes in the slip systems are more clearly reflected in either the lattice rotations or the dislocation structures. However, a line marking a transition in either Fig. 2 or Fig. 4 must designate a change in slip systems, leading to the grain-orientation dependence of the slip systems presented in Fig. 5b. With two exceptions, Fig. 5b is

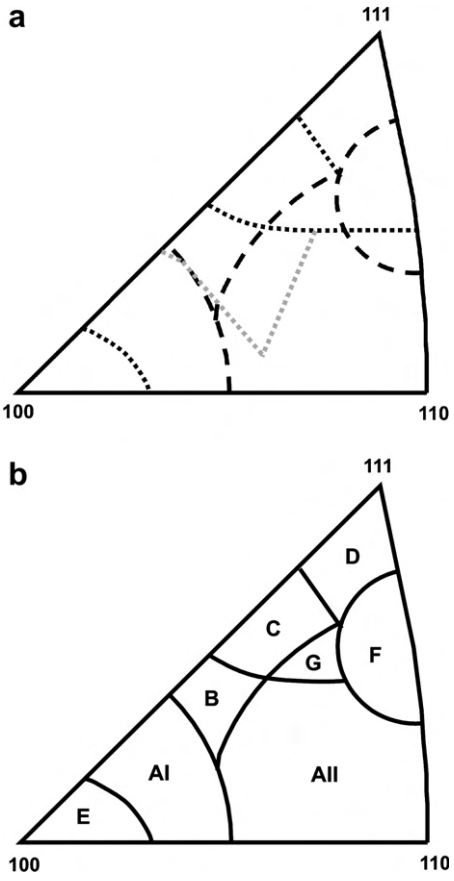

Fig. 5. (a) Superposition of the subdivisions of the stereographic triangle based on lattice rotations from Fig. 2 (dashed) and dislocation structures from Fig. 4 (dotted). (b) The unified subdivision represents the grain-orientation dependence of the slip systems. New labels are attached to the regions, which will be used throughout the remainder of the paper.

merely a repetition of Fig. 5a, but with new labels (A–G) for the slip system regions, which are used throughout the remainder of the paper. The two exceptions and their motivations are:

- Slip system region F corresponds to rotation region 3, although the transition between Type 1 and Type 3 dislocation structures runs through it so that the GNBs in the lower part of region F lie close to the primary slip plane while the GNBs in the upper part do not. The reason for considering region F as one entity is that single crystals on the part of the [1 1 0]–[1 1 1] line delineating region F exhibit a gradual change in the GNB plane from $(1\,1\,\bar{1})$ to near $(4\,4\,\bar{1})$, with all GNBs deviating from the slip plane by rotation around the same axis in the same direction. This indicates the operation of the same slip systems, although with a gradual change in their relative intensities. A further pragmatic argument for not splitting up this region is that the lack of detailed GNB planes for grains in polycrystals with the tensile axis lying in the interior of this region prevents firm conclusions in the subsequent analysis.
- The transition between slip system regions AII and B is fixed to the one given by the lattice rotations because of the sharpness of this transition compared with the uncertain location of the dislocation structure transition caused by extensive overlap in the two types of GNB planes involved.

4. Slip system analysis methods

Having established the subdivision of the triangle into regions with different slip systems, the analysis to determine the identity of these systems can start. This analysis is a three-step process. The first step is to calculate slip systems based on the observed lattice rotations in each region. In the second step, the slip systems are deduced from the dislocation structure. This deduction is based on recently identified relations between slip classes and the crystallographic alignment of the dislocation structure [31]. The third step compares the slip systems calculated from lattice rotations and those deduced from dislocation structures. This section describes the details of these analysis steps, before the analysis is applied to the data in the next section.

4.1. Calculating slip systems from lattice rotations

Traditionally, polycrystal plasticity models first calculate the slip systems based on the grain orientation and the strain or stress boundary conditions. The lattice rotations are calculated subsequently. By contrast, the present analysis calculates the slip systems from an assumed strain and the measured lattice rotations in one process.

Slip systems, lattice rotations and plastic strain are related according to Eq. (1), where the strain and rotations constitute the symmetric and antisymmetric parts, respectively, of the displacement gradient tensor.[1] The five strain components (ε_{ij}) and the three rotation components (r_{ij}) are thus related to the shears on the individual slip systems (γ^k):

$$\begin{aligned} \varepsilon_{ij} &= \sum_{k=1}^{8} \gamma^k (b_i^k n_j^k + b_j^k n_i^k)/2 \\ r_{ij} &= \sum_{k=1}^{8} \gamma^k (b_i^k n_j^k - b_j^k n_i^k)/2 \end{aligned} \tag{1}$$

with $b = (b_1, b_2, b_3)$ and $n = (n_1, n_2, n_3)$ being the unit vectors representing the slip direction and slip plane normal in the sample coordinate system.

In the present work, three strain tensors with different restrictions have been employed, leading to three different calculation methods. It is common to all three methods that the elongation of a grain along the tensile axis is fixed to the nominal elongation of the sample (in this case 6%).

The first method prescribes axisymmetric strain with no shear strains, which is why it will be referred to as the *axisymmetric method* throughout the paper. The strain tensor is

$$\varepsilon = \varepsilon_{\text{nom}} \cdot \begin{pmatrix} -0.5 & 0 & 0 \\ 0 & -0.5 & 0 \\ 0 & 0 & 1 \end{pmatrix} \tag{2}$$

Inserting this strain tensor and the measured rotation for the grain in Eq. (1), the equations can easily be solved to find the unknown shears on the individual slip systems (γ^k). Analogously to the calculations in the Taylor/Bishop–Hill models, many slip system combinations will satisfy the equations, but these require different amounts of plastic work. The common procedure of selecting the systems minimizing the internal work is adopted here, i.e. the slip systems with $(\sum \gamma^i)_{\min}$ are selected, assuming that all slip systems have the same critical resolved shear stress. In contrast to the Taylor/Bishop–Hill model, only one such slip system combination is found, i.e. no ambiguity is encountered. It should be noted that the calculated work can never be smaller than the one obtained by the Taylor/Bishop–Hill model, as this model imposes an axisymmetric strain with no restrictions on the lattice rotation.

A strain tensor allowing asymmetric contraction as well as shear strains has also been devised. The corresponding calculation method is referred as the *unrestricted method*. The only condition is that the largest component of the strain is elongation, i.e.

$$\varepsilon = \varepsilon_{\text{nom}} \cdot \begin{pmatrix} -q & r & s \\ r & -(1-q) & t \\ s & t & 1 \end{pmatrix}; \quad q \in [0;1]; \ \{r,s,t\} \in [-1;1] \tag{3}$$

[1] Except for cases where additional information on the boundary conditions of the grain is available or assumed [35].

The strain tensor in Eq. (3) is not axisymmetric, meaning that the calculated slip systems will depend on the orientation of the grain with respect to the front and side faces of the lath-shaped sample. This has not, however, been of any importance for the conclusions drawn based on the calculations.

Introduction of these wide bounds on the strain components transforms the linear equations in Eq. (1) to

$$\begin{aligned} \varepsilon_{ij}^{\min} &\leqslant \sum_{k=1}^{8} \gamma^k (b_i^k n_j^k + b_j^k n_i^k)/2 \leqslant \varepsilon_{ij}^{\max} \\ r_{ij} &= \sum_{k=1}^{8} \gamma^k (b_i^k n_j^k - b_j^k n_i^k)/2 \end{aligned} \tag{4}$$

where $\varepsilon_{ij}^{\min}$ and $\varepsilon_{ij}^{\max}$ are the bounds on the strain component as defined in Eq. (3). These equations and inequalities are solved by the simplex method [36], again giving solutions with up to eight systems and selecting the one with minimum work. In practice, however, the number of active slip systems is found to be about four.

Finally, the *intermediate method* assumes a strain tensor where the contraction and shear strains are allowed to fluctuate within more restrictive bounds:

$$\begin{aligned} \varepsilon = \varepsilon_{\text{nom}} \cdot \begin{pmatrix} -q & r & s \\ r & -(1-q) & t \\ s & t & 1 \end{pmatrix}; \quad q \in [0.35; 0.65]; \\ \{r, s, t\} \in [-0.15; 0.15] \end{aligned} \tag{5}$$

The bounds on the contraction (q) have been somewhat arbitrarily selected to approximately match the typical variations in the macroscopic contraction of tensile-deformed polycrystalline aluminium samples [37,38]. The bounds on the shear strains (r, s, t) have been set to the same level. Apart from tightening the bounds on the parameters q, r, s and t, the inequalities in Eq. (5) are solved in the same way as those in Eq. (4). The number of active slip systems turns out to be between four and eight.

4.2. Deducing slip systems from dislocation structures

A recent systematic analysis of dislocation structures and slip systems in tension and rolling has resulted in universal relations between the slip systems and the type of dislocation structure [31]. The analysis was conducted by decomposing various combinations of active slip systems into five fundamental slip classes, each resulting in a specific crystallographic alignment of the dislocation structure. One of the classes, however, results only in equiaxed cells and no planar GNBs. The slip classes and examples of GNB planes resulting from a specific combination of slip systems belonging to the class are listed in Table 2. The slip classes may be two-or-more-fold activated in a grain and different slip classes may also be active in the same grain. Twofold activation of a slip class, or activation of two different classes which do not involve any of the same slip systems, results in two independent sets of GNBs. Twofold activation of especially the dependent coplanar and codirectional slip class can occur in several different combinations, of which one leads to two sets of GNBs and the others lead to only one set.

The relations between GNB planes and slip classes have previously been applied to deduce the active slip systems, e.g. in the rolled Brass orientation $(0\,1\,\bar{1})[\bar{2}\,1\,1]$. This example is presented in detail here to illustrate the procedure, which will be applied to the tensile data. The Brass orientation is one of the stable rolling texture components but its intensity is typically underestimated by standard crystal plasticity models like the Taylor/Bishop–Hill model. The crystallographic GNB plane in this orientation has been extensively

Table 2
Summary of the relations between slip pattern classes and dislocation boundaries derived in Ref. [26]

Fundamental slip class	Boundary plane	Slip systems
Single slip	$(1\,1\,\bar{1})$*	−b2
Coplanar slip	$(1\,1\,\bar{1})$*	−b2, b1
Codirectional slip		
*Symmetric***		
Easy cross-slip	(1 0 1)	−b2, −c2
Difficult cross-slip	(0 1 0)	−b2, c2
Two-fold activation of easily cross slipping systems	Equiaxed cells only	E.g. −b2, −c2, −a2, −d2
Dependent coplanar and codirectional slip		
3 systems, with one being coplanar and codirectional, respectively, to the others	$(3\,5\,\bar{1})$	−b2, b1, −d1
Two-fold activation:		
4 systems on 2 slip planes	$(3\,5\,\bar{1})$, $(3\,\bar{1}\,5)$	−b2, b1, −d1, d3
4 systems on 3 slip planes	$(4\,4\,\bar{1})$	−b2, b1, −d1, c2
6 systems on 3 planes	{1 1 5}***	−b2, b1, c2, −c3, −d1, d3

* Note that the GNBs always deviate a little from the exact slip plane. GNBs from the single slip class are rotated slightly away from the slip plane around a {1 1 2} axis while those from the coplanar slip class are rotated around a {1 1 0} axis.

** In the general case, the GNB plane is a linear combination of the two active slip planes weighted by their relative activities so that the GNB lies closer to the more active slip plane. The GNB plane always contains the codirectional slip direction.

*** Different variants of {1 1 5} occur.

investigated and found to consist of two sets of GNBs aligned with two {1 1 1} slip planes. The deviation of both GNB planes from the exact slip planes is by rotation around a {1 1 0} axis, which, according to Table 2, is evidence of activation of the coplanar slip class. The dislocation structure analysis therefore reveals that the active slip systems constitute a twofold activation of this slip class. Interestingly, these systems are in better agreement with predictions based on Schmid factors than those based on the Taylor/Bishop–Hill model and also agree with the stability of the Brass orientation during rolling.

4.3. Comparison of the two sets of slip systems

In the following section, the slip classes and the actual slip systems activated are deduced for all regions of the stereographic triangle. These systems are then compared with those calculated from the rotations. In order to conduct an objective evaluation, quantitative parameters are defined. These parameters designate the fraction of the work ($\sum_i \gamma^i$) that is accounted for by the systems involved in each slip class or twofold activation of the class. More specifically, the parameters are:

Single and double slip:

- F_{sgl}, which is the fraction of the total slip in the grain occurring on the most active slip system.
- F^2_{sgl}, which is the fraction of the total slip in the grain occurring on the most active slip system and its conjugate or critical system (twofold activation of the single slip class).
- F_{copl}, which is the fraction of the total slip in the grain occurring on the most active set of coplanar slip systems.
- F_{codir}, which is the fraction of the total slip in the grain, which occurs on the most active set of codirectional slip systems.

Twofold activation of easily cross-slipping systems:

- F_{cell}, which is the fraction of the total slip which occurs on two or more sets of codirectional slip systems, which are oriented for easy cross-slip.

Dependent coplanar and codirectional slip:

- $F_{\{1\,3\,5\}}$, which is the maximum fraction of the total slip which occurs on three systems, of which one is coplanar and codirectional, respectively, with the two others. This combination leads to a boundary plane near {1 3 5}.
- $F^2_{\{1\,3\,5\}}$, $F_{\{4\,4\,1\}}$, $F_{\{1\,1\,5\}}$, which are the fractions of the total slip accounting for multiple activation of the dependent coplanar and codirectional slip class. This may occur in three different geometries, involving four systems on two or three slip planes or six systems on three slip planes. These geometries lead to two sets of boundaries near {1 3 5}, one boundary near {4 4 1}, or one boundary near {1 1 5}, respectively.

5. Results

5.1. Slip systems from dislocation structures

Not all of the GNB planes listed in Table 2 are actually observed in tension. Table 3 lists the observed planes for each region as extracted by comparison of Figs. 4 and 5b. The slip class associated with the dislocation structure in each region is deduced from Table 2, and the actual slip systems active in each case are also determined. Most of these could be taken directly from the slip system examples in Table 2.

Some of the regions require a little more analysis as several GNB planes are observed. Region AI exhibits GNB planes aligned with three different slip planes, and sometimes two of these coexist in the same grain. All the GNBs are of the type resulting from the single slip class, as evidenced by the small deviation of the GNBs from the ideal slip plane by rotation around {1 1 2} axes, but this single slip must take place on three different slip planes. Twofold activation of the single slip class, i.e. simultaneous slip on two systems, which are neither coplanar nor codirectional, is also possible. Analogously, in region B more than one possibility is deduced, namely one of two systems or both of these. In region C, two different combinations representing the dependent coplanar and codirectional slip class are possible, and these may also be activated simultaneously. Region F is difficult to conclude on as the dislocation structure in this region is less well characterized. For this region the possible GNB planes and the associated slip classes and systems are listed in Table 3.

The slip class deduced dominating in each region is directly related to the previously defined quantitative parameter stating the fraction of the total slip in a grain that is accounted for by the slip class (see Section 4.3). It is expected that the highest parameter derived from the slip systems in a grain must correspond to the slip class deduced from the dislocation structure. The expected high parameters are also included in Table 3.

5.2. Comparison with systems from lattice rotations

For clarity, detailed listings of the slip systems calculated from the lattice rotations with each of the three methods described in Section 4.1 are omitted. The results of the calculations are instead interpreted directly in terms of the nine parameters defined in Section 4.3 relating to the slip classes governing the dislocation structure. As also stated in Ref. [12], there is some scatter in the measured rotations within each region which is obviously also reflected in some variation in the calculated slip systems. This variation is, however, not of a magnitude where it affects the conclusions drawn here. The parameters used are therefore, the average of the parameters for all the grains in each

Table 3
Dislocation structure data, deduced slip class and the active slip systems belonging to this slip class for the different regions of the stereographic triangle in Fig. 5b

Region	GNB plane	Slip class	Slip systems	Expect. parameter	axi	int	unr
AI	$(1\,1\,\bar{1})/(1\bar{1}1)/(1\,1\,1)$	single or two-fold single	−b2/d3/−a2	F_{sgl}/F^2_{sgl}	✓	✓	✓
B	$(1\,1\,\bar{1})/(1\,\bar{1}\,1)$	single or two-fold single	−b2/d3	F_{sgl}/F^2_{sgl}		✓	✓
AII	$(1\,1\,\bar{1})$	single	−b2	F_{sgl}			
C	$(3\,5\,\bar{1})/(3\,\bar{1}\,5)$	one or two-fold dep. coplanar and codirect.	−b2, b1, −d1/ d3, −d1.b1	$F_{\{1\,3\,5\}}/F^2_{\{1\,3\,5\}}$	✓	✓	
G	$(3\,5\,\bar{1})/(3\,\bar{1}\,5)$	one or two-fold dep. coplanar and codirect.	−b2, b1, −d1/ d3, −d1, b1	$F_{\{1\,3\,5\}}/F^2_{\{1\,3\,5\}}$	✓	✓	
D	{1 1 5}	two-fold dep. coplanar and codirect.	−b2, b1, −d1, d3, c2, −c3	$F_{\{1\,1\,5\}}$	✓	✓	
E	Cells only	two-fold easily cross slipping codirectional		F_{cell}	✓		
F	$(4\,4\,\bar{1})$?	two-fold dep. coplanar and codirect.	−b2, b1, −d1, c2	$F_{\{4\,4\,1\}}$	✓		
	$(3\,5\,\bar{1})/(3\,\bar{1}\,5)$?	two-fold dep. coplanar and codirect.	−b2, b1, −d1/ d3, −d1.b1	$F_{\{1\,3\,5\}}/F^2_{\{1\,3\,5\}}$		✓	
	$(1\,1\,\bar{1})$?	coplanar	−b2, b1	F_{copl}			✓

The parameters quantifying the fraction of the slip that is accounted for by the slip class are also listed (see Section 4.3). These parameters are expected to be high when extracted from the slip systems calculated from the lattice rotations using the three methods described in Section 4.1. The last three columns designate whether this is the case for each of the three methods (axi, int, and unr). Note that / separates slip classes or slip systems, which may or may not be active at the same time while, separates classes or systems which must be simultaneously activated. The question marks for region F reflect the uncertainty about the GNB plane, which is why several possibilities are listed.

region. Within two of the regions (AI and E) three rotation trends coexist. For these regions, the grains adhering to each of these trends are treated separately.

All the calculated parameters are tabulated in the Appendix. The data in these tables have been evaluated to see if the parameters with the highest value derived from the calculated slip systems with each of the three methods agree with those listed in Table 3, as expected from the dislocation structure. The last three columns in Table 3 show the result of this comparison. It is seen that at least one of the methods give agreement for regions AI, B, C, D, E, and G and F, while this is not the case for region AII.

For region AII, F_{sgl} is not the highest parameter for any of the three methods. However, for the unrestricted method F_{sgl} is almost as high as F^2_{sgl}, as seen in Table A.2. This shows that the slip is in fact dominated by a single system, which on average accounts for 58% of the total slip calculated with the unrestricted method. As a special case for this region, a calculation with a bound of 0.25 on the strains instead of the 0.15 used in the intermediate method was conducted. This calculation gave parameters comparable to the unrestricted method and shows that realistic slip systems can be obtained while enforcing fairly tight bounds on the strains.

For region F, the dislocation structure alignment is not well characterized, and three different possibilities are listed in Table 3. Each of the three calculation methods give slip systems which are in agreement with one of these. This means that the analysis unfortunately does not contribute to resolve the structure in this region.

5.3. Slip systems

The identified slip systems are reported in Table 4. In the table the dominant systems are those deduced to be highly active based on both dislocation structures and lattice rotations. The dislocation structure analysis does not give quantitative information on the activity of these systems. This information is, however, provided by the calculations based on the lattice rotations. It is seen that the dominant systems account for 54–90% of the total slip, depending on the region and the calculation method. The dominant systems are active in practically all the grains in the region and on average each system accounts for more than 8% of the total slip. The identities and combined activities of major additional systems are also listed in Table 4. A major additional system is defined as one which, on average, accounts for 5% or more of the slip in the region. It is furthermore required that the system is active in half or more of the grains in the region. Together, the dominant and major additional systems account for more than 70% of the slip, and in most cases close to 90%.

It is seen in Table 4 that the three rotation trends in region AI correspond to different relative activities on the primary, critical and conjugate slip systems (−b2, −a2, d3). The three trends in region E also share some systems, but activate them with different intensity.

The difference between regions C and G lies in the consistent activation of systems −b2, b1 and −d1 in region G, while the conjugate system (d3) often replaces

Table 4
Dominant slip systems determined from both dislocation structure and lattice rotations, the fraction of slip they account for as well as major additional systems and the total slip fraction accounted for by major and dominant systems

Region	Dominant slip systems		Slip on dominant (%)	Additional major systems	Total slip on dominant and major (%)
AI-down	$-a2 \gg -b2, d3$	axi	65	$a3, b3, -c3, c2$	92
		int	87	a3	93
		unr	73	$a3, b3$	97
AI-none	$-b2, d3 \gg -a2$	axi	60	$a3, b1, -d1$	92
		int	65	a3	93
		unr	70	$a3, -d2$	98
AI-up	$-b2 \gg d3, -a2$	axi	54	$a3, -d1, b1$	86
		int	63	$-d1$	71
		unr	80	none	80
B	$-b2, d3$	int	54	$-d1, b1, -a2, a3$	96
		unr	69	$-d1, -a2$	89
AII	$-b2$	unr	56	$b1, -a2^*$	78
C	$-b2, b1, -d1, d3$	axi	82	none	82
		int	89	none	89
G	$-b2, b1, -d1$	axi	75	$a3, -c3, c2, d2$	97
		int	79	a3	85
D	$-b2, b1, -d1,$ $d3, c2, -c3$	axi	90	none	90
		int	93	none	93
E-down	$a3, b3, -a2, -d2$	axi	76	$c2, -c3, -b2$	95
E-none	$-b2, -c2, c3,$ $d3, a3, b3$	axi	75	$-a2$	98
E-up	$-b2, -c2, a3, b3$	axi	65	$-a2$	80
F	$-b2, b1, c2, -d1$	axi	87	none	87
	$-b2, b1, -d1$	int	81	c2	89
	$-b2, b1$	unr	75	$-d1$	82

Additional major systems are interpreted as systems, which on average account for 5% or more of the slip in the region and are furthermore active in half or more of the grains.
* In the lower part of AII $-a2$ dominates over b1, while b1 dominates over $-a2$ in the upper part.

or coexists with the primary one in region C. This suggests that the GNBs in region G all align with $(3\,5\,\bar{1})$, while those in region C align with $(3\,5\,\bar{1})$ and/or $(3\,\bar{1}\,5)$. This has yet to be verified experimentally. The difference, however, shows up clearly in the rotations: while the rotations in region G move towards the $\langle 1\,0\,0\rangle$–$\langle 1\,1\,1\rangle$ line, the rotations in region C include a wide span of directions from towards the $\langle 1\,0\,0\rangle$–$\langle 1\,1\,1\rangle$ line to rotations away from this line. Rotations in between these extremes, i.e. more or less parallel to the $\langle 1\,0\,0\rangle$–$\langle 1\,1\,1\rangle$ line, are also seen.

While the detailed dislocation structure in region F is not known, it is clear that the GNBs in the lower part of the region lie closer to a slip plane than in the upper part. Neither inspection of the parameters calculated for each grain nor inspection of the identified slip systems reveal any systematic differences between the lower and upper parts of the region. The homogeneity of the rotations and the calculated slip systems in this region compared with the variations of the dislocation structure cannot be explained at present.

6. Discussion

The lattice rotations and dislocation structures give different information about the slip systems:

- The lattice rotations alone give the identity and relative activities of the calculated systems, but the result depends heavily on the assumed boundary conditions on the strain.
- The dislocation structures give the identity of the dominating slip systems but only little information about the relative activities of these. Nor do they give information about the strain tensor.

The analysis of the preceding sections combined the two types of data and identified slip systems, relative activities and some bounds on the strain tensor. In the following it is argued that the findings are also within the regime commonly considered physical realistic. The implications for modelling of polycrystal plasticity are also discussed.

6.1. Plastic work

In addition to the parameters derived from the calculated slip systems with each of the three methods, the tables in the Appendix include a parameter which relates to the plastic work. Assuming the same critical resolved shear stress on all slip systems, the plastic work is calculated as the sum of the shears on the active systems, $\sum_i \gamma_i$. In the Appendix this is related to the corresponding quantity calculated with the Taylor/Bishop–Hill model[2] (often termed the M-factor), which is commonly believed to constitute an upper limit.

Leaving out region E, which has exceptionally high plastic work, the work from the axisymmetric method amounts to 102–116% of the Taylor/Bishop–Hill work, while the corresponding numbers for the intermediate and unrestricted methods are 94–102% and 79–94%, respectively. Even though the work of the axisymmetric and intermediate methods exceeds the commonly accepted upper bound set by the Taylor/Bishop–Hill model, the magnitude of the work increase is relatively small and cannot be deemed physically unrealistic. It should also be noted that these methods also agree better with the dislocation structures than the unrestricted method.

6.2. Slip systems and stress/strain conditions

The identified slip systems may be compared with the systems predicted by the Taylor/Bishop–Hill model, which enforces strain compatibility, and those with the highest Schmid factors, which are expected to be activated based on stress considerations. The majority of the identified slip systems are also among the slip systems with the highest Schmid factors in the grain. Common systems activated with relatively low – but far from vanishing – Schmid factors are systems b1 and $-$d1. These two systems, on the other hand, are predicted to be active by the Taylor/Bishop–Hill model, together with many of the systems with high Schmid factors. This shows that systems b1 and $-$d1 are activated to maintain some degree of strain compatibility.

Two systems b1 an $-$d1 have a large impact on the dislocation structure, as the combination $\{-\mathrm{b2}, \mathrm{b1}, -\mathrm{d1}\}$ represents the dependent coplanar and codirectional slip class, which results in GNBs which lie far from the slip plane with which GNBs align in the case of single slip on $-$b2. The dislocation structure is therefore a strong indicator for the activation of b1 and $-$d1, and therefore also for general enforcement of some degree of strain compatibility.

The failure of the axisymmetric method for regions AII and B, where it predicts activation of b1 and $-$d1 in disagreement with the dislocation structure, suggests that strain compatibility is not strictly enforced. By contrast to this, only the axisymmetric method succeeds for region E. Regions C, D and G, which all exhibit dislocation structures that require substantial activities on b1 and $-$d1 have been explored with a number of additional calculations to determine how much the bounds on the strain tensor may be relaxed while still activating the systems which agree with the dislocation structure. It was found that the limit is about 0.3–0.4 compared to the 0.15 used here for the intermediate method in Eq. (5).

6.3. Grain-orientation dependence and variations within regions

It is clear from the preceding analysis that the slip systems exhibit a strong grain-orientation dependence, which manifests itself in grain-orientation-dependent lattice rotations and dislocation structures. Closer inspection of the lattice rotations in Fig. 2 reveals that also the variation within each region exhibits grain-orientation dependence. The rotation scatter in regions AII, F and G is much smaller than in the regions closest to the $\langle 1\,0\,0\rangle$–$\langle 1\,1\,1\rangle$ line, i.e. regions E, AI, B, C and D, where variation in the relative activities of the primary and conjugate systems ($-$b2 and d3) – and, for regions AI and E, also of other systems – show up in both lattice rotations and dislocation structures. It is characteristic that these systems are those with the highest Schmid factors. The correlation with the Schmid factors again reveals the importance of the grain orientation, although secondary factors must be invoked to fully explain the variations.

Often local stress/strain variations are suggested to be the origin of different behaviour of grains of similar orientations. Interestingly, predictions based on addition of random stresses to activate multislip in the so-called modified Sachs model [39,40] predicts rotation variations in reasonably good agreement with the present observations, except for regions AI and E in the $\langle 1\,0\,0\rangle$ corner [41]. However, analysis of the predicted systems with this model in relation to the dislocation structure remains to be carried out. The problems of this model and many other models [12] in regions AI and E, together with the fact that the present calculations for region E only succeeds with the axisymmetric method, demonstrate that the coexistence of three distinct rotation trends in the $[1\,0\,0]$ corner of the stereographic triangle cannot be attributed to stress/strain variations.

While local stress/strain conditions may have an impact in some cases, the above conclusion for regions AI and E suggests the existence of another factor, which has not been considered. As the variations depend on the grain orientation, the unconsidered factor must also be related to this. One suggestion may be dislocation interactions. This is supported by the result from dislocation dynamics that slip systems with similar Schmid factors can exclude each other due to interaction between the dislocations they generate [42].

7. Conclusion

The combination of lattice rotations and dislocation structures adds a new dimension to polycrystal plasticity modelling:

[2] The value listed in the Appendix is the ratio between the two types of work, both referring to the same elongation of the grain.

- Slip systems for all grain orientations in tensile-deformed aluminium have been identified which match both the observed lattice rotations and the observed dislocation structures, while keeping both the plastic work and the strain within physically realistic bounds.
- The grain orientation has been established as the primary parameter controlling the slip systems, leading to grain-orientation dependence of lattice rotations and dislocation structures.
- Secondary effects control the selection of the most active slip system among those with the highest Schmid factors. This is reflected in systematic variations in lattice rotations and dislocation structures within each region. The character of these variations differs from region to region in the stereographic triangle, and the variations are therefore also strongly linked to the grain orientation. They could not in all cases be attributed to local variations in the stress/strain conditions. Instead, interaction between the dislocations from the active slip systems may be the factor responsible for this behaviour.

Acknowledgements

The author especially wishes to thank Dr. N. Hansen and Dr. X. Huang for a decade of fruitful discussions on the subjects of this paper. She also gratefully acknowledges the Danish National Research Foundation for supporting the Center for Fundamental Research: Metal Structures in Four Dimensions, within which this work was performed.

Appendix A. Quantitative parameters characterizing the calculated slip system combinations

This appendix contains all the values of the quantitative parameters, which are derived from the slip systems calculated as described in Section 4 from the lattice rotations. The parameters are presented for each of the regions shown in Fig. 5b. For regions AI and E the three rotation trends of the tensile axis (rotation downwards towards [1 0 0], towards the [1 0 0]–[1 1 1] line and no rotation) are treated separately. Table 3 summarizes the agreement between the parameters presented here with those deduced from the dislocation structure. Agreement is obtained when the parameter with the highest value in each of Tables A.1–A.8 is among those expected from the dislocation structure.

The last column in each table displays the parameter $\sum\gamma_i/M_T$, which is the ratio of the calculated plastic work and the plastic work calculated with the Taylor/Bishop–Hill model (the so-called Taylor M-factor). This parameter is introduced and discussed in Section 6.1.

Table A.1
Parameters characterizing the slip systems calculated by the three methods for the three rotation trends in region AI

	F_{sgl} (%)	F^2_{sgl} (%)	F_{copl} (%)	F_{codir} (%)	F_{cell} (%)	$F_{\{135\}}$ (%)	$F^2_{\{135\}}$ (%)	$F_{\{441\}}$ (%)	$F_{\{115\}}$ (%)	$\sum\gamma_i/M_T$
AI – to [100]										
Axisymmetrical	30	47	41	28	0	35	44	45	26	1.16
Intermediate	39	54	53	30	18	16	0	0	0	0.95
Unrestricted	53	74	49	11	0	0	0	0	0	0.90
AI – no rotation										
Axisymmetrical	24	44	37	27	0	43	62	23	0	1.08
Intermediate	34	61	38	12	10	0	0	0	0	0.97
Unrestricted	37	64	44	0	0	0	0	0	0	0.94
AI – to [100]–[111]										
Axisymmetrical	35	49	44	35	27	39	44	18	0	1.13
Intermediate	41	60	40	26	19	34	32	0	0	1.00
Unrestricted	47	68	47	11	0	0	0	0	0	0.93

Table A.2
Parameters characterizing the slip systems calculated by the three methods in region AII

AII	F_{sgl} (%)	F^2_{sgl} (%)	F_{copl} (%)	F_{codir} (%)	F_{cell} (%)	$F_{\{135\}}$ (%)	$F^2_{\{135\}}$ (%)	$F_{\{441\}}$ (%)	$F_{\{115\}}$(%)	$\sum\gamma_i/M_T$
Axisymmetrical	35	46	51	39	2	66	75	58	3	1.07
Intermediate	45	56	56	42	3	65	71	40	3	0.94
Unrestricted	58	71	56	17	0	21	7	0	0	0.79

Table A.3
Parameters characterizing the slip systems calculated by the three methods in region B

B	F_{sgl} (%)	F^2_{sgl} (%)	F_{copl} (%)	F_{codir} (%)	F_{cell} (%)	$F_{\{135\}}$ (%)	$F^2_{\{135\}}$(%)	$F_{\{441\}}$ (%)	$F_{\{115\}}$ (%)	$\sum\gamma_i/M_T$
Axisymmetrical	27	39	43	39	0	62	75	43	15	1.10
Intermediate	35	56	48	29	0	53	50	0	0	0.96
Unrestricted	45	72	44	14	0	0	0	0	0	0.88

Table A.4
Parameters characterizing the slip systems calculated by the three methods in region C

C	F_{sgl} (%)	F^2_{sgl} (%)	F_{copl} (%)	F_{codir} (%)	F_{cell} (%)	$F_{\{135\}}$ (%)	$F^2_{\{135\}}$ (%)	$F_{\{441\}}$ (%)	$F_{\{115\}}$ (%)	$\sum\gamma_i/M_T$
Axisymmetrical	29	35	48	48	0	74	83	74	56	1.09
Intermediate	36	46	53	45	0	76	88	59	19	0.99
Unrestricted	46	67	51	20	0	40	50	0	0	0.88

Table A.5
Parameters characterizing the slip systems calculated by the three methods in region D

D	F_{sgl} (%)	F^2_{sgl} (%)	F_{copl} (%)	F_{codir} (%)	F_{cell} (%)	$F_{\{135\}}$ (%)	$F^2_{\{135\}}$ (%)	$F_{\{441\}}$ (%)	$F_{\{115\}}$(%)	$\sum\gamma_i/M_T$
Axisymmetrical	24	31	41	43	0	63	73	71	90	1.12
Intermediate	31	39	46	57	0	71	81	76	93	1.02
Unrestricted	38	63	51	26	0	50	67	0	0	0.93

Table A.6
Parameters characterizing the slip systems calculated by the three methods for the three rotation trends in region E

	F_{sgl} (%)	F^2_{sgl} (%)	F_{copl} (%)	F_{codir} (%)	F_{cell} (%)	$F_{\{135\}}$ (%)	$F^2_{\{135\}}$ (%)	$F_{\{441\}}$ (%)	$F_{\{115\}}$ (%)	$\sum\gamma_i/M_T$
E – to [100]										
Axisymmetrical	27	32	48	43	76	26	33	11	0	1.40
Intermediate	34	36	62	49	90	0	0	0	0	1.21
Unrestricted	46	50	79	57	0	0	0	0	0	1.09
E – no rotation										
Axisymmetrical	24	43	32	29	80	0	0	0	0	1.02
Intermediate	31	58	39	31	39	0	0	0	0	0.98
Unrestricted	41	74	11	23	0	0	0	0	0	0.97
E – to [100]–[111]										
Axisymmetrical	29	44	41	39	77	18	21	0	0	1.11
Intermediate	35	50	53	40	48	0	0	0	0	1.01
Unrestricted	50	69	37	47	0	0	0	0	0	0.96

Table A.7
Parameters characterizing the slip systems calculated by the three methods in region G

G	F_{sgl} (%)	F^2_{sgl} (%)	F_{copl} (%)	F_{codir} (%)	F_{cell} (%)	$F_{\{135\}}$ (%)	$F^2_{\{135\}}$ (%)	$F_{\{441\}}$ (%)	$F_{\{115\}}$(%)	$\sum\gamma_i/M_T$
Axisymmetrical	36	38	54	46	0	75	81	80	0	1.15
Intermediate	46	51	61	44	0	80	85	0	0	1.01
Unrestricted	65	76	75	15	0	32	38	0	0	0.85

Table A.8
Parameters characterizing the slip systems calculated by the three methods in region F

F	F_{sgl} (%)	F^2_{sgl} (%)	F_{copl} (%)	F_{codir} (%)	F_{cell} (%)	$F_{\{135\}}$ (%)	$F^2_{\{135\}}$ (%)	$F_{\{441\}}$ (%)	$F_{\{115\}}$ (%)	$\sum\gamma_i/M_T$
Axisymmetrical	32	35	57	48	0	77	81	82	13	1.06
Intermediate	38	41	64	51	0	82	66	74	10	0.96
Unrestricted	51	64	73	24	0	42	20	2	0	0.87

References

[1] Sachs GZ. Ver Deu Ing 1928;72:734.
[2] Taylor GJ. J Inst Met 1938;62:307.
[3] Bishop J, Hill R. Philos Mag A 1951;42:1298.
[4] Hutchinson JW. Proc Roy Soc A 1970;319:247.
[5] Mika DP, Dawson PR. Mater Sci Eng A 1998;257:62.
[6] Panchanadeeswaran S, Becker R, Doherty RD, Kunze K. Mater Sci Forum 1994;157–162:1277.
[7] Bhattachayva A, El-Danaf E, Kalidindi SR, Doherty RD. Int J Plast 2001;17:861.
[8] Wu GL, Godfrey A, Liu Q. Mater Sci Forum 2002;408-4:589.
[9] Margulies L, Winther G, Poulsen HF. Science 2001;291:2392.
[10] Winther G, Margulies L, Poulsen HF, Schmidt S, Larsen AW, Lauridsen EM, et al. Mater Sci Forum 2002;408–412:287.
[11] Poulsen HF, Margulies L, Schmidt S, Winther G. Acta Mater 2003;51:3821.
[12] Winther G, Margulies L, Schmidt S, Poulsen HF. Acta Mater 2004;52:2863.
[13] Kalidindi SR, Bhattachayva A, Doherty RD. Adv Mater 2003;15:1345.
[14] Haldrup K, Nielsen SF, Beckmann F, Wert JA. J Microsc – Oxford 2006;222:28.

[15] Kobayashi M, Toda H, Kawai Y, Kobayashi T, Uesugi K, Wilkinson DS, et al. J Jpn Inst Met 2007;71:181.
[16] Nielsen SF, Poulsen HF, Beckmann F, Thorning C, Wert JA. Acta Mater 2003;51:2407.
[17] Poulsen HF. Three-dimensional X-ray diffraction microscopy. Mapping polycrystals and their dynamics. Berlin: Springer; 2004.
[18] Huang X, Hansen N. Scripta Mater 1997;37:1.
[19] Huang X. Scripta Mater 1998;38:1697.
[20] Liu Q, Juul-Jensen D, Hansen N. Acta Mater 1998;46:5819.
[21] Winther G, Huang X, Hansen N. Acta Mater 2000;48:2187.
[22] Huang X, Hansen N. Mater Sci Eng A 2004;387–389:186.
[23] Winther G, Huang X, Godfrey A, Hansen N. Acta Mater 2004;52:4437.
[24] Huang X, Winther G. Philos Mag A 2007;87:5189.
[25] Winther G. Acta Mater 2003;51:417.
[26] Hughes DA, Khan S, Godfrey A, Zbib H. Mater Sci Eng A 2001;309:220.
[27] McCabe RJ, Misra A, Mitchell TE. Acta Mater 2004;52:705.
[28] Wert JA, Liu Q, Hansen N. Acta Metall Mater 1995;43:4153.
[29] Kühlmann-Wilsdorf D. Mater Sci Eng A 1989;113:1.
[30] Basson F, Driver JH. Mater Sci Eng A 1998;A256:243.
[31] Winther G, Huang X. Philos Mag A 2007;87:5215.
[32] Kang J-Y, Bacroix B, Réglé H, Oh KH, Lee H-C. Acta Mater 2007;55:4935.
[33] Randle V, Hansen N, Juul Jensen D. Philos Mag A 1996;73:265.
[34] Kawasaki Y. In: Oikawa, editor. Strength of materials. Sendai: The Japan Institute of Metals; 1994. p. 187.
[35] Kocks UF, Chandra H. Acta Metall 1982;30:695.
[36] Vetterling W, Teukolsky S, Press W, Flannery B. Numerical recipes. Example book (C). Cambridge: Cambridge University Press; 1988.
[37] Peyrac C, Penelle R. In: Kallend J, Gottstein G, editors. Proceedings of ICOTOM 8, 1988. p. 977.
[38] Bate P, An Y. Scripta Mater 2004;51:973.
[39] Leffers T. Phys Status Solidi (a) 1995;149:69.
[40] Leffers T. In: Haasen P, Gerold V, Kostorz G, editors. Proceedings of fifth international conference on strength of metals and alloys, Aachen, 1979. p. 769.
[41] Winther G, Leffers T, Clausen B. In: Szpunar J, editor. Proceedings of ICOTOM 12, Montreal, 1999. p. 399.
[42] Madec R, Devincre B, Kubin L, Hoc T, Rodney D. Science 2003;301:1879.

Author: Grethe Winther
Title: Slip systems, lattice rotations and dislocation boundaries in deformed metals
Division: Materials Research Division

Risø-R-1686(EN)
March 2009

Abstract (max. 2000 char.):
Metals are polycrystals and consist of grains, which are subdivided on a finer scale upon plastic deformation due to formation of dislocation boundaries.
The crystallographic alignment of planar dislocation boundaries in face centred cubic metals, like aluminium and copper, deformed to moderate strains at room temperature are analysed. A major result is that, by contrast to previous beliefs, the boundaries align with specific crystallographic planes, which depend on the crystallographic grain orientation. This grain orientation dependence originates from an underlying dependence of the active slip systems. Actual prediction of the dislocation boundary alignment has become possible through establishment of general relations between slip systems and dislocation boundary planes. The practical relevance of these relations has been exemplified by applying them as a basis for further prediction of the mechanical anisotropy of rolled sheets.
The rotation of the crystallographic lattice in each grain during deformation also exhibits grain orientation dependence, originating from the slip systems. A combined analysis of dislocation boundaries and lattice rotations concludes that the two phenomena are coupled through their common dependence on the slip systems.

ISSN 0106-2840
ISBN 978-87-550-3741-0

Cover :
Selected figures appearing throughout the report

Pages: 92
Tables: 8
References: 140

Information Service Department
Risø National Laboratory for Sustainable Energy
Technical University of Denmark
P.O.Box 49
DK-4000 Roskilde
Denmark
Telephone +45 46774004
bibl@risoe.dk
Fax +45 46774013
www.risoe.dtu.dk